AEROSPACE REPORT NO.
ATR-2006(5195)-1

Triggered Lightning Risk Assessment for Reusable Launch Vehicles at the Southwest Regional and Oklahoma Spaceports

30 January 2006

Prepared by

E. P. KRIDER
Professor, Department of Atmospheric Sciences and
Institute of Atmospheric Physics
The University of Arizona
Tucson, Arizona

J. C. WILLETT
Consultant
Garrett Park, Maryland

G. S. PENG
Computer Systems Research Department
Computer Science and Technology Subdivision

F. S. SIMMONS
Sensor Systems Subdivision
Electronic Systems Division

G. W. LAW and R. W. SEIBOLD
Commercial Launch Systems
Space Launch Projects Directorate

Prepared for

VOLPE NATIONAL TRANSPORTATION SYSTEMS CENTER
U.S. DEPARTMENT OF TRANSPORTATION
Cambridge, MA 02142

Contract No. DTRS57-99-D-00062
Task 12.0

Space Launch Operations

THE AEROSPACE CORPORATION
EL SEGUNDO, CALIFORNIA

Technical Report Documentation Page

1. Report No. DOT-VNTSC-FAA-06-01	**2. Government Accession No.**	**3. Recipient's Catalog No.**
4. Title and Subtitle Triggered Lightning Risk Assessment for Reusable Launch Vehicles at the Southwest Regional and Oklahoma Spaceports		**5. Report Date** January 30, 2006 **6. Performing Organization Code** DOT-RITA-VNTSC-DTS-67
7. Author(s)* E. P. Krider, J. C. Willett, G. S. Peng, F. S. Simmons, G. W. Law, and R. W. Seibold		**8. Performing Organization Report No.**
9. Performing Organization Name and Address U.S. Department of Transportation Research and Innovative Technology Administration Volpe National Transportation Systems Center Aviation Safety Division Cambridge, MA 02142-1093		**10. Work Units No. (TRAIS)** FA-2R; BL411 **11. Contract or Grant No.**
12. Sponsoring Agency Name and Address U.S. Department of Transportation Federal Aviation Administration Office of the Assoc. Administrator for Commercial Space Transportation Washington, DC 20591		**13. Type of Report and Period Covered** Contractor Final Report: January 26 – December 23, 2005 **14. Sponsoring Agency Code** FAA/AST-300

15. Supplementary Notes

*The Aerospace Corporation, El Segundo, CA 90245-4691, under contract to the Volpe National Transportation Systems Center -- Contract No. DTRS57-99-D-00062, Task 12.

Aerospace Corporation Report No. ATR-2006(5195)-1

16. Abstract

The Aerospace Corporation was tasked by the Volpe National Transportation Systems Center to provide technical support to the Federal Aviation Administration, Office of Commercial Space Transportation (FAA/AST), in assessing the risks involved with triggered lightning during suborbital launches and reentries of reusable launch vehicles (RLVs) from the proposed Southwest Regional Spaceport in New Mexico and the proposed Oklahoma Spaceport, Burns Flat, Oklahoma. The Aerospace Corporation is pleased to submit this final report, in accordance with the requirements delineated in Section F, Deliveries or Performance, of Volpe Center Contract No. DTRS57-99-D-00062.

Risk of triggered lightning was studied for five conceptual RLVs originating and/or landing at these proposed spaceports. Three areas were addressed: (1) observed frequencies of cloud-to-ground lightning at the proposed spaceports, including estimates of violation frequencies of the existing lightning launch commit criteria (LLCC), (2) estimates of the ambient fields required for triggering by each of the concept vehicles, including consideration of potential methods for estimating the probability of encountering these field magnitudes from the measured radar returns of thunderstorm anvil clouds, and (3) review of the current LLCC to determine if the criteria are relevant to each suborbital RLV concept, including an evaluation of local geographical effects pertaining to each spaceport to determine whether additional LLCC are necessary to conduct safe launch operations there.

17. Key Words Reusable Launch Vehicle, RLV, Suborbital Launch Vehicle, Triggered Lightning, Spaceport, Southwest Regional Spaceport, Oklahoma Spaceport, Licensing, Regulation, Lightning Launch Commit Criteria	**18. Distribution Statement** PUBLIC RELEASE IS AUTHORIZED.

19. Security Classification. (of this report) None	**20. Security Classification. (of this page)** None	**21. No. of Pages** 148	**22. Price**

Form DOT F 1700.7 (8-72) **Reproduction of completed page authorized**

AEROSPACE REPORT NO.
ATR-2006(5195)-1

TRIGGERED LIGHTNING RISK ASSESSMENT FOR REUSABLE LAUNCH VEHICLES AT THE SOUTHWEST REGIONAL AND OKLAHOMA SPACEPORTS

Prepared by

E. P. KRIDER
Professor, Department of Atmospheric Sciences and
Institute of Atmospheric Physics
The University of Arizona
Tucson, Arizona

J. C. WILLETT
Consultant
Garrett Park, Maryland

G. S. PENG
Computer Systems Research Department
Computer Science and Technology Subdivision

F. S. SIMMONS
Sensor Systems Subdivision
Electronic Systems Division

G. W. LAW and R. W. SEIBOLD
Commercial Launch Systems
Space Launch Projects Directorate

30 January 2006

Space Launch Operations
THE AEROSPACE CORPORATION
El Segundo, CA 90245-4691

Prepared for

VOLPE NATIONAL TRANSPORTATION SYSTEMS CENTER
U.S. DEPARTMENT OF TRANSPORTATION
Cambridge, MA 02142

Contract No. DTRS57-99-D-00062, Task 12.0

TRIGGERED LIGHTNING RISK ASSESSMENT FOR REUSABLE LAUNCH VEHICLES AT THE SOUTHWEST REGIONAL AND OKLAHOMA SPACEPORTS

Prepared

E. P. Krider
Professor, Department of Atmospheric Sciences and
Institute of Atmospheric Physics
The University of Arizona
Tucson, Arizona

J. C. Willett
Consultant
Garrett Park, Maryland

G. S. Peng
Computer Systems Research Department
Computer Science and Technology Subdivision

F. S. Simmons
Sensor Systems Subdivision
Electronic Systems Division

G. W. Law
Commercial Launch Systems
Space Launch Projects Directorate

R. W. Seibold
Commercial Launch Systems
Space Launch Projects Directorate

Approved

S. A. Hayati, Director
Computer Systems Research Department
Computer Science and Technology Subdivision

E. K. Ruth, Systems Director
Commercial Launch Systems
Launch Systems Division

Abstract

The Aerospace Corporation was tasked by the Volpe National Transportation Systems Center to provide technical support to the Federal Aviation Administration, Office of Commercial Space Transportation (FAA/AST), in assessing the risks involved with triggered lightning during suborbital launches and reentries of reusable launch vehicles (RLVs) from the proposed Southwest Regional Spaceport in New Mexico and the proposed Oklahoma Spaceport, Burns Flat, Oklahoma. The Aerospace Corporation is pleased to submit this final report, in accordance with the requirements delineated in Section F, Deliveries or Performance, of Volpe Center Contract No. DTRS57-99-D-00062.

Risk of triggered lightning was studied for five conceptual RLVs originating and/or landing at these proposed spaceports. Three areas were addressed: (1) observed frequencies of cloud-to-ground lightning at the proposed spaceports, including estimates of violation frequencies of the existing lightning launch commit criteria (LLCC), (2) estimates of the ambient fields required for triggering by each of the concept vehicles, including consideration of potential methods for estimating the probability of encountering these field magnitudes from the measured radar returns of thunderstorm anvil clouds, and (3) review of the current LLCC to determine if the criteria are relevant to each suborbital RLV concept, including an evaluation of local geographical effects pertaining to each spaceport to determine whether additional LLCC are necessary to conduct safe launch operations there.

Acknowledgments

The authors are grateful for the valuable consultation and contributions provided by Dr. Richard Walterscheid and Dr. James L. Roeder at The Aerospace Corporation. Gratitude is extended to Ms. Karen Shelton-Mur at the Office of the Associate Administrator for Commercial Space Transportation, Federal Aviation Administration, for valuable guidance on FAA/AST weather-related regulatory and licensing needs. The authors also wish to thank Mr. John J. Sigona and Ms. Ann R. DiMare, both of whom served as the Contracting Officer's Technical Representatives (COTRs) at the Volpe National Transportation Systems Center and provided valuable insight on government needs and regulations.

In Memoriam

This report is dedicated to the memory of Dr. Harry C. Koons. Dr. Koons was one of the original members of an advisory panel that was formed to improve the lightning launch constraints for the national ranges following a lightning-related launch failure in 1987. Over the years, Dr. Koons made seminal contributions to the structure, wording, and content of the NASA/USAF/FAA Lightning Launch Commit Criteria (LLCC) and the associated Definitions. His physical insights, attention to detail, and logical rigor were crucial in developing the LLCC. Dr. Koons was the first to use extreme value statistics in the analysis of cloud electric fields and weather radar reflectivities in ways that have increased both launch availability and launch safety. Harry was open and engaging, and his presence on the Lightning Advisory Panel is greatly missed.

Contents

Figures

Tables

1. Executive Summary

The Aerospace Corporation was tasked by the Volpe National Transportation Systems Center to provide technical support to the Federal Aviation Administration, Office of Commercial Space Transportation (FAA/AST), in assessing the risks involved with triggered lightning during suborbital launches and reentries of Reusable Launch Vehicles (RLVs) from the proposed Southwest Regional Spaceport in New Mexico and the Oklahoma Spaceport, Burns Flat, Oklahoma. The Aerospace Corporation is pleased to submit this Final Report, in accordance with the requirements delineated in Section F, Deliveries or Performance, of Volpe Center Contract No. DTRS57-99-D-00062.

The purpose of this study was to determine the risk of triggered lightning during suborbital launches of five different RLV concept vehicles originating and/or concluding at the above proposed spaceports. This report covers:

- A survey of the threat (probability) of natural and triggered lightning due to convective and layered clouds, both seasonally and diurnally, at each spaceport.
- A risk level of triggered lightning performed on each RLV concept vehicle by analyzing the vehicle design (i.e., shape, materials), propellants, and type of operations (i.e., launch altitude, launch platform) at each of the launch sites.
- Review of the current Lightning Launch Commit Criteria (LLCC) to determine if the criteria are relevant to each suborbital RLV concept.
- Evaluation of local geographical effects pertaining to each spaceport and a determination of additional LLCC (if any) necessary to conduct safe launch operations for a given RLV design.
- Pros/Cons of current electric field measurement techniques and a discussion of new techniques (if any) for direct measurement of the electric field inside the clouds.

1.1 Introduction

Oklahoma and New Mexico are each actively seeking to obtain a license to operate a launch site, from the Federal Aviation Administration, Office of Commercial Space Transportation (FAA/AST). Because commercial space activities are anticipated at both launch sites, The Aerospace Corporation was tasked by the Volpe National Transportation Systems Center to provide technical support to FAA/AST in assessing the risks involved with triggered lightning during suborbital launches and reentries of reusable launch vehicles (RLVs) from each of these proposed launch sites.

Risk of triggered lightning was studied for five conceptual RLVs originating and/or landing at these proposed spaceports. Three areas were addressed: (1) observed frequencies of cloud-to-ground lightning at the proposed spaceports, including estimates of violation frequencies of the existing lightning launch commit criteria (LLCC), (2) estimates of the ambient fields required for triggering by each of the concept vehicles, including consideration of potential methods for estimating the probability of encountering these field magnitudes from the measured radar returns of thunderstorm anvil clouds, and (3) review of the current LLCC to determine if the criteria are relevant to each suborbital RLV concept, including an evaluation of local geographical effects pertaining to each spaceport to determine whether additional LLCC are necessary to conduct safe launch operations there.

1.2 Triggered Lightning

At least 80–90% of all lightning strikes to flying aircraft and spacecraft are "triggered," in the sense that they are locally initiated by the penetration of a large conductor into a sufficiently large region of high-intensity ambient electrostatic field. This fact was first conclusively demonstrated by Mazur et al. [1984], who used a UHF radar to document the initial spatial development of lightning discharges *away from* an instrumented F-106 aircraft when it was struck. Recordings of currents and electric-field changes on board other aircraft have been interpreted to indicate that such triggered strikes invariably begin with a positive "leader" propagating away from an extremity on which positive charge had been induced by the ambient field, followed after a few milliseconds by the development of a negative leader from a negatively charged extremity, propagating in the opposite direction [e.g., Boulay et al., 1988; Mazur, 1989]. Here the term "leader" denotes a highly ionized, conducting, filamentary channel extending into virgin air. The term "positive streamer," in contrast, will always refer to the poorly conducting "corona" space-charge waves [e.g., Dawson and Winn, 1965; Phelps and Griffiths, 1976] that are an important component of the advancing "head" of a positive leader.

Detailed study of the triggering phenomenon (as well as other important aspects of lightning) has been facilitated by rocket-triggering techniques. "Classical" rocket-triggered lightning [St. Privat D'Allier Group, 1985] is initiated by a small rocket lifting a grounded wire aloft under a thunderstorm. This technique was pioneered by Newman et al. [1958, 1967]. The key to its success is likely a hypothesis by Brook et al. [1961] that the sufficiently rapid introduction of a grounded conductor into a high-field region might actually initiate the discharge.

It is now well established that classical rocket-triggered lightning normally begins with an upward-propagating, positive leader that moves from the tip of the triggering wire toward a negatively charged cloud. Most "upward-initiated" discharges to towers [Uman, 1987, Chapter 12] are also initiated by positive leaders. The onset conditions for the latter discharges are somewhat different from those for rocket-, aircraft-, and spacecraft-triggered lightning, however, because a fixed tower tends to be surrounded by considerable corona space charge, which inhibits leader formation, whereas this space charge is blown away by the rapid motion of flying vehicles.

Very similar positive leaders have been shown to initiate "altitude" triggered lightning [e.g., Laroche et al., 1989], which is produced when a small rocket lifts an ungrounded wire aloft. Altitude-triggered discharges are believed to be a good analog for lightning strikes to flying aircraft and spacecraft. For all of the above reasons, we focus here on the extended development of a positive leader as the proximate cause of triggered strikes to spacecraft, and we use triggering conditions derived from experiments with classical rocket-triggered lightning to estimate the conditions for such strikes.

The initiation and continued propagation of positive leaders from conducting objects has been studied in detail in the laboratory, using sparks up to tens of meters in length, but to a much lesser extent on the scale of lightning discharges in the free atmosphere [e.g., Bazelyan and Raizer, 1998, 2000; Willett et al., 1999]. Material from these references that is relevant to the triggering conditions will be summarized here.

Basically, there are three conditions that must be satisfied in order to initiate and propagate a positive leader.

First, “breakdown” must occur in a small volume of air near the surface of the object in question, in order to produce free electrons in sufficient quantities to carry an electric current. This means that at normal temperatures and pressures the local electric field must reach a value near 3.0 MV/m, and when this occurs, a phenomenon called “glow corona” is produced.

Second, the current in the corona region must be amplified to the point where positive streamers occur. These streamers propagate outward from the breakdown region, further heating a small volume that is called the “stem,” and the stem is where the positive-leader channel begins.

Third, the *ambient* field must be large enough over a sufficiently large volume of space that the positive leader, once it has been initiated, will continue to grow and propagate (i.e., the potential at its tip will remain large enough relative to the local ambient potential to sustain propagation). This last condition is what we will refer to as “leader viability.”

We identify leader viability with the triggering conditions for several reasons. First, long, thin conductors like classical rocket-triggering wires are known to create air breakdown near their tips, initiate positive streamers, and even produce short, nonviable positive leaders long before — at much shorter wire lengths or in much weaker ambient fields than — they trigger lightning. Second, even shorter and stubbier conductors, such as large aircraft, are known to be in corona much of the time, due to charging by their engines and/or by particle impaction inside clouds, without triggering lightning. Thus it appears that the ambient field, rather than the locally enhanced field at the extremities of a flying vehicle, is the key determinant of triggering. Third, the net charge on such a vehicle is usually unknown, making it difficult or impossible to calculate the conditions for localized breakdown by the familiar enhancement-factor approach. Finally, the enhancement factor estimated from the nose radius of curvature and the effective length (including the exhaust plume) of any of the RLVs of interest here (assuming it to be uncharged) predicts the onset of breakdown at a higher ambient field than that required to produce leader viability (as determined from the data and model described in Section 1.4). Thus the leader-viability approach affords a margin of safety in these cases.

1.3 Possible Solutions

There are two ways to reduce the risk of triggered lightning — hardening the vehicle, or avoiding the hazard. The former is not considered in any detail here because the weight (and testing) requirements are generally prohibitive and expensive for all but military rockets. Therefore, avoidance was the main focus of the present study.

1.3.1 *In Situ E* Measurements

In situ measurement of the ambient electrostatic field is undoubtedly the best way to determine whether any particular cloud along or near the planned flight path poses a triggered-lightning hazard to any particular RLV. This is because most clouds do not give a clear indication to any known remote-sensing technique (e.g., morphology or radar reflectivity) of whether or not they are electrified and capable of triggering lightning. The obvious exceptions are cumulonimbus clouds and any clouds that are producing natural lightning; clearly, any such clouds should always be avoided. Developing cumuli should also be avoided because they are capable of becoming electrified very rapidly.

Some types of clouds, such as “thick clouds” and “thunderstorm debris clouds” (as defined in the current LLCC), are statistically known to constitute a hazard in a relatively small percentage of cases.

Thus, in the absence of direct measurements, they should be avoided, even though avoidance may produce unnecessary launch delays and scrubs. In such cases, an *in situ* measurement capability could virtually eliminate false alarms and maximize launch availability, without compromising safety. Unfortunately, the only appropriate method of obtaining *in situ* electric field measurements — a high-performance aircraft instrumented with five or more field mills (an Airborne Field Mill, or ABFM, system) — is expensive and both technically and operationally difficult.

The use of an *in situ* measurement capability, such as outlined above, to reduce the false alarms that would otherwise be inherent in any cloud-based avoidance criteria (like the current LLCC) requires a knowledge of the electric-field conditions that are necessary to trigger lightning with the vehicle in question. To this end, the electric-field magnitudes that constitute a threat to five concept RLVs are estimated below. The electric-field "threshold" for triggering lightning is vehicle, engine, altitude, and velocity dependent. More theoretical and experimental work is needed on all of these dependencies, although some estimates can be made with reasonable confidence.

1.3.2 Cloud-Based Rules

The existing LLCC are examples of cloud-based avoidance criteria. Although they are believed to be very safe, these rules were developed for large orbital boosters like the Titan and the Space Shuttle, and they do produce false alarms and reduce launch availability. Nevertheless, they should be applied to flight operations of the RLVs of interest here until and unless an operational ABFM and/or further statistical analysis of existing ABFM experiments enable some of the rules to be tailored to smaller launch vehicles.

Note that the most important of these rules, *whether an operational ABFM is used or not*, are (A) to avoid all clouds that are producing any type of natural lightning and (B) to avoid cumulus clouds that may become electrified in just a few minutes and could produce natural (or triggered) lightning. Note also that measurements of surface electric fields using a Ground-Based Field-Mill system (GBFM, as opposed to an ABFM) are incorporated into certain of these LLCC, where they are important for both adding safety (detection of additional hazards) and providing some relief from the otherwise very conservative cloud-based rules. It should be emphasized that a GBFM is not a substitute for an ABFM because of the electrical charges on screening layers that can accumulate at cloud boundaries, even if the GBFM system has the necessary areal extent for sensitivity to the clouds of interest.

1.4 Triggering Models

We now briefly review four possible models for predicting the viability of a positive leader, hence a lower bound on the triggering conditions, in classical rocket-triggered lightning. [In this section, we will consider triggering only at altitudes near the surface, i.e., at standard temperature and pressure (STP)]. Two simple models are the following: A) A leader might become viable when the magnitude of the ambient field is larger than the potential gradient found in a DC arc that carries the same current — only a few kilovolts per meter at typical leader currents of a few amperes. This is probably a necessary condition, but fortunately for us, it is not sufficient. B) It has also been suggested that triggering can occur when the potential "spanned" by the triggering wire exceeds about 3.5 MV. This might be called the "constant-potential-spanned" criterion. It turns out to be overly simplistic, however, when compared to two more sophisticated models of leader propagation that cannot be discussed in any detail here.

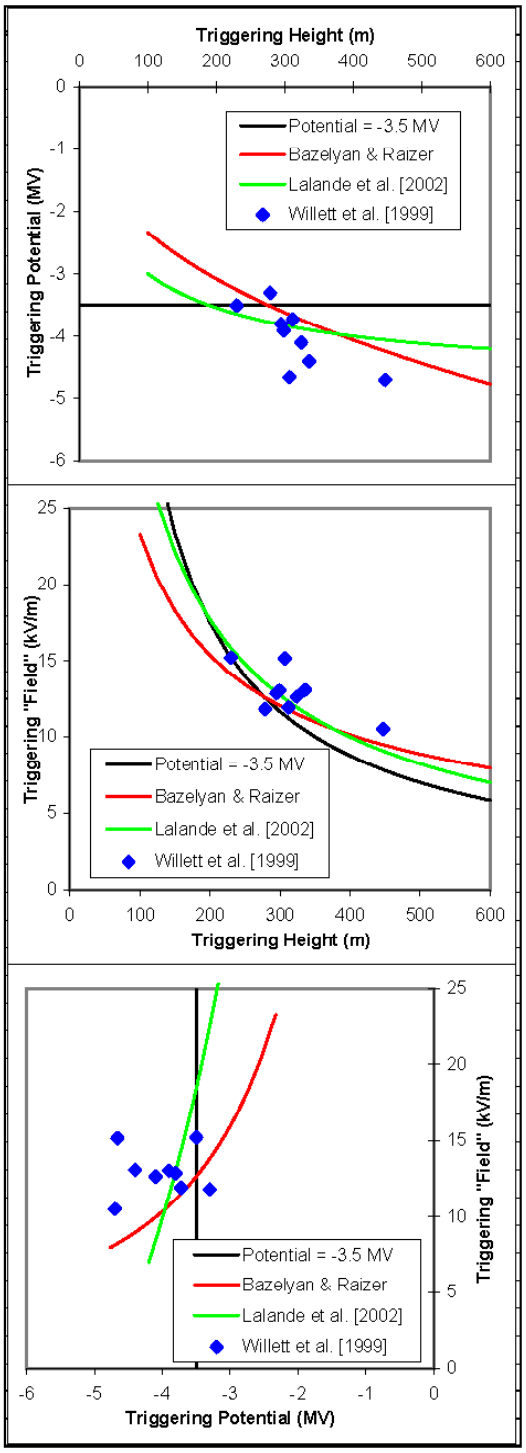

Figure 1-1. Comparison of the "Constant-Potential-Spanned," Bazelyan and Raizer [2000], and Lalande et al. [2002] Positive-Leader Models with the Data of Willett et al. [1999].

These two models of the physical development of positive leaders have led to predictions of the ambient field (assumed uniform) *vs*. wire length that is required for a viable upward positive leader in classical, rocket-triggered lightning: C) Aleksandrov et al. [2005] have presented a formula corresponding to a model that was developed previously by Bazelyan and Raizer [2000]. D) Lalande et al. [2002] gave a comparable formula corresponding to their very different physical model.

In Figure 1-1 we show the predictions of models B, C, and D, plotted together with the direct measurements of Willett et al. [1999]. (Note that we are plotting the average measured electric field between the surface and the triggering height, as opposed to the field at the triggering height, because models C and D both assume a uniform ambient field.) The black curves in Figure 1-1 represent the assumption that a viable positive leader will be initiated whenever the potential spanned by the triggering wire exceeds a constant threshold of 3.5 MV — model B above. The red curves are for model C of Bazelyan and Raizer, and the green curves are for model D of Lalande et al. The data of Willett et al. can be seen to agree reasonably well with all three of these models, giving little to recommend one over any of the others. Nevertheless, the relatively limited data available from lightning strikes to instrumented aircraft (not shown) appears to conclusively rule out model B and to favor model C over model D. For this reason, and because the Bazelyan and Raizer model is safer — it predicts a smaller triggering field for a conductor of any given length in the size range relevant to our RLVs — we adopt model C for present purposes. Clearly, however, more work needs to be done on the models of triggering and their validation.

1.5 Altitude and Velocity Dependence of Triggering

The altitude dependence of electrical breakdown in long sparks is essentially unknown. The triggering field threshold for any given vehicle might range anywhere from the $p^{3/2}$ dependence on ambient pressure at constant temperature that was found for the positive-streamer "stability field" by Phelps and Griffiths [1976] down to the $p^{1/3}$ dependence that has been measured for DC arc drops [see Raizer, 1991, Fig. 10.15], or even lower. Here we compromise on the p^1 dependence that is implied by Paschen's Law at constant temperature, with the understanding that this behavior is quite uncertain at present.

The vehicle-velocity dependence of triggering is believed to be a threshold that is based on the ion-drift velocity in the geometrically enhanced electric field at the altitude of interest, as originally suggested by Brook et al. [1961]. Most estimates of this velocity threshold at STP are lower than the flight speeds of any of the RLVs of interest, except during balloon ascents or the late stages of parachute descents. Given that the small-ion mobility increases with altitude approximately in inverse proportion to air density, our assumption that the triggering field increases in proportion to density suggests that the threshold speed may be approximately altitude independent.

1.6 Five Vehicle Types and Two Spaceports

1.6.1 Representative Suborbital Vehicle Concepts

In order to determine the electric fields that could trigger lightning to suborbital vehicles, the types of vehicles and their trajectories must be known. Because this information is difficult to obtain or unavailable for the five suborbital vehicle concepts being considered, representative vehicle configurations were developed that closely resemble currently proposed suborbital vehicle concepts. The five vehicle configurations are described below.

1) Horizontal takeoff and landing (HTHL) vehicle with jet engines and rocket engines. This vehicle takes off using jet engines and proceeds to an airborne launch point, where it then climbs to apogee using rocket power and glides to a landing on a runway.
2) Ferried and horizontal landing vehicle with rocket engines (referred to as "Air Launch vehicle"). The vehicle is carried aloft by a carrier aircraft to the drop point, where it is released and climbs to apogee using rocket power, and glides to a landing on a runway.
3) HTHL vehicle with rocket engines. This vehicle takes off using rocket engines, climbs to apogee using rocket power, and glides to a landing on a runway.
4) Vertical takeoff and landing (VTVL) vehicle with rocket engines. This vehicle takes off vertically using rocket engines, coasts to apogee, and lands by rocket-powered descent.
5) Balloon takeoff-carrying launch vehicle to altitude. At altitude, the vehicle will climb to apogee using rocket power and lands using a parachute landing system.

Table 1-1 presents information on each of the five vehicles that were used to perform triggered lightning analyses.

1.6.2 Spaceports

New Mexico has proposed to establish the Southwest Regional Spaceport near Upham, New Mexico, approximately 45 miles north of Las Cruces and 30 miles east of Truth or Consequences. This

location is along the western boundary of the White Sands Missile Range, and will benefit from the controlled airspace around the Missile Range. The proposed Spaceport will encompass a 27-square-mile site consisting of open, generally level, rangeland with an average elevation of 4700 ft. The plans for the Spaceport facility call for a launch complex, a landing strip and aviation complex, a payload assembly complex, a support facilities complex, and a system development complex.

The Oklahoma Spaceport is being developed at the Clinton-Sherman Industrial Airpark at Burns Flat, Oklahoma, approximately 100 miles west of Oklahoma City. The Clinton-Sherman Airpark encompasses approximately 3,000 acres and has two runways of 13,500 ft and 5,200 ft. The Spaceport has an operational control tower and an instrument landing system (ILS) capability that can support a full range of aircraft operations. The Spaceport has multiple commercial-size hangars that can accommodate multiple suborbital vehicle companies, and has adequate access to air, ground, and rail transportation modes. The spaceport also has access to manufacturing facilities and the facilities of Oklahoma's Western Technology Center, and will coordinate all suborbital flights from its spaceport operations center, which is under development. Current plans are for the Oklahoma Spaceport to be operational in 2006.

Table 1-1. Representative Vehicle Design Information

Vehicle Number	1	2	3	4	5
Vehicle Type	**HTHL w/ Jet Engines**	**Air Launch**	**HTHL w/ Rocket Engines**	**VTVL**	**Balloon Launch**
Vehicle Length	40.0 ft	21.2 ft	24.3 ft	23.2 ft	18.0 ft
Vehicle Wingspan	25.0 ft	14.4 ft	17.0 ft	N/A	N/A
Vehicle Diameter	5.0 ft	5.0 ft	5.0 ft	5.0 ft	5.0 ft
Nose Radius of Curvature	1.7 ft	4.2 ft	4.2 ft	2.0 ft	3.0 ft
Vehicle Gross Weight	18,000 lb	9,103 lb	13,276 lb	10,724 lb	8,500 lb
Fuel Type	JP-1 and RP-1	Rubber	RP-1	Ethanol	RP-1
Oxidizer Type	Liquid Oxygen	Nitrous Oxide	Liquid Oxygen	Liquid Oxygen	Liquid Oxygen
Rocket Sea Level Thrust (total)	23,800 lb	10,500 lb	13,300 lb	14,500 lb	10,000 lb
Engine Firing Altitude	24,000 ft	50,000 ft	0 ft	0 ft	"80,000 ft"
Engine Burn-out Altitude	150,000 ft	173,000 ft	144,000 ft	114,000 ft	"206,000 ft"
Rocket Burn Time	74.4 sec	96.7 sec	145.1 sec	85.0 sec	"100 sec"
Total Flight Time	1537.4 sec (25.6 min)	973.8 sec (16.2 min)	914.7 sec (15.2 min)	869.7 sec (14.5 min)	"90 - 110 min"
Furthest Distance from Takeoff Site	36 nmi	28 nmi	12 nmi	14 nmi	"10 - 100 km, depending on winds"

1.7 Estimation of Vehicle Plume Lengths

The electrical conductivity of a plume is primarily a function of its electron density; the particle content might also be a secondary factor. The electron density is strongly dependent on the temperature and the presence of easily ionized trace species, mainly sodium and potassium compounds, in the fuel. Soot particles are produced by the combustion of hydrocarbon fuels such as JP-1 and RP-1 with liquid oxygen or nitrogen/oxygen compounds used as oxidizers. One possible effect of these particles might be the thermionic production of electrons consequent to their reaction with entrained air. (Temperatures in the mixing layer of O_2/RP-1 plumes generally reach about 2400

K at low altitudes, hundreds of degrees hotter than the exhaust at the nozzle exit.) The governing plume parameter in triggering lightning is assumed to be an effective length, to be combined with a vehicle body length. The question is how to define an effective plume length with respect to the electrical conductivity.

There are a number of ways in which an effective plume length might be estimated. One method might be to use the distance along the axis where the temperature drops to a specified value. A more casual definition might be simply to use the visible length of the plume, but this would be highly subjective because, in photography, the visible length will depend on both the exposure and the degree of halation of the film. Visible plume lengths are also functions of the concentrations of soot that produce most of the visible radiation. (An O_2/ethanol plume is virtually invisible in daylight.) However the plume lengths are defined, they also vary strongly with the engine size, i.e., with thrust or mass flow of propellants, and with the nozzle configuration. The nozzle expansion ratio governs the exit pressure, and the maximum propulsive efficiency occurs with the pressure matched to the ambient conditions. In practice, the expansion ratio is optimized for some intermediate altitude in the missile flight.

Here we base our estimates of the conducting lengths of RLV plumes on (A) the visible plume length scaled from two video images of SpaceShipOne during a test flight and (B) scaling to the other vehicles in proportion to the square root of engine thrust, on the assumption of single nozzles with the same expansion ratios and fuel-oxidizer mixtures in all cases. (The value for the Titan IV was scaled in a similar way from video images of that vehicle.) We further assume that (C) these plumes are all under-expanded throughout the altitude range of interest for triggered lightning (roughly 0–10 km), so that their lengths do not change much with altitude. Obviously the results, given in the third column of Table 1-2, are quite uncertain in terms of the actual conductive lengths of these plumes.

The overall electrical effective length of each vehicle during the boost phase has been estimated in the last column of Table 1-2 as one-half of the sum of vehicle length plus conducting plume length. For a long, thin, uncharged conductor of actual length equal to that sum, this value of electrical effective length, when multiplied by the ambient-field magnitude (assumed uniform and parallel to the conductor's long dimension), would give the correct potential difference between each tip of the conductor and the nearby ambient atmosphere. Nevertheless, the proper value of electrical effective length to use in the Bazelyan and Raizer model might range from something less than half the vehicle length (if the plume actually has no effect at all) to as much as the sum of vehicle plus plume length (if the tip of the conducting plume acts as a potential equalizer), so this value is also quite uncertain.

Table 1-2. Estimated Plume Lengths

System	Vehicle length, m	Conducting plume length, m	Electrical effective length, m
Concept 1	12.2	29	21
Concept 2	6.5	13	10
Concept 3	7.4	16	12
Concept 4	7.1	18	13
Concept 5	5.5	12	9
Titan IV	60	300	180

1.8 Triggering Conditions

The ambient electric-field thresholds that are required for triggering have been estimated for each of the concept RLVs (except the Concept 5 spacecraft, for reasons that are discussed briefly below) at two altitudes, 0 and 10 km, both during boost phase (with the exhaust plume) and during landing (without the plume). These thresholds are summarized and compared with similar estimates for the Titan IV in Table 1-3. Triggering conditions during the glide phase have not been given for the Concept 4 vehicle because this vehicle is designed to land vertically, breaking first with a parachute and then with its rocket motor. Thus, the exhaust plume may play a role during landing as well as during launch.

Table 1-3. Estimated Electric Fields for Triggering

	Boost Phase		Glide Phase	
System	Surface, kV/m	10 km, kV/m	Surface, kV/m	10 km, kV/m
Concept 1	60	20	125	42
Concept 2	93	31	182	61
Concept 3	83	28	169	56
Concept 4	79	26	--	--
Concept 5	--	--	--	--
Titan IV	16	5	--	--

Although these field thresholds are quite uncertain in absolute terms, they should be reasonably comparable between vehicles at the same altitude. Thus, they do provide a quantitative basis for the following three conclusions:

A) For vehicles that are designed for unpowered horizontal landings (Concept vehicles 1, 2, and 3), there is a significant increase in triggering threshold (or, qualitatively, a reduction in the likelihood of lightning strikes) during the glide phase of the flight.

B) During the glide phase, these three concept RLVs have higher triggering thresholds than those of medium-sized aircraft (which have been measured to be on the order of 45 kV/m at 4–5 km altitudes).

C) Not surprisingly, each concept RLV has much higher triggering fields than the Titan IV. This is typical for large, orbital boosters that the current LLCC have been designed to address.

The following additional conclusion is less certain because conventional aircraft do not have electrically significant exhaust plumes and, consequently, are not strictly comparable to space vehicles during the boost phase:

D) Although Concept 1, the largest vehicle, has an appreciably lower triggering threshold as compared to the other concepts, during boost phase they are all comparable to the triggered-lightning threshold of medium-sized aircraft.

Our last conclusion is not based on quantitative triggering conditions, but rather on the balloon-launched nature of the 5th Concept RLV:

E) Launch conditions for the Concept 5 vehicle will have to be even more rigorous than specified by the current LLCC because of the large balloon that is required to lift the vehicle to 80,000 ft. altitude before ignition. Wind shear, turbulence, and icing must all be avoided, in addition to lightning. Therefore, we believe that neither triggered-lightning conditions nor even the LLCC are relevant in this case.

1.9 Analysis of Lightning Risk and Convective Cloud Cover for Two Proposed Commercial Spaceport Sites

1.9.1 Introduction

A climatological study was performed for two proposed commercial spaceport locations. Frequency of natural lightning, percentage of cloud cover, and cloud top temperatures were analyzed to determine the risk of natural or triggered lightning to anticipated suborbital launch activity at these sites. Diurnal and seasonal variability of natural cloud-to-ground lightning at the proposed spaceports was compared to existing federal launch ranges at Cape Canaveral, Florida (CAPE), and Vandenberg Air Force Base, California (VAFB), in order to assess relative lightning risk. The site of the proposed Southwest Regional Spaceport (SWRS) is in New Mexico, approximately 45 miles north of Las Cruces, 30 miles east of Truth or Consequences and just outside the western boundary of the White Sands Missile Range. The Oklahoma Spaceport (OS) is being developed at the former Clinton-Sherman Air Force Base (CSAFB) at Burns Flat, Oklahoma, approximately 100 miles west of Oklahoma City. The southern portion of White Sands Missile Range (WSMR), approximately 40 miles distant from SWRS, was also included in this study.

1.9.2 Data

Data from a nearly fifteen-year lightning climatology study [Schaub, 1996] of all cloud-to-ground lightning strikes detected by the National Lightning Detection Network (NLDN) within a 100 km radius from the latitude and longitude coordinates in Table 1-4 was collected. The climatology study includes periods before and after the NLDN system upgrade in 1995. Only periods after the upgrade were selected for further analysis.

The 15-year climatology study suggested that January and July would provide the greatest spread in seasonal behavior. The January and July 1999 periods were selected for further analysis at both potential sites. July 1999 appeared to be an anomalously lightning-prone month at SWRS and an anomalously lightning-free month at CSAFB.

Data was also collected for January and July 2004, and the result was opposite from 1999. CSAFB had nearly twice as many cloud-to-ground strikes as SWRS in July 2004.

Cloud data from the Cloud Depiction and Forecast System (CDFS2) [Zamiska and Giese, 1996] was also used to investigate the relationship between the occurrence of convective clouds and lightning and the applicability of cloud-based lightning launch commit criteria (LLCC). CDFS2 is a global cloud analysis product that uses sensor data from the Defense Meteorological Satellite System (DMSP). It identifies clouds by types, percent coverage, and top and base heights for up to four layers.

Temperatures from the European Center for Medium Range Forecasting (ECMWF) global analysis model grid were also used.

The following analysis uses data from three independent databases. While the data can give the locations and times that clouds and lightning were observed, it cannot establish that a particular cloud generated lightning. The temperatures were obtained from a global analysis model and cannot be expected to exactly represent the actual temperatures within a cloud.

Table 1-4. Site Coordinates and Cloud-to-Ground Lightning Occurrence within 100 km

	CSAFB	SWRS	WSMR	CAPE	VAFB
Lat	35.3 N	32.8 N	32.3 N	28.4 N	34.7N
Lon	99.2 W	107 W	106.5W	80.6 W	120.5W
1990-2004 Total	1825240	2123004	968680	3268359	14076
Jan Total	7991	1232	542	24	216
Jan Avg	533	82	36	2	14
Jan 1999	137	22	-	-	-
Jan 2004	3	46	-	-	-
July Total	287810	745058	356042	813906	3091
July Avg	19187	49671	23736	54260	206
July 1999	6068	63932	-	-	-
July 2004	61473	30336	-	-	-

1.9.3 Lightning Climatology

The climatology of naturally occurring cloud-to-ground lightning at all five sites was examined for seasonal and diurnal variability (Tables 1-5 and 1-6). Vandenberg is shown likely to be lightning free year-round. Cape Canaveral is less than 80% likely to be lightning free for day-of-year (DOY) ~139–284 (May 19 – October 11), or ~146 days a year. CSAFB is less than 80% likely to be lightning free for DOY ~93–262 (April 3 – September 10), or ~169 days a year. The proposed SWRS is less than 80% likely to be lightning free for DOY ~144–273 (May 24 – September 30), or ~129 days a year.

Despite the proximity of WSMR and SWRS, significant differences in their lightning climatology were seen. WSMR experienced roughly half as many lightning strikes as the proposed SWRS. Notably, the number of days that a site will be lightning free is not strongly dependent on the total number of lightning strikes at that site. The likelihood that WSMR will be lightning free on any given day is similar to that for SWRS, except that the duration of the lightning season at WSMR is 39 days shorter (June 17 – September 15). The difference is due to the influence of just two outliers in the SWRS climatology, May 24 and September 30. Similarly, the length of the lightning season at CSAFB would have been only 120 days if two outliers had been excluded.

The natural lightning seasons at the two potential spaceport sites are on par with or shorter than for Cape Canaveral, the most lightning-prone existing launch site. Even though SWRS had a shorter lightning season than CSAFB, it experienced twice the number of lightning strikes and for more hours per day (in season) as CSAFB.

1.9.4 Local Effects

Initially, coordinates of the southern end of WSMR were used as a proxy for the proposed SWRS location. The two sites were expected to be similar as they are adjacent and have similar elevations. However, to rule out localized effects, the climatology was later compiled using the exact coordinates of the proposed SWRS. The result showed that the proposed SWRS had roughly twice as many lightning strikes in 1990–2004 than the southern end of WSMR.

Table 1-5. Approximate Number of Days with Less than 80% Probability of Being Lightning Free (Greater than 20% chance of lightning within 100 km on that day of year)

Site	DOY Range	Date Range	No. Days With High Lightning Probability	Length of Main Season (Days, Excluding Outliers)	Length of Entire Season (Days, Including Outliers)
VAFB	N/A	N/A	0	0	0
CAPE	139 – 284	May 19 – October 11	129	146	146
CSAFB	93 – 262	April 3 – September 10	47	120	169
SWRS	144 – 273	May 24 – September 30	86	90	129
WSMR	168 – 258	June 17 – September 15	84	90	90

Table 1-6. Times of Minimum and Maximum Probability of Naturally Occurring Lightning in July

Site	Min (Universal Time)	Min (Local Time)	Max (Universal Time)	Max (Local Time)
CAPE	0900	0400	2000	1500
WSMR	1500	0800	2200	1500
SWRS	1500	0800	2200	1500
CSAFB	1600	1000	2300	1700

Note: VAFB is omitted because it is nearly lightning free in July.

The site of the proposed SWRS is near a bend in a small mountain range on the western edge of WSMR. The mountain range between WSMR and SWRS appears to block the flow of monsoonal moisture from the southwest. The monsoonal flow is primarily responsible for mesoscale convective systems in southwestern continental US (CONUS). A graph of the latitude and longitude coordinates of measured lightning strikes near SWRS in July 1999 (Figure 1-2) illustrates this effect. The density of lighting strikes is much higher to the west of the proposed SWRS and the mountain range. Even the northeastward bend in the mountain range near SWRS is apparent in the lightning statistics; the

boundary between the lightning-prone and nonlightning-prone areas also bends to the north-northeast there. WSMR, which is inside of a protected valley, experienced much fewer lightning strikes in the same time period.

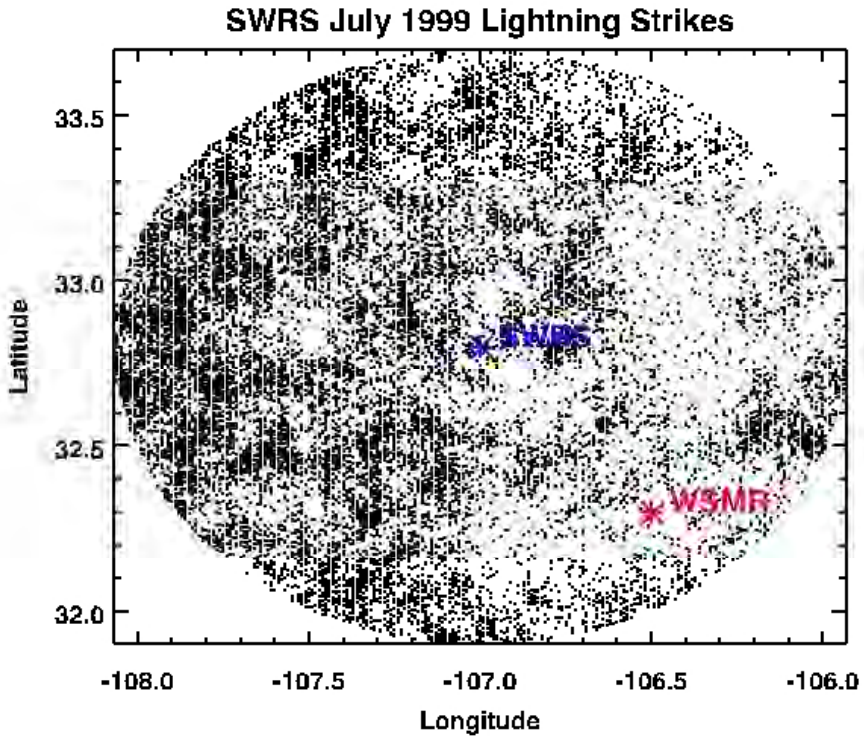

Figure 1-2. Each small black dot represents one lightning strike observed by the National Lightning Detection Network (NLDN) during July 1999, which was a very stormy period in the area. Lightning occurs much less frequently in the WSMR valley floor than at SWRS.

1.9.5 Clouds and Lightning

Several LLCC [Krider, 1999] developed for Expendable and Reusable Launch Vehicles on the federal ranges require that launches be delayed if lightning storms are in the area and if the associated clouds remain in the vicinity of the launch area. Lightning and convective cloud data were combined to clarify the correlations. The dates and hours of observed convective clouds (black crosses) and lightning strikes (red diamonds or triangles) within a 100 km radius circle of the proposed SWRS and CSAFB were plotted (Figures 1-3 and 1-4).

Between 1999 and 2004, CDFS2 cloud analysis became available hourly instead of every 3 hours. Times are rounded *down* to the next whole hour (or 3-hour) time period. In general, lightning is observed during or following times in which convective clouds are observed.

As expected, there was a correlation between observation of cumulus and cumulonimbus clouds and lightning occurrence. However, a high correlation was also observed between altocumulus clouds and lightning occurrence even though altocumulus clouds are not generally associated with natural lightning. The CDFS2 system possibly misidentifies cumulus clouds as altocumulus clouds because

satellite cloud identification can sometimes incorrectly locate the cloud top heights by up to three kilometers too high [Naud et al., 2004].

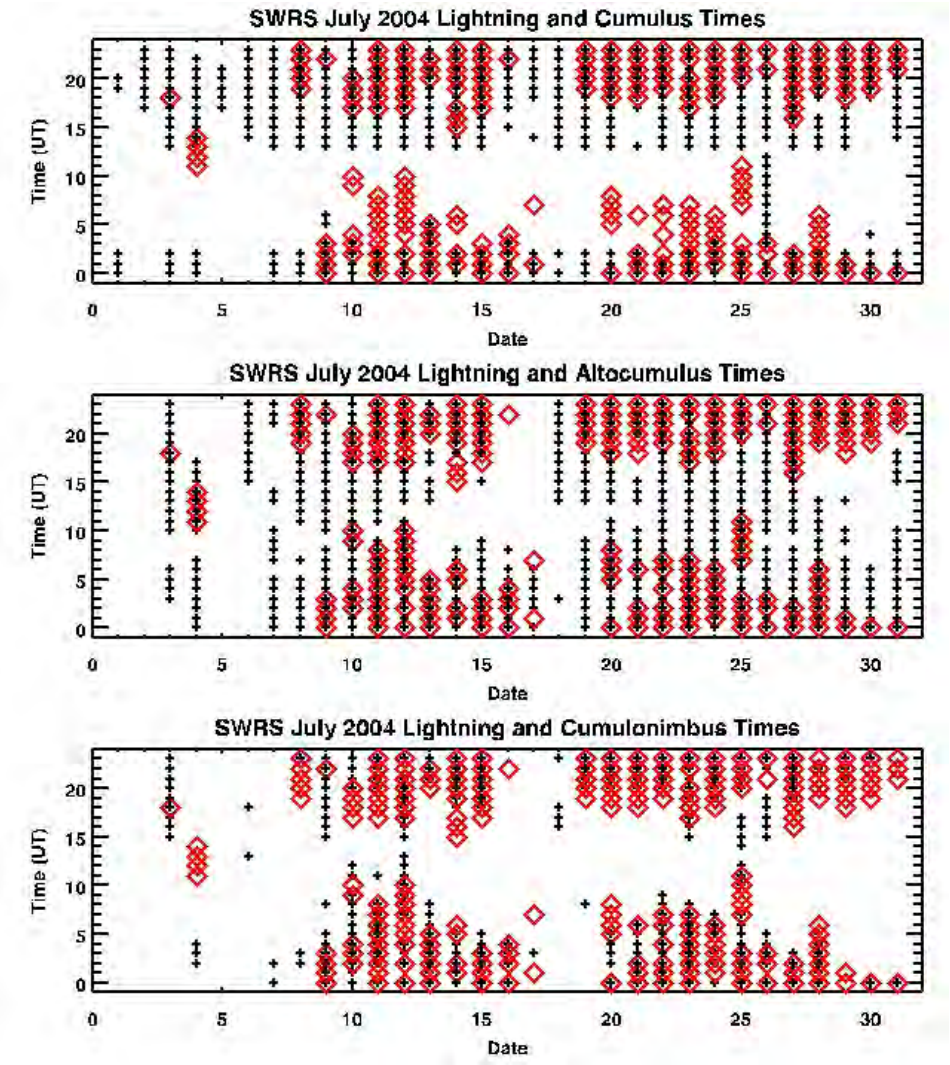

Figure 1-3. July 2004 dates and hours (UT) that convective clouds (black +) and lightning (red diamonds) were observed within 100 km of SWRS. Local time is UT minus 7 hours.

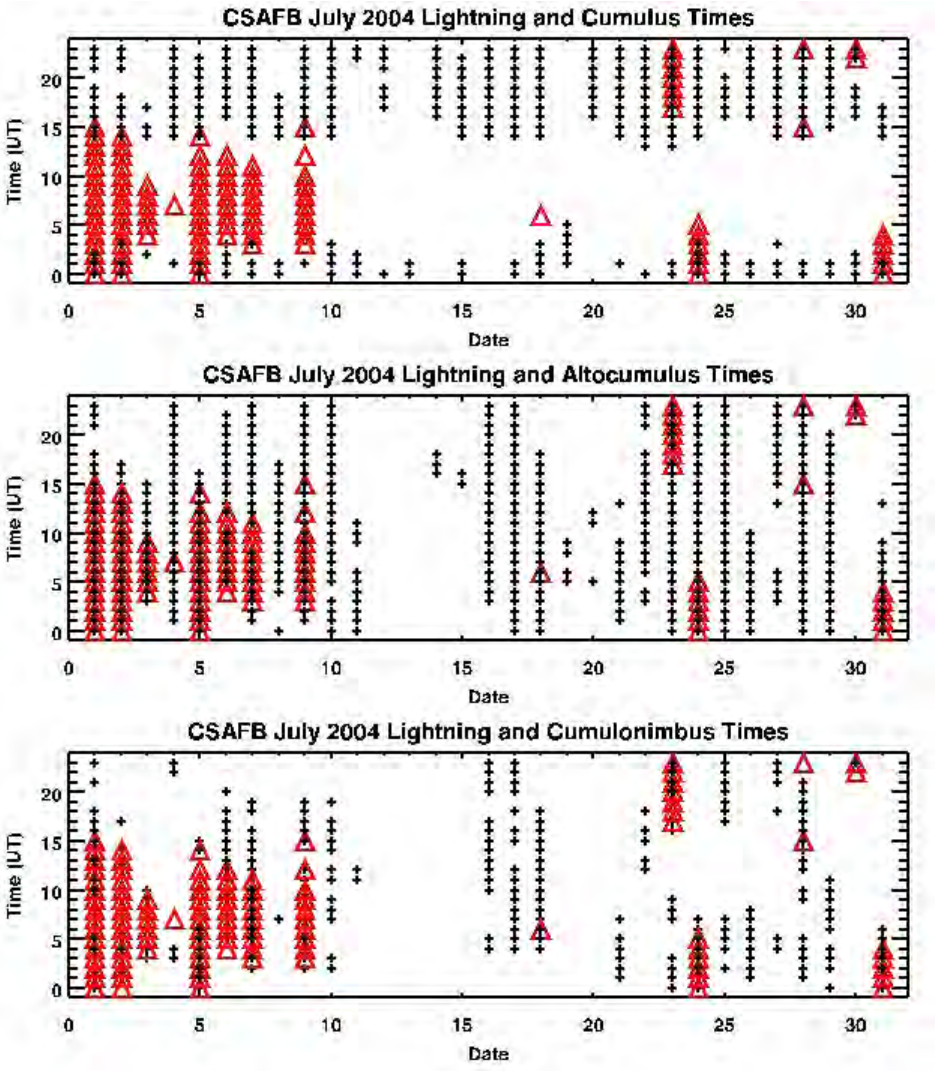

Figure 1-4. July 2004 dates and hours (UT) that convective clouds (black +) and lightning (red triangles) were observed within 100 km of CSAFB. Local time is UT minus 6 hours.

1.9.6 Cloud Temperature-Based LLCC

Some of the cloud-based LLCC are based on cloud microphysical properties. Cloud electrification peaks where water and ice are both present, around –10ºC. Existing cloud-based LLCC also specify that the flight path must not come within 0, 5, or 10 nautical miles of cumulus clouds with cloud tops higher than the –5ºC, –10ºC, and –20ºC isotherms, respectively. Since this required knowledge of the heights of the isotherms at specific times and places and CDFS2 does not give cloud temperature information, incorporation of a third database was required. The European Center for Medium Range Forecasting (ECMWF) global analysis model grid was used.

The data at the tiles containing CSAFB and the proposed SWRS were vertically interpolated to obtain the isotherm geopotential heights for 5ºC, –5ºC, –10ºC, and –20ºC (red, green, aqua, blue lines) (Figures 1-5 and 1-6).

Where the surface temperature is colder than 5ºC, the 5ºC isotherm line (shown in red) is set at 0. The terrain elevation of CSAFB grid tile is 590 m. Terrain elevation at SWRS grid tile is 1534 m. This is an average over the entire tile and not the actual elevation at the site. In general, wintertime surface temperatures are lower at CSAFB than at SWRS.

Comparison of the July 1999 and 2004 data show that the cumulus (and possibly also the altocumulus) cloud tops at the proposed SWRS reach the –10ºC, and –20ºC isotherm altitudes more frequently than those at CSAFB. This increases the chances of violating the LLCC dependent on cloud top temperatures. There were no noticeable differences for cumulonimbus cloud top temperatures.

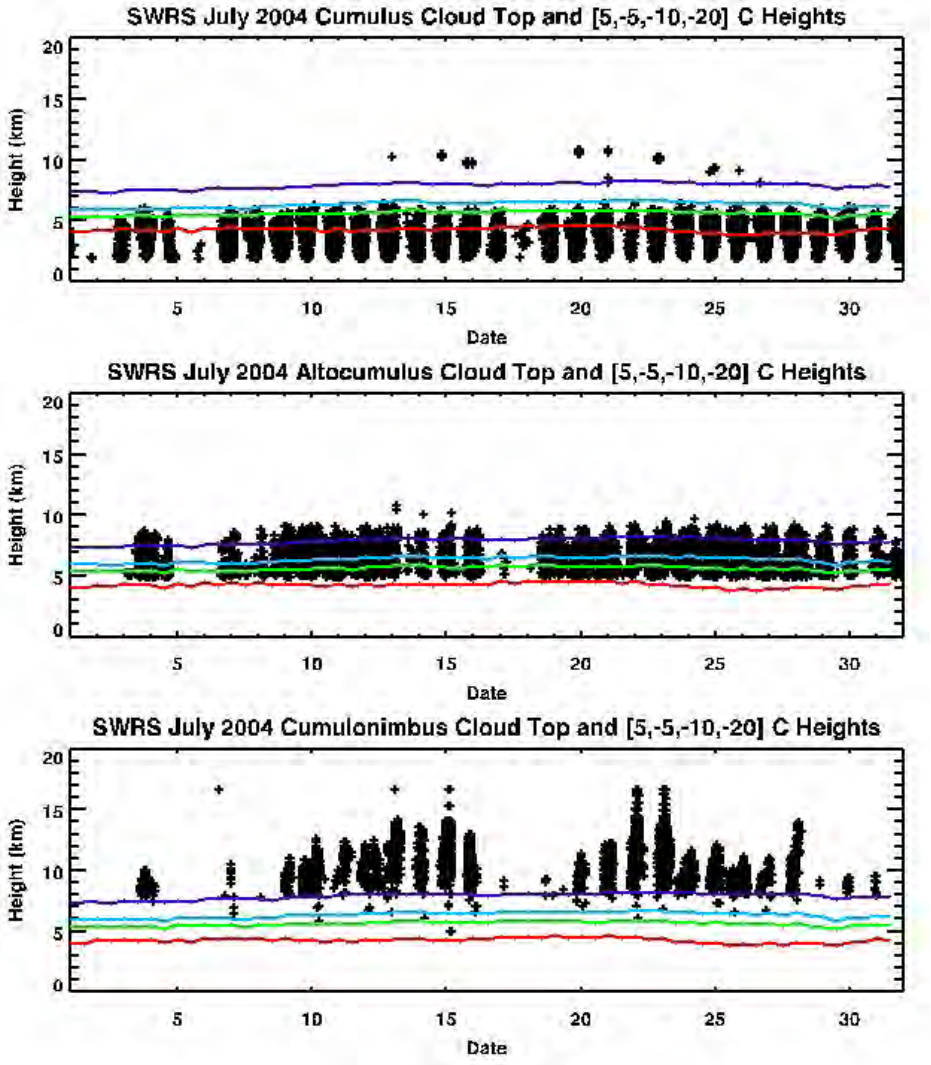

Figure 1-5. Cloud top heights for selected cloud types are shown in black (+). Isotherm heights for 5, –5, –10, and –20ºC are shown in red, green, aqua, and blue, respectively.

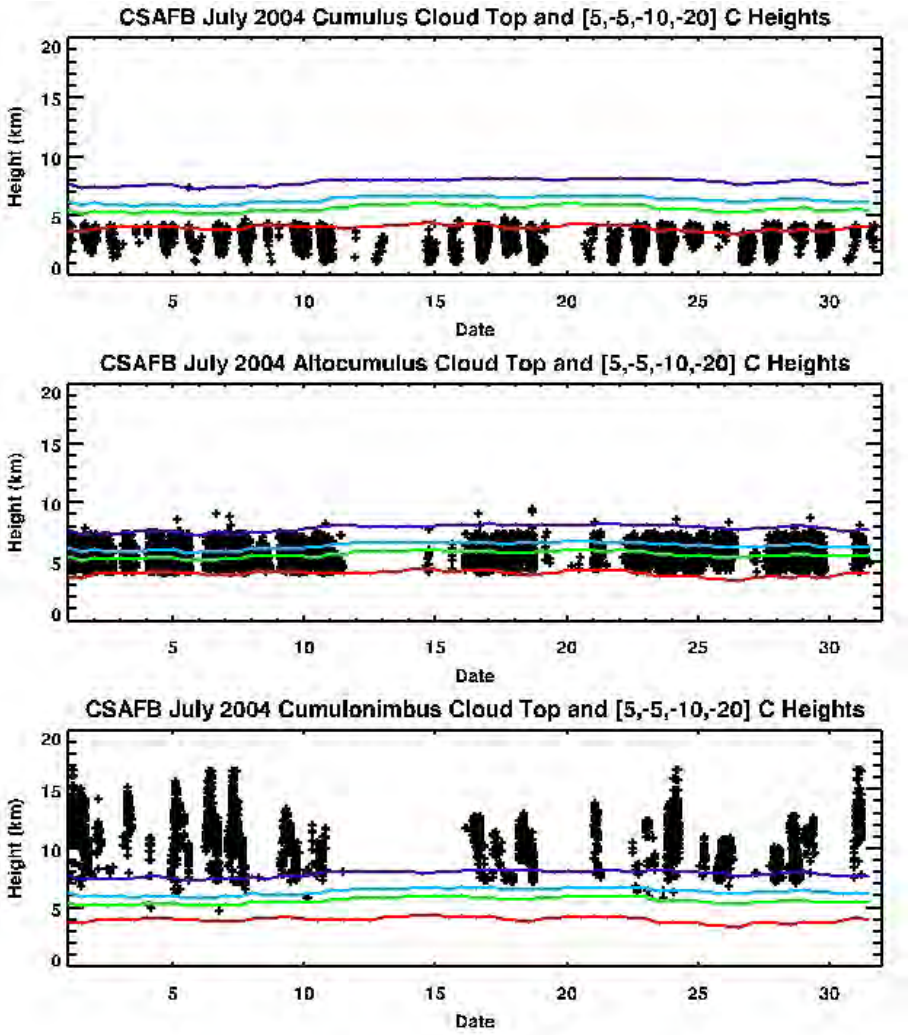

Figure 1-6. Cloud top heights for selected cloud types are shown in black (+). Isotherm heights for 5, –5, –10, and –20°C are shown in red, green, aqua, and blue, respectively.

1.9.7 Climatology Summary

A nearly 15-year climatology study of naturally occurring cloud-to-ground lightning strikes showed that the proposed SWRS experiences significantly more lightning strikes overall than CSAFB. However, year-to-year variability is high, and cloud-to-ground data from July 2004 indicated twice the amount of lightning strikes at the proposed OS than at the proposed SWRS.

The proposed launch sites at OS and SWRS are more than 20% likely to experience lightning for seasons spanning 120 and 90 days a year, respectively. The main lightning season begins at the end of May and lasts through early September in Oklahoma. In New Mexico, it begins in mid-June and lasts until early October.

A more detailed discussion with numerous additional graphs is presented in Section 3.3.

2. Background

2.1 Historical Lightning Strike Incidents

2.1.1 Aircraft Strikes/Damage

Figure 2-1 shows two frames from a Japanese video of an aircraft taking off from the Kamatzu Air Force Base on the coast of the Sea of Japan during the winter. The lightning is obviously triggered, since it is branched both upward and downward away from the aircraft, indicating the direction of propagation. Such events are usually unexpected, especially as they often occur in clouds that are not producing natural lightning. If they occur near the ground, they are likely to include the multiple return strokes that are typical of cloud-to-ground lightning, as happened in this case, making them particularly destructive. There is no known remote-sensing technique that is capable of reliably detecting this hazard.

2.1.2 Apollo 12 Incident and Motivation for LLCC

Apollo 12 and Atlas-Centaur 67 were the only two U.S. missions ever struck by lightning. In each case, the presence of the launch vehicle in an elevated atmospheric electric field is thought to have triggered the lightning.

Apollo 12 was launched on November 14, 1969, from Kennedy Space Center in Florida. Major electrical disturbances, subsequently attributed to vehicle-triggered lightning, were observed at 36.5 and 52 seconds into the mission. Nine nonessential sensors with solid-state circuits were permanently damaged. Temporary upsets included loss of communication, flashing and sounding of various warning lights and alarms, disconnection of three fuel cells from the power bus, loss of attitude reference by the inertial platform, and disturbances to the timing system, clocks, and other instruments. The mission was able to continue.

At launch, a cold front was passing through the area. Tops of isolated cumulus congestus clouds within a range of 48 kilometers reached a maximum of 7 kilometers. In the vicinity of the launch complex, clouds were reported at altitudes between 240 and 455 meters, with overcast between 600 and 3030 meters. The freezing level was near 3758 meters. No other lightning was reported in the area six hours prior to or after launch.

The vehicle apparently triggered a lightning discharge to ground at 36.5 seconds, when it was at about 1940 meters, and then triggered an intracloud discharge at 52 seconds, when it was at about 4364 meters. In the 20 minutes prior to launch, radioactive electric field probes indicated that the electric field at the launch site was rapidly varying. However, no calibration of the probes was available.

2.1.3 Atlas-Centaur 67 Incident; Origin of Current LLCC

The Atlas-Centaur 67 rocket, carrying the FltSatCom (Fleet Satellite Communications) satellite, was launched on March 26, 1987, from Cape Canaveral. Weather conditions were similar to those at the time of the Apollo 12 launch. A broad cloud mass covered most of Florida and the Gulf of Mexico, and a nearly stationary cold front extended across northern Florida in a southwest-northeast orientation well north of Cape Canaveral.

A squall line, also oriented southwest-northeast, was centered over the eastern Gulf, moving eastward over Florida. It produced substantial amounts of cloud-to-ground lightning activity throughout the day, but most of this activity was well west of the Cape.

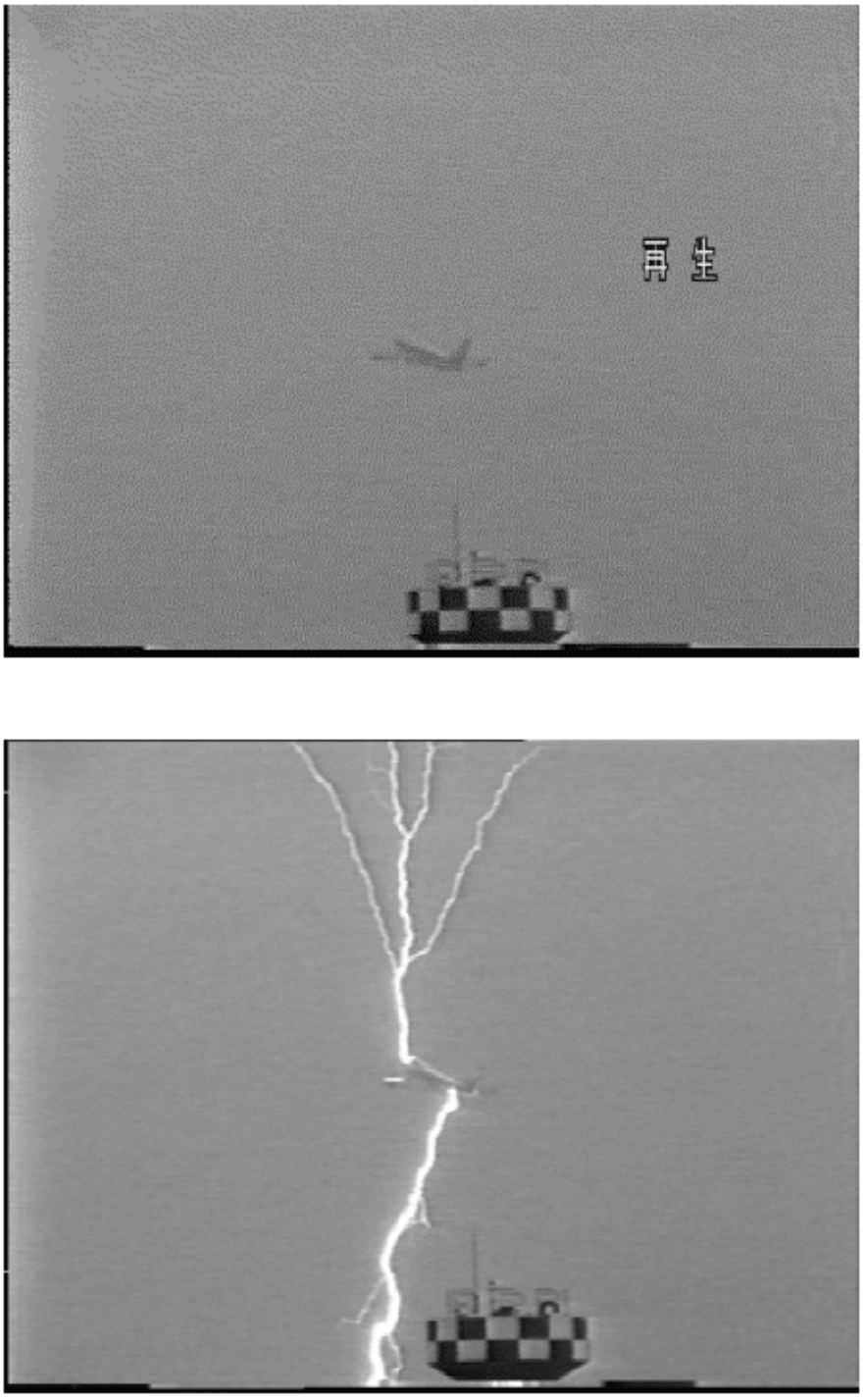

Figure 2-1. Lightning strike on airplane.
[Photograph reprinted with permission of Professor Zen I. Kawasaki, Osaka University]

At the launch site heavy rain fell, and layered clouds were reported at an altitude between 2424 and 6061 meters. No cloud-to-ground lightning was observed within 9 kilometers of the launch site in the 42 minutes prior to launch, and only one strike occurred within 18.5 kilometers during this time. At launch, the intensity of the electric field at the field mill site closest to the launch site was –7.8 kilovolts per meter.

At 49 seconds after launch, when the vehicle's altitude was about 3636 meters, a lightning flash was observed. That flash produced at least four strokes to ground as recorded by television cameras. At the time of the strike, the air temperature at the vehicle altitude was 4 degrees Celsius. The freezing altitude was 4242 meters. The vehicle was inside a cloud with a radar echo level of 10 dBZ (radar reflectivity units), far below the value of 40 dBZ generally associated with strong electrification in a thunderstorm.

After the incident, examination of the ground-based electric field mill records indicated that a small cloud discharge probably occurred in the vicinity of the launch pad about two minutes before launch. Members of the press also reported seeing a cloud discharge at about that time.

The lightning strike caused a memory upset in the vehicle guidance system; the upset then caused the vehicle to commence an unplanned yaw rotation. The stresses associated with this motion caused the vehicle to begin breaking apart. Approximately 40 percent of the telemetry outputs showed anomalous electrical behavior at the time of the event. About 70 seconds after liftoff the Range Safety Officer ordered the vehicle destroyed. Substantial portions of the payload fairing were subsequently recovered from the Atlantic Ocean, and these pieces showed physical evidence of being struck by lightning.

2.2 The Problems

2.2.1 Natural-Lightning Hazards to Aircraft

A search on the Internet was made for several pertinent topics. The first was for lightning information on composite aircraft. It was found that seven small, composite aircraft have been or are being certified for lightning protection. They are the Beech Aircraft Starship 2000, the Cirrus SR-20 and SR-22, the Diamond DA20 Katana and DA40, the Eagle Aircraft 150B, and the Lancair Columbia 300. A search of the individual Web sites showed that each prominently advertised a "lightning protection system" but gave no details.

A section of the Code of Federal Regulations (CFR), 14 CFR part 25.581, covers lightning protection. Subsection (c) states that "for nonmetallic components, compliance with paragraph (a) of this section may be shown by (1) designing the components to minimize the effect of a strike; or (2) incorporating acceptable means of diverting the resulting lightning current so as not to endanger the airplane."

Aircraft made of advanced composite materials, which are much less conductive than aluminum, are made with an embedded layer of conductive fibers or screens designed to carry lightning currents. It is important that we determine if such embedded layers are used in the RLVs. If not it will dramatically affect their interaction with the atmospheric electric field.

The second search was for lightning hazards to aircraft in general. A comprehensive review article was found: [M. A. Uman and V. A. Rakov, 2003]. In this they summarize data that shows that the bulk of the electric field strikes to aircraft occur at altitudes between 1 and 7 km. They state that triggering occurs "in an ambient electric field typically near 50 kV/m..." and that "the aircraft

extremities provide the region of high electric field needed to initiate a lightning discharge by enhancing the ambient electric field to breakdown values, 3×10^3 kV/m near sea level and about half that value at 6 km altitude." We used these values as initial guides and 'sanity' checks for our study. It was our intent to determine the breakdown values for each RLV concept and from that, determine the ambient field needed for breakdown.

2.2.2 Triggered Lightning

At least 80–90% of all lightning strikes to flying aircraft and spacecraft are "triggered," in the sense that they are locally initiated by the penetration of a large conductor into a sufficiently large region of high-intensity ambient electrostatic field. This fact was first conclusively demonstrated by Mazur et al. [1984], who used an ultra-high-frequency (UHF) radar to document the initial spatial development of lightning discharges *away from* an instrumented F-106 aircraft when it was struck. Recordings of currents and electric-field changes on board other aircraft have been interpreted to indicate that such triggered strikes invariably begin with a positive "leader" propagating away from an extremity on which positive charge had been induced by the ambient field, followed after a few milliseconds by the development of a negative leader from a negatively charged extremity, propagating in the opposite direction [Boulay et al., 1988; Mazur, 1989b]. (Here the term "leader" denotes a highly ionized, conducting, filamentary channel extending into virgin air. The term "positive streamer," in contrast, will always refer to the poorly conducting "corona" space-charge waves [e.g., Dawson and Winn, 1965; Phelps and Griffiths, 1976] that are an important component of the advancing "head" of a positive leader.)

A small percentage of aircraft strikes appear to result from the chance interception of naturally occurring lightning flashes; perhaps some are triggered by large ambient-field changes that were produced by nearby natural lightning. These events need not concern us here, however, because they can easily be prevented by avoiding any clouds that are producing natural lightning (see Sections 2.3.2.2 and 3.2.2). Triggered lightning represents a severe hazard precisely because it often occurs in clouds that produce little or no natural lightning.

Detailed study of the triggering phenomenon (as well as other important aspects of lightning) has been facilitated by rocket-triggering technology. "Classical" rocket-triggered lightning [St. Privat D'Allier Group, 1985] is initiated by a small rocket towing a grounded wire aloft under a thunderstorm. This technique was pioneered by Newman et al. [1958, 1967]. The key to its success is likely an observation by Brook et al. [1961] that the sufficiently rapid introduction of a grounded conductor into a high-field region might actually initiate the discharge. It is now well established that this type of lightning normally begins with a positive leader propagating upward from the tip of the triggering wire toward a negatively charged cloud. Apparently identical positive leaders have been shown to initiate "altitude" triggered lightning [Laroche et al., 1989b], which is produced by a similar rocket towing an ungrounded wire aloft and appears to constitute a good analog for triggering by aircraft and spacecraft, and most "upward-initiated" discharges to towers [Uman, 1987, Chapter 12]. (The onset conditions for the latter are somewhat different from those for rocket-, aircraft-, and spacecraft-triggered lightning, however, because a fixed tower tends to be surrounded by considerable corona space charge, inhibiting leader formation, most of which is blown away by the rapid motion of flying vehicles.)

Although the positive leader itself probably does not constitute a serious threat to a flying vehicle, the negative leader may, and their subsequent development into a discharge several kilometers in length usually results in large currents and current derivatives that can cause both direct and indirect damage (see Section 2.2.1). Since the positive leader is believed to constitute the initial stage of all triggered

strikes to such vehicles, however, it (and especially the conditions for its formation and continued propagation) is an important subject of study in its own right.

Considerable information is available on the phenomenology of rocket-triggered positive leaders, including currents measured at the base of the triggering wires and electric-field changes at the ground produced by these currents [e.g., Laroche et al., 1988; Lalande et al., 1998], and propagation velocities and other interesting optical characteristics [Idone, 1992; Idone and Orville, 1988]. Very briefly, during their first few hundred meters of propagation such leaders have average currents of a few amperes, normally exhibit pulsing with peak currents of several tens of amperes, and propagate at speeds ranging from a few times 10^4 to a few times 10^5 m/s. Unfortunately, the conditions required to initiate a viable positive leader, especially from a spacecraft producing a significant exhaust plume, are not sufficiently understood.

2.2.2.1 Qualitative Discussion of Conditions for Triggered Lightning

The initiation and continued propagation of positive leaders from conducting objects has been studied in detail in the laboratory, using sparks up to tens of meters in length, but to a much lesser extent on the scale of lightning discharges in the free atmosphere [e.g., Bazelyan and Raizer, 1998, 2000]. Material relevant to the triggering conditions will be summarized here, and more details can be found in later sections. (See especially Sections 2.2.3 and 3.1.2.)

Basically, there are three conditions that must be satisfied in order to initiate and propagate a positive leader. First, "breakdown" must occur in a small volume of air near the surface of the object in question, in order to produce free electrons in sufficient quantities to carry an electric current. At normal temperatures and pressures this means that the local electric field must reach a value near 3.0 MV/m, and when this occurs a phenomenon called "glow corona" is produced. Second, the current in the corona region must be amplified to the point where "streamers" occur. Positive streamers propagate outward from the breakdown region, further heating a small volume that is called the "stem," and the stem is where the positive-leader channel begins. Third, the *ambient* field must be large enough over a sufficiently large volume of space that the positive leader, once it has been initiated, will continue to grow and propagate (i.e., the potential at its tip will remain large enough relative to the local ambient potential to sustain propagation). This last condition is what we will refer to as "leader viability."

The breakdown (first) condition can be computed relatively easily once the geometry of the conducting object and its orientation relative to the ambient electrostatic field are known. If the conductor is uncharged, a geometrical "enhancement factor" can be computed and used to estimate the maximum field that will be present on the surface of the object simply by multiplying the ambient field intensity by this factor. The enhancement increases with the length of the conducting object (in the direction of the ambient field) and with the inverse of local radius of curvature of the object's extremities. If the conductor carries a net charge, there will be another contribution to the field on the surface due to this charge (which can also be computed fairly easily), and this must be added to the enhanced ambient field. However, since the magnitude of the charge on the vehicle is usually not known, and since this charge can change rapidly as a result of particle impaction and/or corona discharges from the object, the determination of breakdown conditions is problematic. Nevertheless, the geometric enhancement factor remains the most familiar tool for estimating the risk of triggering lightning by airborne vehicles. (Perhaps this is because the same mathematical approach is often used to define the various "zones" of lightning attachment to aircraft surfaces.)

The leader-initiation (second) condition can be approximately summarized by the requirement that the potential difference between the object its environment (i.e., the potential due to the ambient field) exceeds about 400 kV at standard conditions. If the object is uncharged and generally symmetrical with respect to the direction of the ambient field, then this condition will be met whenever the length of the object in the direction of the field, multiplied by the magnitude of the field, exceeds about 800 kV. In this case, we can say the positive and negative extremities of the object each "span" a potential difference of 400 kV. (Of course, no leader can be initiated unless the initial breakdown condition is also satisfied.)

The "leader-viability" (third) condition is conceptually more complex but is probably the most important condition in practice. When a sufficiently long and thin conductor is exposed to a high electric field at normal temperatures and pressures (e.g., the wire in classical rocket-triggering lightning), air breakdown always occurs before a positive-leader is initiated, and this in turn precedes positive-leader viability. For example, in rocket-triggered lightning, there are always indications of both air breakdown and leader initiation — the "precursors" described in Section 2.2.3 — before the triggered lightning flash begins. In this case, the enhancement factor is actually irrelevant, since it is a much less stringent condition than the one for leader viability.

It is worth asking, "How long and thin are the RLVs of interest in our case?" The answer to this question can be estimated roughly as follows: Bazelyan and Raizer [2000, p. 54] give an approximate formula for the geometrical field enhancement at the tips of an uncharged, cylindrical rod of length, H, with hemispherical tips of radius, r_0. (This formula is accurate for such a rod when the factor, H/r_0, is in the range, 10 to 50. It is, however, a rather crude approximation for the complex, three-dimensional structure of an RLV.) In Section 3.1.2 we review two recent models of leader viability and adopt the model of Bazelyan and Raizer [2000, Section 4.1.1] for use throughout this report. Anticipating a result from that section, we require the *enhanced* field to equal the breakdown value in the same *ambient* field that is required for leader viability (Equation 4 in Section 3.1.2.1), and we solve for the tip radius. This approach yields a curvature radius, $r_0 \approx 0.093\ H^{2/5}$, at which both the breakdown and the leader-viability conditions are satisfied simultaneously. (For all smaller values of r_0, the object is effectively long and thin, in the sense that breakdown will occur in smaller ambient fields than the threshold for leader viability.)

Using the above criterion, the concept RLVs considered in this report turn out *not* to be long and thin. In the case of a space vehicle during boost phase, the electrical effective length, H in the above formula, equals $(D + L)/2$, where D is the length of the vehicle itself and L is the length of the conducting portion of its exhaust plume, as discussed in Section 3.1.5.5. Looking ahead to vehicle data reported in Section 3, and taking numbers for the actual nose radii of curvature from Table 3-2 and for D and L from Table 3-4 in the two extreme cases, we find that the "Concept 5" vehicle — the shortest — has a nose radius of 91 cm, whereas the radius required for breakdown in the same ambient field as for leader viability is only about 30 cm. For the "Concept 2" vehicle — the longest — the nose radius of curvature is 52 cm, whereas the "breakeven" radius is only about 41 cm. (By way of comparison, the "breakeven" radius for Titan would be about 50 cm, using a slightly different approximation for the enhancement factor that is more appropriate for long, thin vehicles.) Thus with the above criterion, it would appear that triggering a positive leader is controlled by the breakdown condition and that it is the leader-viability condition that is irrelevant.

In spite of the above, we remain profoundly skeptical of using just the nose radii and the electric field enhancement factors to estimate the leader-triggering conditions, even for these relatively small RLVs. First, there are almost certainly small-scale features on the vehicles (e.g., wingtips, pitot tubes, radio antennae, and other protrusions) that have much smaller radii of curvature than the nose.

Second, there are likely to be imperfections in implementing the theoretical design that have even smaller local radii of curvature. Third, any flights inside clouds will involve impactions of ice and/or water particles that will certainly produce very small radii of curvature for a brief instant. Fourth, during conditions of particle impact, and perhaps even because of the action of the rocket engines themselves, these vehicles will likely be highly charged, and any such charging can produce breakdown and corona discharges from extremities of the vehicle surfaces. The latter point is supported by many observations of aircraft going into corona while flying in clouds that are not electrified. For example, Thomas et al. [2004, Fig. 13] have used a lightning-mapping system to track the corona discharges produced by a commercial aircraft flying through a cirrus cloud. Similarly, when the Space Shuttle has flown through cirrus during landings at the NASA Kennedy Space Center, it has been tracked by a similar lightning-mapping system [Frank Merceret, private communication, October 2005]. For all of the above reasons, we will assume that the leader-viability criterion is a more reliable criterion (and also the safer one in the present context) than the simple enhancement-factor approach.

2.2.3 Results of a Key Field Experiment

From first principles [e.g., Smythe, 1968, Sections 2.19 and 3.11], it is evident that the energy that drives all lightning discharges is extracted from the ambient electrostatic field. Therefore, one would like to know the ambient-field intensity, and its spatial distribution, associated with both unsuccessful and successful triggering attempts. Unfortunately, it is well known that surface-based measurements can be "screened" from more intense fields aloft by a layer of corona-produced space charge [e.g., Standler and Winn, 1979]. There are few *in situ* measurements aloft from which to determine the necessary or sufficient conditions for propagation of positive leaders or with which to explain variations in their behavior. Therefore, Willett et al. [1999] conducted a major field experiment in Florida during the summer of 1996.

The objective of this experiment was, in effect, to extend experimental work on long laboratory sparks from tens-of-meter to kilometer-length scales. When conditions appeared favorable for rocket-triggered lightning, a special sounding rocket was launched to profile the vector ambient electrostatic field through the lowest few kilometers of the atmosphere. The sounding rocket was followed a few seconds later by a classical triggering rocket, and the currents and field changes of any positive leaders so initiated were recorded. For present purposes, the field profiles and the heights at which triggered lightning flashes were initiated are of primary interest. A summary of the data is presented here.

Figure 2-2 shows the lower part of all nine measured ambient-field profiles. Here, the magnitude of the vector field is plotted as a function of height from the surface to 500 m altitude. Note that the field increases rapidly with height near the ground (due to the corona-space-charge layer) and then becomes relatively uniform over the height range in which triggering occurred (230–447 m in this experiment). As the triggering rocket ascended in this environment, brief leader-like discharges ("precursors") began at heights of 102–213 m, but successful positive leaders were not initiated until 164 ±38 m higher (mean ± standard deviation), where the magnitude of the ambient field was only 2.9 ±1.2 kV/m greater. Nevertheless, the magnitude of the ambient potential difference between ground and the triggering altitude (obtained by line integration of the vector field along the sounding-rocket trajectory) was 2.4 ±0.4 MV (2.5 times, on average) larger than that at the precursor-initiation height. (Note that this difference between the occurrence of precursor discharges and the onset of a viable leader exemplifies the well known fact that breakdown fields, or even bursts of positive streamers, at the wire tip are not sufficient to trigger lightning.) Thus it appears that the leader may have been waiting, not for the triggering rocket to fly into a region of higher ambient field, but for the

triggering wire to “span” a threshold potential difference. More details can be found in Figures 2-3 and 2-4, as discussed below.

A significant shortcoming of the present data set is that the range of ambient field magnitudes aloft that were encountered during the experiment is relatively narrow — less than a factor of two — and similar for the range of triggering heights. This makes it difficult to determine from scatter plots like those in Figure 2-4 whether the ambient field intensity, the potential spanned by the wire, or some other property of the field profile is actually the condition for triggering. For the same reason it is also difficult to use this data alone for model validation (see Section 3.1.2).

A loose, quasi-theoretical argument for a threshold potential difference can be given as follows: Laboratory measurements show that direct-current (DC) arc discharges with currents comparable to those observed in rocket-triggered lightning by Willett et al. [1999] and others have longitudinal potential gradients of a few kilovolts per meter of channel length [e.g., King, 1961]. Thus, one might expect a leader to propagate indefinitely in fields of that magnitude at standard conditions. Nevertheless, a discharge channel takes time and heating to develop to the point where its conductivity can be maintained by thermal ionization, as in an arc. Calculations of electrostatic conditions on thin, prolate, conducting ellipsoids in a uniform field show that significant field enhancements do not extend more than a small percentage of the total length of the ellipsoid beyond its tip. (The dependence on axis ratio is very weak.) Thus, a competition may exist between the ambient field intensity and the dimensions of the enhanced-field region, on the one hand, and the time and energy that are required to create a “thermalized” channel that can become self-propagating, on the other. The playing field can be tilted in favor of a successful leader either by lengthening the conductor or by increasing the ambient field intensity, in either case increasing the total potential difference that is spanned by the conductor.

Willett et al. [1999] have tabulated two different threshold potential differences, (A) that for precursor onset (see Figure 2-3) and (B) that for initiating a viable leader (see Figure 2-4). (The green traces on each graph represent the corresponding regression lines.) The former can be considered to define the conditions that are safe, i.e., viable leaders do not form when the triggering wire spans only 1.6 ±0.3 MV. The latter defines the conditions in which triggered lightning will likely occur, i.e., 4.0 ±0.5 MV.

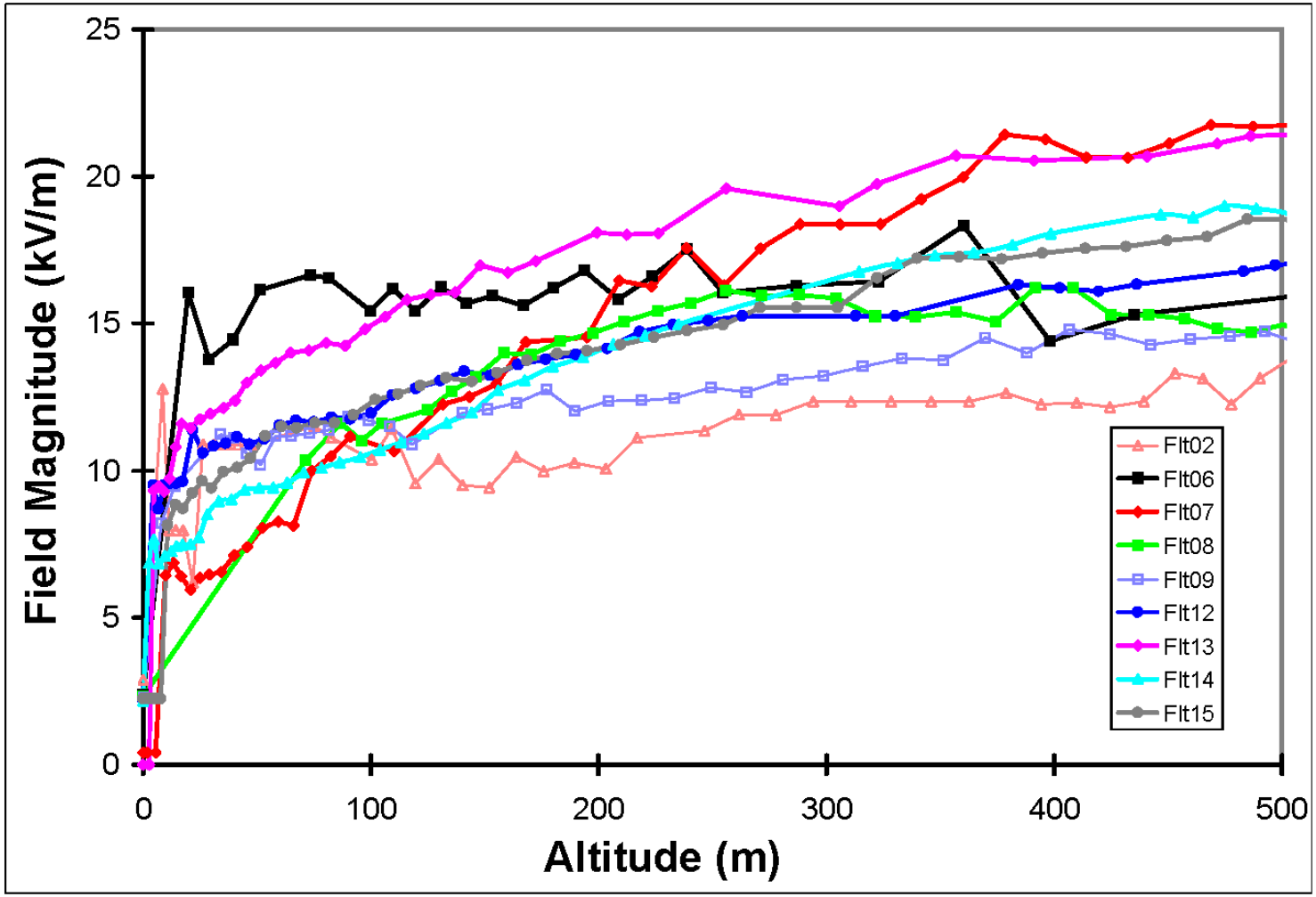

Figure 2-2. Profiles of ambient-field magnitude from Willett et al. [1999]

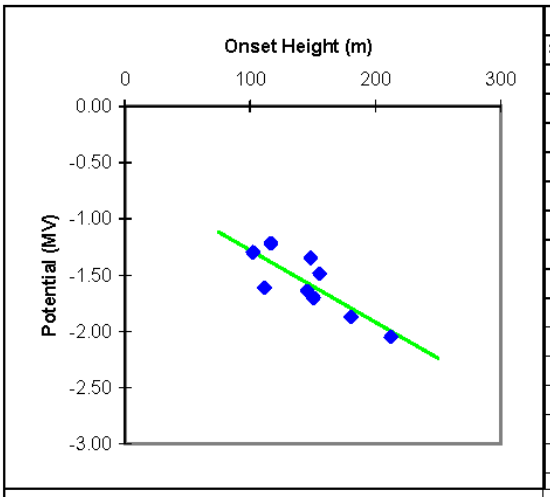

Flight #	Onst.Alt., (m)	V(h) (MV)	Emag(h) (kV/m)	"-V(h)/h" (kV/m)
2	213	-2.05	10.7	9.6
5	116	-1.22	12.9	10.5
6	112	-1.61	15.8	14.4
7	156	-1.49	13.3	9.6
8	148	-1.35	13.3	9.1
12	146	-1.64	13.3	11.3
13	102	-1.30	15.0	12.7
14	181	-1.87	13.5	10.3
15	151	-1.70	13.3	11.3
Prec. Alt. based on model trajectory				

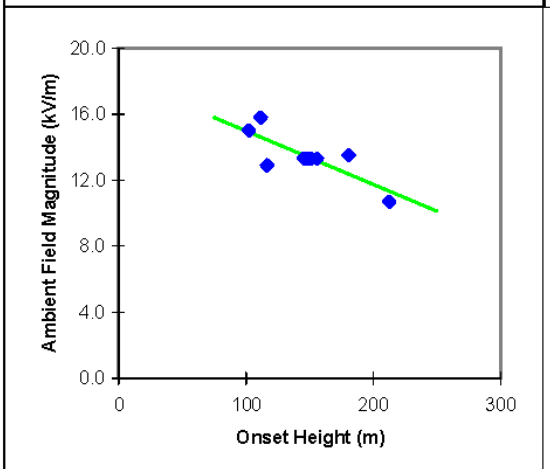

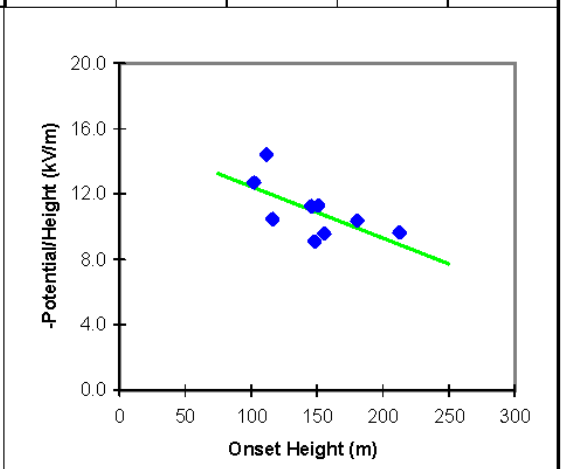

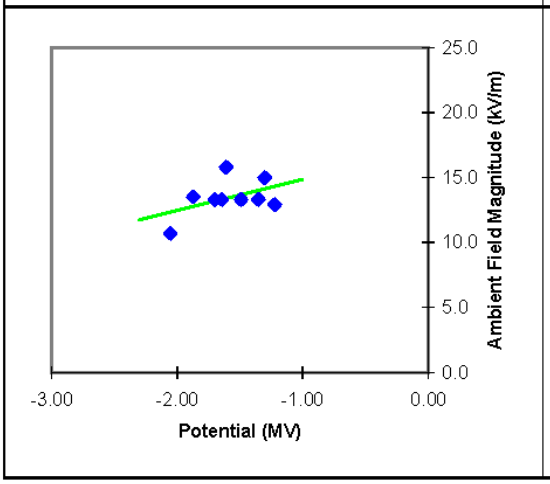

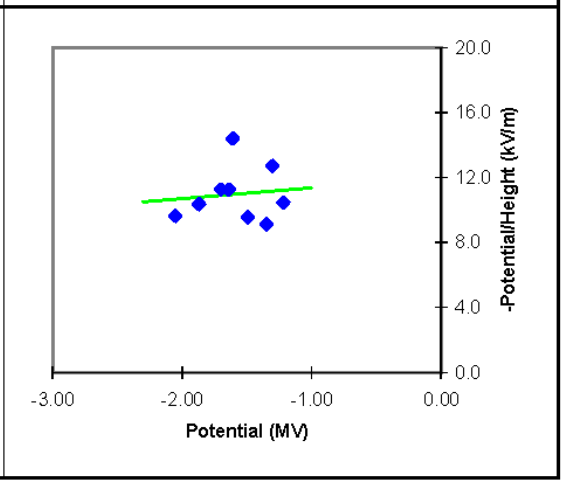

Figure 2-3. Precursor-onset conditions from Willett et al. [1999]. Note that the electric field has been plotted in two different ways: On the left side, the magnitude of the vector field at the triggering height is used. On the right is the average field between the surface and the triggering height, which is slightly smaller because the field increases with height.

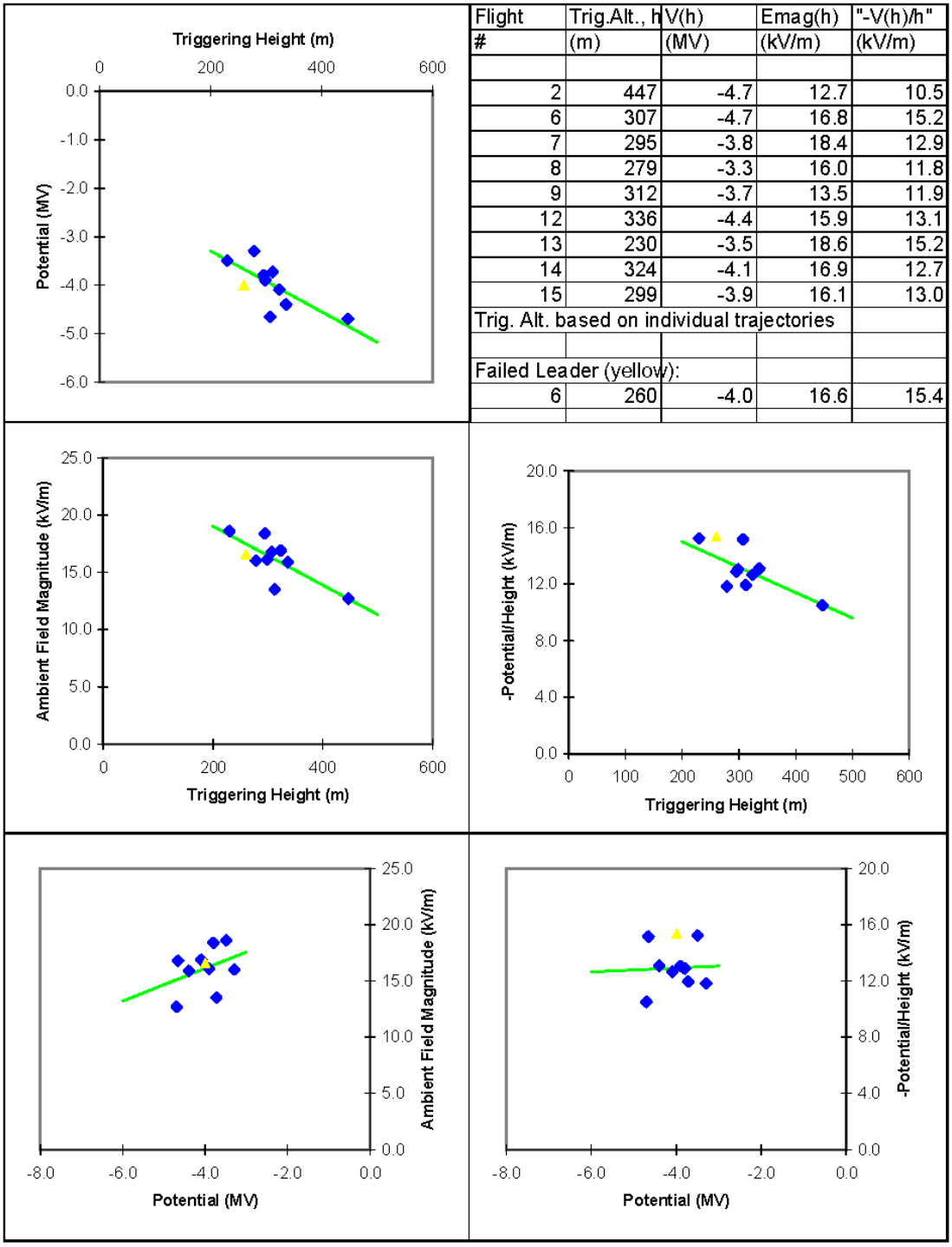

Flight #	Trig.Alt., h (m)	V(h) (MV)	Emag(h) (kV/m)	"-V(h)/h" (kV/m)
2	447	-4.7	12.7	10.5
6	307	-4.7	16.8	15.2
7	295	-3.8	18.4	12.9
8	279	-3.3	16.0	11.8
9	312	-3.7	13.5	11.9
12	336	-4.4	15.9	13.1
13	230	-3.5	18.6	15.2
14	324	-4.1	16.9	12.7
15	299	-3.9	16.1	13.0
Trig. Alt. based on individual trajectories				
Failed Leader (yellow):				
6	260	-4.0	16.6	15.4

Figure 2-4. Leader-onset conditions from Willett et al. [1999]. The yellow points represent a significant, but ultimately failed, leader that occurred in Flight 6, prior to onset of a viable leader. Otherwise as in Figure 2-3.

2.3 Possible Solutions

There are two obvious solutions to the problem of triggered lightning — hardening and avoidance. The former will not be considered in any detail here, as the resulting weight penalty is generally prohibitively expensive for all but military rockets. The latter is, of course, the main focus of the present study.

2.3.1 Lightning Hardening

All commercial passenger aircraft are required by the FAA to be "hardened" to withstand lightning strikes because such events cannot be entirely avoided. That this hardening has been successful is demonstrated by the fact that such aircraft are struck frequently (about once every 3000 flight hours) but generally sustain only minor damage. The main reason that serious damage or destruction are relatively rare is undoubtedly that passenger aircraft have traditionally been constructed almost entirely out of aluminum skin and structural elements, which are excellent conductors of electricity. Nevertheless, careful attention is given to electrical bonding among the various metal parts, to the use of adequate metal thickness over fuel tanks and in other sensitive areas, to the correct mounting and protection of electrical fixtures such as lights and antennae, and to numerous other details.

Composite materials are known to be highly vulnerable to physical damage by lightning ("direct effects") and also provide little or no shielding for internal electronic components against the associated electrical transients ("indirect effects"). Where such materials must be used for their lighter weight or transparency to electromagnetic waves, conducting foil or mesh, diverter strips, and other techniques have been developed to guide lightning currents harmlessly over the external surfaces.

Test standards and techniques are well developed to validate the various hardening technologies. Current test standards are outlined briefly by Rakov and Uman [2003, Section 10.5], and the whole subject of lightning protection for aircraft is described by Fisher et al. [1999]. Here we will assume that the weight penalties associated with vehicle hardening will not be acceptable for RLVs.

2.3.2 Lightning Avoidance

For vehicles that are not hardened, avoidance remains the only option. *In situ E* measurement [with an airborne field mill (ABFM) — see Sections 2.1.4 and 2.3.2.1.1] and/or cloud-based rules (like the existing LLCC — see Sections 2.1.5 and 3.2.2 — and the Space-Shuttle flight rules — not discussed herein) can enable RLVs to avoid situations in which strikes by triggered and/or natural lightning are likely. These two approaches to avoidance are further described in the following sections.

2.3.2.1 *In situ E* Measurements

In situ measurement of the ambient electrostatic field is undoubtedly the best way to determine whether certain types of clouds in and near the planned flight path pose a lightning hazard to any particular RLV. This is because most clouds do not give a clear indication to any known remote-sensing technique (e.g., morphology or radar reflectivity) of whether or not they are dangerously charged electrically. (Notable exceptions are cumulonimbus clouds and any clouds that are producing natural lightning, both of which must always be avoided. Developing cumuli should also be avoided because they are capable of becoming electrified very rapidly.)

Some types of clouds, such as "thick clouds" and "thunderstorm debris clouds" (as defined in the current LLCC), are statistically known to constitute a hazard in a relatively small percentage of cases.

Thus they should be avoided, in the absence of direct measurements, even though such avoidance will result in unnecessary launch delays and scrubs. In such cases an *in situ* measurement capability could virtually eliminate false alarms, maximizing launch availability, without compromising safety. Unfortunately, the only appropriate method of obtaining *in situ E* measurements is quite expensive and is both technically and operationally difficult, as briefly described in the next section.

2.3.2.1.1 Operational Platform for *In situ E* Measurements

The only acceptable electric-field-measurement platform for launch support is a high-performance aircraft (or perhaps a Remotely Piloted Vehicle — RPV) instrumented with five or more shutter-type field mills and fully calibrated as a system. This was the fundamental conclusion of a workshop organized by the U.S. Air Force after the Atlas/Centaur-67 disaster [Barnes and Metcalf, 1988]. Similar, though less detailed, recommendations were also made by The Aerospace Corporation [Lightning Review Committee, 1988] and the National Research Council [Panel on Meteorological Support for Space Operations, 1988].

Without going into detail on the subject here, the primary reasons for this specific recommendation are as follows: Polarimetric radars are the only remote-sensing tools that appear attractive for the purpose [e.g., Scott et al., 2001]. This is because of their ability to rapidly survey large volumes of cloud and because they have been shown capable of detecting the reorientation of ice crystals due to electric fields inside of highly electrified clouds. Unfortunately, this technique has never been calibrated quantitatively in terms of ambient electric-field intensity and, in any case, does not apply to clouds that lack a significant population of small, nonspherical ice crystals. Thus, an *in situ* measurement is essential. The electrical state of even stratiform clouds can change fairly rapidly. Therefore, a high-performance aircraft is required to permit the investigation of any potentially hazardous clouds along the planned flight path within minutes of the planned launch time. Five or more shutter-type mills are necessary to permit the redundant determination of all three components of the vector ambient field plus the charge (or potential) on the aircraft itself. Both the redundancy and the vehicle charge are helpful in assessing the accuracy of the ambient-field measurement. The full-system calibration (as opposed to just a calibration of each individual field mill) is probably the most difficult requirement to achieve. This calibration is necessary to separate the effects of the aircraft itself from those of the ambient field that is to be measured. Other key recommendations include a dedicated aircraft, a well trained flight crew and ground team, real-time data transmission to a ground station, and coordination with a meteorological radar for data interpretation and aircraft vectoring.

Such airborne measurement platforms, sometimes associated with ground controllers, have been operated in a research environment with varying degrees of success, but it must be emphasized that an operational ABFM system remains to be designed and implemented for launch support. As discussed in Section A.3, the French research organization, ONERA, instrumented both a CV-580 and a Transall aircraft to determine the ambient field immediately prior to direct lightning strikes during 1985 and 1988, respectively. Laroche et al. [1989] states that the former installation was calibrated by numerical solution of Laplace's equation on a mesh representation of the aircraft, whereas the latter was calibrated by laboratory measurements on a scale model. The Naval Research Laboratory installed a separate set of four field mills on the same CV-580 aircraft, obtaining their calibration from maneuvers in the fair-weather field as described by Bailey and Anderson [1987]. Somewhat more recently SRI International, in collaboration with Aeromet, Inc., installed a system of eight field mills on a Learjet 36A and calibrated it with the scale-model approach [Kositsky et al., 1991]. Most recently, an RPV has been instrumented with six field mills (among many other instruments) by the NASA Marshall Space Flight Center (MSFC) and the NASA Goddard Space Flight Center, calibrated

in the fair-weather field, and used to measure vector fields above thunderstorms [e.g., Farrell et al., 2003].

Of most relevance here were two implementations on high-performance aircraft by NASA/MSFC, the first on a NASA Langley Lear 28/29 that was flown from 1990 into 1992 ("ABFM I") [Fisher et al., 1992] and the second on a University of North Dakota Cessna Citation II that was flown from 2000 through 2001 in collaboration with the National Center for Atmospheric Research ("ABFM II") [e.g., Bateman et al., 2003]. These systems utilized five and six shutter mills, respectively, and were both calibrated by maneuvers in the fair-weather field, as variously described by J. C. Bailey, D. M. Mach, W. Koshak, and H. J. Christian [unpublished reports]. These implementations were particularly noteworthy because of their close coordination with radar through the use of ground stations that received the electric-field data and aircraft location via telemetry and so were able to overlay this information on a meteorological radar display in real time. Thus a ground-based "controller" was able efficiently to vector each aircraft through clouds of interest. They serve as good models for a potential operational system.

Important progress has been made in the theory and practice of instrumenting and calibrating an ABFM over the past two decades. It is now understood that space charge is always emitted by the aircraft itself in a high-field environment and that this space charge can render impossible the measurement of one or more components of the ambient field, especially if it passes close to one or more of the field mills [Jones et al., 1993]. It is also regarded as vital by many investigators that there be some way to verify the calibration and performance of the actual ABFM system in flight. This has led to the requirement for redundancy (five or more mills), to detect errors caused by emitted charge as well as other problems, and to the popularity of the fair-weather calibration procedure. (The fair-weather field is often uniform, vertically directed, and constant.) Nevertheless, fair-weather calibration places severe demands on the instrumentation, since the individual mills must accurately measure field intensities of only a few tens of V/m (magnitudes that would be trivial in most operational uses), and it is not as simple as it might appear [e.g., Bailey and Anderson, 1987].

Winn [1993] proposed a novel calibration method that addresses both of these problems. This method does not require systematic placement, nor even knowledge of the placement, of the individual mills on the aircraft, nor does it require knowledge of the ambient-field magnitude and direction. The only requirements are that the ambient field be constant in magnitude and direction during aircraft maneuvers and that the field at each mill be a linear combination of the three components of the vector ambient field and of the charge on the aircraft. One drawback of Winn's method is that it is unable to directly compute the aircraft charge (or potential), but this drawback is not as important as its advantages. Mo et al. [1998] have taken advantage of Winn's calibration method to instrument an aircraft with field mills in distinctly unconventional locations, where they are well away from the streams of space charge that are emitted in high fields by the aircraft. They have demonstrated in this way the ability to accurately measure ambient fields as large as 150 kV/m.

Further developments regarding the calibration of an ABFM have been published by Koshak et al. [1994], Mach and Koshak [2003], and Koshak et al. [2005], and more is expected from this group at NASA/MSFC in the near future.

2.3.2.1.2 Requirement for a Triggering Threshold

The use of an *in situ* measurement capability, such as outlined above, to reduce the false alarms that would otherwise be inherent in any cloud-based system of rules like the current LLCC requires a knowledge of the electric-field conditions that are necessary to trigger lightning with the space

vehicles in question. To this end, the electric-field magnitudes that constitute a hazard to our five concept RLVs are estimated in Section 3.1 below. The electric-field "threshold" for triggering lightning is vehicle, engine, altitude, and velocity dependent. More theoretical and experimental work is needed on all of these dependencies, although some estimates can be made with reasonable confidence.

2.3.2.2 Cloud-Based Rules

The existing LLCC are examples of cloud-based rules. Although they are believed to be very safe, they do produce false alarms that significantly reduce launch availability. Note that the most important of these rules, *whether or not an operational ABFM is used*, are (A) to avoid clouds that are producing any type of natural lightning and (B) to avoid cumulus clouds that may become electrified in just a few minutes and produce natural (or triggered) lightning. Note also that measurements of electric field with a Ground-Based Field-Mill system (GBFM, as opposed to an ABFM) are incorporated into certain of these LLCC, where they are important for both adding safety (detection of additional hazards) and providing some relief from the otherwise very conservative cloud-based rules. (It should be emphasized that a GBFM is no substitute for an ABFM. Even if the GBFM system has the necessary areal coverage for sensitivity to the clouds of interest, charge inside clouds aloft may be invisible to instruments on the ground because of screening layers on the surfaces of the clouds themselves.) The existing LLCC, proposed FAA Lightning Flight Commit Criteria (LFCC), and their rationales are discussed in Sections 3.2.2 and 3.2.3 below.

3. The Current Study

Here we review lightning avoidance by RLVs and specifically by the five concept vehicles that are described in Section 3.1.5 below. The existing literature on the measurement of *E* aloft in support of space launches has been reviewed above (see Section 2.3.2.1.1), leading to the conclusion that an ABFM is the only suitable tool. This addresses the fifth bullet in Section 1.0. In Section 3.1, the vehicles and their flight profiles are analyzed in an effort to quantify the expectation that they are less likely to trigger lightning than the larger expendable launch vehicles (e.g., Titan and Delta) and the Space Shuttle, for which the existing LLCC were developed. This is responsive to the second bullet in Section 1.0. Before any quantitative estimates can be made, however, we need to review the state of our present understanding of the triggering conditions (see Section 3.1.2 to 3.1.4 below). In Section 3.2 the existing LLCC are reviewed in order to determine their applicability to the proposed RLV concepts. This is responsive to the third bullet in Section 1.0. In Section 3.3, the climatology of the proposed inland launch sites for these RLVs is analyzed, both to determine the applicability of the existing LLCC and to identify the need for any additional rules specific to these sites. This is responsive to the first and fourth bullets in Section 1.0. Finally, in Section 3.4, we summarize what can be quantified at present about the risk of triggered lightning to these vehicles.

Two points should be noted about the proposed RLVs: A) Because they are physically smaller and have less powerful engines than ICBM-type boosters, it is to be expected that their lightning-triggering thresholds (expressed in terms of the ambient electric field, as described in Section 3.1.5.5) will be correspondingly higher. Given our present incomplete understanding of the physics of triggering and the difficulty of measuring or inferring the ambient fields aloft, however, it will be difficult to exploit this advantage. B) Because the suborbital RLVs (a) are piloted, hence not required to carry remote-destruct systems, (b) use relatively nontoxic fuels, (c) will operate in remote areas, and (d) are expected to require good visibility for the duration of their flights, the FAA might allow their operators more discretion than is given to the operators of large orbital boosters by the National Ranges.

3.1 Estimate Quantitative Triggering Conditions

3.1.1 Threshold Electric Environment for Triggering

The threshold electric environment for triggering is relevant primarily to an *in situ* measurement of *E* (see Section 2.3.2.1 above) and secondarily to the present, radar-based, anvil rules (see Sections 3.2.2 and 3.2.3). Application of these new rules to smaller vehicles (and presumably higher field thresholds) at mid-latitude, continental launch sites introduces the following two difficulties.

3.1.1.1 Radar vs. Field Relationship for Anvils

The radar vs. field relationship on which the anvil rules are based has been developed for quasi-maritime, subtropical anvils, and it might not be valid for thunderstorm anvils that develop in a continental air mass that contains a different aerosol and/or humidity profile. This question should be considered further by experts in cloud physics.

3.1.1.2 Radar Parameters Corresponding to Higher Field Thresholds

If the existing ABFM dataset is found to be applicable, then an extreme-value statistical analysis previously performed by Dr. Harry Koons will need to be repeated in order to quantify the radar parameter(s) that corresponds to the higher field threshold(s).

3.1.2 Models of Positive-Leader Viability and Their Validation

We now briefly review five conceivable models for predicting positive-leader viability, hence lower bounds on the triggering conditions, in classical rocket-triggered lightning. [In this section only triggering at surface conditions — essentially at standard temperature and pressure (STP) — is considered. What little is currently known about the air-density, or altitude, dependence will be reviewed in Section 3.1.3.] The first three such "models" have already been alluded to in Section 2.2.3: A) Triggering might occur whenever the geometrically enhanced field intensity at the wire tip exceeded the "breakdown field" — about 3 MV/m at STP. Unfortunately this is well known to be a necessary, but far from sufficient, condition for triggering. B) A leader might become viable as soon as the ambient field magnitude exceeds that of the potential gradient found inside a DC arc channel carrying the same current — only a few kilovolts per meter, based on measured positive-leader currents of a few amperes. This is probably necessary, but, fortunately for us, it is also not sufficient. In the experiment described in Section 2.2.3, for example, precursor discharges do not develop into viable leaders, even in field magnitudes approaching 20 kV/m, until the length of the triggering wire approximately doubles. C) In Section 2.2.3 it was suggested that a potential that is spanned by the triggering wire of about 4 MV might be both necessary and sufficient to initiate lightning. This plausible but fairly simplistic "model" is compared with two more sophisticated models of leader propagation below.

Two serious attempts to model the physical mechanism of the positive leader have led to predictions of triggering conditions: (D) Aleksandrov et al. [2005] and (E) Lalande et al. [2002] have both presented curves of ambient field (assumed uniform) vs. wire length required to initiate a viable upward positive leader in classical rocket-triggered lightning.

3.1.2.1 The Bazelyan and Raizer Model

We discuss first the semi-empirical model of Aleksandrov et al. [2005], which is by far the simpler of the two and is essentially that presented previously by Bazelyan and Raizer [2000, Section 4.1.1]. These authors write a fundamental equation for the potential balance at the leader tip:

$$\Delta U_t = -E_c L - [-E_0(H + L)] \qquad (1)$$

The first term on the right side is the potential (relative to Earth) of the leader tip, assuming a uniform voltage gradient, $-E_c$, inside a leader channel of length, L, extending upward from the tip of a grounded wire. The second term is the ambient potential near the leader tip, assuming a uniform vertical ambient field, E_0 (positive upward), and a wire length, H. Thus, ΔU_t represents the potential difference between the leader tip and the ambient atmosphere at the same height. From laboratory experiments with long sparks, ΔU_t must remain at least 300–400 kV in order to maintain leader propagation [Bazelyan and Raizer, 2000, p. 139].

A much more stringent condition, however, is that ΔU_t must remain constant or increase with L to keep the leader viable. This obviously requires a minimum ambient field, $E_0 = E_c$, reducing (1) to ΔU_t

$= E_c H$. Bazelyan and Raizer [2000, Section 4.1.1] find this minimum field with the help of two other relationships involving the leader current, i, assumed uniform along the channel:

$$i = C_l \Delta U_t V_L, \text{ where } C_l = 2\pi\varepsilon_0/\ln(L/R) \text{ and } V_L = a(\Delta U_t)^{1/2} \quad (2)$$

$$E_c = b/i \quad (3)$$

Here C_l is the effective capacitance per unit length of the leader, ε_0 is the dielectric permittivity of air, R (also assumed uniform) is the effective radius of the envelope of corona space charge surrounding the leader channel, V_L is the leader propagation speed (the physics of which Bazelyan and Raizer [2000, Section 4.1.1] admit is not yet well understood), $a = 15$ m/(sV$^{1/2}$) is an empirical constant estimated from data on long laboratory sparks, and $b = 3.0 \times 10^4$ VA/m is another empirical constant approximating laboratory data on the potential gradient in arc-like leader channels. (Note that Equation 3 specifies a significantly larger potential gradient for any given current below about 25 A than that measured in laboratory DC arcs [e.g., King, 1961]. For more discussion of arc potential gradients, see Section 3.1.2.3.) Substituting for E_c in the simplified version of (1) from (3), and then substituting for i from (2), Aleksandrov et al. [2005] find the minimum ambient field as

$$E_0 = [b\ln(L/R)/(2\pi\varepsilon_0 a)]^{2/5} H^{-3/5} \approx 3.7 \text{ X } 10^5 \, H^{-3/5} \quad (4)$$

where the numerical coefficient, 3.7×10^5 Vm$^{-2/5}$, results from taking $\ln(L/R) \approx 2.3$.

It is important to understand what is happening in this model. According to Equation 2, the "fan" of positive streamers at the leader head supplies current to the channel in proportion to the leadertip's potential difference, ΔU_t, times its speed, V_L (which itself depends weakly on ΔU_t). This current, in turn, determines the leader's internal voltage gradient through (3). Because an appreciable current must be maintained to keep E_c relatively low, a viable leader will always have ΔU_t much larger than the minimum of 300–400 kV. The lower the ambient field, the longer the triggering wire must be in order to span this required potential difference. It turns out that a nonviable leader — a precursor — can propagate in ambient fields lower than the minimum given by (4), but ΔU_t will decrease with time (because $E_0 < E_c$) until such a precursor stops. Thus, the Bazelyan and Raizer model predicts not only the triggering conditions, $E_0(H)$, but also the existence of precursors. (It should also be noted that this model agrees in principle with the assertion of "model" B above — $E_0 \geq E_c$ — but shows that a conductor of considerable length is required to get the discharge past the precursor stage.) On the other hand, this model substantially overpredicts the inferred length of the precursors, and it implies leader potential gradients of a few tens of kV/m for reasonable triggering-wire lengths.

3.1.2.2 The Lalande et al. Model

A quite different and much more complex model of classical rocket-triggered lightning has been described most recently by Lalande et al. [2002] and Gallimberti et al. [2002], based heavily on earlier work by Bondiou and Gallimberti [1994]. This time-dependent model attempts to represent the detailed physics of the discharge in a fully self-consistent manner, including both global electrostatic effects (e.g., the competition between field enhancement at the leader head by its relatively conducting, grounded channel, and "screening" of the leader head by space charge that has been distributed by positive streamers propagating in that enhanced field), and plasma-physical effects (e.g., the formation of new leader channel by the positive streamers that diverge from its head, and the subsequent "thermalization" of that channel by continued current input from this streamer fan). The full model is too complex to discuss further here, but Lalande et al. [2002, Equation 1] have

used it to compute what they call the "stabilization field" for development of a viable positive leader from a grounded triggering wire — essentially comparable to $E_0(H)$ in our Equation (4):

$$E_{stab}(H) = 306.7/(1 + H/6.1) + 21.6/(1 + H/132.7) \quad (5)$$

Lalande et al. [2002, Section 4.4] also describe a simplified electrostatic model, based on their full model, that illustrates the latter's behavior. Since they are able to essentially duplicate (5) with this simplified model, we take a closer look at it here. Rewriting their fundamental Equation 3 in notation similar to our (1), we have

$$\Delta U'_t = -E_c L - [-E_0(H + L)] - \Delta U_{ce} \quad (6)$$

where the new term, ΔU_{ce}, is the (positive) increment of potential that is contributed, at the location of the leader tip, by all of the corona space charge around and ahead of the leader channel. The authors give formulae from which to compute ΔU_{ce} using assumed values for the charge per unit length in the corona-space-charge envelope, $q_{ce} \approx 50$ μC/m (assumed uniform), its radius around the leader channel, $a_{ce} \approx 0.5$ m (also assumed uniform), and the distance of its leading edge (the front of the positive-streamer fan) ahead of the leader tip, L_c. This third parameter has a significant effect on ΔU_{ce} and must be computed implicitly from

$$L_c = \Delta U'_t / E_s \quad (7)$$

where $E_s \approx 450$ kV/m is the average field inside a positive-streamer fan, from laboratory measurements, and L_c typically equals a few meters. Like the Bazelyan and Raizer model, this simplified model predicts the occurrence of precursors at ambient fields less than $E_{stab}(H)$; it also overpredicts their length, but not by as much.

q_{ce} and ΔU_{ce} are essential aspects of the full leader model of Lalande et al. [2002]. These authors argue that a well defined quantity of charge must be injected from the streamer fan in order to form a unit length of new leader channel. The opposite charge remains in the corona envelope, which then exerts an electrostatic effect on leader behavior via ΔU_{ce}. Further, Lalande et al. [2002] argue that E_c is usually negligible compared to E_0, since their model of thermalization normally predicts channel potential gradients of only a few kV/m. In calculations with their simplified model, they appear to set $E_c = 0$.

This is conceptually quite different from the Bazelyan and Raizer model (see Section 3.1.2.1), where the leader current is computed from a capacitance per unit length times ΔU_t (effectively a charge per unit length) — see Equation 2 — and the electrostatic effect of the corona envelope does not appear explicitly in Equation 1. Lalande et al. [2002] describe leader viability primarily as a balance between the ambient field, which increases $\Delta U'_t$ as L increases, and the field produced by the corona envelope, which decreases $\Delta U'_t$ as L and/or L_c increases. In contrast, Bazelyan and Raizer [2000, Section 4.1.1] emphasize the balance between ambient field and channel potential gradient.

Nevertheless, the Bazelyan and Raizer model does not actually ignore ΔU_{ce}. In fact, the main contribution to the difference, ΔU_t in Equation 1, between the potential of the leader tip and that of the ambient field nearby must be precisely ΔU_{ce}, since the effects of the only other charges in the vicinity — surface charge on the wire and that on the leader channel itself — are negligible [Y. Raizer, private communication, November 17, 2005]. Thus, it would be incorrect to equate ΔU_t with $\Delta U'_t$ in Equation 6; a comparison of Equations 1 and 6 shows instead that $\Delta U'_t \approx 0$. Note that in this case Equation 7 no longer makes sense for estimating the streamer length. Lalande et al. [2002] do not

clearly state the meaning of $\Delta U'_t$ — they say above their Equation 3 only that "the potential difference available to sustain the leader propagation is a function of the potential drop [$\Delta U'_t$]" — but it would appear that there is an important electrostatic error in the simplified model of Lalande et al. [2002, Section 4.4]. We are unable to determine at this time whether their full numerical model, from which Equation 5 was derived, contains a similar error.

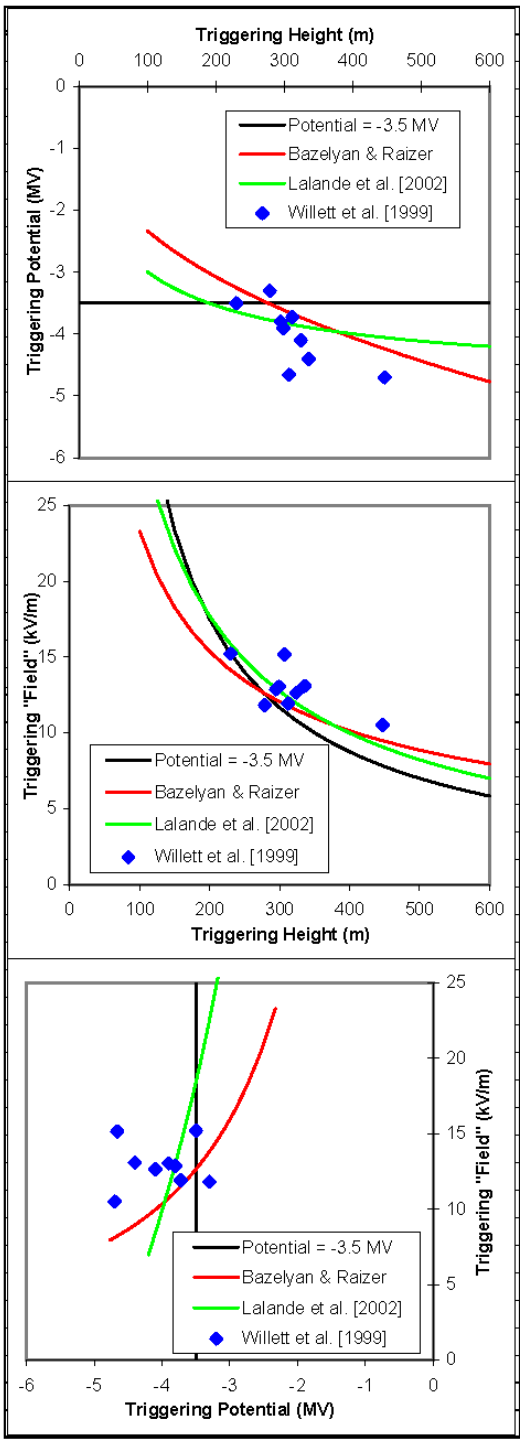

As mentioned above, the charge per unit length on the leader, including its corona envelope, is written as $C_l \Delta U_t$ in the model of Bazelyan and Raizer [2000, Section 4.1.1]. That is, it is directly proportional to the leader-tip potential difference, as required by electrostatics, instead of being equal to a constant q_{ce}, as assumed in Lalande et al. [2002, Section 4.4]. The latter assumption also appears unreasonable, but we are again unable to determine whether the full numerical model of Lalande et al. [2002] also makes this assumption. In any case, these two apparent errors in Lalande et al. [2002, Section 4.4] are sufficient reason to question the origins of Equation 5.

3.1.2.3 Model Comparison and Validation

In Figure 3-1, three of the above-described models are overplotted on the measurements of Willett et al. [1999], shown previously in Figure 2-4. (Note that we have displayed the average field between the surface and the triggering height here, as opposed to the field magnitude at the triggering height, because the two more sophisticated models both assume uniform ambient field.) The black curves in the figure represent the assumption that a viable positive leader will be initiated whenever the potential spanned by the triggering wire exceeds a constant potential — 3.5 MV in this case. This might be called the "constant-potential-spanned" model — (C) from above. The red curves correspond to Equation 4 — the Bazelyan and Raizer model of Section 3.1.2.1 — and the green curves are from Equation 5 — the Lalande et al. model of Section 3.1.2.2. Although one might pick the Bazelyan and Raizer model as best representing the apparent trend of the data points, the fact is that there is little here to recommend one of these three models over the others.

Figure 3-1. Comparison of the "Constant-Potential-Spanned," Bazelyan and Raizer [2000], and Lalande et al. [2002] Positive-Leader Models with the Data of Willett et al. [1999].

In addition to the rocket-triggering experiments of Willett et al. [1999], there have been at least four major field campaigns to measure lightning strikes on board instrumented aircraft [Uman and Rakov, 2003]. Two of these aircraft, the FAA CV-580 in 1985 and the French Transall C-160 in 1988, carried calibrated systems of electrostatic field mills that allowed the measurement of ambient field immediately prior to a number of strikes. The data from these systems has been summarized and interpreted by Laroche et al. [1989a] and by Lalande and Bondiou-Clergerie [1997]. The tables given in the latter report do not completely match those in the former, but Laroche et al. [1989a] omit data that is essential to our purposes. Therefore, the data of Lalande and Bondiou-Clergerie [1997] has been taken to be authoritative and are re-interpreted here in an effort to assess the triggering conditions for these aircraft.

Table 3-1. Ambient Field Immediately Prior to Aircraft Strikes

Event	Altitude	E_x	E_y	E_z	U	Density	reduced $\|E\|$	reduced $\|E_h\|$	reduced U
(#)	(ft)	(kV/m)	(kV/m)	(kV/m)	(kV)	(nondim.)	(kV/m)	(kV/m)	(kV)
CV-7	14000	33	-18	20	-1370	0.65	65	58	-2107
CV-9	14000	4	-25	-1	-1510	0.65	39	39	-2322
CV-10	1800	-28	-3	11	-310	0.95	32	30	-327
CV-12	18000	-43	-20	-20	-600	0.57	90	83	-1052
CV-13	18000	-61	-29	-50	-705	0.57	147	118	-1236
CV-14	16000	50	-14	8	-830	0.61	86	85	-1362
CV-15	16000	60	-3	34	-1240	0.61	113	99	-2035
CV-17	14000	65	-14	55	-890	0.65	133	102	-1369
CV-18	14000	61	-5	19	-1100	0.65	99	94	-1692
CV-19	18000	27	12	-17	-1440	0.57	60	52	-2525
CV-20	14000	49	-3	6	-1000	0.65	76	76	-1538
CV-21	14000	41	-5	43	-760	0.65	92	64	-1169
CV-22	14000	7	-25	-3	-800	0.65	40	40	-1230
CV-25	14000	34	23	51	-600	0.65	101	63	-923
CV-28	15000	-16	-38	-17	-650	0.63	71	66	-1033
T-3	15000	33	-19	-40	-1950	0.63	88	60	-3098
T-7	14000	45	-7	-26	-840	0.65	81	70	-1292
T-8	14000	31	15	-60	85	0.65	106	53	131
T-11	14000	58	-5	17	-1335	0.65	93	90	-2053
T-12	14000	37	-36	-54	-1890	0.65	115	79	-2907

Lalande and Bondiou-Clergerie [1997] state that 30 direct lightning strikes to the CV-580 and 12 to the Transall were recorded during their respective campaigns. Of these, ambient-field data is presented from 22 events, two of which are unambiguously identified as “intercepted” strikes and have been omitted here. There remain 15 strikes to the CV-580 and five to the Transall that are suitable for further analysis. This data is listed in Table 3-1, which shows aircraft altitude; the field components in the forward direction (E_x), to port (E_y), and upward (E_z) relative to the aircraft; vehicle potential (U); relative air density at altitude (estimated from the U.S. Standard Atmosphere); and “reduced” values of the vector field magnitude ($|E|$), of the magnitude of the “horizontal” components ($|E_h| = [E_x^2 + E_y^2]^{1/2}$), and of U. These last three entries have been reduced to surface conditions by dividing the corresponding measured values by relative air density, on the implicit assumption that the triggering conditions scale with density according to Paschen’s Law. Some such reduction is required

in order to compare these results on an equal footing with the rocket-triggering data of Willett et al. [1999]. Note, however, that this assumption has *not* been validated, as will be further discussed in Section 3.1.3.

The uncertainty of the measurements themselves must also be emphasized. Measurement of the ambient field from an aircraft is not easy in the best of circumstances; it becomes difficult inside clouds, where particle impaction may charge the vehicle strongly, and especially so at high field intensities, where corona discharges are inevitable. Laroche et al. [1989a] give estimated uncertainties of the various field components ranging between roughly ±5 and ±30 kV/m, with E_y the most uncertain component on the CV-580 and E_z the most uncertain on the Transall. (E_x seems to be the most accurately determined component on both aircraft, having uncertainties toward the low end of this range.) In summary, individual measurements are probably only 20–50% accurate.

The dimensions of these aircraft (including a tail boom on the CV-580 and both nose and tail booms on the Transall) are given by Laroche et al. [1989a] as 32 m wingspan by 28 m long (CV-580) and 40 m wingspan by 40 m long (Transall). The tail heights are only about 7 m and 11 m, respectively; so we focus on the horizontal components of the ambient field as critical for triggering, and we take the relevant aircraft dimensions to be 30 and 40 m, respectively.

If a flying vehicle were uncharged at the time of a lightning strike, it would be appropriate to use 1/2 its maximum dimension (i.e., 15 m for the CV-580 and 20 m for the Transall) to estimate the conductor-vs.-ambient potential difference at each of its two extremities at the time of positive-leader initiation. (See further discussion of this issue in Section 3.1.5.5.) Both Laroche et al. [1989a] and Lalande and Bondiou-Clergerie [1997] point out, however, that both aircraft were consistently (in every case but one) negatively charged, their potentials averaging about –1460 and –1840 kV, respectively — roughly in proportion to their capacitances. These large negative potentials, most likely due to a combination of tribo-electric and corona charging, probably made it more difficult to launch a positive leader, thereby increasing the ambient field intensity required to trigger lightning. Nevertheless, we have little choice but to neglect the aircraft charge and use 1/2 the dimensions in what follows, with the understanding that this probably results in some overestimation of the ambient fields required to initiate a positive leader from an uncharged vehicle of comparable size. (With a time-dependent model of positive-leader development, such as the full model of Lalande et al. [2002], it would be possible to take account of the capacitance and initial charge of the aircraft — perhaps of negative-leader initiation as well — in determining leader viability. This would require both access to, and validation of, the specific model, however, we can claim neither.)

Figure 3-2 shows the reduced data from Table 3-1, plotted together with the surface data of Willett et al. [1999], in comparison to the three models discussed above. For the aircraft data we have taken $D/2$ as the effective length, $|E_h|$ as the average field, and $-|E_h|D/2$ as the spanned potential, where D is 30 m for the CV-580 and 40 m for the Transall. In spite of the scatter, measurement uncertainty, altitude-scaling, and neglect of vehicle charge in the aircraft data, they clearly rule out the constant-potential-spanned model (the black curves) in comparison with the other two models. Figure 3-3 shows a magnified view of these graphs to emphasize the aircraft data. Once again, although one might favor the Bazelyan and Raizer model (red curves) as passing closer to the “center of mass” of these data points, all of the uncertainties make it difficult to argue convincingly that this model is better than the model of Lalande et al. [2002] (green curves). Henceforth, we use the Bazelyan and Raizer model (Equation 4) to represent triggering at surface conditions, primarily because of its relative simplicity and small number of parameters.

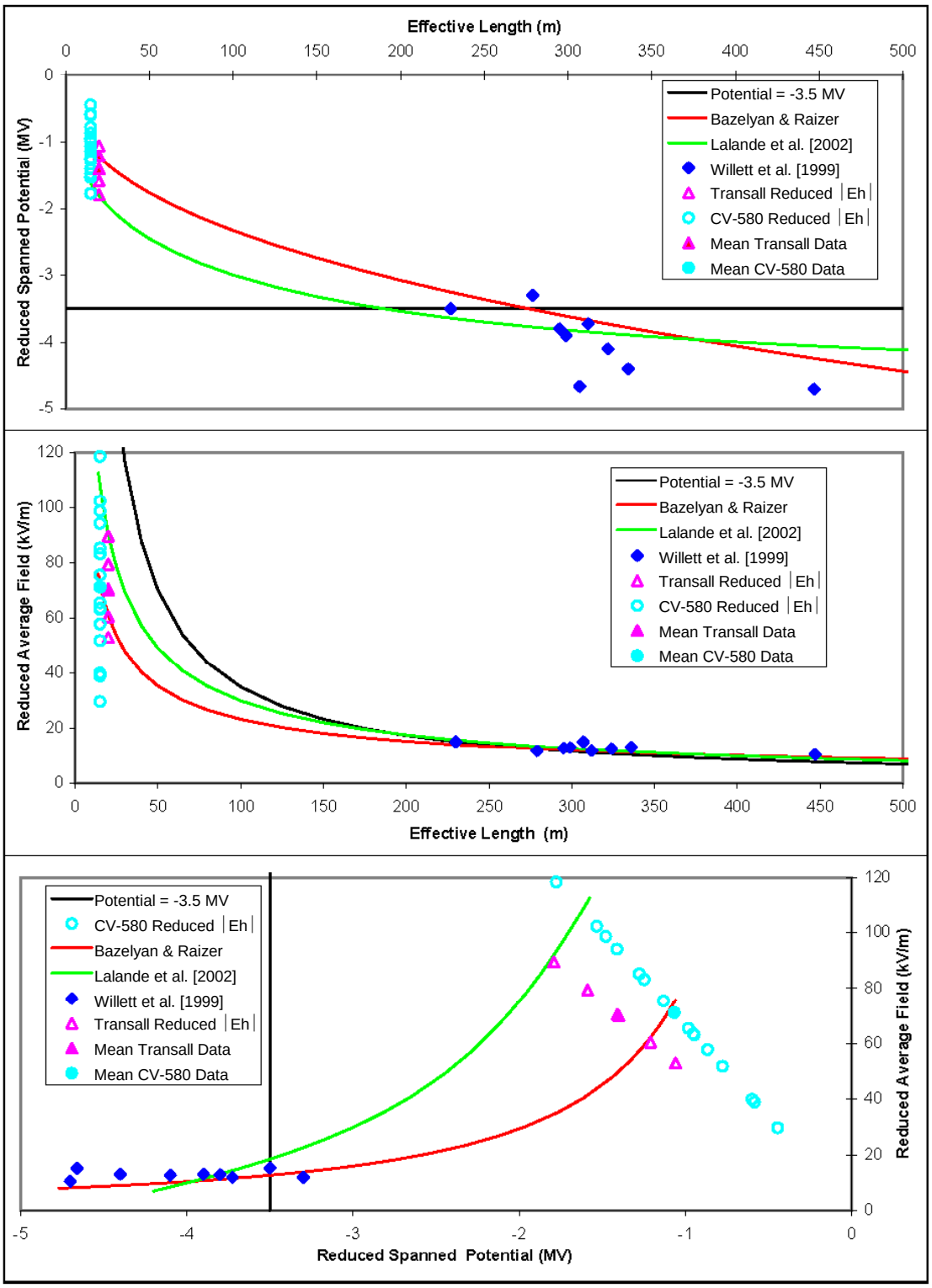

Figure 3-2. Comparison of Models with Data. As in Figure 3-1, but with the aircraft-triggering data added.

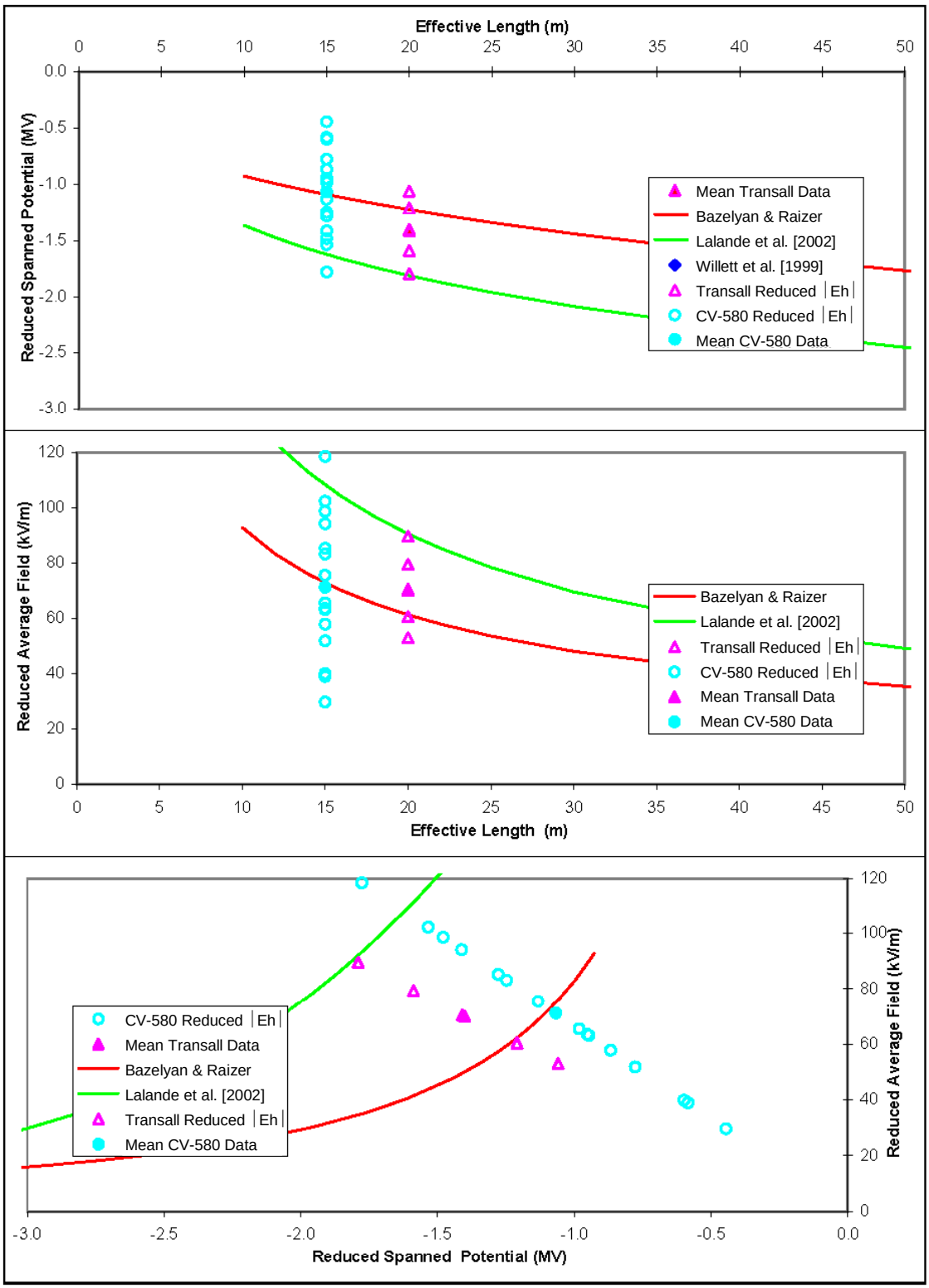

Figure 3-3. Comparison of Models with Data. As in Figure 3-2, but cropped to focus on the aircraft-triggering data.

A cautionary note is required, however, to the use of Equation 4 for our present purposes: The measured fields for aircraft triggering have been increased by as much as 75% by the (quite uncertain) density scaling that was applied to reduce them to surface conditions. If Paschen's Law turns out to exaggerate significantly the altitude dependence of the actual triggering conditions, then the Bazelyan and Raizer model might not correctly represent the size dependence of these conditions. In that case, this model could dangerously overpredict the ambient field intensity required to trigger lightning with small vehicles.

3.1.3 Altitude (Density) Dependence of Triggering

The altitude dependence of long-spark breakdown is essentially unknown. Looking at the simple models described in Section 3.1.2, one can see several places where a pressure and/or temperature dependence would likely enter. In the Bazelyan and Raizer model this could happen through the parameter, b, of the leader channel's internal potential gradient, E_c, in Equation 3; through a in the leader's propagation speed, V_L, in (2); or weakly through L/R in the capacitance per unit length, C_l, also in (2). In the Lalande et al. [2002] model, on the other hand, it could happen through several parameters in the increment of leader-tip potential difference that is contributed by the corona space charge, ΔU_{ce}, in Equation 6 — the charge required to create a unit length of new leader channel, q_{ce}; the corona radius, a_{ce}; or the longitudinal extent of the active corona fan, L_c, via E_s in (7). It could even happen in this model through the minimum value of leader-tip potential difference at which the leader is assumed to stop (not discussed).

There is at least one research group [Bazelyan, Aleksandrov, Konchakov, and Raizer, currently under contract to NASA/KSC] that is studying this altitude dependence, but for the time being it must be estimated from that of other, only partially applicable, electrical-discharge processes. There are three obvious candidates: Paschen's Law (constant E_0/N, where E_0 is ambient-field intensity and N is gas molecular density) is the most familiar air-density dependence in electrical breakdown, but it strictly applies only to volume breakdown by the Townsend process (or, on a much larger scale, by "runaway electrons"). Paschen's Law is known *not* to apply, however, to the positive streamers that feed current into the head of a positive leader. The air-pressure, p, dependence of the positive-streamer "stability field," E_s, is the strongest known for any important long-spark process — the 3/2 power of air pressure at constant temperature [Phelps and Griffiths, 1976]. Nor does Paschen's Law apply to the longitudinal field inside a DC arc. This third dependence is not as well known as that for positive streamers, as further summarized below, but measurements suggest only the 1/3 power of ambient pressure, and even this may be an overestimate.

The current-voltage characteristic (CVC) of the "positive column" (excluding the electrode regions) of DC arcs in air at atmospheric pressure has been the subject of considerable experimental investigation, but we are aware of only one study that measured the pressure dependence of the CVC of such arcs. Figure 3-4 shows some of this data, replotted from Figure 10.15 of Raizer [1991]. "Free-air" data has also been included in Figure 3-4 from Raizer [1991, Fig. 10.16] and from King [1961] (at atmospheric pressure only).

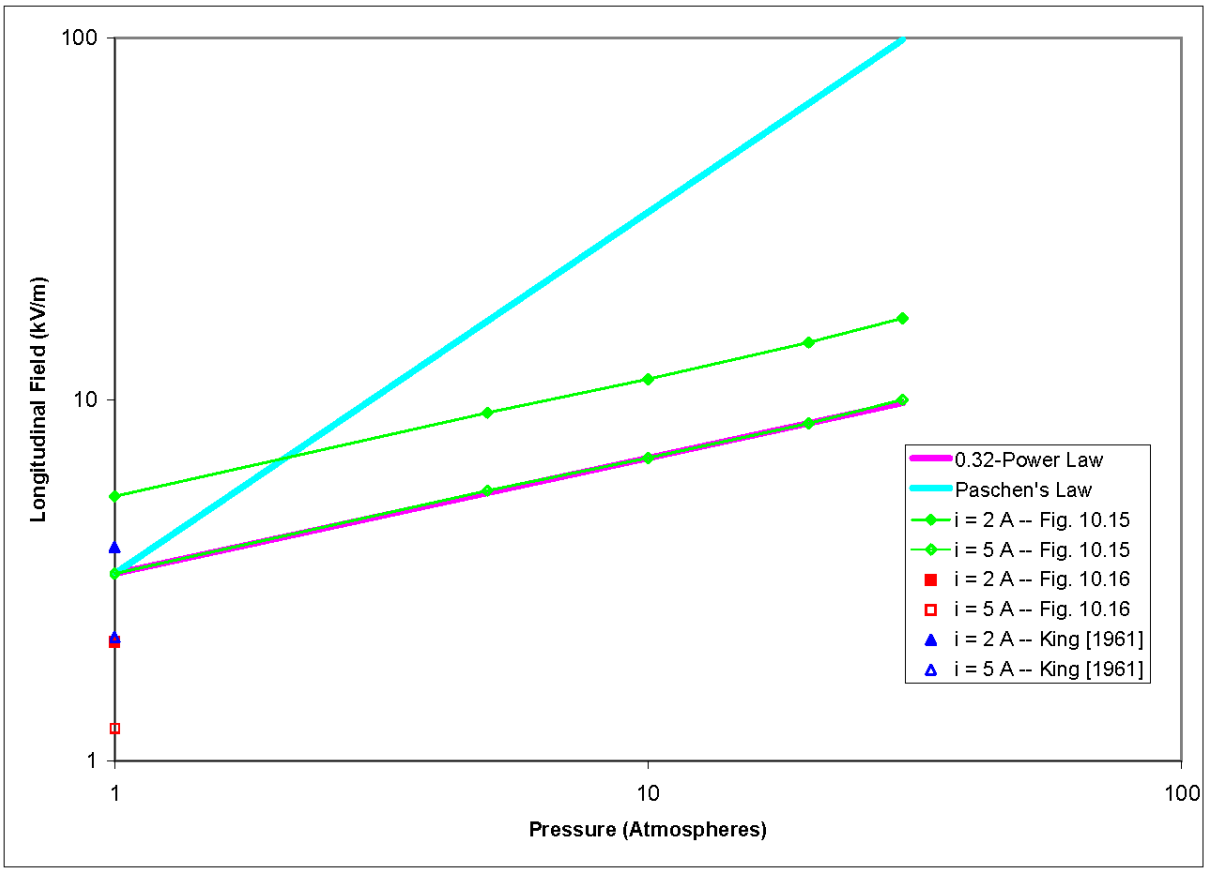

Figure 3-4. Experimental Data on Arc Potential Gradient vs. Pressure

Several comments are in order here. First, the measured longitudinal field in Raizer [1991, Fig. 10.15] appears to depend on the 0.32 power of ambient pressure (magenta line) at both 2 A (solid green diamonds) and 5 A (hollow green diamonds), in dramatic contrast to Paschen's Law (cyan line). This observed dependence might be exaggerated, however, as the measurements were apparently made on arcs that were confined inside cooled tubes. Second, data replotted from Raizer [1991, Fig. 10.16] (red symbols), specifically for unconfined arcs, indicates significantly lower potential gradients in free air. Raizer [1991, p. 273] offers the following comments on these issues: "If the pressure is increased at a fixed current, the field is enhanced (Fig. 10.15). The enhancement is caused by increased radiative losses and, possibly, by a certain increase in heat transfer from plasma to the [tube] walls, dictating enhanced power per unit length, $W = Ei$. At equal currents, stronger field is required to sustain the plasma in a tube than in an arc burning in free atmosphere, because the transfer is more intense [in the tube] and more power is needed (Fig. 10.16)." Third, the data on DC arcs that is summarized in Figure 3-4 appears to be relevant to the lightning-initiation problem because the time constants for adjustment of these arcs to changes in current (order 100 μs [e.g., Edels and Graffmann, 1969; Latham, 1986]) are short compared to the leader-development times (a few milliseconds). Finally, we believe that the free-air data of King [1961] (blue symbols) is more quantitatively compelling than that from Raizer [1991, Fig. 10.16] because King's measurements were acquired with very careful attention to the experimental techniques so as not to compromise the free-air nature of the arcs in question, nor to underestimate the tortuous channel length. Therefore, we take the minimum electric field that is required to maintain a 2 to 5 A arc in the free atmosphere to

be in the range from 3.9 to 2.2 kV/m at atmospheric pressure. We further take the pressure dependence of this field to be no stronger (and probably weaker) than the 0.32 power.

Note that, by quoting arc gradients at specific currents, we tacitly assume that the minimum current required to maintain a positive leader will not change substantially with altitude. Since this current is supplied to the leader channel by streamer processes at the leader tip, and since it is largely controlled by the leader-propagation speed (the physics of which is not well understood), there is no guarantee that this assumption is valid.

The positive-streamer scaling as $p^{3/2}$ is probably extreme for the triggering conditions, since it applies only to a small portion of the leader structure, but the estimated DC-arc scaling as $p^{1/3}$ might be too weak for the long spark as a whole. Therefore it is recommended here that the Paschen's Law scaling be used until the behavior of positive leaders at high altitude is better understood. More research is clearly required to understand the altitude dependence of the triggering conditions.

3.1.4 Velocity Dependence of Triggering

The vehicle-velocity dependence of triggering is believed to be a threshold that is based on the ion-drift velocity in the geometrically enhanced electric field at the altitude of interest. The basic argument, originally due to Brook et al. [1961], is that space charge tends to accumulate in the air around a long, thin conductor embedded in a high ambient electrostatic field as a result of corona discharges from its tips. If the conductor is motionless relative to the air, this charge partially shields it from the otherwise greatly enhanced field. If the conductor is moving rapidly, however, it will tend to leave the space charge behind, eliminating the shielding. How fast the conductor has to move to escape this charge sufficiently for triggering depends on the ion-drift velocity in the enhanced field near the conductor's tips.

A complete analysis of the situation is obviously complex, but rough estimates of the threshold speed at surface pressure may be made as follows: An extreme upper bound can be derived from the breakdown field (see Section 3.1.2). A somewhat more realistic estimate can be obtained by assuming the field to be limited (near the positive tip) by the positive-streamer stability field (see E_s in Section 3.1.2.2). Taking the small-ion mobility to be about 1.2×10^{-4} m^2/(Vs), the resulting speeds become 360 m/s and 54 m/s, respectively. Recently Aleksandrov et al. [2005] have stated that a speed of only about 20 m/s is sufficient to overcome the shielding effect of corona space charge, but no details of this theoretical derivation were offered.

Although systematic experiments have not been carried out, to our knowledge, speeds that are sufficient for lightning initiation can be obtained from rocket-triggering technology and from strikes to flying aircraft. Two early types of triggering rockets that were used successfully by French triggering experts flew at 170 m/s, and their most recent design flies at 220 m/s, according to St. Privat D'Allier Group [1985]. Laroche et al. [1989a] asserted, "The critical velocity lies around 100 m/s for an electric field equal to one-third of the breakdown field in normal conditions. The [CV-580 and Transall] aircraft were flown at about the same speed, around 100 m/s, so they were both in the same favorable conditions to trigger..." All of these observed speeds are consistent with the above estimates.

The density (or altitude) dependence of this speed threshold would depend to some extent on the details of the shielding mechanism. Given that both the breakdown field and the positive-streamer stability field decrease with air density (see Section 3.1.3) and that the small-ion mobility increases

approximately in inverse proportion to density, however, it seems likely that the threshold speed is approximately altitude independent.

3.1.5 Five Vehicle Types and Concomitant Triggering Conditions

In the following sections we describe the concept RLVs and their launch sites, and then we estimate the electrical lengths of their exhaust plumes and the resulting triggering conditions.

3.1.5.1 Representative Suborbital Vehicle Concepts

In order to determine the electric fields that could trigger lightning to suborbital vehicles, the specific vehicle and trajectory characteristics must be known. As this information is difficult to obtain or unavailable from the various suborbital vehicle companies, five representative suborbital vehicle configurations were developed that closely resembled currently proposed suborbital vehicle concepts. The five representative vehicles are:

1) Horizontal takeoff and landing vehicle with jet engines and rocket engines. This vehicle takes off using jet engines and proceeds to an airborne launch point, where it then climbs to apogee using rocket power and glides to a landing on a runway.
2) Ferried and horizontal landing vehicle with rocket engines (referred to as "Air Launch vehicle"). The vehicle is carried aloft by a carrier aircraft to the drop point, where it is released and climbs to apogee using rocket power, and glides to a landing on a runway.
3) Horizontal takeoff and landing vehicle with rocket engines. This vehicle takes off using rocket engines, climbs to apogee using rocket power, and glides to a landing on a runway.
4) Vertical takeoff and landing vehicle with rocket engines. This vehicle takes off vertically using rocket engines, coasts to apogee, and lands by rocket-powered descent.
5) Balloon takeoff-carrying launch vehicle to altitude. At altitude, the vehicle will climb to apogee using rocket power and lands using a parachute landing system.

3.1.5.1.1 Horizontal Takeoff with Jet and Rocket Engines Representative Vehicle

The Horizontal Takeoff with Jet and Rocket Engines vehicle is designed to take off from the airport of origin using jet engines to climb to approximately 20,000 to 30,000 ft. At that altitude, the rocket engines light off to begin the suborbital trajectory. After rocket engine burn-out, the vehicle coasts to the 100 km altitude, and then re-enters the atmosphere. The vehicle then either re-lights its jet engines for a powered landing or glides back to the airport of origin for an unpowered landing. The vehicle is controlled by a single pilot who controls the vehicle during all portions of the flight, including emergency situations. The vehicle also carries up to three passengers during the flight. The gross takeoff weight of the representative vehicle is 18,000 lb. The vehicle length is 40.0 ft, with a wingspan of 25.0 ft. The horizontal takeoff with jet and rocket engines representative vehicle is presented in Figure 3-5.

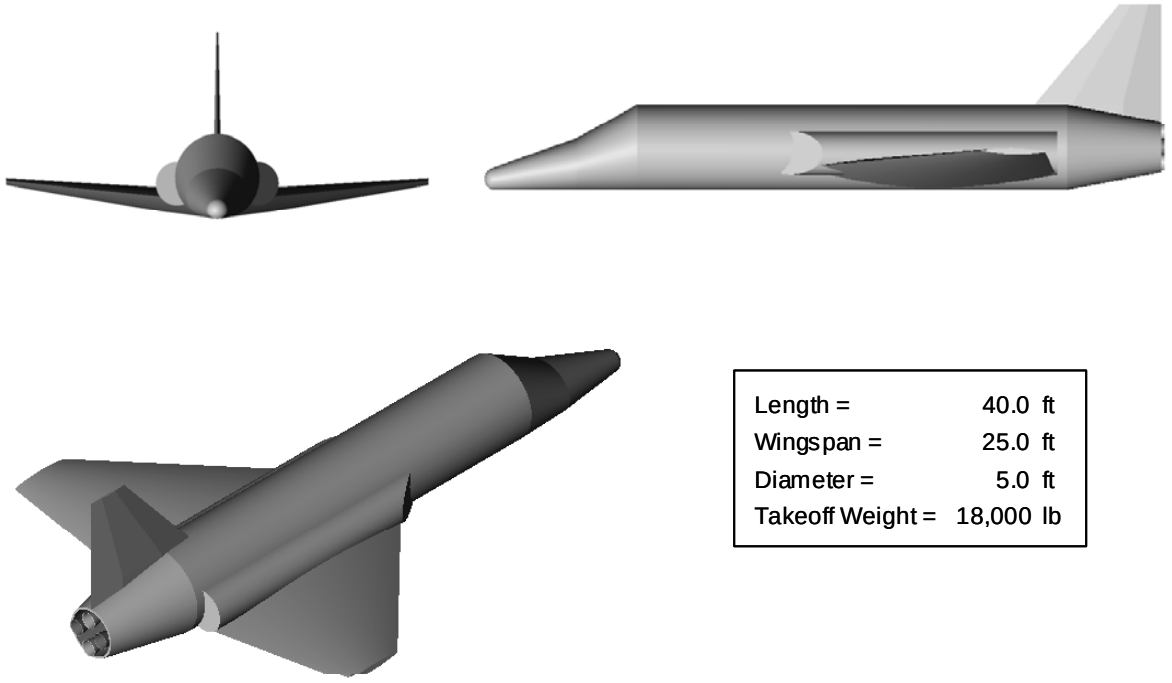

Figure 3-5. Horizontal Takeoff with Jet and Rocket Engines Representative Vehicle

3.1.5.1.2 Air Launch Representative Vehicle

The Air Launch vehicle is designed to be carried on the back of an aircraft to approximately 40,000 to 50,000 ft. At that altitude, the vehicle separates from the aircraft, and the rocket engines light off to begin the suborbital trajectory. After rocket engine burn-out, the vehicle coasts to the 100 km altitude, and then re-enters the atmosphere. The vehicle then glides back to the airport of origin for an unpowered landing. The vehicle is controlled by a single pilot who controls the vehicle during all portions of the flight, including emergency situations. The vehicle also carries up to two passengers during the flight. The gross weight of the vehicle is 9,103 lb. The vehicle length is 21.1 ft, with a wingspan of 14.4 ft. The Air Launch vehicle is presented in Figure 3-6.

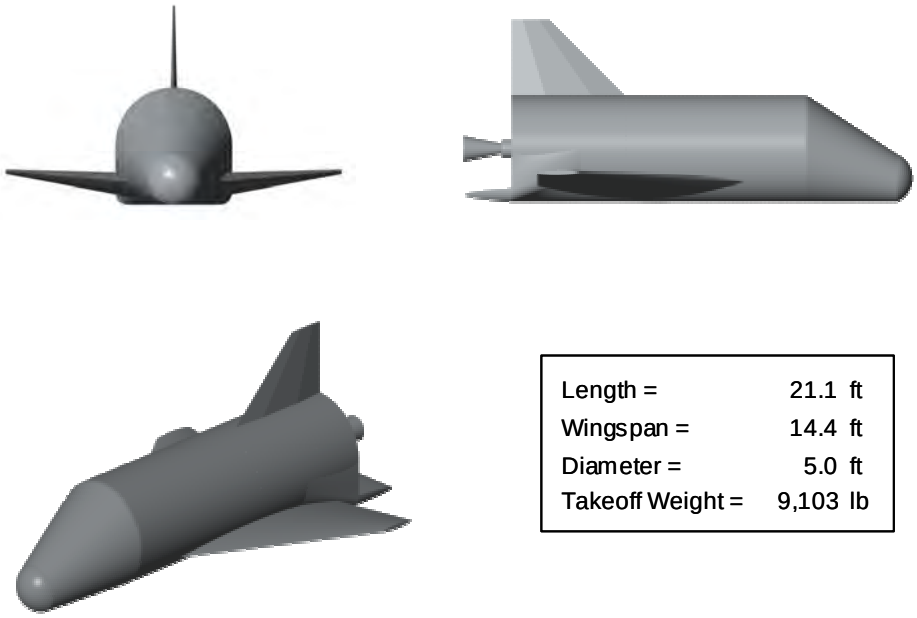

Figure 3-6. Air Launch Representative Vehicle

3.1.5.1.3 Horizontal Takeoff with Rocket Engines Representative Vehicle

The Horizontal Takeoff with Rocket Engines vehicle is designed to take off from the airport of origin using two of its four rocket engines. Once clear of the runway, at an altitude of approximately 1 nm, the remaining two rocket engines light off to begin the suborbital trajectory. After rocket engine burn-out, the vehicle coasts to the 100 km altitude, and then re-enters the atmosphere. The vehicle then glides back to the airport of origin for an unpowered landing. The vehicle is controlled by a single pilot who controls the vehicle during all portions of the flight, including emergency situations. The vehicle also carries up to two passengers during the flight. The gross takeoff weight of the vehicle is 13,276 lb. The vehicle length is 24.3 ft, with a wingspan of 17.0 ft. The Horizontal Takeoff vehicle is presented in Figure 3-7.

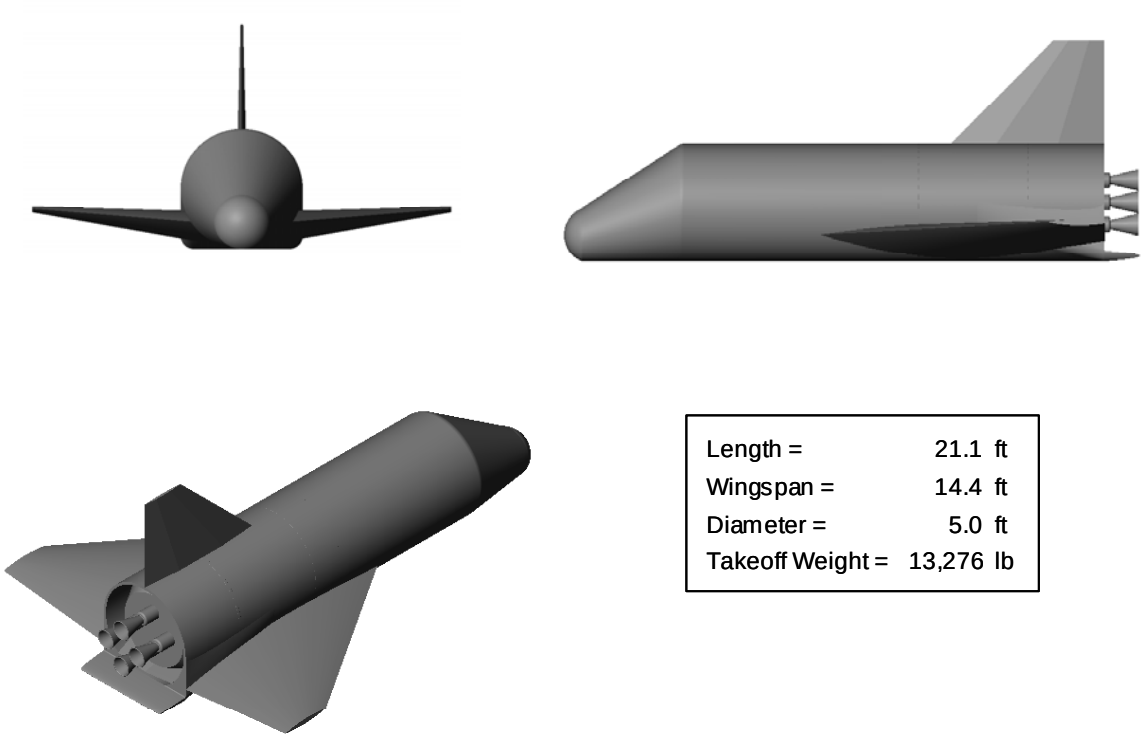

Figure 3-7. Horizontal Takeoff with Rocket Engines Representative Vehicle

3.1.5.1.4 Vertical Takeoff and Landing Representative Vehicle

The Vertical Takeoff and Landing vehicle is a single-stage vehicle that launches using rocket engines. After rocket engine burn-out, the vehicle coasts to the 100 km altitude, and then re-enters the atmosphere. The vehicle deploys a parachute to reduce airspeed. The parachute is then jettisoned and the vehicle's engines re-light for a powered vertical landing at a downrange site. The vehicle is controlled by a single pilot, and carries up to two passengers during the flight. The gross takeoff weight of the vehicle is 10,724 lb. The vehicle length is 23.2 ft and its diameter is 5.0 ft. The Vertical Takeoff vehicle is presented in Figure 3-8.

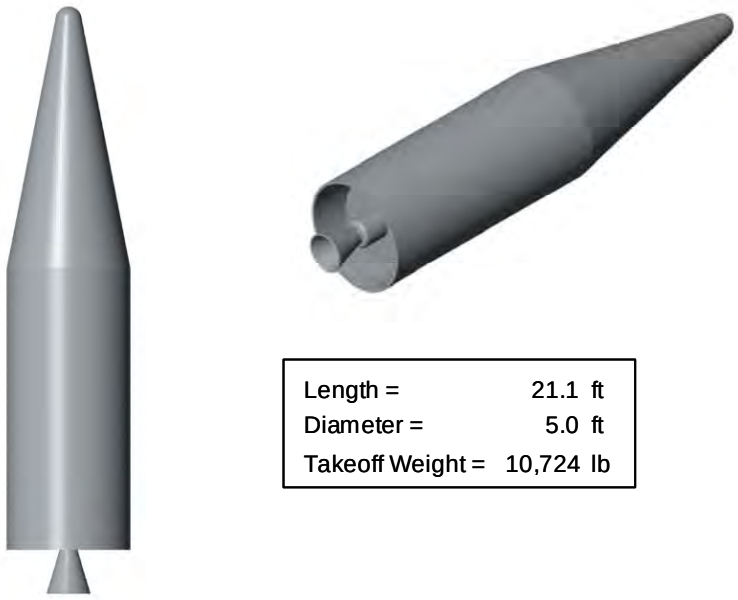

Figure 3-8. Vertical Takeoff and Landing Representative Vehicle

3.1.5.1.5 Balloon Takeoff Representative Vehicle

The Balloon Takeoff vehicle is designed to be carried to approximately 80,000 ft by a large helium balloon. At that altitude, the vehicle separates from the balloon, and the rocket engines light off to begin the suborbital trajectory. After rocket engine burn-out, the vehicle coasts to the 100 km altitude, and then re-enters the atmosphere. The vehicle then deploys a ballute to both protect the vehicle during high-temperature reentry and cushion the vehicle's landing. The vehicle deploys a parachute at 25,000 ft to reduce airspeed. When the landing occurs, the inflated cone at the base of the ballute slightly deforms, and the rocket falls to one side and is supported by the ballute. The vehicle is controlled by a single pilot who controls the vehicle during all portions of the flight, including emergency situations. The vehicle also carries up to two passengers during the flight. The gross weight of the vehicle is 8,500 lb. The vehicle length is 18.0 ft, with a wingspan of 5.0 ft. The Balloon Takeoff vehicle is presented in Figure 3-9.

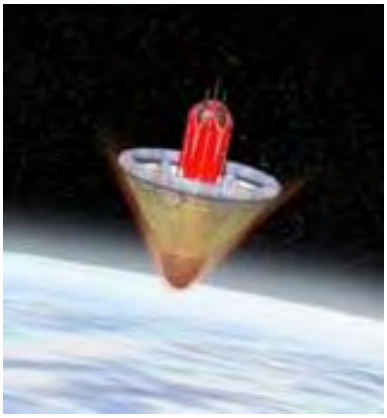

Length =	18.0	ft
Diameter =	5.0	ft
Takeoff Weight =	8,500	lb

Figure 3-9. Balloon Takeoff Representative Vehicle.
[Drawings reprinted with permission of ORVA Space Group / The da Vinci Project]

Table 3-2 presents additional information on each of the five vehicles, as required to perform triggered lightning analyses.

Table 3-2. Representative Vehicle Design Information

Vehicle Number	1	2	3	4	5
Vehicle Type	**HTHL w/ Jet Engines**	**Air Launch**	**HTHL w/ Rocket Engines**	**VTVL**	**Balloon Launch**
Vehicle Length	40.0 ft	21.2 ft	24.3 ft	23.2 ft	18.0 ft
Vehicle Wingspan	25.0 ft	14.4 ft	17.0 ft	N/A	N/A
Vehicle Diameter	5.0 ft	5.0 ft	5.0 ft	5.0 ft	5.0 ft
Nose Radius of Curvature	1.7 ft	4.2 ft	4.2 ft	2.0 ft	3.0 ft
Vehicle Gross Weight	18,000 lb	9,103 lb	13,276 lb	10,724 lb	8,500 lb
Fuel Type	JP-1 and RP-1	Rubber	RP-1	Ethanol	RP-1
Oxidizer Type	Liquid Oxygen	Nitrous Oxide	Liquid Oxygen	Liquid Oxygen	Liquid Oxygen
Rocket Sea Level Thrust (total)	23,800 lb	10,500 lb	13,300 lb	14,500 lb	10,000 lb
Engine Firing Altitude	24,000 ft	50,000 ft	0 ft	0 ft	"80,000 ft"
Engine Burn-out Altitude	150,000 ft	173,000 ft	144,000 ft	114,000 ft	"206,000 ft"
Rocket Burn Time	74.4 sec	96.7 sec	145.1 sec	85.0 sec	"100 sec"
Total Flight Time	1537.4 sec (25.6 min)	973.8 sec (16.2 min)	914.7 sec (15.2 min)	869.7 sec (14.5 min)	"90 - 110 min"
Furthest Distance from Takeoff Site	36 nmi	28 nmi	12 nmi	14 nmi	"10 - 100 km, depending on winds"

3.1.5.2 Spaceports

For this analysis, two proposed spaceports were evaluated, the Southwest Regional Spaceport in New Mexico and the Oklahoma Spaceport.

3.1.5.2.1 Southwest Regional Spaceport

New Mexico has proposed to establish the Southwest Regional Spaceport near Upham, New Mexico, approximately 45 miles north of Las Cruces and 30 miles east of Truth or Consequences. This location is along the western boundary of the White Sands Missile Range, and will benefit from the controlled airspace around the Missile Range. The proposed Spaceport will encompass a 27-square-mile site consisting of open, generally level, range land with an average elevation of 4700 ft. The plans for the Spaceport facility call for a launch complex, a landing strip and aviation complex, a payload assembly complex, a support facilities complex, and a system development complex.

The location of the Southwest Regional Spaceport, and its proximity to the White Sands Missile Range, is presented in Figure 3-10.

Figure 3-10. Location of Southwest Regional Spaceport

3.1.5.2.2 Oklahoma Spaceport

The Oklahoma Spaceport is being developed at the Clinton-Sherman Industrial Airpark at Burns Flat, Oklahoma, approximately 100 miles west of Oklahoma City. The Clinton-Sherman Airpark encompasses approximately 3,000 acres and has two runways of 13,500 ft and 5,200 ft. The Spaceport has an operational control tower and an instrument landing system (ILS) capability that can support a full range of aircraft operations. The Spaceport has multiple commercial-size hangars that can accommodate multiple suborbital vehicle companies, and has adequate access to air, ground, and rail transportation modes. The spaceport also has access to manufacturing facilities and the facilities of Oklahoma's Western Technology Center, and will coordinate all suborbital flights from its spaceport operations center, which is under development. Current plans are for the Oklahoma Spaceport to be operational in 2006.

The location of the Oklahoma Spaceport is presented in Figure 3-11.

Figure 3-11. Location of Oklahoma Spaceport

3.1.5.3. Estimation of Vehicle Plume Lengths

Natural lightning occurs when the potential gradient along a particular path exceeds the level required to ionize atmospheric components. A rocket launch can trigger a lightning bolt in perturbing the gradient by consequence of the greater electrical conductivity of the vehicle body and the exhaust plume. The effect of vehicle bodies is treated elsewhere in this report. This section is concerned with the exhaust plume.

The electrical conductivity of a plume is primarily a function of its electron density; the particle content might also be a secondary factor. The electron density is strongly dependent on the temperature and the presence of easily ionized trace species, mainly sodium and potassium compounds, in the fuel. Of concern here are the soot particles produced by the combustion of hydrocarbon fuels such as JP-1 and RP-1 with liquid oxygen or nitrogen/oxygen compounds used as oxidizers. These particles, mostly composed of amorphous carbon, are relatively poor electrical conductors; their contribution to the conductivity of plumes is certainly questionable. Indeed, the possible effect might lie more in the thermionic production of electrons consequent to their reaction with entrained air. (Temperatures in the mixing layer of O_2/RP-1 plumes generally reach about 2400 K at low altitudes, hundreds of degrees hotter than the exhaust at the nozzle exit.) The governing plume parameter in triggering lightning is assumed to be an effective length combined with an effective vehicle body length. The question is how to define an effective plume length with respect to the electrical conductivity.

It is difficult to calculate plume conductivities for two reasons, both related to nonequilibrium effects. Electron densities calculated by means of the Saha equation,[1] which derives from the Boltzmann equation characterizing systems in equilibrium, generally underpredicts the values required to correlate with radar cross sections.[2] This is quite understandable because a rocket exhaust plume exhibits nonequilibrium effects in a number of ways. It is a complex structure involving the flow of gases not generally in local thermal equilibrium, laden with particulate matter, interacting with the atmosphere chemically and kinetically. The directed supersonic velocity of the gases with respect to the vehicle body exceeds the thermal velocities of the exhaust at the nozzle exit, and the overall plume velocity relative to the atmosphere varies from subsonic to hypersonic throughout the flight of a space launch vehicle. Soot concentrations are not calculable with the standard rocket performance codes, which assume complete equilibrated combustion in the chamber and well mixed flow through the nozzle into the exhaust. (Accordingly, for applications of those codes in calculations of infrared emission from plumes, an assumed or empirically determined value of carbon soot mass fraction is assigned.)

There are a number of ways in which an effective plume length can be defined. One method might be the length where the temperature along the axis drops to a specified value. A casual definition might involve the visible length, but this is a highly subjective matter. In visible photography, the apparent length is quite dependent on the exposure. In the photographs to be presented below, the exposures were very short, selected to bring out the interior shock structure. [Actually, had the exposures been sufficient to record the engine hardware in these broad daylight photos, the plume images would have been highly saturated with halation (a blurring or spreading of light around bright areas on a photographic image). Halation is a factor affecting the apparent length.] Visible plume lengths are

[1] The Saha equation provides the degree of ionization, expressible as an electron density, as a function of the temperature, density, and ionization energies of the gaseous constituents, see for example Weinstein's World of Physics, <scienceworld.wolfram.com>

[2] This assertion is based on conversations many years ago with analysts concerned with the cross sections of the exhaust plumes of RF-guided Atlas missiles in the early stages of their development.

also functions of the concentrations of soot that produce most of the visible radiation. (An O_2/ethanol plume on the other hand is virtually invisible in daylight.) However plume lengths are defined, they vary strongly with the engine size, i.e., thrust or mass flow of propellants, and with the nozzle configuration. In the latter regard, the nozzle expansion ratio governs the exit pressure. The maximum propulsive efficiency occurs with the pressure matched to the ambient conditions. In practice, the expansion ratio is optimized for some intermediate altitude in the missile flight. (Off-optimum operation introduces pressure forces, which create the periodic "Mach diamond" structure characteristic of exhausts at low altitudes.) Of course, an engine with multiple nozzles would differ in its attributes from one with a single nozzle. Finally, there is the matter of relating a visible plume length to an effective electrical-conductive length.

All of those complexities contribute to difficulties in making rigorous calculations with available detailed codes for describing rocket engine operation and performance and plume attributes. In fact, simple "scaling laws" are frequently used instead for estimating infrared intensities of missiles for which no direct observations are available.[3] For present purposes, estimates of the visible lengths of the exhaust plumes for several propulsion systems under consideration in this report can be used to illustrate this approach. Since the systems considered here, with one exception, can be expected to exhibit soot in significant mass fractions, visible plume lengths can be estimated by scaling in a manner analogous to the scaling of intensities with thrust. The exception is the propellant combination of ethanol and liquid oxygen, which burns more cleanly, not producing appreciable soot, although the chemistry of the combustion is not that different than for hydrocarbon fuels.[4] These relative thrust-dependent lengths, however, must be considered in the context of other engine design and performance factors being the same. Consequently, the following example is intended to illustrate the process of scaling, not to produce absolute values for use in establishing a triggered-lightning criterion.

Scaling relations were originally developed to relate properties, e.g., infrared (IR) intensities, for unobserved or yet to be developed systems to those that have been observed. Accordingly, intensities can be approximately estimated relative to that of a specific missile selected as a reference case. For illustration, a similar procedure can be used to estimate visible plume lengths. For soot-laden exhausts the visible emission is mostly thermal emission from the carbon particles as they react with entrained air. The apparent length in this case depends on the rate at which the hot carbon particles are consumed. In so doing, use is made of the fact that, other parameters (propellants, mixture ratio, nozzle expansion ratio) being the same, the plume length is proportional to the nozzle throat diameter. Since the thrust under these constraints is proportional to the nozzle throat area, the effective plume length would vary as the square root of the thrust. This thrust-scaling relationship is illustrated in Figure 3-12, which depicts the plumes from static tests of an Atlas booster engine (150,000 lbf thrust) and an Atlas vernier engine (1000 lbf thrust), both operating at an O_2/RP-1 mixture ratio of about 2.4. The photo exposures were selected to emphasize the plume structure. The respective lengths are about 17 and 2 m, based on nozzle exit diameters of 1.2 and 0.1 m. (It should be kept in mind that, at the same mixture ratio, smaller engines are less efficient than larger ones so that the mass fraction of soot would be somewhat greater.[5]) The preceding exercise referred to operations at the same altitude, in this case at sea level. As the ambient pressure decreases, the plume expands to a greater diameter and lengthens accordingly, the length-to-diameter ratio remaining relatively the same, which introduces another complication.

[3] See Chapter 6, [Simmons, 2000].
[4] See Chapter 9, ibid.
[5] See Chapter 10, ibid.

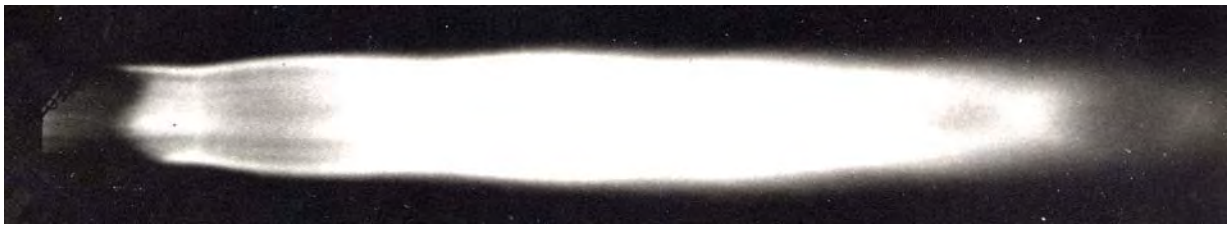

Booster

Vernier

Figure 3-12. Atlas Plumes (not to scale)

Accordingly, Table 3-3 indicates the relative plume lengths to be expected for the propulsion systems considered here, assuming single nozzles in all cases. Of course, further analysis would be needed to establish a relationship between an apparent plume length based on visible emission from soot particles and the possible relation to the electrical conductivity of the plume.

Table 3-3. Estimated Plume Lengths

Vehicle	Propellants	Thrust, lbf.	Vehicle length, ft	Visible plume length, m
Concept 1	O_2/RP-1	23,800	40	6.7
Concept 2	Rubber/N_2O	10,500	21.2	4.4
Concept 3	O_2/RP-1	13,300	24.3	5.0
Concept 4	O_2/ethanol	14,500	23.2	NA
Concept 5	O_2/RP-1	10,,000	18.8	4.3

The above analysis was presented to illustrate the process of scaling as an alternative to a much more complex and not necessarily more dependable procedure using detailed plume codes.[6] The results should not be considered as directly applicable for establishing a launch criterion. If that is to be based in part on an estimate of plume electrical conductivity, then some direct experimental data on that property of exhaust plumes is essential. To the author's knowledge such data does not exist. Experiments to fulfill that requirement should be neither difficult nor expensive. They could be carried out with a model thrust chamber/nozzle assembly capable of handling different propellants, including O_2 with RP-1 as well as ethanol, over a range of mixture ratios. A comparable model for a hybrid motor also should be tested. From such studies a more rigorous definition of an effective electrical plume length could be established and scaling relations developed. Subsequent measurements on full-scale engines in static tests would be required to validate those relations. The personnel of the Aerospace Testing Alliance, the operators of the AF Arnold Engineering and Development Center at Tullahoma, TN, are singularly well qualified and equipped to carry out such experiments. Presumably, such tests could also be conducted at the NASA Glenn Laboratory in

[6] See Chapter 4, [Simmons, 2000].

Cleveland, OH. Finally, those experimental studies should be accompanied by appropriate theoretical analysis. For that, the considerable information on the radar cross sections of plumes in the classified and unclassified literature[7] should be exploited.

3.1.5.4 Estimates of Plume Electrical Lengths

It has been pointed out in the previous section that, although a credible scaling law for exhaust-plume length exists (proportional to the square root of thrust), for various reasons the "paradigm" from which to scale our RLV plumes is not obvious. The examples given in Figure 3-12 were deliberately under-exposed to illustrate the shock structure within those Atlas plumes — quite unlike the nighttime video images of Titan and Shuttle that have been used to estimate the electrical effective length of those vehicles [Frank Merceret, personal communication, January 5, 2004]. Further, there remains the question of how to relate the extent of the visible plume to its conducting extent.

A paradigm that is both more similar to the Titan and Shuttle imagery and closer in scale to the other RLVs under consideration here is a video image from flight #2 of SpaceShipOne (see Figure 3-13). Although this is a daytime image, the apparent brightness gradient at the tip of the plume is large enough that it should be reasonably representative of a comparable nighttime image. (The difference in engine type leads to a difference in visible-plume characteristics — incandescent soot particles for SpaceShipOne vs. incandescent aluminum-oxide particles for the Titan and Shuttle solid rocket boosters (SRBs) — casting doubt on their comparability, but there appears to be no readily available way to avoid this difficulty.)

Figure 3-13. Video image of SpaceShipOne and plume taken from chase aircraft during X Prize flight No. 2. [Photograph reprinted with permission of Scaled Composites, LLC]

We can make use of Figure 3-13 to obtain a crude estimate of the conducting length of the RLV plumes, as follows: Using the dimensions of the Concept 2 vehicle (similar to SpaceShipOne) that were given in Table 3-2, we calculate the length of the visible plume in this image to be about 13 m

[7] e.g., archived at the MDA Advanced Missile Signature Center at AEDC, Arnold Air Force Base, Tullahoma, TN.

— considerably longer than the result obtained in Table 3-3 by scaling from the underexposed Atlas images. Again making use of the scaling law and the thrust values from Table 3-2, we arrive at plume lengths for the other RLVs given in Table 3-4, below. As with Titan and Shuttle, these incandescent lengths are taken as approximately equal to the lengths of the corresponding 1000 F isotherms [Frank Merceret, personal communication, January 5, 2004], which are, in turn, assumed to be roughly equal to the conducting lengths. (We have estimated the length of the Concept 4 vehicle's plume in the same manner, since we expect its thermal structure to scale similarly to that of the other RLVs, even though its plume should be much less visible without significant soot to illuminate it.) Finally, the last column of the table gives the estimated electrical effective length of the entire launch vehicle during boost phase, $H = (D + L)/2$ (D is the vehicle length and L is the conducting length of its exhaust plume), as explained in the next section, 3.1.5.5.

Also included in Table 3-4 are corresponding estimates for the Titan IV. As mentioned above, Titan may not be truly comparable to our RLVs because of the different engine types. For example, the soot particles in the plume of SpaceShipOne (our paradigm taken from Figure 3-13) might have been completely consumed, possibly leading to an underestimate of the conducting length, whereas the aluminum-oxide particles in the Titan and Shuttle plumes probably remained hotter than the surrounding gases, possibly leading to an overestimate. Even admitting these uncertainties, however, it is clear that the electrical effective length of all of the RLVs is much shorter (hence, the ambient electric-field threshold required for triggering is considerably larger) than that of Titan.

Table 3-4. Re-estimated Plume Lengths

Vehicle	Vehicle length, m	Conducting plume length, m	Electrical effective length, m
Concept 1	12.2	29	21
Concept 2	6.5	13	10
Concept 3	7.4	16	12
Concept 4	7.1	18	13
Concept 5	5.5	12	9
Titan IV	60	300	180

One might reasonably ask, "How do the conducting lengths of all of these plumes scale with altitude (or ambient pressure)?" Both the video observations and the models indicate that the Titan and Shuttle plumes do not lengthen significantly between the surface and at least 10 km altitude [Frank Merceret, personal communication, January 5, 2004]. (This is a reasonable upper bound for the height of electrified clouds other than severe thunderstorms, which would not be penetrated in any case.) A probable explanation is that the nozzle expansion ratios were designed for maximum propulsion efficiency at or above 10 km, so that the plumes were overexpanded in that altitude range. Overexpanded plumes remain approximately constant in diameter (and in length) with increasing altitude, rather than expanding (and lengthening) with altitude as they would above their maximum-efficiency altitude. We assume that this is also true of the conceptual RLVs under consideration here, so we neglect any altitude dependence of the electrical effective length.

3.1.5.5 Pulling It All Together: Triggering Conditions

We have selected a model that relates the overall length of a long, thin conductor at any given altitude to the ambient-field intensity required to trigger lightning (see Sections 3.1.2.1 and 3.1.3). We have defined the physical dimensions of the concept RLVs themselves (Section 3.1.5.1) and estimated the conducting lengths of their exhaust plumes during boost phase (Section 3.1.5.4). We are therefore in position to estimate the ambient fields required to trigger lightning by each of these vehicles at any given altitude. First, however, some further discussion is required of the concept of an electrical effective length.

In validating our chosen triggering model against available data on lightning strikes to instrumented aircraft (Section 3.1.2.3), we used 1/2 the maximum aircraft dimension as the effective length, H, in Equation 4, based on the assumption that these aircraft were uncharged (which was actually incorrect in those cases). The factor of 1/2 comes from that fact that a long, thin, uncharged conductor of length, D, oriented parallel to a uniform, ambient, electrostatic field, E_0, will "float" to the ambient potential at its center. Thus, the difference between the potential of the conductor and the ambient potential near either extremity is $E_0D/2$. (This is in contrast to classical rocket-triggered lightning, where the lower end of a vertical triggering wire of length, H, is grounded and the ambient potential difference at its tip is therefore E_0H, with no factor of 1/2.)

The potential of an airborne vehicle will not remain fixed, however, during the initiation of an upward positive leader from its tip. The leader will increase the overall conducting length of the vehicle-leader system (although it will still remain net uncharged), effectively increasing the altitude of the ambient potential to which the whole conducting system floats (at least until a negative leader begins to propagate from its opposite extremity). Thus, such a floating vehicle will be even less than half as effective at triggering as a grounded wire of the same length (which always remains fixed at ground potential).

Extending this argument to a spacecraft during the boost phase involves additional complexities. First, the electrical length of the spacecraft is normally assumed to be the sum of the vehicle length, D, and the conducting length of its exhaust plume, L. Thus, the total effective length for triggering would be $(D + L)/2$. Second, the rocket engine might not be electrically passive but might act to charge the vehicle/ plume system inductively, for example, like a water-dropper or a flame potential equalizer. Perala et al. [1994] have made this assumption, asserting that the trailing end of the conductive plume acts as a potential equalizer, which charges the conducting part of the system in such a way that the longitudinal electric field vanishes there and the lower extremity of the conducting plume is anchored at the local ambient potential. If this is the case, the effective length would be $D + L$, without the factor of 1/2. Third, the engine might actively charge the system in one polarity or the other by charge transfer due to triboelectrification of particles in the exhaust or to chemical processes associated with the combustion (see below).

It can be questioned, however, whether any of the above effects of the exhaust plume can compete with current input from a positive leader initiating from the tip of the vehicle. Nanevicz and Hilbers [1973, p. 40] deduced from precipitation-charging measurements on an instrumented Titan IIIC (although with a completely different type of engine from the RLVs of present interest) that the exhaust plume was capable of discharging about 310 μA of negative charge without an appreciable rise in vehicle potential. Nevertheless, a positive leader would supply a current of a few amperes (based on measurements in rocket-triggered lightning), which would probably overwhelm the potential-equalizing capabilities of the exhaust plume, returning us to the situation of the flying

aircraft, described above. At best, the exhaust nozzles themselves might become the effective potential equalizer, reducing the electrical effective length of the flying system to *D*.

Nanevicz and Hilbers [1973, p. 31] also concluded that the Titan engines *do* actively charge the vehicle, but only between the altitudes of about 650 ft. (where the plume was taken to disconnect from ground) and 12,000 ft. (where the vehicle self-charge had returned to essentially zero). The vehicle charge was observed to saturate (producing a self-potential of –200 kV — presumed to be the corona threshold — in a near-zero ambient field) between about 1400 and 2500 ft altitude. Nevertheless, this negative charging current was estimated to be only 100 μA. Again, we assume here that the leader current would overwhelm such a small charging current.

An additional consideration is the polarity of the ambient field with respect to the vehicle trajectory. We have tacitly assumed that the launch is occurring in a field of foul-weather polarity, so that a positive leader would be initiated (if at all) at the nose of the vehicle. Once a space vehicle has encountered a high field of one polarity, however, it is likely to also penetrate a high field of the opposite polarity. Little or nothing is known about initiation and/or propagation conditions within the exhaust plume for a leader of either polarity. The only thing that might help us here is the assumption that the rocket exhaust acts as a potential equalizer, tending to limit or eliminate the electric field near the conducting end of the plume. The first stage of the triggering process would then have to be the initiation of a leader from the nose of the vehicle. In foul-weather fields, this would be a positive leader, as assumed throughout this report. In fair-weather fields, it would be a negative leader, which would require a substantially stronger field to propagate [e.g., Lalande et al., 2002, Fig. 19]. Thus, the field required to sustain a positive leader should constitute a lower bound on the triggering field for arbitrary vehicle orientation.

More research is clearly needed on the conductivity distribution in real exhaust plumes, and on the effects of this distribution (and other plume dynamics) on the vehicle potential as a function of leader current. Meanwhile, we will assume for present purposes that the electrical effective length of the vehicle/plume system is $H = (D + L)/2$. The actual effective length might range from less than $D/2$ to as large as $D + L$, however, so it seems prudent to assign an extreme range of at least [–67%, +100%] to this parameter. (For our RLVs Table 3-4 suggests that $L \sim 2D$.)

Using the values of *D* from Table 3-2 and of *L* from Table 3-4 to compute *H* for each RLV during boost phase, for insertion into Equation 4, and also using the crude altitude dependence of the triggering field proposed in Section 3.1.3, we estimate the triggering thresholds listed in the second and third columns of Table 3-5. Note, however, that this approach clearly does not apply to the da Vinci spacecraft, which is designed to be lofted above 24 km (hence, through any electrified clouds) by a large balloon.

Table 3-5. Estimated Triggering Fields

Vehicle	Boost Phase		Glide Phase	
	Surface, kV/m	10 km, kV/m	Surface, kV/m	10 km, kV/m
Concept 1	60	20	125	42
Concept 2	93	31	182	61
Concept 3	83	28	169	56
Concept 4	79	26	—	—
Concept 5	—	—	—	—
Titan IV	16	5	—	—

During the glide phase of the flight (i.e., on landing), the exhaust plume is not an issue for most vehicles, so the electrical effective lengths are correspondingly shorter. For the fourth and fifth columns of the table we have used $H = D/2$ in Equation 4 to determine the triggering thresholds. Note, however, that this approach probably does not apply to the fourth concept vehicle, which is designed to land vertically, breaking first with a parachute and then with thrust from its rocket motor, nor to the balloon-launched concept vehicle (Concept 5), which is designed to parachute to the ground.

The length of the conducting portion of the plume, *L*, is rather uncertain, but we assume the effect of this to be included in our nearly factor-of-two uncertainty in *H*, discussed above. Further, our model for the triggering field as a function of *H* is probably uncertain over an extreme range of about ±60%: Note, for example, the differences between the Bazelyan and Raizer model and the Lalande et al. model, as well as the scatter in the aircraft data, that are illustrated in Section 3.1.2.

Finally, the altitude dependence is poorly known, as discussed in Section 3.1.3. For example, if we assume that the triggering fields measured on aircraft (see Table 3-1) are correct at their typical altitudes of 4–5 km, and if the pressure dependence is actually much weaker than we have assumed, the deduced triggering fields could be smaller than indicated at the surface or larger than indicated at 10 km. Thus the the triggering field could vary over an extreme range of [−40%, +0%] at the surface and [–0%, +70%] at 10 km because of uncertainty in the altitude dependence. The results of the Russian study mentioned earlier may help clarify this uncertainty.

Combining all of these individual uncertainties on the assumption that they are statistically independent suggests overall extreme ranges for the triggering field of [–94%, +72%] at the surface and [–85%, +100%] at 10 km, not that we really expect the results to stray this far from the estimates in Table 3-5.

For purposes of comparison, the triggering field for Titan (see Table 3-4) has been estimated by the same method and entered in the last row of Table 3-5. Notice that it is smaller than that of the largest RLV (Concept 1) by a factor of 3.6. Note also that, although individual triggering fields in this table are quite uncertain, their ratios are much more reliable, since they are all affected in the same way by most of the uncertainties. Thus, we can say with reasonable certainty that all of these RLVs are considerably less prone to trigger lightning than Titan.

3.2 Relevancy of Existing LLCC to Proposed RLV Concepts

3.2.1 Cloud Electrification

On May 10, 1752, a retired French dragoon, acting on instructions from Thomas-Francois Dalibard, drew sparks from a 40-foot iron rod that had been carefully insulated from the ground when a thundercloud passed overhead. This experiment had been suggested by Benjamin Franklin and had been set up at the village of Marly-la-Ville, near Paris, to determine whether clouds that produce lightning are electrified or not [Cohen, 1990, Chapter 6]. These sparks proved for the first time that thunderclouds contain electricity and that lightning is an electrical discharge. A few weeks later (but before he knew about the results at Marly-la-Ville), Franklin performed his famous kite and key experiment (electrically equivalent to the experiment at Marly-la-Ville), and in September he installed a tall rod on the roof of his house to study the characteristics of storm electricity. This rod had a gap where he could observe, and chimes were mounted on each side of the gap (see Figure 3-14). The upper portion was carefully insulated from the house, and the lower portion ran down a stairwell and was connected to a well. A small ball was suspended on silk thread between the chimes, so that it

would ring the bells whenever the rod became electrified. The purpose of all this was to study the characteristics of storm electricity and to determine whether the electricity in thunderstorms was the same as the electricity that was generated by friction. Franklin described the results of his observations as follows:

> "I found the bells rang sometimes when there was no lightning or thunder, but Only a dark cloud over the rod; that sometimes after a flash of lightning they would suddenly stop; and at other times, when they had not rung before, they would, after a flash, suddenly begin to ring; that the electricity was sometimes very faint, so that when a small spark was obtained, another could not be got for sometime after; at other times the sparks would follow extremely quick, and once I had a continual stream from bell to bell, the size of a crow-quill. Even during the same gust there were considerable variations." [Labaree et al., Vol. 5, 1962, p. 62]

Franklin also used this apparatus to measure the polarity of thunderclouds, and he summarized those observations as follows:

> "…that the clouds of a thunder gust are most commonly in a negative state of electricity, but sometimes in a positive state." [Labaree et al., Vol. 5, 1962, p. 71]

This short description of storm electricity remained the state of the art for the next 150 years [Schonland, 1950, p. 22], and Franklin's observations underscore several factors that are important for the FAA Lightning Flight Commit Criteria: (1) clouds can be highly electrified and not produce natural lightning; (2) lightning often appears with little advance warning; (3) lightning can both create and destroy cloud electricity; and (4) the amount and polarity of the electric fields aloft are highly variable both within a storm and from storm to storm.

Figure 3-14. The apparatus that Benjamin Franklin used to study cloud electricity. [Courtesy, E. Philip Krider, private collection, reprinted with permission]

In the following, we will give a brief review of what is known today about the electrical structure of thunderclouds, and then we will summarize the mechanisms that have been proposed to explain this electrification. Since space is limited, we will cite just a portion of the relevant literature, but we will try to emphasize the work in New Mexico and Oklahoma. Readers who are interested in more details should consult Mason [1971, Chapter 9], Latham [1981], Illingworth [1985], NAS [1986, Chapters 7–10], Williams [1988], Saunders [1988], Black and Hallett [1998], and MacGorman and Rust [1998] and the references cited therein.

3.2.1.1 Observations

Since the work of Franklin, there have been numerous *in situ* and remote measurements of the electrical structure of thunderclouds. Most *in situ* measurements have been of the cloud electric field, E, and E-field sensors have been carried into clouds on balloons, aircraft, and rockets. The remote measurements have typically been of lightning and/or the changes in the electric field that are caused by lightning.

3.2.1.1.1 *In situ* Measurements

Figures 3-15 and 3-16 show the results of balloon soundings of the vertical electric field inside a small thunderstorm in New Mexico [Byrne et al., 1983] and a larger storm in Oklahoma [Stolzenburg et al., 2002], respectively. In each of these figures, the average volume charge density can been estimated from the rate that the field increases (positive) or decreases (negative) with height, assuming that the cloud charges are horizontally stratified and constant with time. These soundings are consistent with the classic tripole model of the thundercloud charge distribution, i.e., negative charge is concentrated at altitudes that are above (i.e., colder than) the freezing level (0ºC), a larger volume of positive charge is at higher altitudes, and a small region of positive charge is at lower altitudes [Williams, 1989]. The sketch in Figure 3-16 shows a more complicated charge structure that depends on the cloud dynamics, but there is still negative charge at altitudes where the cloud temperature is between –5ºC and –20ºC, and there are layers of positive charge both above and below that region.

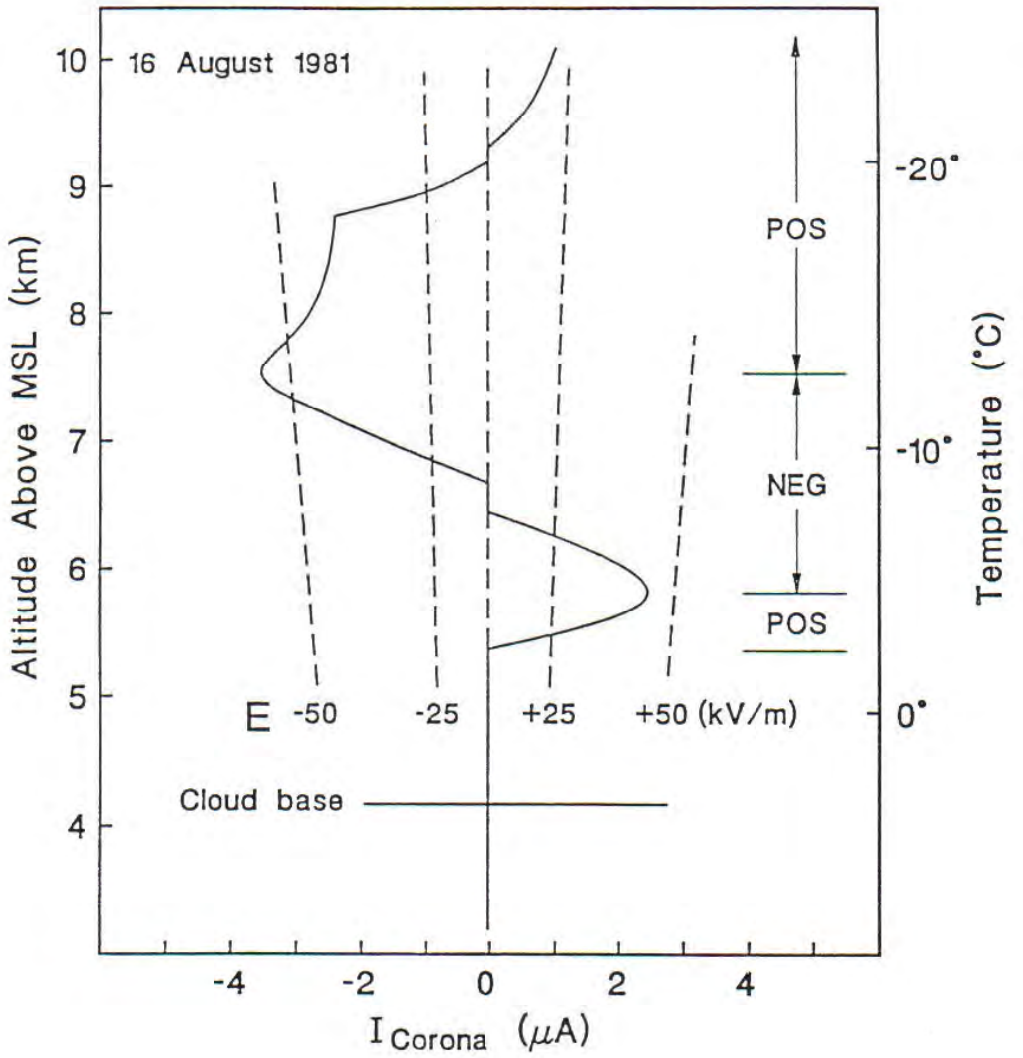

Figure 3-15. Balloon measurements of corona current and the inferred vertical electric field, E, vs. altitude and air temperature inside a small thunderstorm in New Mexico. Charge regions are labeled positive (pos) or negative (neg) on the right. The total time to acquire the record above cloud base was about 11 minutes. [Adapted from Byrne et al., 1983]

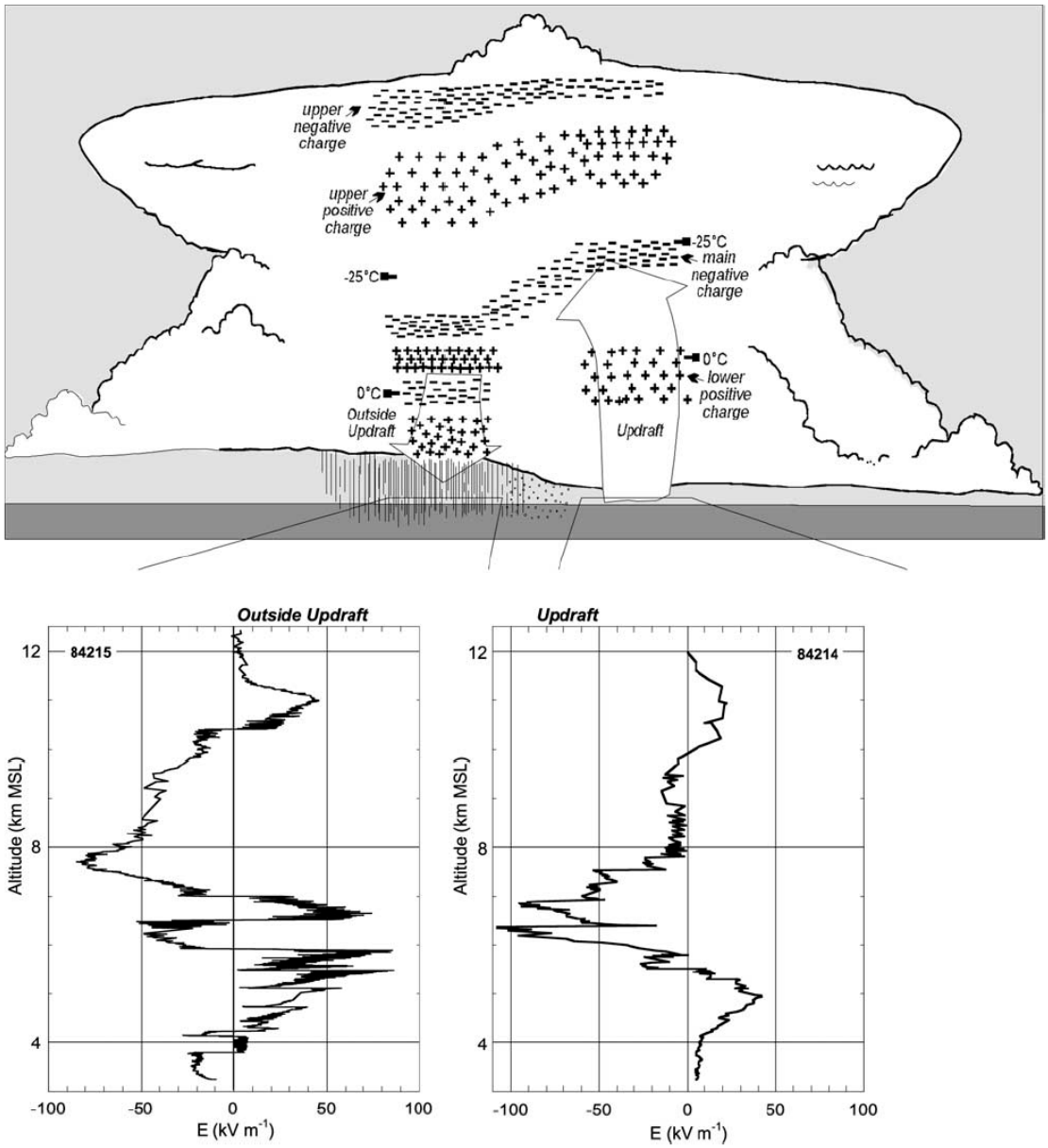

Figure 1. Basic conceptual model of the charge structures within and outside the updraft of thunderstorm convection, and an electric field (E) sounding representative of each charge structure. The updraft has four main regions of charge and a relatively simple E profile. Outside the updraft there are six main region of charge, and the E profile is more complicated at and below middle levels in the cloud. Adapted from *Stolzenburg et al.* [1998a].

Figure 3-16. Model of Charge Structures [Adapted from Stolzenburg et al., 2002]

Figure 3-17 shows an aircraft sounding of the horizontal electrical field, i.e., the field parallel to the axis of the airplane, and the cloud microphysics inside a small thunderstorm in New Mexico [Dye et al., 1988, 1992], and Figure 3-18 shows the aircraft trajectory superimposed on the cloud radar reflectively [Dye et al., 1992]. The electric field in Figure 3-17 is consistent with the cloud having a concentrated volume of negative charge centered (the open circle in Figure 3-18) near a region of moderate radar reflectively (> 25 dBZ), where the air temperature is about –12 ºC. The liquid water content (LWC) of the cloud is of the order of 1 gram per cubic meter in this region, and there is also a high concentration of ice crystals (and supercooled water drops) and a high ice-particle collision frequency per unit volume (see Figure 3-17).

3.2.1.1.2 Measurements Outside the Cloud

Today we know that measurements of cloud electric fields, both at the surface (like Benjamin Franklin's) and aloft, can be strongly affected by "screening layers," or the space charge that accumulates on conductivity gradients in the atmosphere, especially near the ground and at the boundaries of the cloud [Holzer and Saxon, 1952; Kasemir, 1959; Brown et al., 1971; Hayes and Roble, 1979]. In order to avoid this problem, Workman and Holzer [1939, 1942], following a suggestion by C. T. R. Wilson [1920], used multiple-station measurements of lightning-caused changes in the electric field (ΔE) to infer the locations and magnitudes of the changes in the cloud charge that are caused by lightning. More recently, Krider, Krehbiel, and their co-workers [Jacobson and Krider, 1976; Krehbiel et al., 1979; Maier and Krider, 1986; Krehbiel, 1986; Koshak and Krider, 1989; Krider, 1989; Murphy et al., 1996] have made similar measurements with more sensors and more sophisticated analysis techniques. If one assumes that a lightning discharge to ground (or one of its component strokes) deposits a charge that, to first order, is spherically symmetric, e.g., a single point charge, Q, or, in the case of a cloud discharge, a point-dipole, P, then the parameters of such a distribution can be inferred by fitting the ΔE measurements to the model. The analysis begins by assuming the simplest model, i.e., a model with the smallest number of unknown parameters, and then a search is made for the model parameters that minimize (in a least-squares sense) an error function involving those parameters and the measured ΔEs. If the minimum in the error function is small and consistent with the expected measurement errors, the search procedure stops and the parameters are regarded as valid. If the error is large, then the search can be repeated using a more complex charge model (i.e., more parameters), and if necessary there can be additional searches, until a satisfactory fit is obtained. The inferred charge parameters will never be unique, of course, but if the error function is small and if the parameters are physically reasonable, the solutions are usually regarded as valid.

Figure 3-19 shows the results of fitting two simple charge models to the field changes produced by lightning during a small (left) and a large (right) thunderstorm at the NASA Kennedy Space Center [Krider, 1989]. The open circles show the locations of point charge solutions (Q-model) that describe the field changes produced when cloud-to-ground (CG) flashes remove negative charge from the cloud (or equivalently deposit positive charge). The arrows (or P-vectors) show the locations and magnitudes of point-dipole fits to field changes produced by cloud discharges. It should be noted in Figure 3-19 that all P-vectors at high altitude point downward and those at low altitude point upward. When a P-vector is located at an altitude that corresponds to the negative charge region (the Q-solutions), it tends to be horizontal. This symmetry is consistent with the classic tripole model of the cloud charge distribution (see Section 3.2.1.1.1), i.e., a concentration of negative charge at subfreezing temperatures in the central part of the cloud with a larger volume of positive charge at higher altitudes. The P-vectors at low altitudes are caused by cloud discharges between the lower positive charge region and the central negative region. Again, it should be noted that the inferred Q-region (negative charge) is centered where the ambient air temperature is between –10ºC and –20ºC,

and the spatial separation between the negative and upper positive regions depends on the size and intensity of the storm.

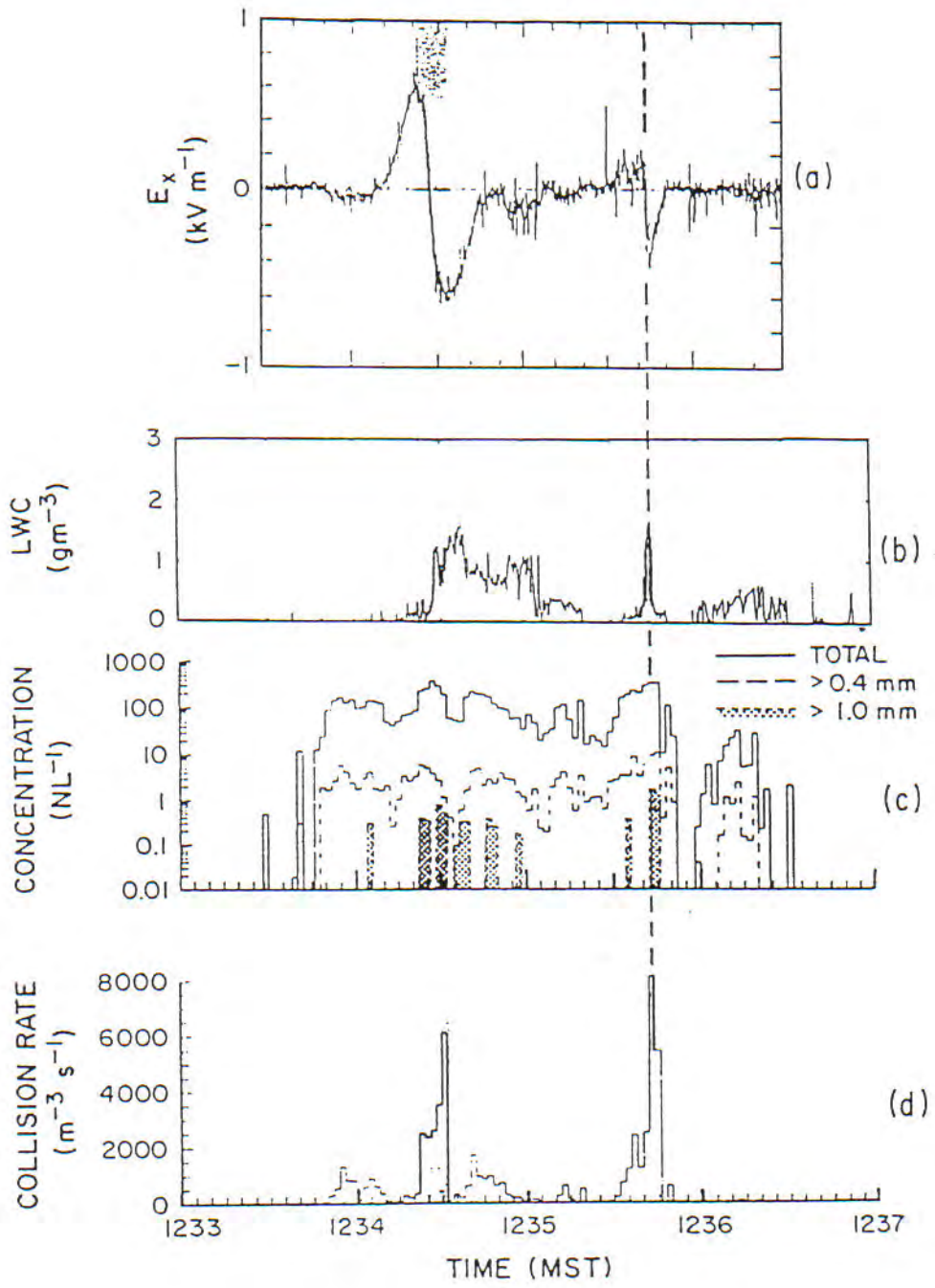

Figure 3-17. Aircraft measurements of (a) the horizontal component of the electric field inside a New Mexico thunderstorm, (b) the cloud liquid water content, LWC, (c) the average ice particle concentrations at various particle sizes, and (d) the total ice-particle collision rate per unit volume. The faint vertical shading and dashed vertical line show the locations of two regions of net negative charge. [Adapted from Dye et al., 1992]

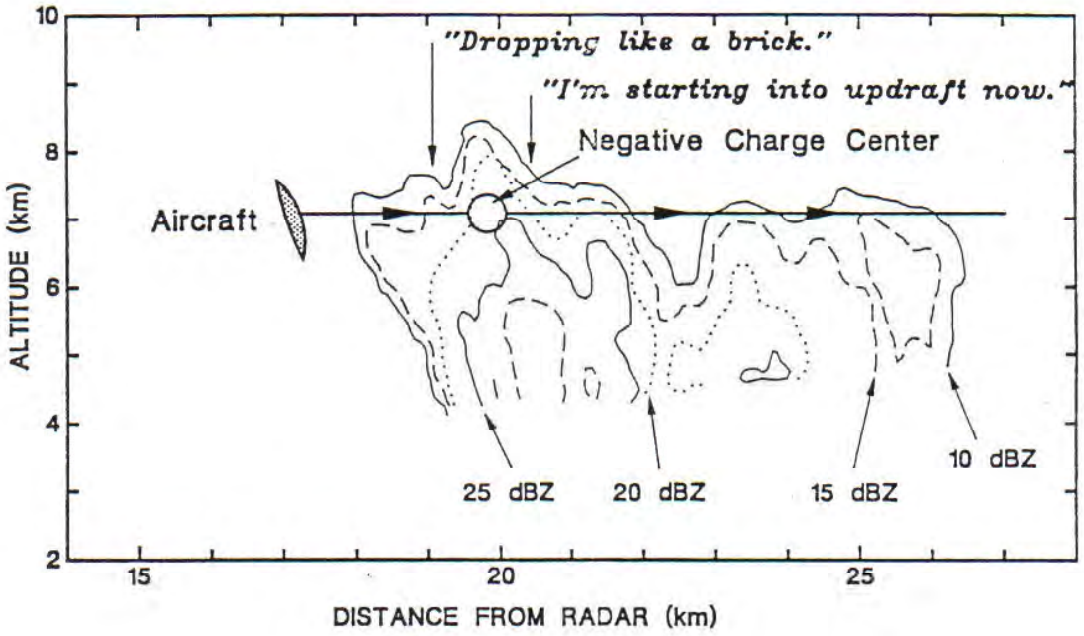

Figure 3-18. The cloud radar reflectivity and aircraft track for the storm shown in Figure 3-17. An inferred region of negative charge is shown (circle) together with voice comments from the pilot. [Adapted from Dye et al., 1992]

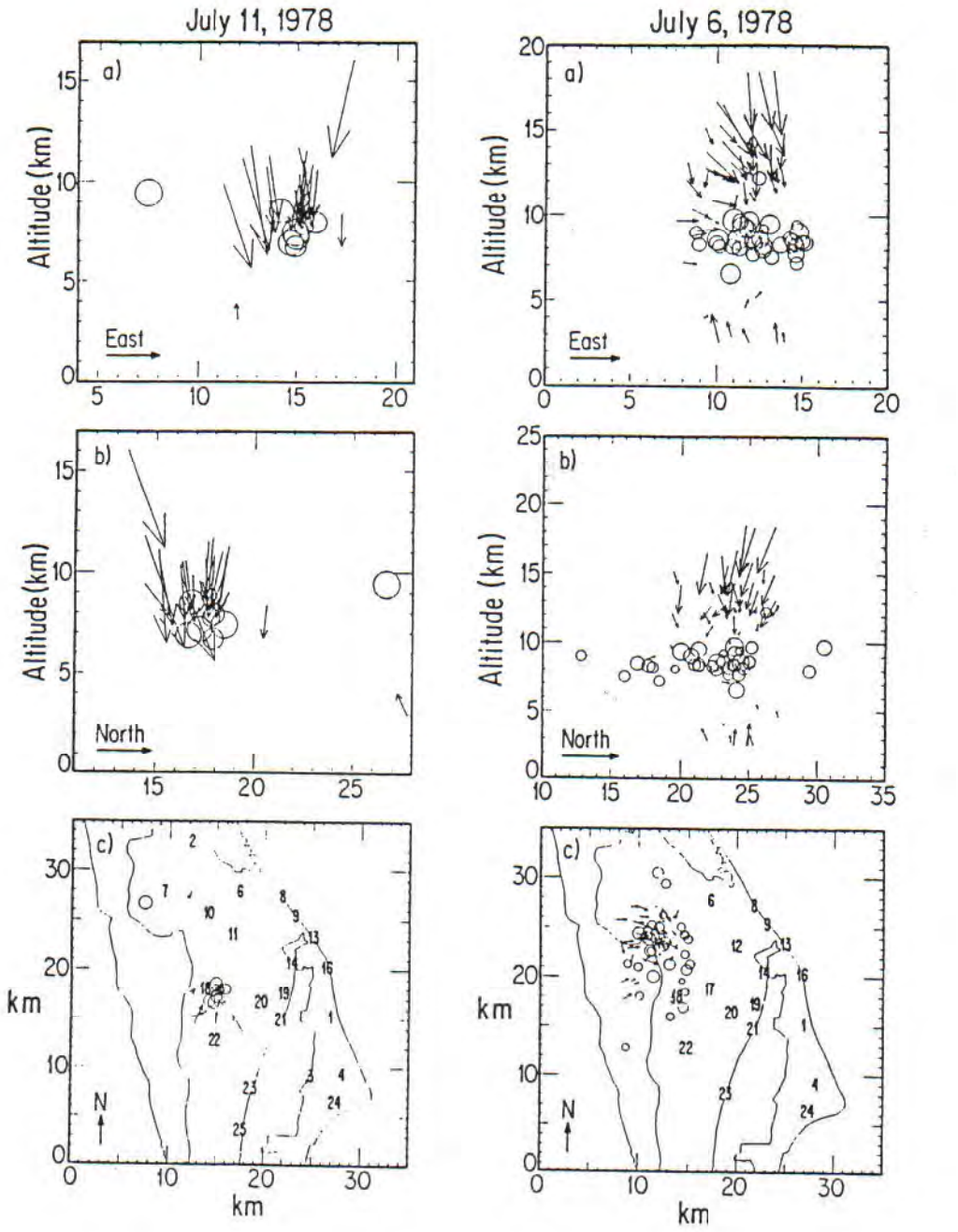

Figure 3-19. Three views of lightning-caused changes in thundercloud charge distributions. The changes caused by the cloud-to-ground flashes (open circles) and intracloud discharges (arrows) in a small storm (left) show a compact cluster of flashes, and the changes during a portion of an active storm (right) show a larger separation between the inferred negative and the upper positive charge regions. [Adapted from Krider, 1989]

Studies of lightning field changes in New Mexico and Japan have found results similar to those shown in Figure 3-19 and are summarized in Figure 3-20. Note how the inferred negative charge region is close to the –10ºC to –20ºC temperature level regardless of where the storm (and the 0ºC level) is located. [Note: The –10ºC to –20ºC region is where convective clouds contain both supercooled water droplets and ice crystals [Mason, 1971].]

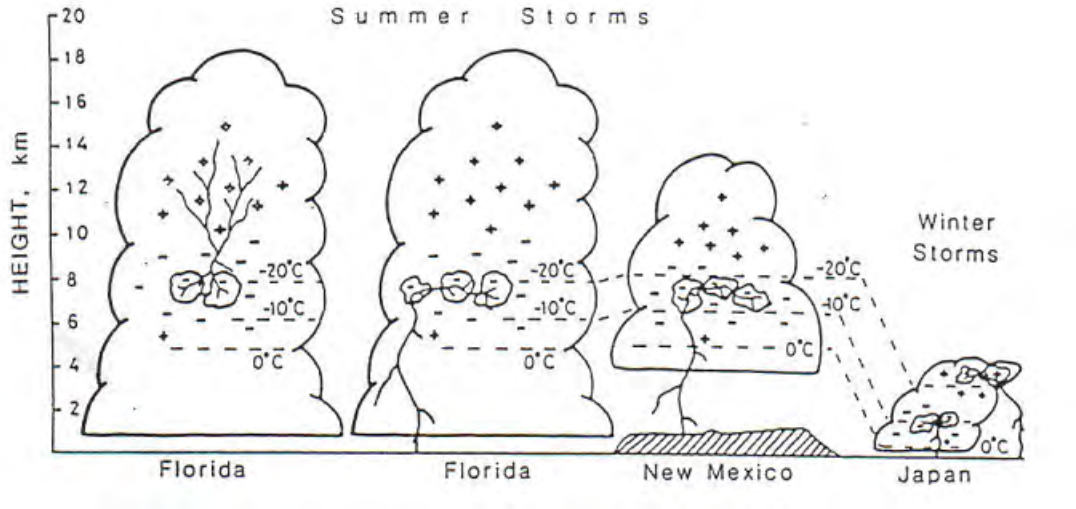

Figure 3-20. Sketches showing the altitudes of the cloud charges in different geographic locations as inferred from analyses of lightning field changes. Note that the temperature levels at which the negative charge accumulates are similar in a wide variety of storm types. [Adapted from NAS, 1986, Chapter 8]

3.2.1.1.3 LDAR/LMA Lightning Mapping Systems

In recent years, VHF lightning mapping systems that are termed the Lightning Detection and Ranging (LDAR) systems or Lightning Mapping Arrays (LMAs) have been developed to detect and locate the sources of VHF radio impulses produced by lightning and to trace how these sources evolve in both space and time [Proctor, 1971; Rison et al., 1999; Krehbiel et al., 2000; Boccippio et al., 2001a and 2001b; Thomas et al., 2001; Thomas et al., 2004]. The VHF emissions are measured at multiple stations with precise time-synchronization, and the source locations are computed using time-of-arrival techniques. LMA systems can trace the geometrical development of lightning channels with a time-resolution of 100 μs or less and a spatial accuracy of a few tens of meters [Thomas et al., 2004]. Currently, LMA systems are operating in both New Mexico and Oklahoma, and in the future we expect that these systems will be extremely valuable for insuring flight safety in those regions.

An important feature of LMA technology is that the amplitude and spatial pattern of the VHF sources can also be used to infer the location and polarity of the charge regions in which the sources originate [Thomas et al., 2001]. The VHF radiation produced by negative polarity breakdown processes is about 10 times larger than the radiation produced by positive breakdown; therefore, the LMA systems detect more pulses above the detection threshold when positive regions of cloud charge are “tapped” by negative breakdown than when the negative regions are being tapped by positive breakdown. Examples of the VHF sources produced by an intracloud lightning discharge between the central negative charge region and the upper positive region in a New Mexico storm are shown in Figure 3-21 (left), and a CG discharge that started inside the cloud near the central negative region and then went to ground via the lower positive charge center is shown in Figure 3-21 (right).

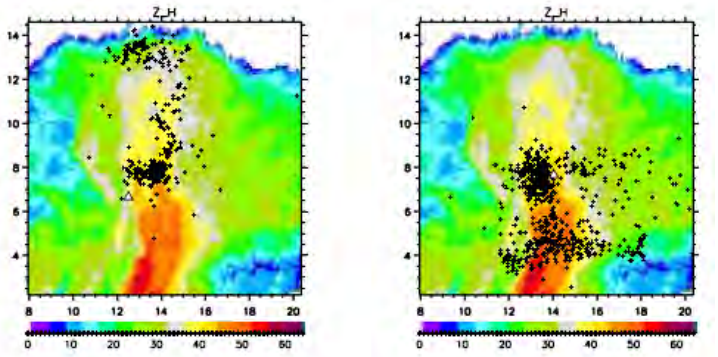

Figure 1. VHF radiation sources for an intracloud discharge (left) and a cloud-to-ground discharge (right), overlaid on a vertical radar scan through the discharges for a storm on August 2, 1999. Distances are in km above mean sea level and away from the radar, respectively. The intracloud discharge occurred at 21:06:20, 16 seconds before the radar scan. The cloud-to-ground discharge occurred at 21:08:10. The triangles denote the initial radiation event for each flash.

Figure 3-21. Maps of lightning VHF radiation taken from [Thomas et al., 2001]

3.2.1.1.4 Severe Thunderstorms and Supercells

The electrical structure of large, severe thunderstorms and supercells presents a difficult challenge for experimenters, but it is of considerable interest to forecasters and to the public at large [Lang et al., 2004]. One aspect of these storms that is still not understood is their tendency to occasionally produce large numbers of positive cloud-to-ground (CG) flashes compared to the normal, warm-season thunderstorms we have been discussing. In a typical summer thunderstorm, 90% or more of the CG flashes transfer negative charge from the central region of the cloud to ground, but sometimes large storms produce predominantly positive CG (PPCG) flashes, sometimes approaching 100% [Krehbiel et al., 2000; Rust and MacGorman, 2002]. A recent effort to understand better the microphysical and dynamical processes that lead to PPCG storms has been described by Lang et al. [2004].

3.2.1.1.5 Electrical Structure of Disturbed Weather, Stratiform Clouds, and Anvils

The electrical structure of disturbed weather and stratiform clouds has received relatively little attention compared to cumulus clouds and thunderstorms, even though the electric fields in such clouds are often very large. Simpson [1949] has given what is still today the best description of the variations in the surface electric field (or potential gradient) that are caused by disturbed weather in the United Kingdom. Clouds that produce steady rainfall are characterized by elevated fields that undulate between positive and negative polarities in a wavelike fashion for 90 minutes or more. Shower clouds often exhibit high fields, like thunderstorms, but without the abrupt transitions that are caused by lightning. Balloon soundings of the electric field inside winter nimbostratus clouds in the U.S. show vertical fields of 1 to 12 kV/m and horizontal fields ranging between 0.2 and 28 kV/m [Rust and Trapp, 2002].

Figure 3-22 shows a sketch of the geometry of a typical mesoscale convective system (MCS) in the Midwestern U.S. Here, it is clear that the threat posed by the trailing stratiform region of MCSs to flight operations will extend over a much larger distance (and for a longer time) than a typical thundercloud.

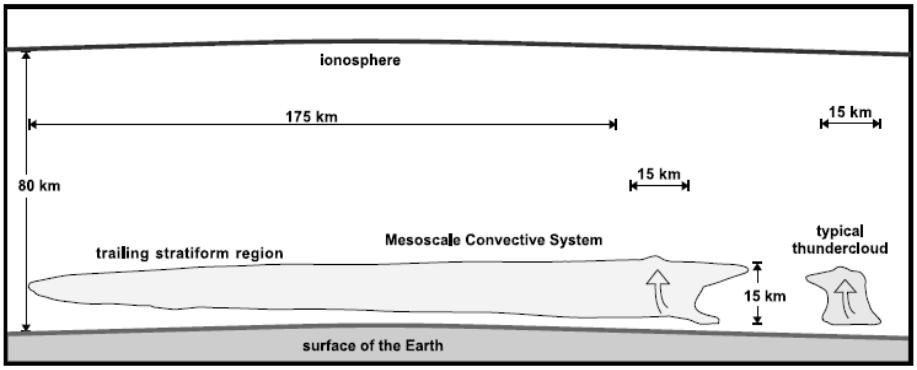

Figure 1. Schematic depiction of a typical isolated thunderstorm and a typical MCS drawn to scale. The curved surface of the Earth and the typical height of the ionosphere are also shown (to scale). The drawing illustrates the fact that the horizontal scale of the MCS is about 10 times that of the isolated storm and about twice the distance from the Earth's surface to the ionosphere.

Figure 3-22. Sketch of the geometry of MCS relative to a typical thunderstorm. [Davydenko et al., 2004]

Balloon soundings of the electric fields in the convective region of MCSs are generally similar to the soundings in normal, warm-season thunderstorms but with more structure [see Stolzenburg et al. [1998a,b,c and 2002]. Soundings in the trailing stratiform region by Schuur et al. [1991], Stolzenburg et al. [1994], Shepherd et al. [1996], Marshall et al. [2001], Stolzenburg et al. [2001], and others are summarized in Figure 3-23. The electric fields in the trailing stratiform region are large, and such clouds are often associated with lightning flashes that propagate horizontally tens to hundreds of kilometers [Mazur et al., 1998; Marshall, 2000], sometimes producing multiple ground contacts along the way.

12,372 STOLZENBURG ET AL.: SERIAL SOUNDINGS THROUGH AN MCS

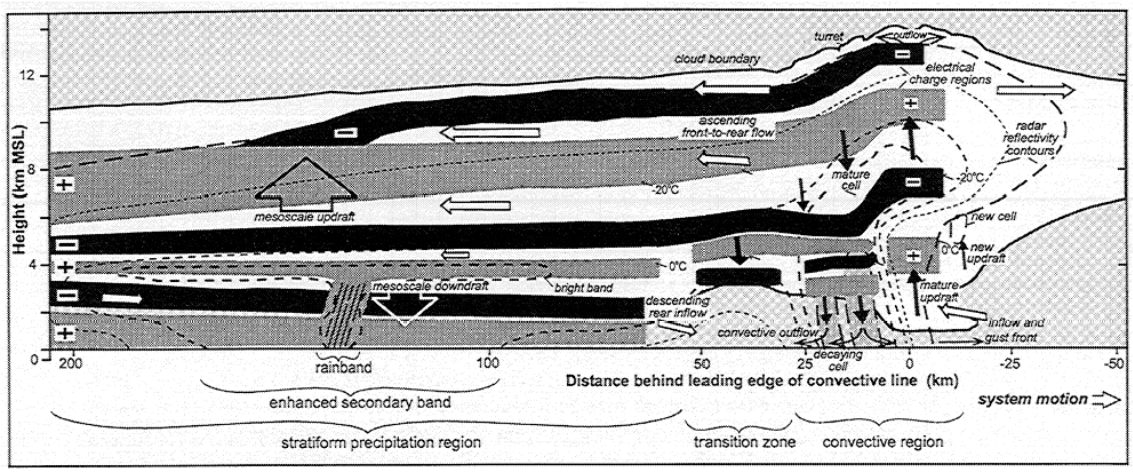

Figure 1. Conceptual model of the charge structure in an idealized mesoscale convective system from *Stolzenburg et al.* [1998a]. Positive charge regions have light shading and negative charge regions have dark shading. Solid and open arrows depict the convective scale vertical motions and the mesoscale, system-relative airflows throughout the system, respectively.

Figure 3-23. Sketch of the charge structure of an ideal MCS [Stolzenburg et al., 2001].

Marshall et al. [1989] and Byrne et al. [1989] have made balloon soundings of the electric field inside thunderstorm anvils, and they find fields in excess of 50 kV/m for long periods of time. Because anvils often cover large areas for long times, this cloud type can significantly affect launch and flight operations.

A comprehensive dataset on the electrical and microphysical structure of thunderstorm anvil and debris clouds has been assembled in two Airborne Electric Field Measuring (ABFM) campaigns near the NASA Kennedy Space Center, Florida. The second ABFM project has been summarized by Dye and Lewis [2004a], and a copy of that Summary is included as Appendix A. The complete Final Report by Dye and Lewis [2004b] is available on a restricted Web site at http://box.mmm.ucar.edu/abfm/webpage/Reports/Reports.html together with several other valuable reports and conference presentations.

The main purpose of the ABFM campaign was to measure the radar reflectivity of both attached and detached anvil clouds, in conjunction with *in situ* electric fields and the microphysical composition of the clouds, all as a function of time. The results show that anvils with a high radar reflectivity usually contain high electric fields, and conversely, anvils with a low reflectivity (and no internal cells of convection) are usually electrically benign.

The electrical structure of thunderstorm debris clouds that do not produce lightning has been studied by Marshall and Lin [1992] and by the ABFM campaign cited above. Marshall and Lin found that the electric fields remained high, 35 kV/m and 71 kV/m, inside debris clouds for at least 20 minutes after the last lightning flash.

3.2.1.2 Mechanisms of Electrification

In order for a cloud to become electrified over spatial scales on the order of kilometers, there must be two types of processes — first, there must be a small-scale process that electrifies the individual cloud particles and/or elements of precipitation, and second, there must be another, large-scale process that separates these charges, preferentially according to their polarity, by distances of the order of kilometers. Since the water droplets and/or ice crystals that are present at the cloud boundaries will become electrified when atmospheric ions attach to their surfaces, some investigators believe that the organized motion of the cloud screening layers by the cloud dynamics will produce a large-scale separation of the charge [Vonnegut, 1991; Moore et al., 1992]; however, today most investigators believe that the large-scale process is dominated by precipitation. For example, if collisions between the cloud hydrometeors separate charge, and if this separation causes the larger particles to have a charge of predominantly one polarity, then because the larger particles will fall faster with respect to cloud air than the oppositely charged, small particles, precipitation will ultimately cause a large-scale separation of charge.

Many mechanisms have been proposed for the small-scale process that, when acting in conjunction with precipitation, will electrify a thundercloud. Some mechanisms depend on, or are enhanced by, the presence of an external electric field (via electrostatic induction) [Mason, 1988], and others, the so-called “non-inductive processes,” do not involve an external field. In 1957, Reynolds and co-workers [Reynolds et al., 1957] showed that when a simulated hailstone was rotated in an artificial cloud containing both ice crystals and supercooled water drops, the hailstone acquired a negative charge that was sufficient to explain the electrification of thunderclouds. Subsequent experiments by other investigators under a wide variety of conditions [Takahashi, 1978; Jayaratne et al., 1983; Williams et al., 1991; Saunders et al., 1991; Takahashi and Miyawaki, 2002; and Evila et al., 2005] have found similar results, so today most investigators believe that the dominant small-scale

mechanism is a non-inductive process involving collisions between soft hail or graupel particles and ice crystals, in the presence of supercooled water drops [see, for example, Williams, 1988; Saunders, 1988; Black and Hallett, 1998; and MacGorman and Rust, 1998].

3.2.1.2.1 Non-Inductive Ice-Ice Collisions

Laboratory experiments show that the charge acquired by a simulated hail or graupel particle undergoing collisions with ice crystals (in the presence of supercooled water drops) is a function of the size of the crystal, the velocity of the collision, the temperature of the hail, and the liquid water content (LWC) of the cloud [Takahashi, 1978; Saunders et al., 1991; Takahashi and Miyawaki, 2002]. When the hail temperature is below a so-called "reversal temperature," typically around –10ºC at moderate values of LWC, the charge acquired by the hail is negative. When the temperature of the hail is warmer than the reversal temperature, it charges positively, as shown in Figure 3-24. The reversal temperature is also a function of the cloud LWC (see Figure 3-25), and computer models show that a non-inductive charging mechanism involving ice-ice collisions can indeed produce charge distributions that are consistent with both the *in situ* and remote measurements of thunderstorms in New Mexico and Oklahama that are discussed in Sections 3.2.1.1.1 to 3.2.1.1.5 [Baker et al., 1995, 1999; Ziegler et al., 1991; Ziegler and MacGorman, 1994; Helsdon et al., 2001, 2002].

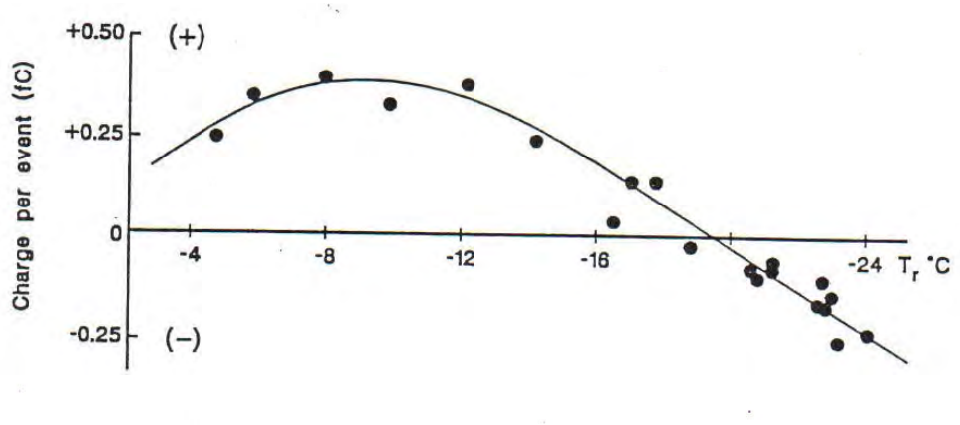

Figure 3-24. The charge acquired by a riming hail particle during collisions with ice crystals is a function of the temperature of the hail (and the cloud liquid water content). [Adapted from Jayaratne et al., 1983]

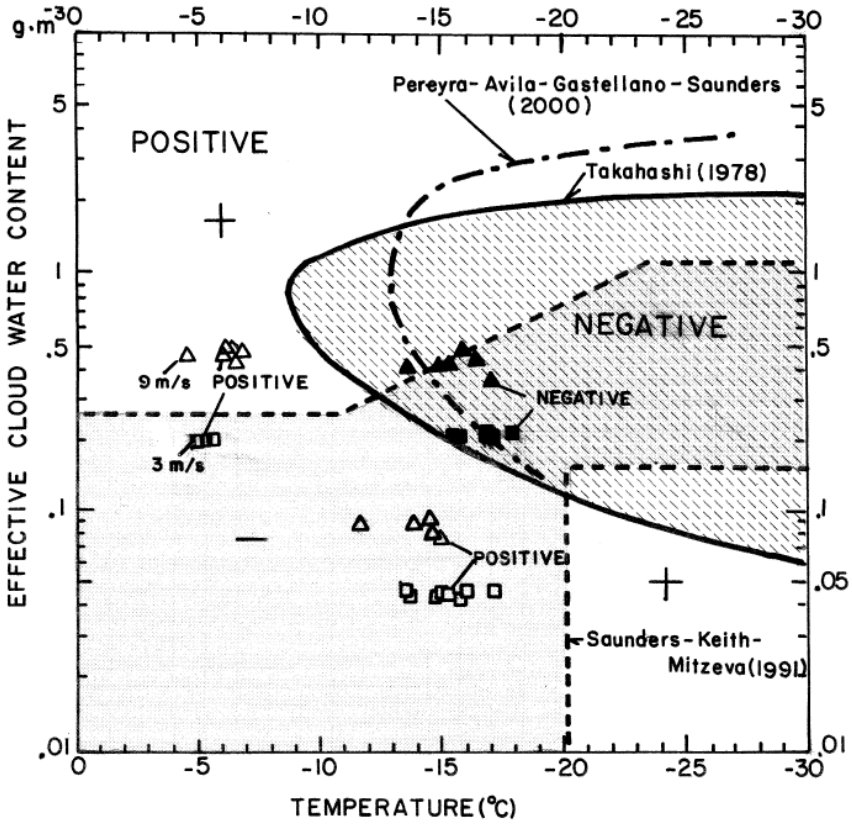

FIG. 7. Similar to Fig. 6 except for the use of "effective" cloud water content (EW—amount of water actually collected by the riming rod). Results of Saunders et al. (1991) and Pereyra et al. (2000) also are plotted.

Figure 3-25. The reversal temperature is also a function of the cloud LWC [Takahashi and Miyawaki, 2002]

3.2.1.2.2 Physics of the Charge Transfer During Ice-Ice Collisions

Several investigators have suggested that the magnitude and polarity of the charge that is transferred in ice-graupel collisions is controlled by the rates at which the ice surfaces are growing by deposition (condensation) or sublimating (evaporation) [Baker et al., 1987, 1989; Mason and Dash, 2000; and Dash et al., 2001]. The surface that is growing the fastest at the time of the collision acquires a positive charge. When both surfaces are evaporating, the surface that is evaporating the slowest becomes positively charged. Unfortunately, there is still no consensus about the reason(s) for this behavior, but mechanisms that have been proposed include differences in the ice surface potentials, thermoelectric effects acting on the riming ice surfaces, and the effects of irregular ice surfaces [Avila et al., 2005]. Baker and Dash [1989] have suggested that there may be liquid-like layers (LLL) on ice surfaces that have an excess concentration of negative ions on the outer portion of the LLL. If this is the case, then when two such LLLs collide, the thicker layer may transfer some of its mass, together with its negative charge, to the thinner LLL, and leave positive charge behind. Since the surfaces that are growing fastest will also have thicker LLLs, the Baker-Dash mechanism does appear to describe practically all the laboratory results to date, at least qualitatively [Mason and Dash, 2000; Dash et al., 2001].

3.2.1.2.3 Other Mechanisms

In their study of the electrical structure of stratiform clouds, Shepherd et al. [1996] found surprisingly high electric fields and charge densities near the melting (0ºC) level and the radar bright band, and they point out that this enhanced electrification cannot be explained by an ice-graupel collision process. They review other mechanisms and suggest that a melting mechanism [Drake, 1968] may dominate the electrification in such clouds near the 0ºC level.

Latham [1991] has shown that the convective clouds initiated by large, wildland fires can produce lightning, and Vonnegut et al. [1995] have suggested that the dominant mechanism producing this electrification may not be ice-graupel collisions but one or more influence mechanisms based on electrostatic induction.

3.2.1.3 Cloud Electrification Conclusions

At this point, we still need more information about the microphysical, electrical, and dynamical structure of thunderclouds before we can make further evaluations of the non-inductive, ice-graupel collision mechanism (coupled with precipitation), the detailed physics that underlies this process, and other possible mechanisms. Among the parameters that are still to be determined are the number of ice-ice collisions, the LWCs, and the temperatures in the different regions of a thundercloud; the sizes of the ice crystals and collision velocities in these regions; and what charges are present on the ice crystals, water drops, and precipitation particles (all as a function of size). Several experiments are currently under way both in the laboratory and in nature to learn more about the electrical structure of clouds and the mechanisms of electrification. Hopefully, these efforts will soon provide explanations for the fascinating phenomena of cloud electrification that Benjamin Franklin and many others have been documenting for over 250 years.

3.2.2 Proposed FAA Lightning Flight Commit Criteria (LFCC)

The proposed FAA Natural and Triggered Lightning Flight Commit Criteria (LFCC, also termed the Lightning Launch Commit Criteria, or LLCC, by NASA and the Air Force) are listed in Appendix B together with the Definitions, Explanations and Examples. (This version of the LFCC was approved by the USAF/NASA Lightning Advisory Panel — LAP — in July of 2004.) Revised Anvil Rules, incorporating a radar exception, were approved by the LAP on 1 February 2005 and are incorporated into Appendix B together with some additional definitions. It should be noted in Appendix B that the Definitions are given first because they are an integral part of the LFCC, and the logic and wording of the LFCC depend in a critical way on these definitions. It should also be noted that each of the LFCC requires *clear and convincing evidence* to trained weather personnel that its constraints are *not violated*. Under some conditions, trained weather personnel can make a clear and convincing determination that the LFCC are not violated based on visual observations alone. However, if the weather personnel have access to additional information such as measurements from weather radar, lightning sensors, electric field mills, and/or aircraft, and this information is within the criteria outlined in the LFCC, it would allow a launch to take place where a visual observation alone would not.

Each of the proposed Natural and Triggered Lightning Flight Commit Criteria (LFCC) are paraphrased below (in italics), and they are followed by a short rationale. For further details, the reader can consult the Titan Program [1988], Krider et al. [1999], Dye et al. [2006], and Willett et al. [2006].

3.2.2.1 Lightning (Appendix B, Section C)

*Do not fly within 10 nm of any type of lightning, or any cloud that has produced it, within the past 30 min. An exception is allowed if the cloud has moved beyond 10 nm **and** if an electric field mill within 5 nm of the **lightning** (and any other mills within 5 nm of the flight path) have shown benign readings for at least 15 minutes.*

Any cloud that is producing natural lightning (either intracloud, cloud-to air, or cloud-to-ground) will contain electric fields that are large enough to trigger lightning to any airborne vehicle. Further, natural lightning itself can be a hazard both by attaching directly to a vehicle in flight (approximately 10% of the strikes to aircraft are the interception of an ongoing flash) and by the indirect effects induced on the vehicle. A delay of 30 minutes is an interval beyond which the chance of an additional lightning discharge in a given thunderstorm cell is very low [Holle et al., 1999; Holle et al., 2003; and Murphy et al., 2005]. Also, the chance that any lightning discharge will propagate beyond a distance of 10 nautical miles from the parent thunderstorm is low [McNamara, 2002; Nelson, 2002], and the chance that it would propagate in a direction that affects the vehicle is even lower.

3.2.2.2 Cumulus Clouds (Appendix B, Section D)

For purposes of this section, "cumulus clouds" do not include altocumulus, cirrocumulus, or stratocumulus clouds.

*Do not fly within 10 nm of any cumulus cloud that has a top above the -20°C temperature level and within 5 nm of any cumulus cloud that is above -10°C. Do not fly through a cumulus cloud that is above the +5°C level. An exception is allowed for any cumulus cloud top between ±5°C if that cloud is not precipitating **and** if a field mill within 2 nm of that top (and any other mills within 5 nm of the flight path) have shown benign readings for at least 15 minutes.*

Cumulus clouds contain convection that can grow and strengthen very rapidly, and if the cloud top exceeds the –20°C level, there is a good chance that an electrification mechanism involving ice-ice collisions (see section 3.2.1) has already created, or soon will be creating, high electric fields. Therefore, such clouds should be treated as if they were already producing natural lightning.

Cumulus clouds that reach the –10°C level but have not exceeded the –20°C level are not as likely to be highly electrified, but since the latent heat released by the freezing of liquid drops can rapidly enhance convection and the growth of precipitation [Szymanski et al., 1980], potentially leading to rapid electrification, the region within 5 nautical miles of any cumulus cloud that reaches the –10°C level should be avoided.

Cumulus clouds that reach the –5°C level but do not exceed the –10°C are not likely to be highly electrified, but such clouds should not be penetrated because clouds with tops in this height range often grow rapidly and could become electrified by the time the vehicle would penetrate the cloud.

Cumulus clouds with tops between the +5°C and the –5°C levels have the potential to grow rapidly and become electrified by the time the vehicle flies through the cloud, especially if they are precipitating. However, if such a cloud is not precipitating and if all electric field measurements made close to the cloud and near the flight path have been low for 15 minutes or longer, then rapid growth and electrification are unlikely. Small cumulus clouds are not likely to contain significant screening layers (unlike stratiform clouds and anvils) because of the mixing and entrainment that takes place at their boundaries, so a nearby field mill can be relied upon to indicate the electrical state of such clouds.

3.2.2.3 Attached Anvil Clouds (Appendix B, Section E)

Do not fly within 10 nm of any non-transparent, attached anvil for at least 30 minutes after the last lightning discharge occurs in the parent cloud or anvil, and do not fly within 5 nm of an attached anvil for 3 hours after the last lightning discharge in the parent cloud or anvil. Never penetrate an attached anvil cloud. If the anvil cloud is everywhere colder than 0°C ***and*** *if its volume-averaged, height-integrated, radar reflectivity (VAHIRR) is less than 10 dBZ-km, exceptions are allowed to both the 5 nm standoff distance and the no-penetration requirement after 30 minutes.*

In Section 3.2.1.1.5, we have seen that electric fields measured inside anvil clouds attached to their parent thunderstorm are frequently very large for long periods of time. If the parent thunderstorm has stopped producing lightning for at least 30 minutes, the observed fields at distances between 5 and 10 nautical miles from the anvil are low and flight can occur in that region. If lightning has not occurred for 3 hours, the observed fields are low everywhere outside the cloud, so under those conditions, flight can occur within 5 nautical miles of an attached anvil. If weather radar measurements are available, a radar-based exception can be applied to attached anvil clouds.

3.2.2.4 Detached Anvil Clouds (Appendix B, Section F)

For purposes of this section, detached anvil clouds are never considered debris clouds.

Do not fly within 10 nm of a non-transparent, detached anvil for 30 minutes after detachment, or within 5 nm for 3 hours after it, or its parent cloud before detachment, produces lightning. Do not penetrate a non-transparent, detached anvil for 3 hours after it is observed to detach, or for 4 hours after it has produced lightning. The duration of the 5 nm standoff requirement is reduced to 30 minutes after lightning if a field mill within 5 nm of the cloud (and any other mills within 5 nm of the flight path) have shown benign readings, ***and*** *if the cloud radar reflectivity has been less than 10 dBZ, for at least 15 minutes. The 5 nm standoff requirement can also be reduced to 30 minutes, and the no-penetration requirement reduced to 30 minutes after lightning, if all parts of the cloud are colder than 0°C* ***and*** *if its volume-averaged, height-integrated, radar reflectivity (VAHIRR) is less than 10 dBZ-km.*

The measurements described in Section 3.2.1.1.5 show that, after anvil clouds become detached from their parent thunderstorms, the electric fields can persist for a long period of time in the absence of internal cells of convection. If the detached anvil, and its parent cloud before detachment, have not produced lightning for at least 30 minutes, the observed fields between 5 and 10 nautical miles outside the cloud are well below the threshold for triggering lightning. If lightning has not occurred for 3 hours, the fields within 5 nautical miles of a detached anvil are below the threshold for triggering lightning. Note that a field mill exception permits flight within 5 nautical miles, but not penetration, of certain detached anvil clouds because screening layers can build up on detached anvils and prevent the detection of high fields within them from the ground. If weather radar measurements are available, a radar-based exception can be applied to detached anvil clouds.

3.2.2.5 Debris Clouds (Appendix B, Section G)

Do not fly within 5 nm of a non-transparent debris cloud for 3 hours after it detaches or decays from its parent cloud ***and*** *for 3 hours after it produces lightning. An exception to the 5 nm standoff requirement is allowed if a field mill within 5 nm of the debris cloud (and any other mills within 5 nm of the flight path) have shown benign readings,* ***and*** *if the cloud radar reflectivity has been less than 10 dBZ, for 15 minutes.*

In Section 3.2.1.1.5, we have seen that thunderstorm debris clouds can contain high electric fields for long periods of time. In the absence of any convective development that generates further charge, as indicated by lightning, the electrification should decay away after a 3-hour interval. Note that the field mill exception permits flight within 5 nm, but not through certain debris clouds because screening layers might build up on these nonconvective clouds and prevent the detection of high fields within them from the ground.

3.2.2.6 Disturbed Weather (Appendix B, Section H)

Do not fly through a non-transparent cloud associated with disturbed weather that produces cloud tops colder than 0 °C and either moderate to greater precipitation or evidence of melting precipitation within 5 nm of the flight path.

In Section 3.2.1.1.5, we have seen that disturbed weather often produces high electric fields, especially when there is evidence of melting precipitation or a radar bright band in the clouds aloft. The mechanism(s) for producing this electrification are not understood and may be different from non-inductive ice-ice collisions, so vehicles should not fly through such clouds.

3.2.2.7 Thick Cloud Layers (Appendix B, Section I)

Do not fly through a non-transparent cloud layer that is thicker than 4500 feet and contains temperatures between 0°C and -20°C (nor any non-transparent cloud layer that is connected to such a thick cloud layer within 5 nm of the flight path). An exception is allowed if the thick cloud layer contains no liquid water ***and*** *has never been associated with a convective cloud.*

A non-inductive charging mechanism involving ice-ice collisions requires the presence of supercooled water drops in a region of the cloud that has appreciable numbers of ice-ice collisions. A thick cloud that encompasses the 0º to –20ºC temperature levels will usually contain supercooled water, and can also include imbedded cells of convection. Imyanitov et al. [1972, Chapter 1] have reported maximum electric fields of 20 kV/m in altostratus clouds with an average thickness of 1300 meters, and the ABFM I campaign also found fields of the order of 10 kV/m in thick Florida clouds.

3.2.2.8 Smoke Plumes (Appendix B, Section J)

Do not fly through any cumulus cloud that develops from a smoke plume for 60 minutes after it has detached from that plume.

Latham [1991] has documented that convective clouds initiated by large, wildland fires can produce lightning, and Vonnegut et al. [1995] have suggested that the dominant mechanism for creating this electrification may not be ice-ice collisions but one or more influence mechanisms involving electrostatic induction. Since the mechanism(s) for producing cloud electricity when the cloud is connected to a smoke plume are still not understood, a delay of at least 60 minutes is required after detachment to ensure flight safety.

3.2.2.9 Surface Electric Fields (Appendix B, Section K)

Do not launch if any electric field mills within 5 nm of the flight path have exhibited readings in excess of 1 kV/m in the past 15 minutes. The field threshold can be raised to 1.5 kV/m if all clouds within 10 nm of the flight path are transparent or both have tops warmer than +5°C and have not been part of convective clouds with tops colder than -10°C for at least 3 hours.

Two key facts support this rule. First, extended volumes of space that contain elevated electric fields can constitute a potential energy source for triggering lightning. Therefore, any indication of elevated fields aloft must be regarded as a threat, whether or not any particular cloud type is present. Second, when the electric field overhead increases, the field at the ground tends to be "clamped" or limited to a steady value between 3 and 5 kV/m, depending on the site, because of corona emissions from the surface. Thus, when any surface electric field measurement approaches 2 kV/m (a value appropriate for the Kennedy Space Center), it may not provide a true indication of the electric field aloft.

A cloud-based exception can be granted if the surface field is below a threshold for producing appreciable corona space charge so that this field can be regarded as indicative of conditions aloft. In particular, it has been observed that splashing waves and bubbling in the surf zone, power line corona, and other sources of electricity in fair weather produce elevated fields near the ground but do not pose a threat for triggering lightning. These processes rarely produce fields in excess of 1500 V/m at the Kennedy Space Center.

3.2.2.10 Triboelectrification (Appendix B, Section L)

Do not fly through any cloud that is colder than -10ºC at vehicle velocities less than 3000 ft/s unless the vehicle has been treated or hardened against surface discharges.

Any collisions of the space vehicle with ice particles have the potential for separating charge and causing discharges on insulating surfaces. In order to avoid this possibility, the launch vehicle must either be treated for surface electrification or it must be shown that surface discharges will not be hazardous to the vehicle or its payload.

3.2.3 On the Applicability of the Current LLCC and LFCC to RLVs

It is clear from the comparison of triggering conditions in Section 3.1.5.5 that the concept RLVs described in this report are considerably less prone to trigger lightning than are the large orbital boosters for which the present LLCC and LFCC (see Appendix B) were developed. Nevertheless, without further data and/or analysis we cannot recommend that the proposed commercial, suborbital launches ignore *any* of these LLCC. Here we rank the individual LLCC in order of importance and indicate qualitatively which ones might be relaxed and by what means.

Most important is the "Lightning" Rule (see Section 3.2.2.1), which should be applied to all flights of any aerospace vehicles that are not hardened against lightning effects. Not only is natural lightning both a direct and an indirect threat to the vehicle under these conditions, but also the triggered lightning threat is large whenever natural lightning is present. There is no safe way of relaxing this rule other than by hardening the vehicle.

Almost as important is the "Cumulus Cloud" Rule (Section 3.2.2.2). Cumuli with tops colder than –20ºC are likely to be electrified and must be treated as though they were already producing natural lightning. The smaller cumuli that are described in this rule can also develop into thunderstorms vary rapidly and should be avoided.

The "Smoke Plumes" (Section 3.2.2.8) and Surface Electric Fields (Section 3.2.2.9) Rules should not be waived for RLVs either. Violations of the former are relatively rare events that are not well enough understood to safely ignore. Violations of the latter constitute our best ground-based indication of truly hazardous conditions aloft (except for possibly natural lightning) and should never be ignored unless the cause of the elevated field is understood and known to be benign.

Aircraft have been struck when flying in “Anvil Clouds” (both attached (Section 3.2.2.3) and detached (Section 3.2.2.4), “Debris Clouds” (Section 3.2.2.5), “Disturbed Weather” (Section 3.2.2.6), and “Thick Cloud Layers” (Section 3.2.2.7) [e.g., Imyanitov et al., 1972; Harrison, 1965]. Therefore, it is certainly not safe for RLVs to penetrate any of these clouds unless the prescribed conditions are met. Nevertheless, there are two ways in which these five rules might be relaxed for RLVs. The first and most effective way is to use an operational ABFM to probe the clouds along the proposed flight path and determine whether or not they are electrified (see Section 2.3.2.1). The second way is to re-analyze the ABFM I data to determine more appropriate standoff distances for RLVs from these clouds, as is recommended in Section 4.1.1. It seems probable that such an analysis would significantly reduce, or possibly even eliminate, the standoff distances for RLVs in all of these rules.

A special case is afforded by anvil clouds. A great deal of data on the relationship between radar reflectivity and ambient electric field in both attached and detached anvils is readily available from the ABFM II campaign. This data could be re-analyzed fairly easily to determine more appropriate radar thresholds for RLVs, based on their higher electric-field thresholds. This approach is recommended in Section 4.1.2.

The “Triboelectrification” Rule (Section 3.2.2.10) does not refer to a triggered-lightning hazard, *per se*, and will not be discussed further here.

3.3 Lightning Climatology

Lightning climatology of each of the proposed sites was studied. Cloud climatology and its correlation with actual lightning were also studied. The lightning climatologies for the proposed sites were compared with those for existing launch ranges.

Data was collected from two sites in New Mexico, the White Sands Missile Range (WSMR), and the proposed Southwest Regional Spaceport (SWRS). Data was collected from the former Clinton-Sherman Air Force Base (CSAFB), which is the site of the proposed Oklahoma Spaceport (OS), Cape Canaveral Air Force Station, Florida (CAPE), and Vandenberg Air Force Base (VAFB), California. The data from the Cape Canaveral and Vandenberg sites was used in order to compare the lightning risk at the proposed spaceport sites with those at existing launch ranges. The lightning climatologies of VAFB and CAPE can be used along with their established history of LLCC-based launch holds to extrapolate how the LLCC will affect launch availability and restrictions at SWRS and OS. Significant differences in the lightning climatology for WSMR and SWRS, which are approximately 70 km apart, were seen.

The Air Force Combat Climatology Center (AFCCC) in Asheville, North Carolina, provided the data. AFCCC polled their databases for all lightning strikes between 1 January 1990 and 30 September 2004 (31 December 2004 for SWRS) within a 100 km radius from the latitude and longitude coordinates in Table 3-6. The database contains all cloud-to-ground lightning strikes measured by the National Lightning Detection Network (NLDN). The NLDN underwent a significant upgrade in 1994. The 15-year climatology study includes periods before and after the system upgrade. Only periods after the upgrade were selected for further analysis.

Table 3-6. Site Coordinates and Cloud-to-Ground Lightning Occurrence within 100 km

CG STRIKES	CSAFB	SWRS	WSMR	CAPE	VAFB
Latitude	35.3 N	32.8 N	32.3 N	28.4 N	34.7 N
Longitude	99.2 W	107 W	106.5 W	80.6 W	120.5 W
1990–2004 total	1,825,240	2,123,004	968,680	3,268,359	14,076
Jan Total	7991	1232	542	24	216
Jan Avg	533	82	36	2	14
Jan 1999	137	22	-	-	-
Jan 2004	3	46	-	-	-
July Total	287,810	745,058	356,042	813,906	3,091
July Avg	19,187	49,671	23,736	54,260	206
July 1999	6,068	63,932	-	-	-
July 2004	61,473	30,336	-	-	-

January and July 1999 were selected for further analysis of observed clouds and lightning at both potential sites. The 15-year climatology study suggested that January and July would provide the greatest spread in seasonal behavior.[8] July 1999 appeared to be an anomalously lightning-prone month at SWRS and an anomalously lightning-free month at CSAFB. Data collected for 2004 showed the opposite effect.

Cloud data from the Cloud Depiction and Forecast System (CDFS2) were also used to investigate the relationship between the occurrence of convective clouds and lightning and the applicability of cloud-based LLCC. CDFS2 is a global cloud analysis product, which uses sensor data from the Defense Meteorological Satellite Program (DMSP). It provides heights for cloud tops and cloud bases for up to four cloud layers, percent of coverage, and cloud types. The ten available cloud types are Cirrus (Ci), Cirrocumulus (Cc), Cirrostratus (Cs), Altocumulus (Ac), Altostratus (As), Nimbostratus (Ns), Stratocumulus (Sc), Stratus (St), Cumulus (Cu), and Cumulonimbus (Cb). CDFS2 also underwent a significant upgrade between 1999 and 2004. The 1999 data was binned every 3 hours, while the 2004 data was binned hourly. The horizontal grid-spacing also improved.

Initially, coordinates of the southern end of the WSMR were used as a proxy for the proposed SWRS. The two sites were expected to be similar as they are adjacent and have similar elevations. However, to rule out localized effects, the climatology was later compiled using the exact coordinates of the proposed SWRS. The result showed that the proposed SWRS had roughly twice as many lightning strikes in 1999–2004 than the southern end of WSMR.

Figures 3-26 and 3-27 show the local geography in southern New Mexico. The site of the proposed SWRS is near the bend in the small mountain range on the western edge of WSMR. The mountain range between the WSMR and the SWRS appears to block the flow of monsoonal moisture from the southwest. The monsoonal flow is primarily responsible for mesoscale convective systems in the southwestern continental U.S. (CONUS). Figure 3-28, a plot of the latitude and longitude coordinates of measured lightning strikes near SWRS in July 1999, illustrates this effect. In Figure 3-28, the

[8] The initial intent was to use data from the International Satellite Cloud Climatology Project (ISCCP), which covers only the period 1983–1999. However, difficulties were experienced with analyzing daily data required for this study. AFCCC then provided Cloud Depiction and Forecast System V2 (CDFS2) data, which enabled analysis of more recent years.

density of lighting strikes is much higher to the west of the proposed SWRS and the mountain range. The bend in the mountain range is also apparent in the lightning statistics; the boundary between the lightning-prone and nonlightning-prone areas bends to the NNE near the proposed SWRS. WSMR, which is inside the protected valley, experienced much fewer lightning strikes in the same time period. Note that the mountain range is an area with a high density of naturally occurring lightning. The area to the north of the mountain range would best be avoided during the monsoonal season.

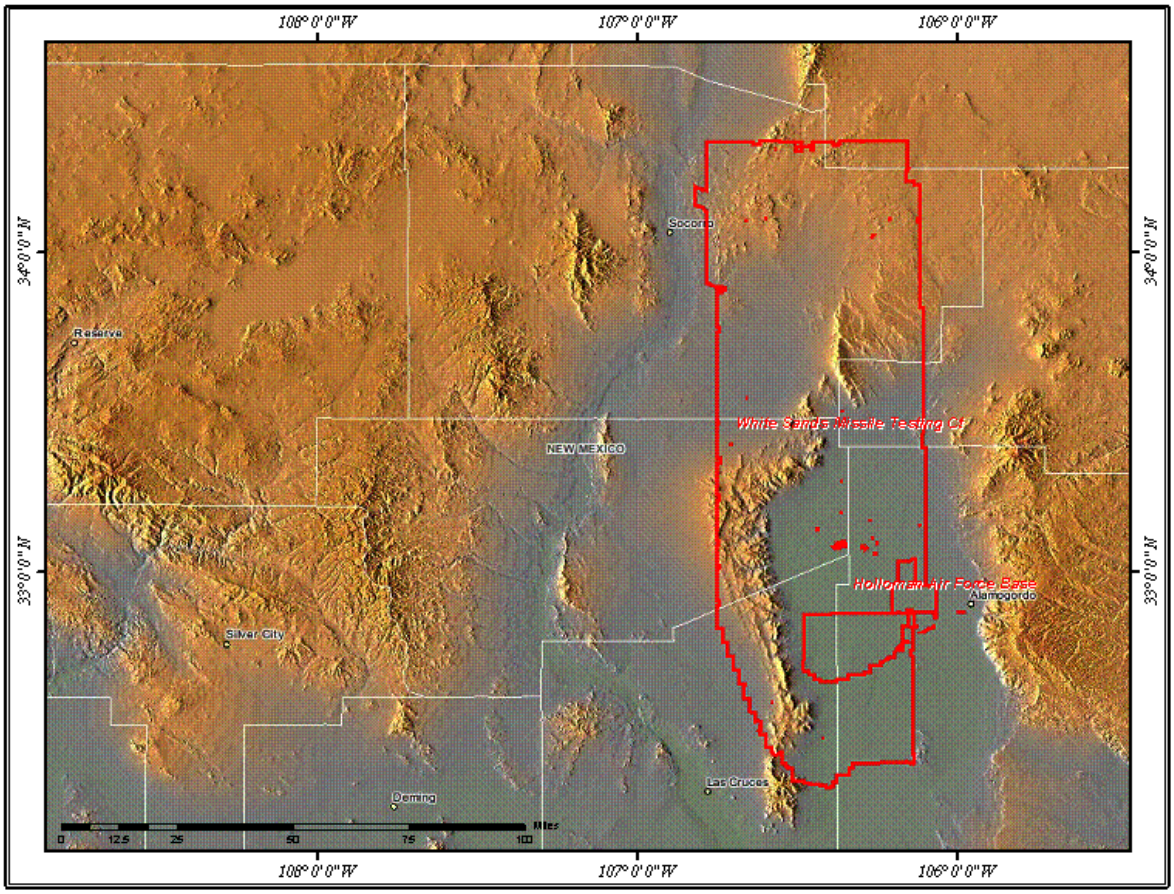

Figure 3-26. Shaded relief map of southern New Mexico. SWRS is at [32.8N, 107W]; WSMR is at [32.3N, 106.5W]. A small mountain range on the southwestern edge of WSMR protects the interior from monsoonal moisture flow from the southwest. This greatly diminishes the lightning risk in WSMR.

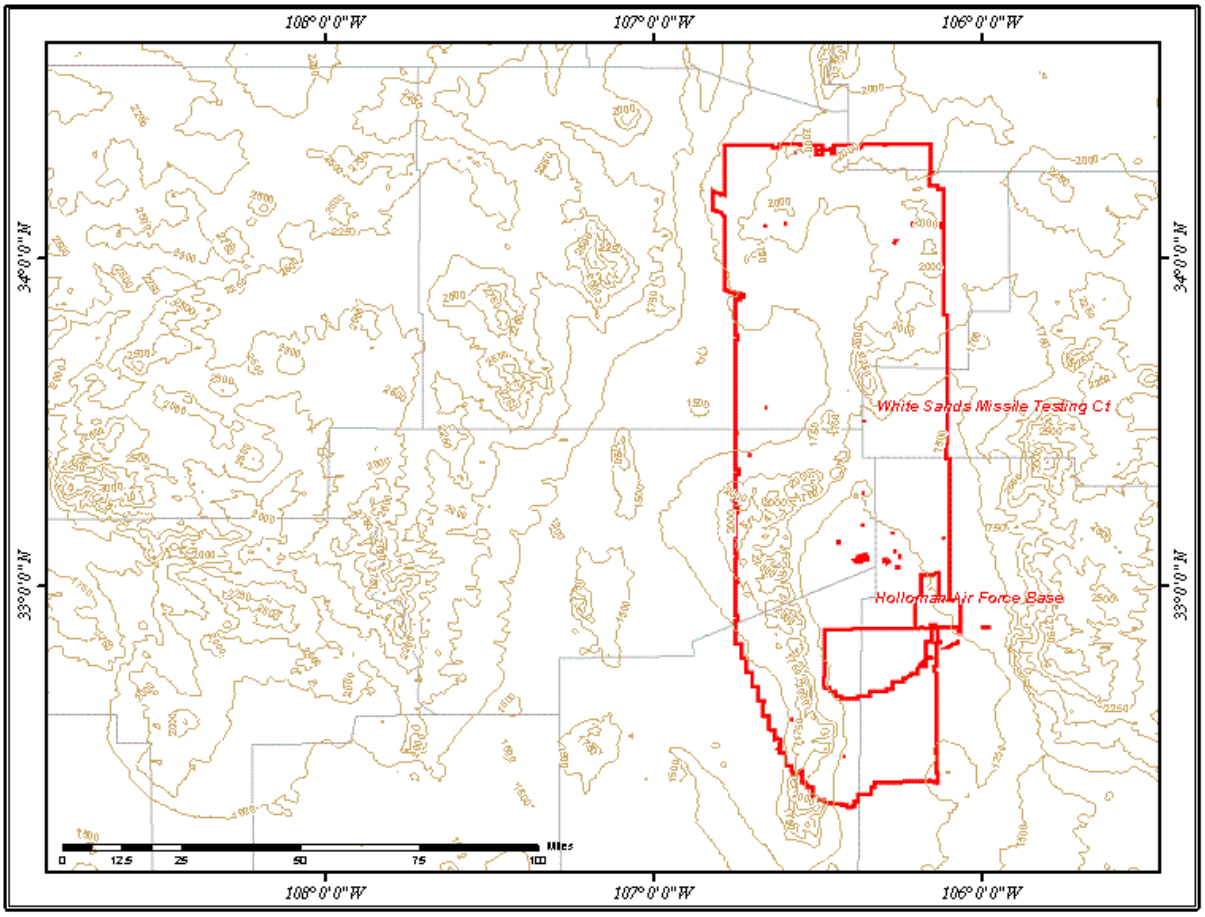

Figure 3-27. Contour map of southern New Mexico showing that SWRS and WSMR are at roughly the same elevation, but have very different surrounding topography.

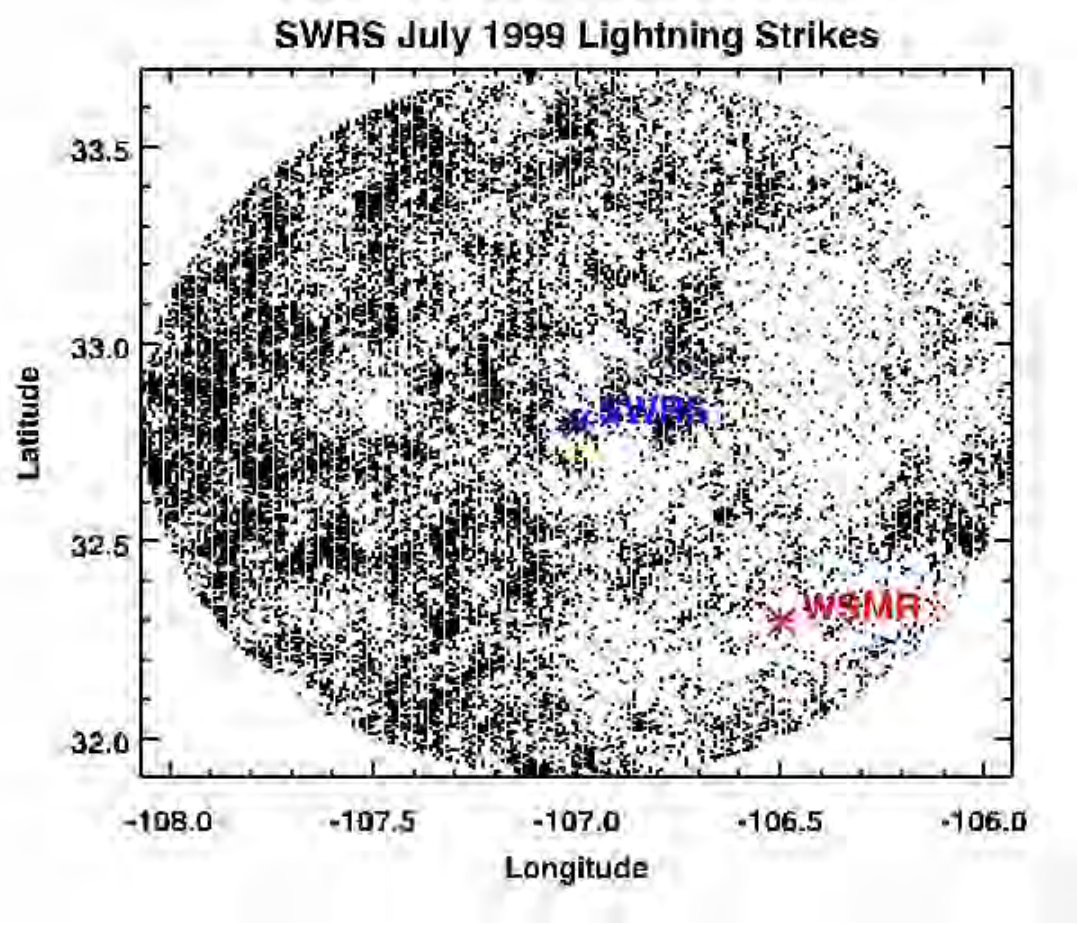

Figure 3-28. Each small black dot represents one lightning strike observed by the National Lightning Detection Network (NLDN) during July 1999, which was a heavily stormy period in the area. Much less frequent lightning occurs in the interior of the WSMR than in the adjacent area to the west.

3.3.1 Likelihood of Lightning-free Days

The existing ranges were reviewed, followed by the New Mexico sites and then the CSAFB. The results are illustrated in Figures 3-29 through 3-33.

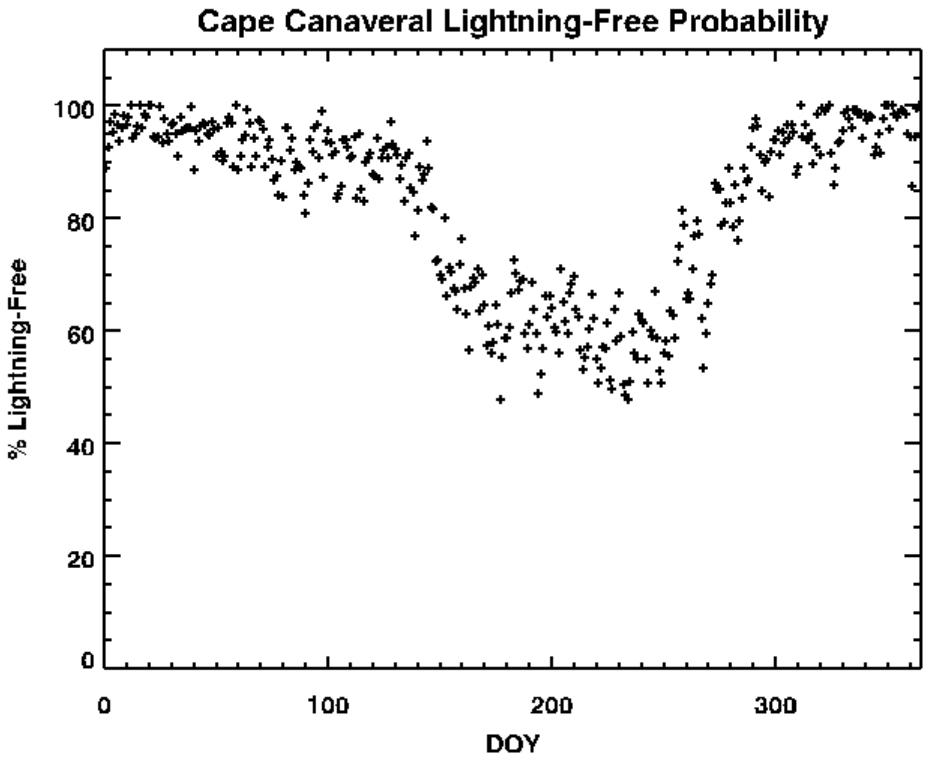

Figure 3-29. Probability that a day of year (DOY) will be lightning free at Cape Canaveral.

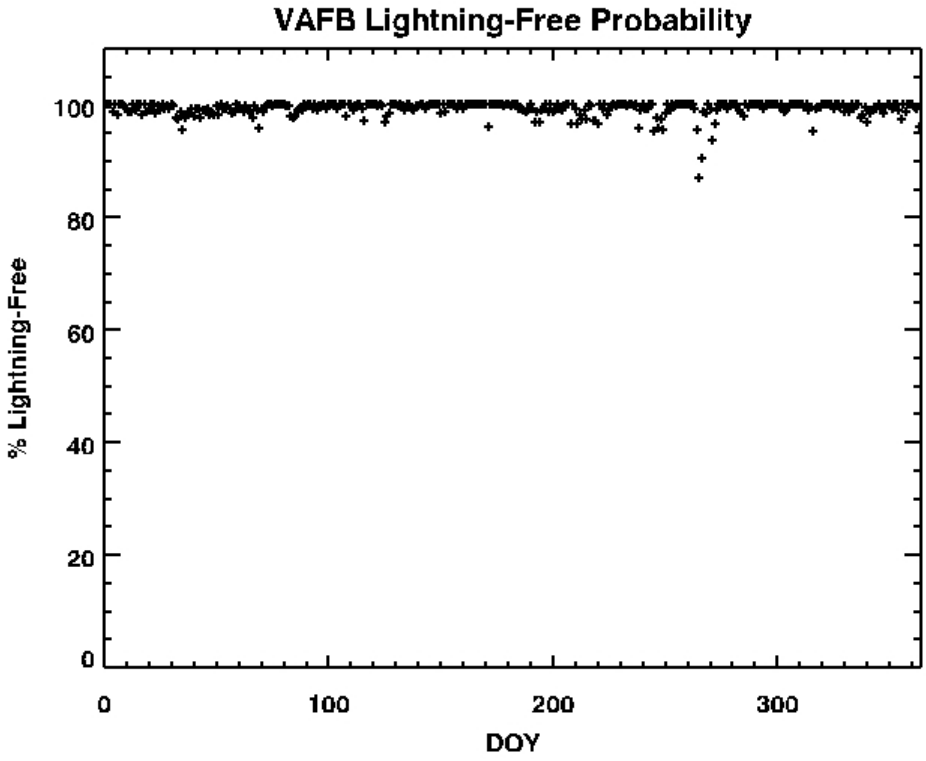

Figure 3-30. Probability that a DOY will be lightning free at Vandenberg AFB.

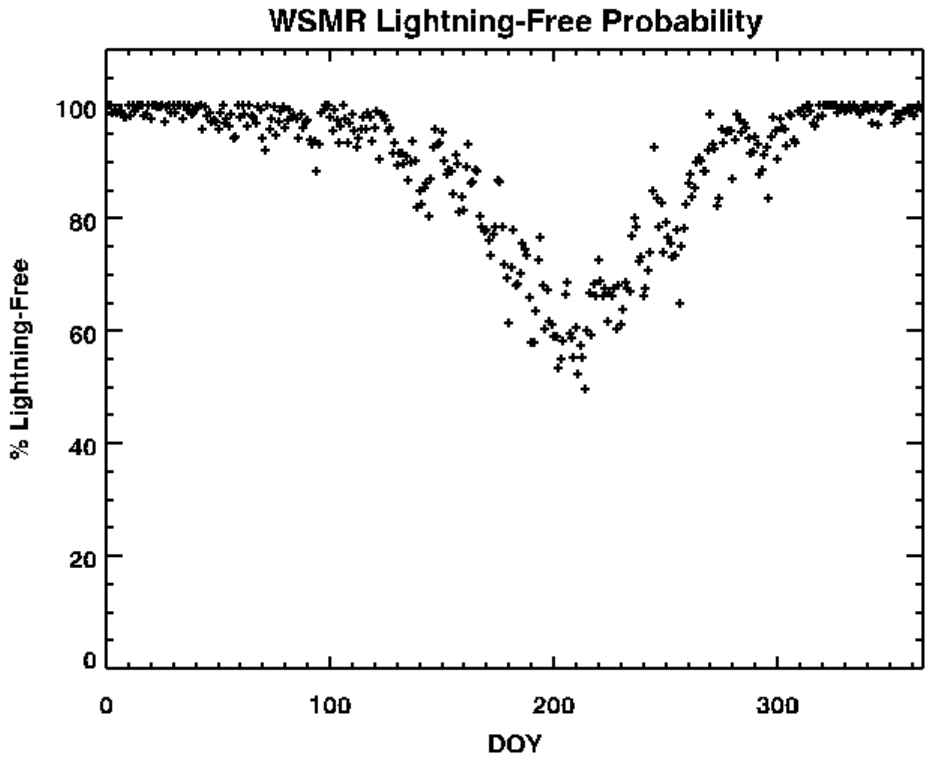

Figure 3-31. Probability that a DOY will be lightning free at White Sands Missile Range.

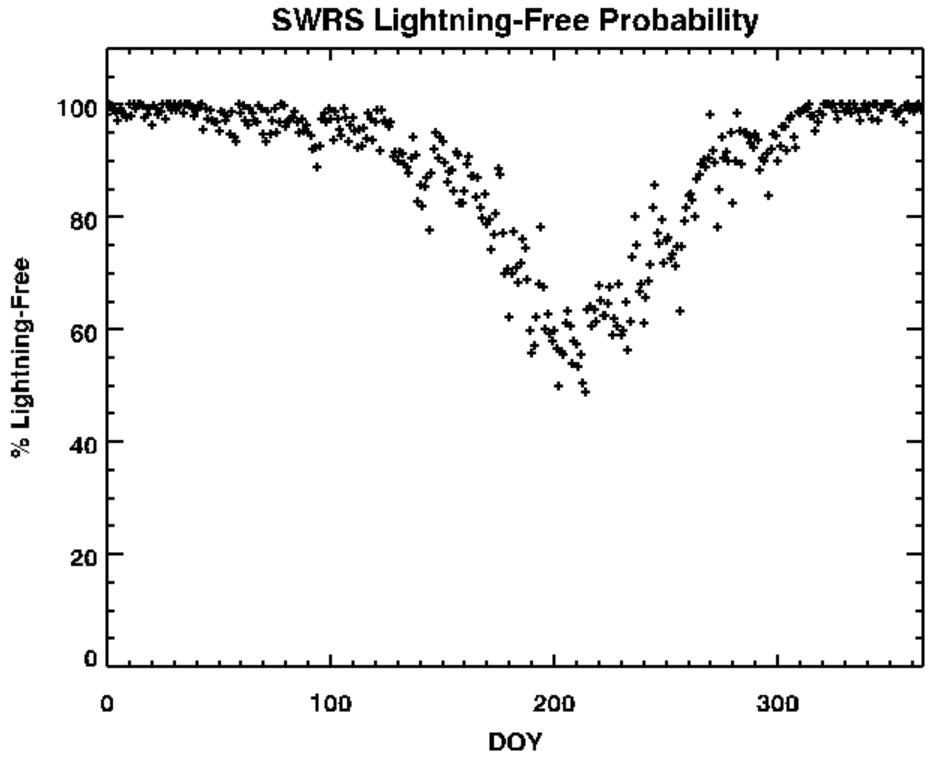

Figure 3-32. Probability that a DOY will be lightning free at Southwest Regional Spaceport.

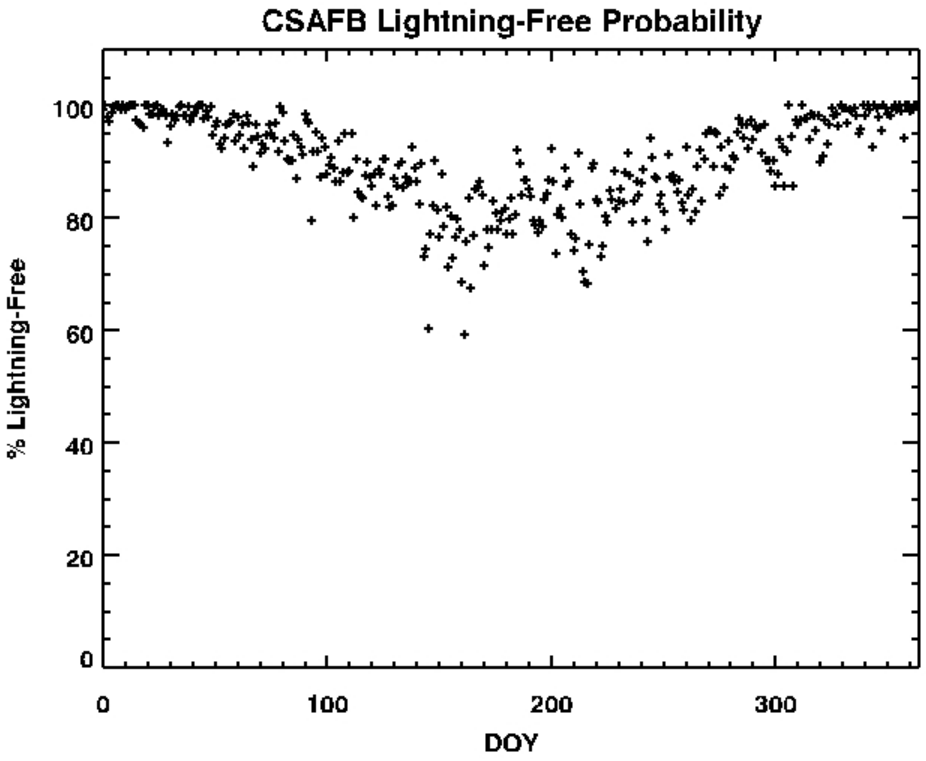

Figure 3-33. Probability that a DOY will be lightning free at Clinton-Sherman AFB.

Outliers in the thunderstorm climatology can significantly extend the lightning season. A single outlier on day-of-year (DOY) 93 stretches the lightning season at CSAFB from 120 days to 169 days. Note also that the number of days that a site will be lightning free is not strongly dependent on the total number of lightning strikes at that site. WSMR experienced roughly half as many lightning strikes as the proposed SWRS, but the likelihood that it will be lightning free on any given day is almost identical to that for SWRS (with the exception of two outliers at DOY 144 and 273).

The following generalizations *exclude* outliers that fall more than 14 days away from the main lightning season (Table 3-7). The proposed SWRS and WSMR are less than 80% likely to be lightning free for DOY ~168–258 (June 17 – September 15), or ~91 days a year. CSAFB is less than 80% likely to be lightning free for DOY ~143–262 (May 20 – September 17), or ~120 days a year. Cape Canaveral is less than 80% likely to be lightning free for DOY ~139–284 (May 30 – October 7), or ~146 days a year. SWRS has a greater than 20% chance of experiencing lightning nearly twice as many days as CSAFB. Both of the two potential spaceport sites have fewer lightning-prone days than Cape Canaveral, the most lightning-prone existing launch site. Vandenberg is shown likely to be lightning free year-round.

Table 3-7. Approximate Days with Less than 80% Probability of Being Lightning Free (Greater than 20% chance of lightning within 100 km on that day of year)

Site	DOY Range	Date Range	No. Days With High Lightning Probability	Length of Main Season (Days, Excluding Outliers)	Length of Entire Season (Days, Including Outliers)
VAFB	N/A	N/A	0	0	0
CAPE	139 – 284	May 19 – October 11	129	146	146
CSAFB	93 – 262	April 3 – September 10	47	120	169
SWRS	144 – 273	May 24 – September 30	86	90	129
WSMR	168 – 258	June 17 – September 15	84	90	90

3.3.2 Diurnal Effects

Rockets can be launched on days with lightning present, but only if the lightning occurs well away from the launch site and launch time. The diurnal influence of each site was reviewed. The results are illustrated in Figures 3-34 through 3-38.

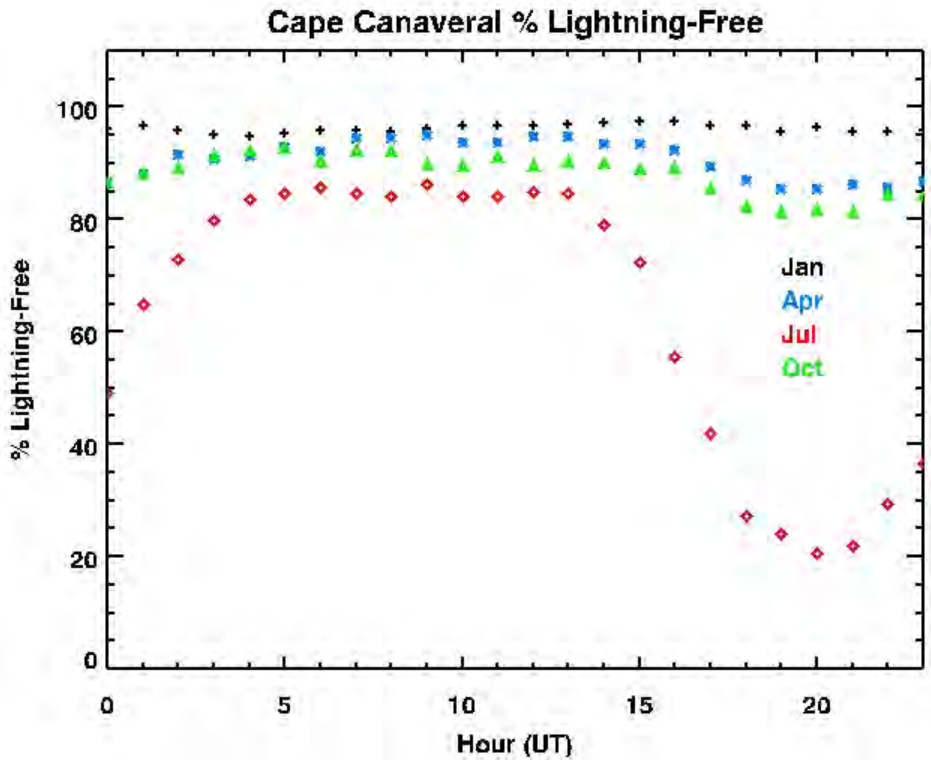

Figure 3-34. Probability that an hour will be lightning free in each month at the Cape. Note: Local time is Universal Time (UT) minus 5 hours.

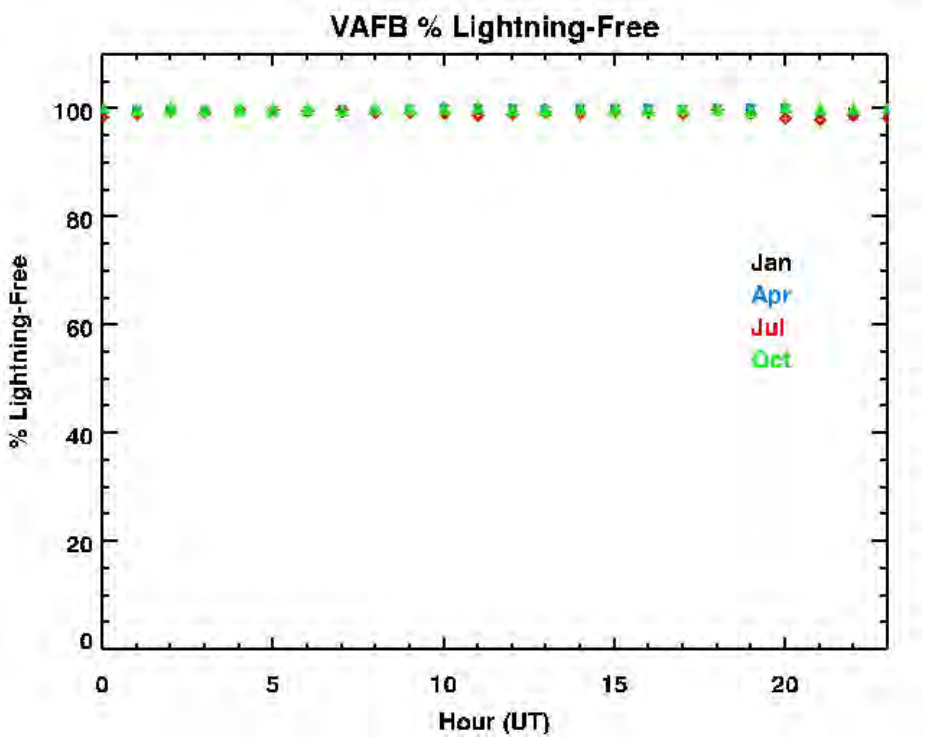

Figure 3-35. Probability that an hour will be lightning free in each month at Vandenberg AFB. Note: Local time is Universal Time (UT) minus 8 hours.

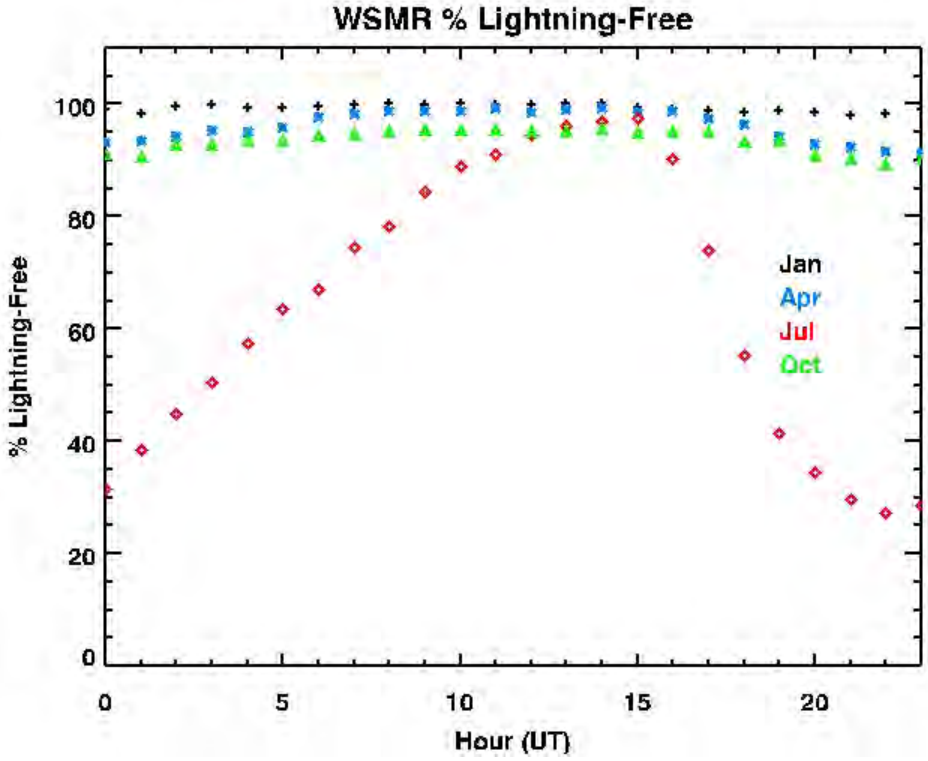

Figure 3-36. Probability that an hour will be lightning free in each month at White Sands Missile Range. Note: Local time is Universal Time (UT) minus 7 hours.

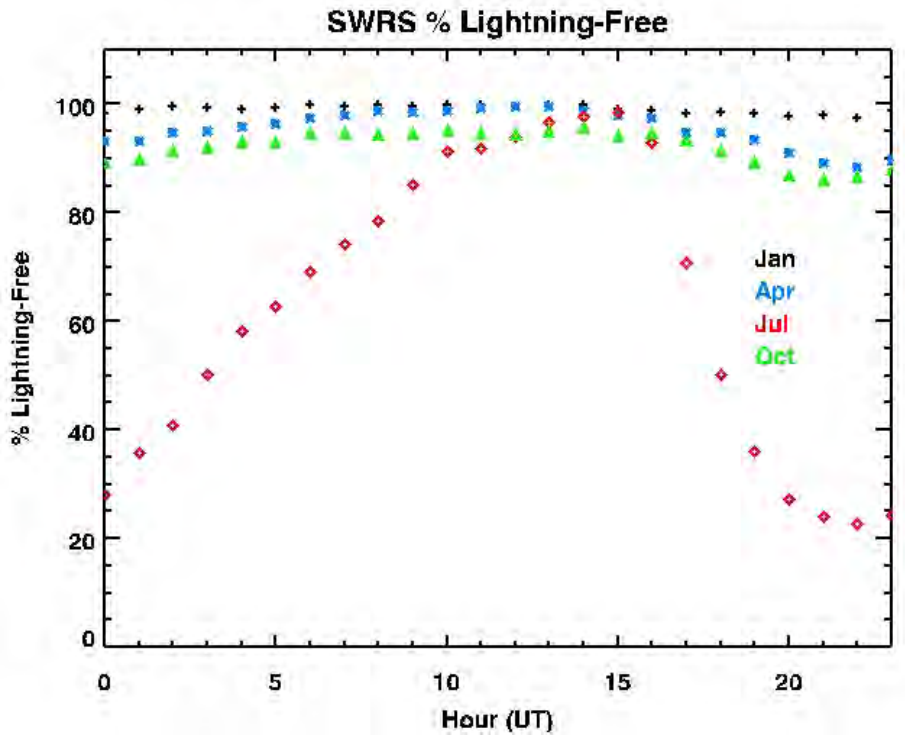

Figure 3-37. Probability that an hour will be lightning free in each month at Southwest Regional Spaceport. Note: Local time is Universal Time (UT) minus 7 hours.

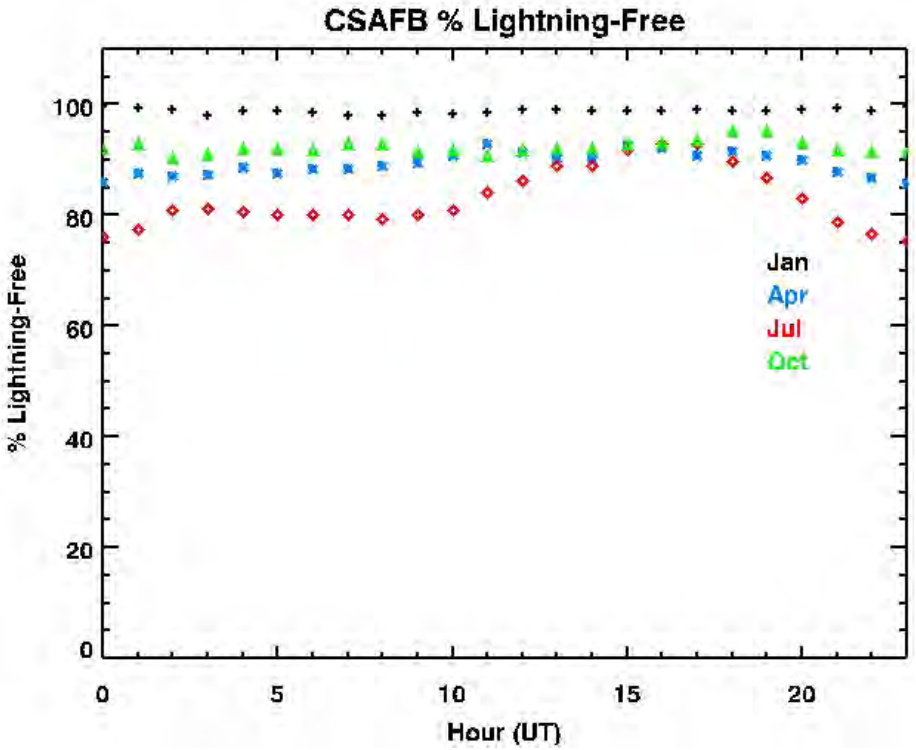

Figure 3-38. Probability that an hour will be lightning free in each month at Clinton-Sherman AFB. Note: Local time is Universal Time (UT) minus 6 hours.

Lightning activity at Cape Canaveral peaks at 2000 universal time (UT) or 1500 local time (LT). Midnight to 0800 LT are reliably lightning free year-round. In New Mexico, July lightning activity peaks at 2200 UT or 1500 LT. 0200 to 0900 LT are reliably lightning free in NM. At Clinton-Sherman AFB, most hours are reliably lightning free, with the possible exception of summer evenings, when the Great Plains low level jet (LLJ) appears (Table 3-8).

Table 3-8. Times of minimum and maximum probability of naturally occurring lightning in July[9]

Site	Min (UT)	Min (LT)	Max (UT)	Max (LT)
CAPE	0900	0400	2000	1500
WSMR	1500	0800	2200	1500
SWRS	1500	0800	2200	1500
CSAFB	1600	1000	2300	1700

The 100 km radius is a generous envelope. Existing lightning launch commit criteria demand only that the launch site and flight path be >10 nm (18.5 km) from lightning and clouds or thunderstorms producing lightning. Thus, the statistics presented above might overstate the probability of naturally occurring lightning within the launch path. However, the NLDN measures cloud-to-ground lightning strikes only. It gives no information about intra-cloud lightning, which might be even more common than cloud-to-ground lightning. In addition, the NLDN does not detect lightning with 100% efficiency. Thus, the statistics presented here *understate* the risk of triggered lightning. They do illustrate the relative risk of lightning at each of the five sites and their seasonal and diurnal influences.

Figure 3-39 depicts all lightning strikes detected within a 100 km radius from CSAFB in July 2004. The distribution is more isotropic than for the analogous plot in Figure 3-28. Table 3-9 shows the number of lightning strikes within circles of radius 100 and 18.5 km centered at each proposed site. If the distributions were perfectly isotropic, the number of lightning strikes in each circle would scale by r^2. The lightning distribution at SWRS is more anisotropic than for CSAFB.

[9] VAFB is omitted because it is nearly lightning free in July.

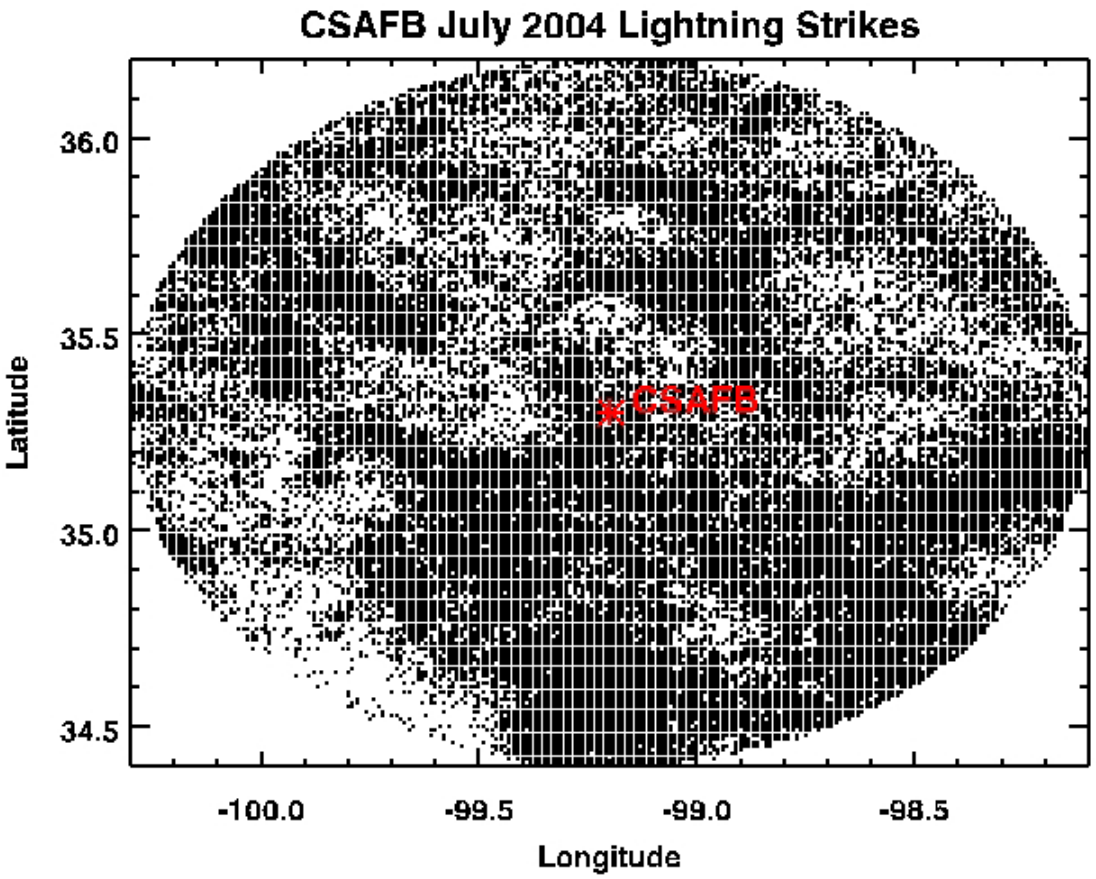

Figure 3-39. Each small black dot represents one lightning strike observed by the National Lightning Detection Network (NLDN) during July 2004, which was a relatively stormy July for the area.

Table 3-9. Lightning Occurrence within 100 and 18.5 km

July	SWRS		CSAFB	
Year	**1999**	**2004**	**1999**	**2004**
Within 100 km	63932	30336	6068	61473
Within 18.5 km	7496	952	309	1926
Ratio[10]	8.5	32	20	31

3.3.3 Cloud and Lightning Correlations

Several LLCC require that launches be held if lightning storms are in the area and if the associated clouds remain in the vicinity of the launch area. Lightning and convective cloud data were combined to clarify the correlations (Figures 3-40 through 3-47). The dates and hours of observed convective clouds (black crosses) and lightning strikes (red diamonds or triangles) within a 100 km radius circle of the SWRS and CSAFB were plotted. As expected, there was a correlation between observation of cumulus and cumulonimbus clouds and lightning occurrence. However, a high correlation was also observed between altocumulus clouds and lightning occurrence even though the LLCC specifically

[10]A perfectly isotropic lightning distribution would yield a (# w/in 100 km)/(# w/in 10 km) ratio of 29.

state that they do not apply to altocumulus clouds. The CDFS2 possibly misidentifies cumulus clouds as altocumulus clouds because satellite cloud identification can erroneously identify cloud top heights up to three kilometers too high [Naud et al., 2004]. Between 1999 and 2004, CDFS2 cloud analysis became available hourly instead of every 3 hours. Times are rounded *down* to the next whole hour (or 3-hour) time period. In general, lightning is observed during or following times in which convective clouds are observed.

The following figures contain data from independent databases. While the data can give the locations and times that clouds and lightning were observed, it cannot establish that a particular cloud generated lightning.

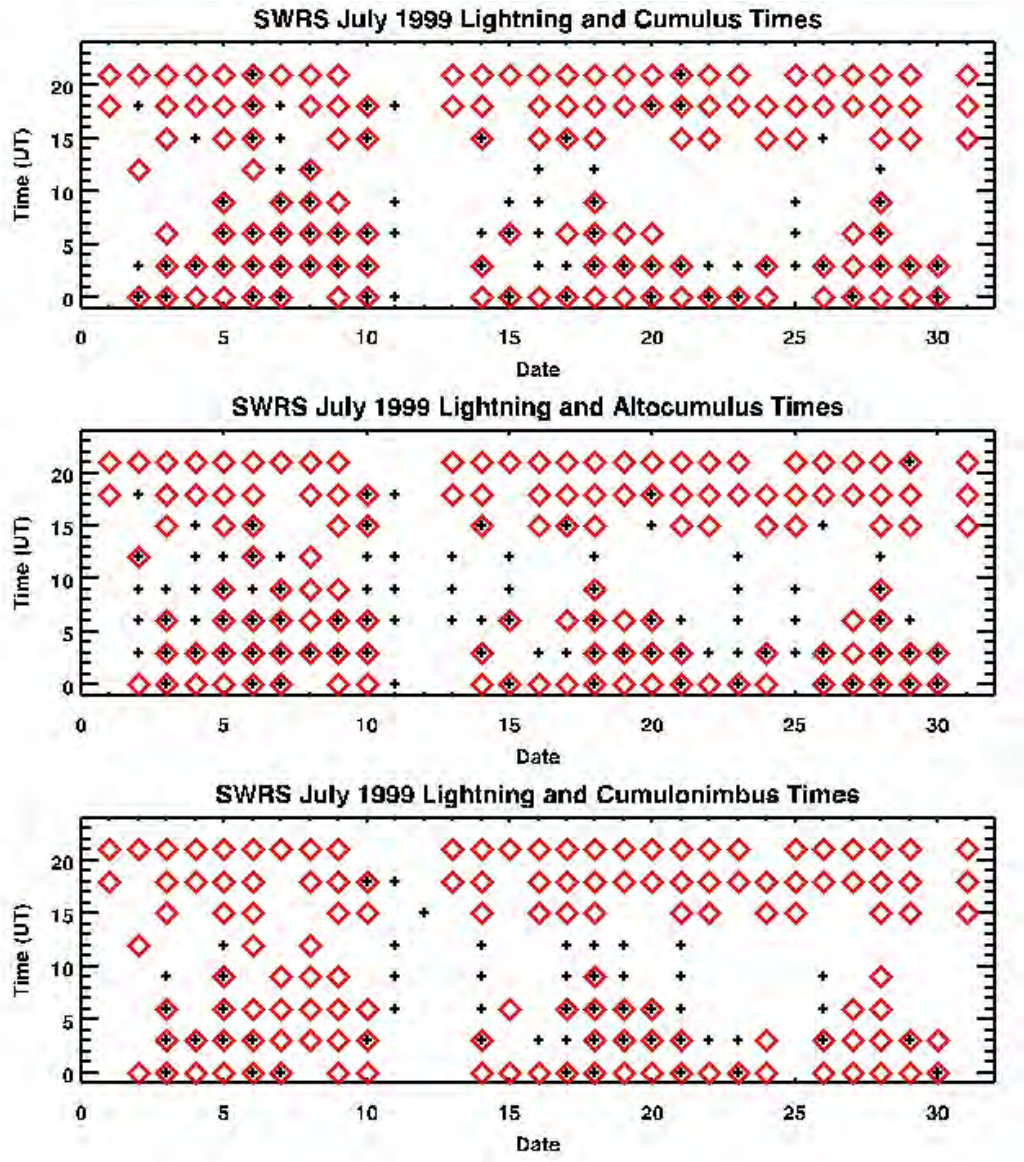

Figure 3-40. Dates and hours that convective clouds (black +) and lightning (red diamonds) were observed within 100 km of SWRS. LT = UT – 7 hours. Late afternoon and evening hours are most prone to lightning. Early morning hours are most likely to be lightning free.

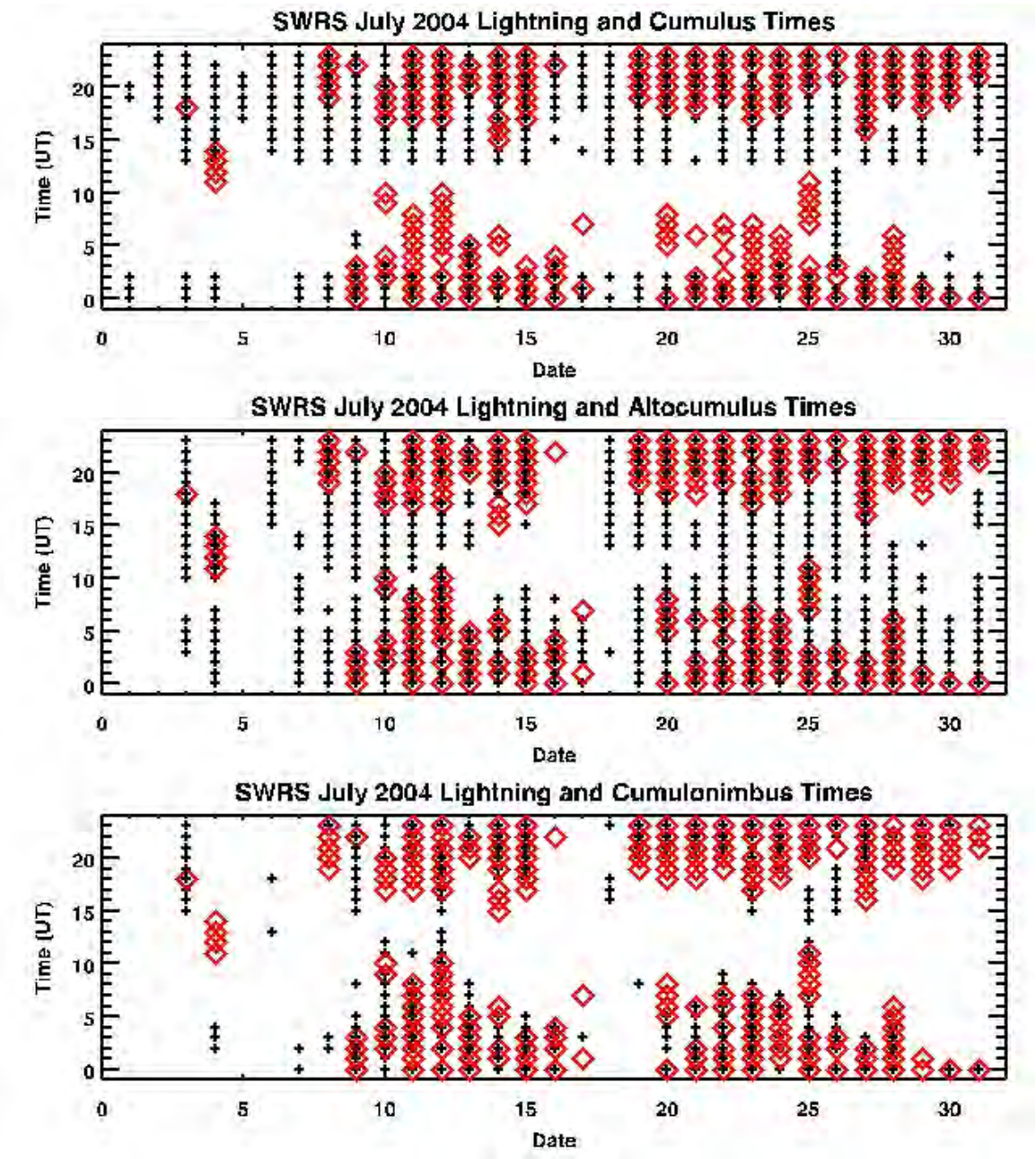

Figure 3-41. Dates and hours that convective clouds (black +) and lightning (red diamonds) were observed within 100 km of SWRS.

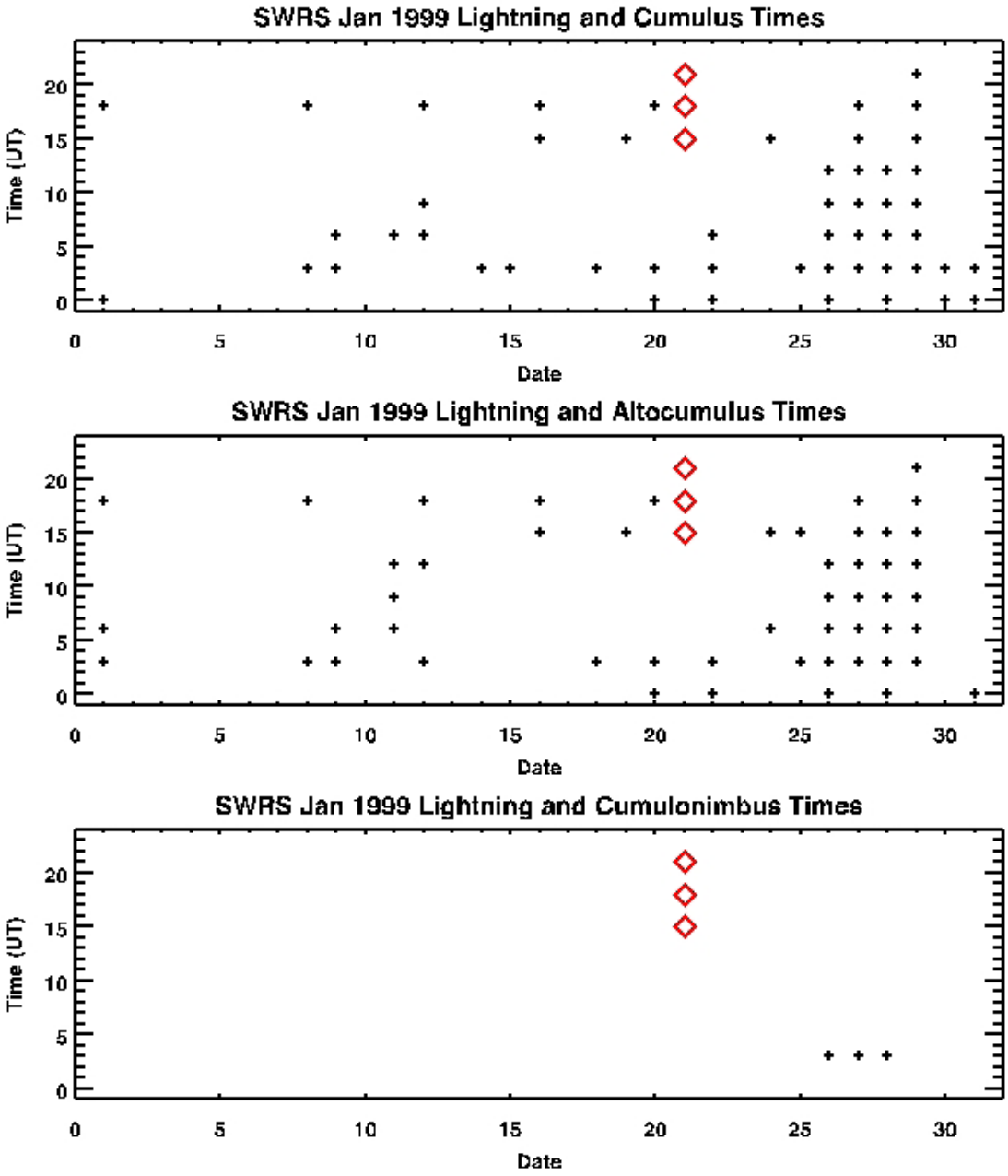

Figure 3-42. Dates and hours that convective clouds (black +) and lightning (red diamonds) were observed within 100 km of SWRS. Lightning occurs infrequently in the winter.

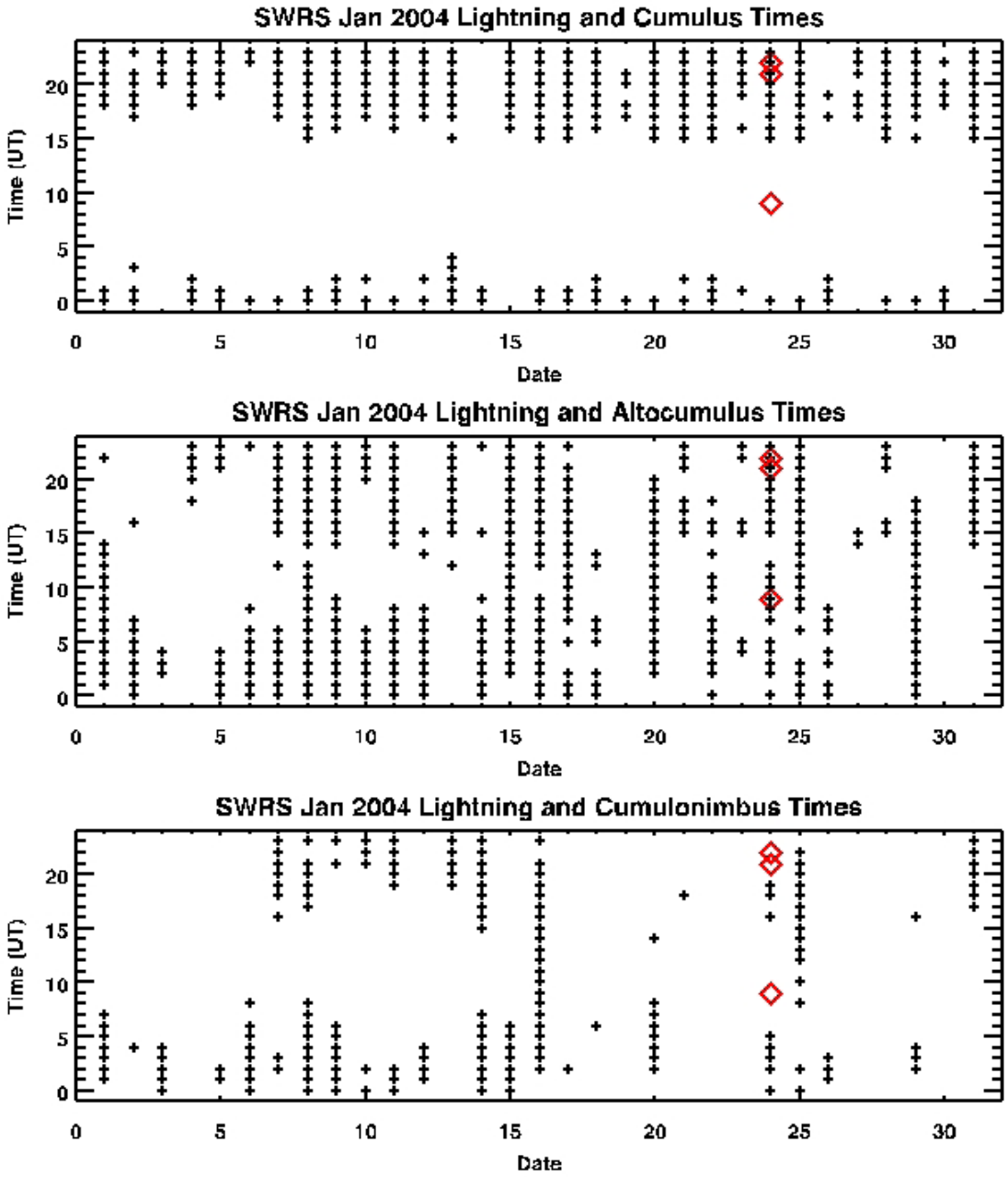

Figure 3-43. Dates and hours that convective clouds (black +) and lightning (red diamonds) were observed within 100 km of SWRS. Lightning occurs infrequently in the winter.

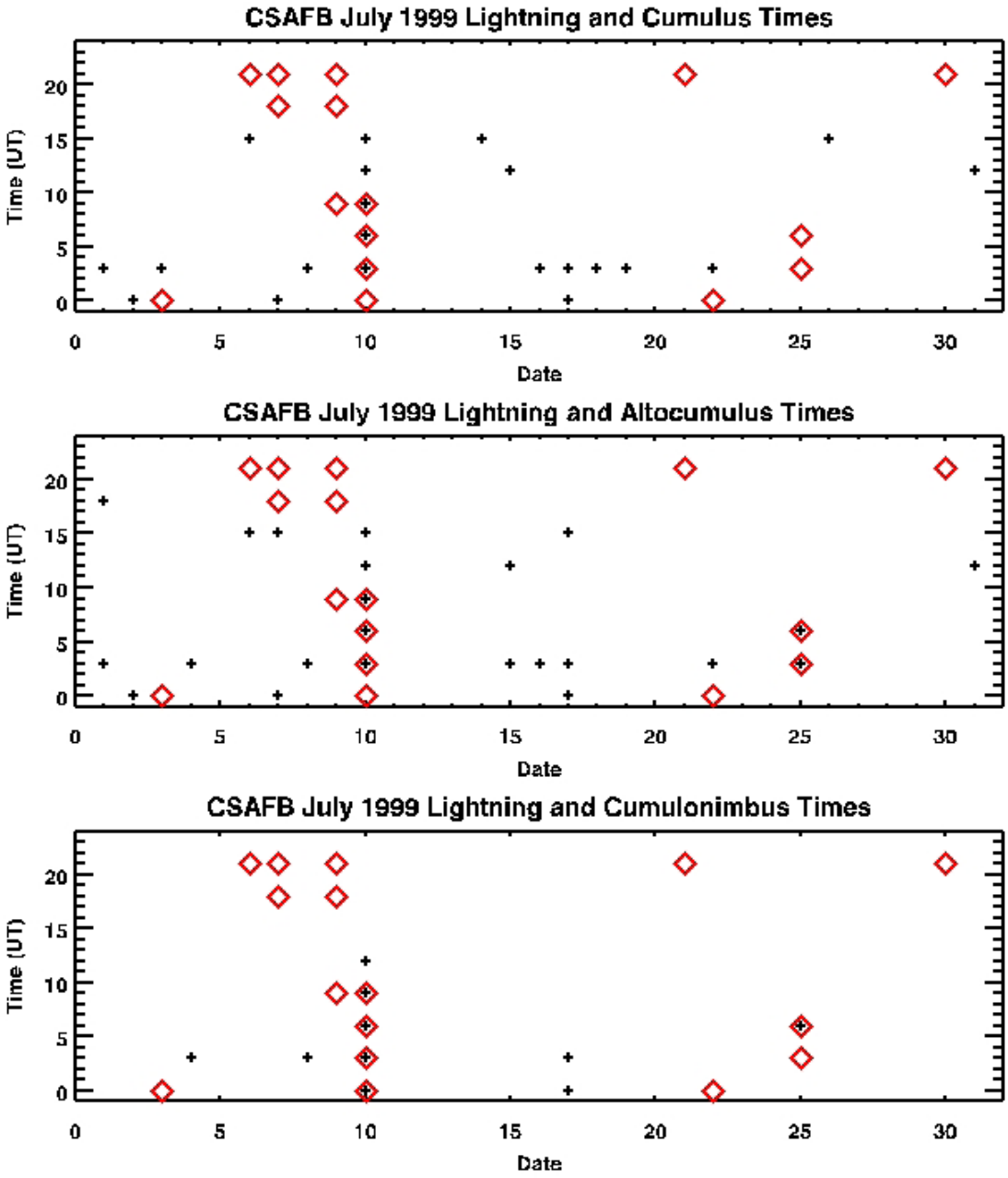

Figure 3-44. Dates and hours that convective clouds (black +) and lightning (red diamonds) were observed within 100 km of CSAFB. This was an anomalously nonstormy July for the region. LT = UT – 6 hours. Thunderstorm occurrence in the Midwest coincides with the approximately 2-week period of global Rossby waves.

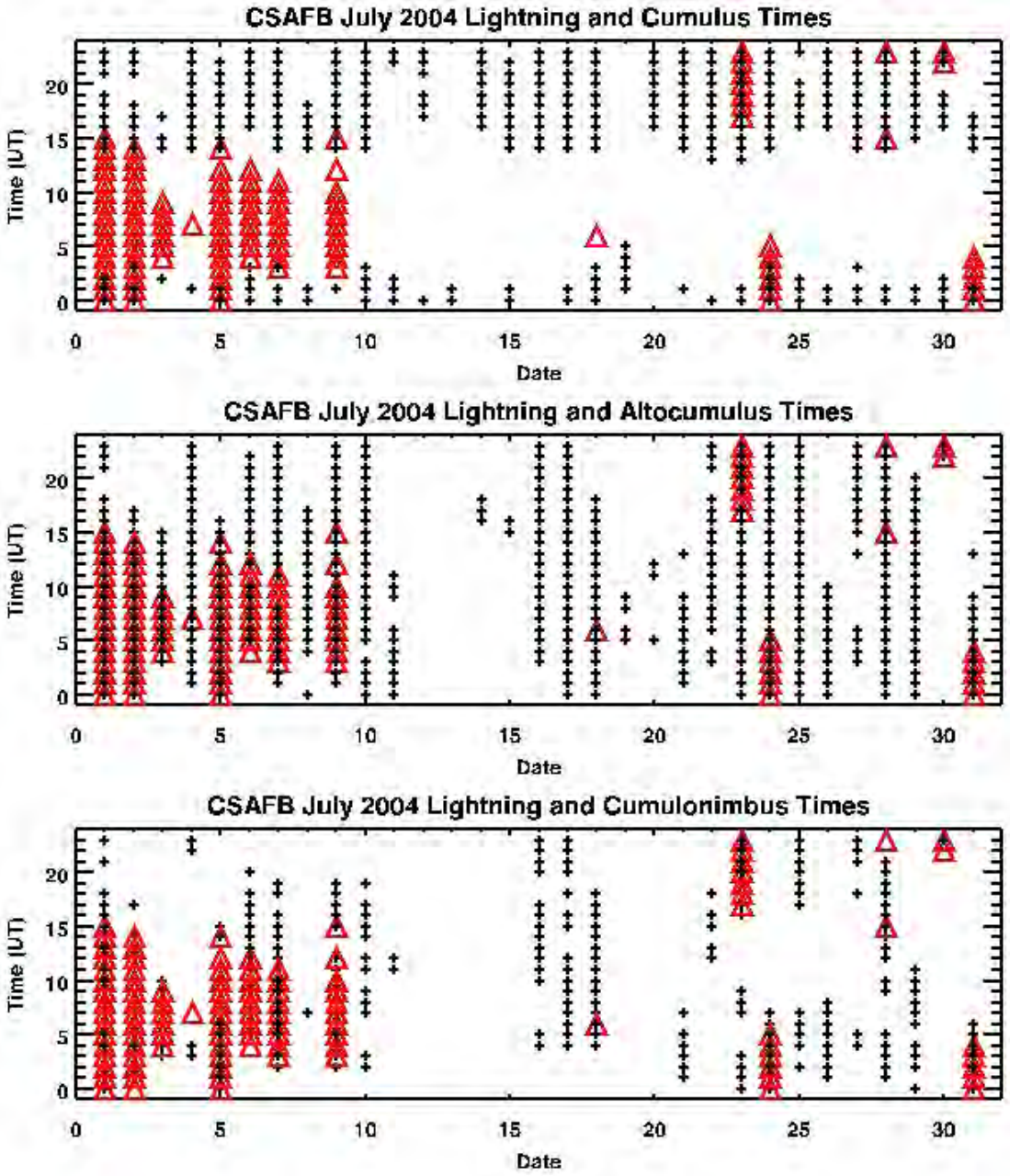

Figure 3-45. Dates and hours that convective clouds (black +) and lightning (red triangles) were observed within 100 km of CSAFB.

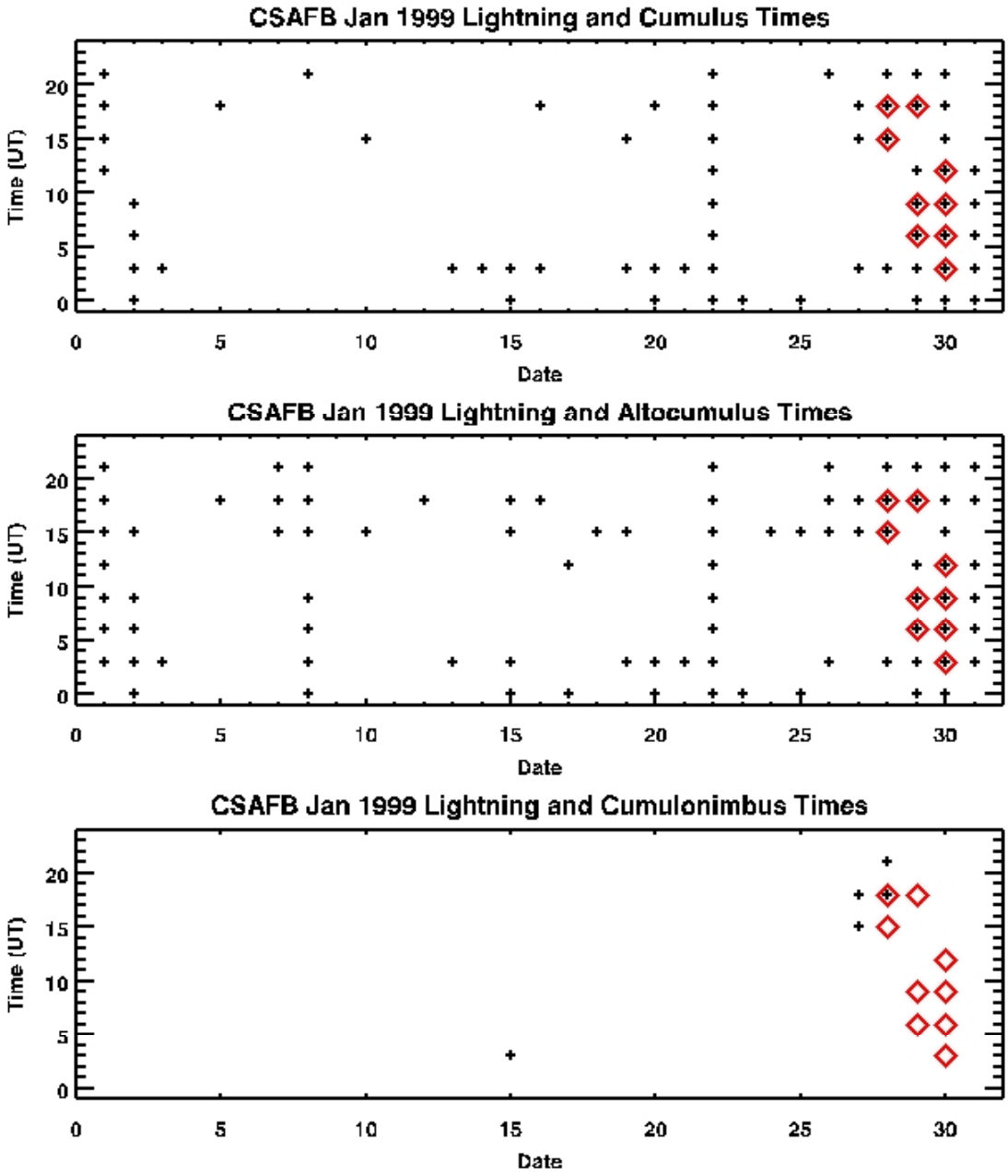

Figure 3-46. Dates and hours that convective clouds (black +) and lightning (red diamonds) were observed within 100 km of CSAFB. Lightning occurs infrequently in the winter.

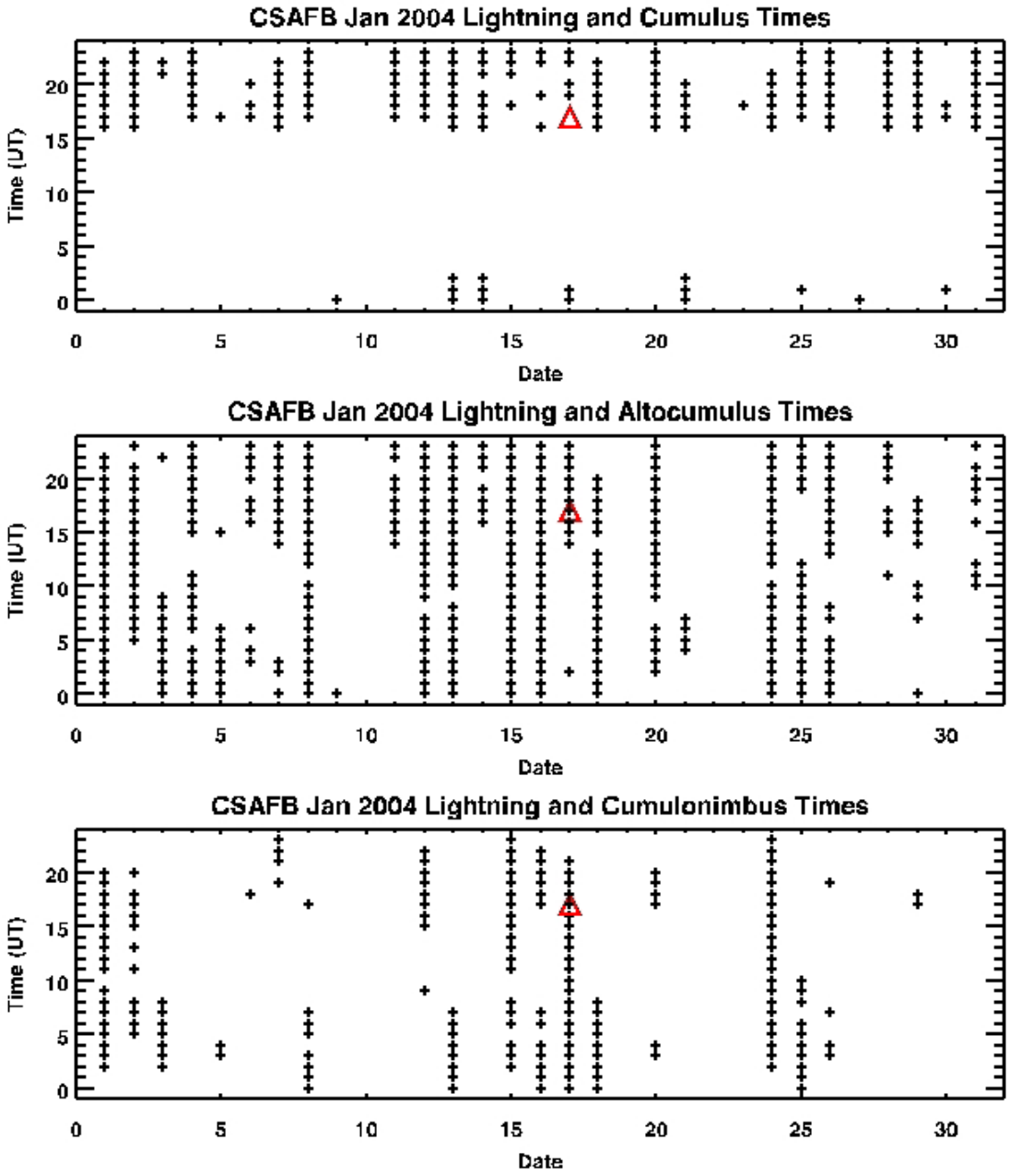

Figure 3-47. Dates and hours that convective clouds (black +) and lightning (red triangle) were observed within 100 km of CSAFB. Lightning occurs infrequently in the winter.

3.3.4 Temperatures within Clouds

Some of the cloud-based LLCC are based on cloud microphysical properties.[11] Cloud electrification peaks where water and ice are both present, around –10ºC. Existing cloud-based LLCC also specify that the flight path must not come within 0, 5, or 10 nautical miles of cumulus clouds with cloud tops higher than the –5ºC, –10ºC, and –20ºC isotherms, respectively. Since this required knowledge of the

[11] See Section 3.2.2 for a detailed explanation of the rationales for the cloud-based LLCC.

heights of the isotherms at specific times and places and CDFS2 does not give cloud temperature information, incorporation of a third database was required. The European Center for Medium Range Forecasting (ECMWF) global analysis model grid was used. This model is archived at the National Center for Atmospheric Research (NCAR). The model output is stored on isobaric (constant pressure) surfaces on a 2.5-degree latitude/longitude grid. The vertical levels are packed more densely near the surface and the tropopause.

The data at the tiles containing CSAFB and the proposed SWRS were vertically interpolated to obtain the isotherm geopotential heights for 5°C, –5°C, –10°C, and –20°C (red, green, aqua, blue lines)[12] (Figures 3-48 through 3-55).

Where the surface temperature is colder than 5°C, the 5°C isotherm line (shown in red) is set at 0. The terrain elevation of CSAFB grid tile is 590 m. Terrain elevation at SWRS grid tile is 1534 m. This is an average over the entire tile and not the actual elevation at the site. In general, wintertime surface temperatures are lower at CSAFB than at SWRS. Cold surface temperatures increase launch risk (e.g., spacecraft icing and frozen O-rings) and may cause launch delays.

Comparison of the July 1999 and 2004 data shows that the cumulus (and possibly altocumulus) cloud tops reach colder temperatures at the proposed SWRS than at CSAFB. There were no noticeable differences for cumulonimbus cloud top temperatures.

[12] The January 1999 data was archived on only 15 vertical levels instead of the usual 21 vertical levels. The reason was not documented on the database help pages. This exaggerated some numerical artifacts for the lower isotherms at CSAFB in January, where the surface was cooler than 5°C.

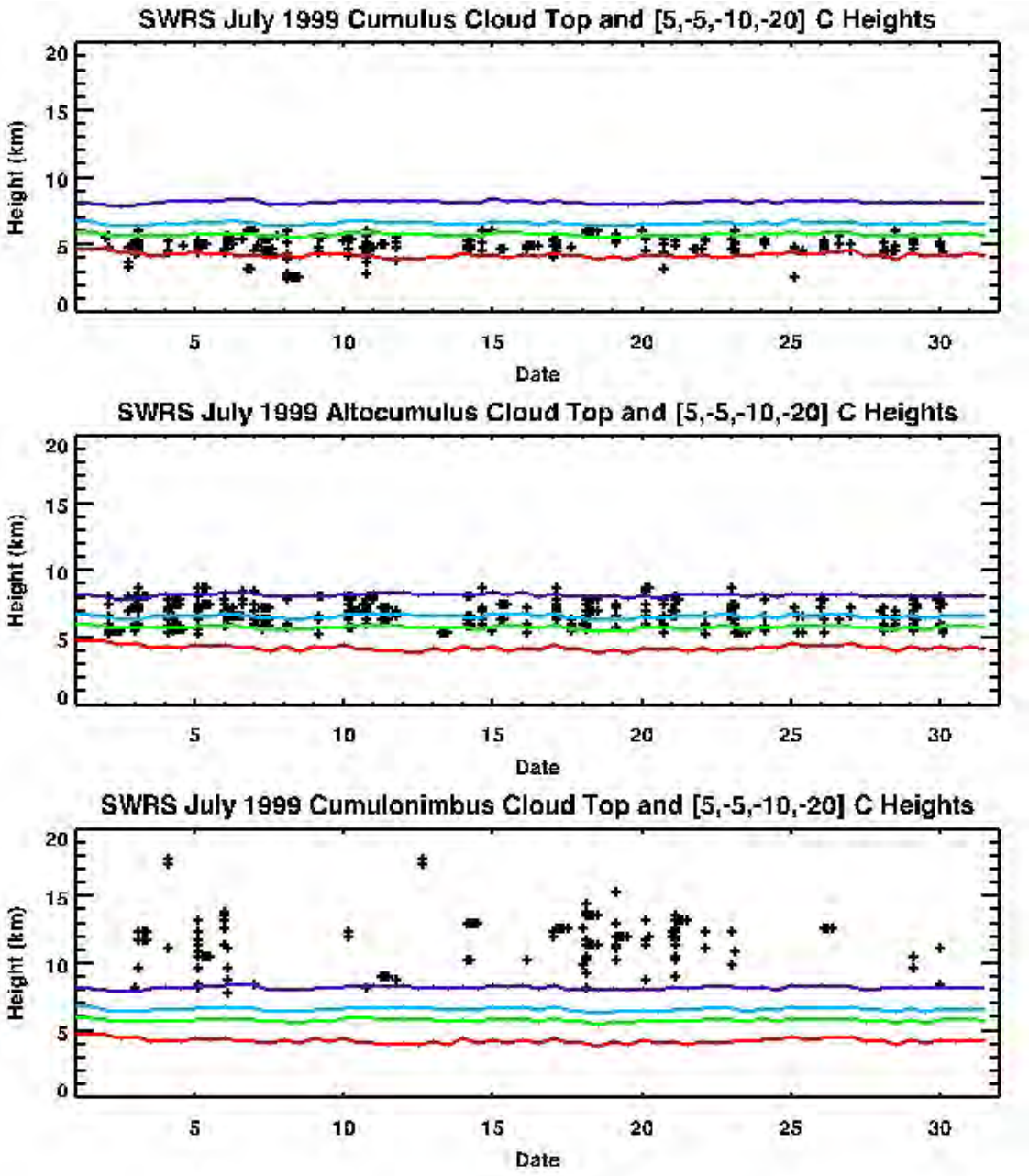

Figure 3-48. Cloud top heights for selected cloud types are shown in black (+). Isotherm heights for 5, –5, –10, and –20°C are shown in red, green, aqua, and blue, respectively.

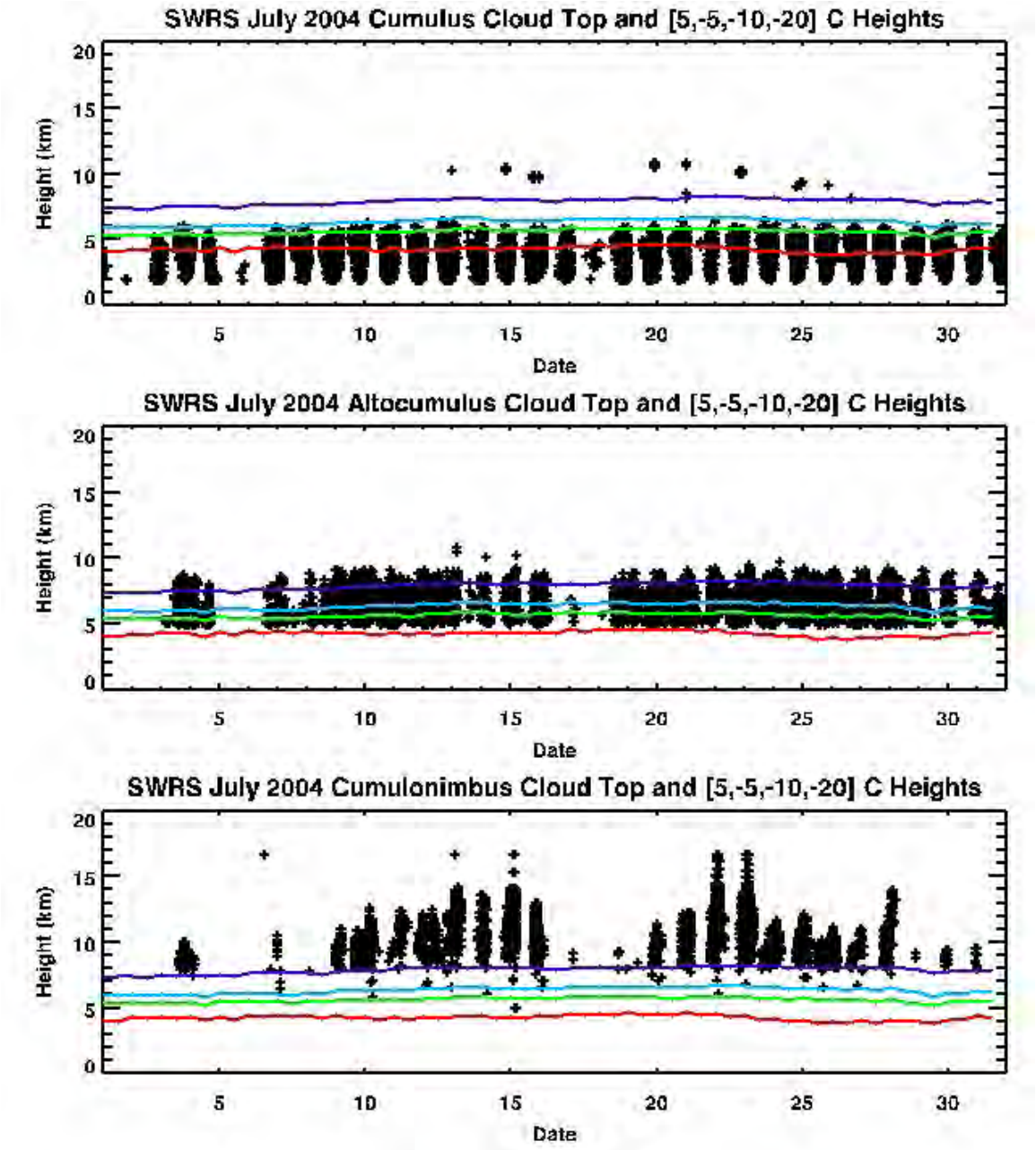

Figure 3-49. Cloud top heights for selected cloud types are shown in black (+). Isotherm heights for 5, –5, –10, and –20°C are shown in red, green, aqua, and blue, respectively.

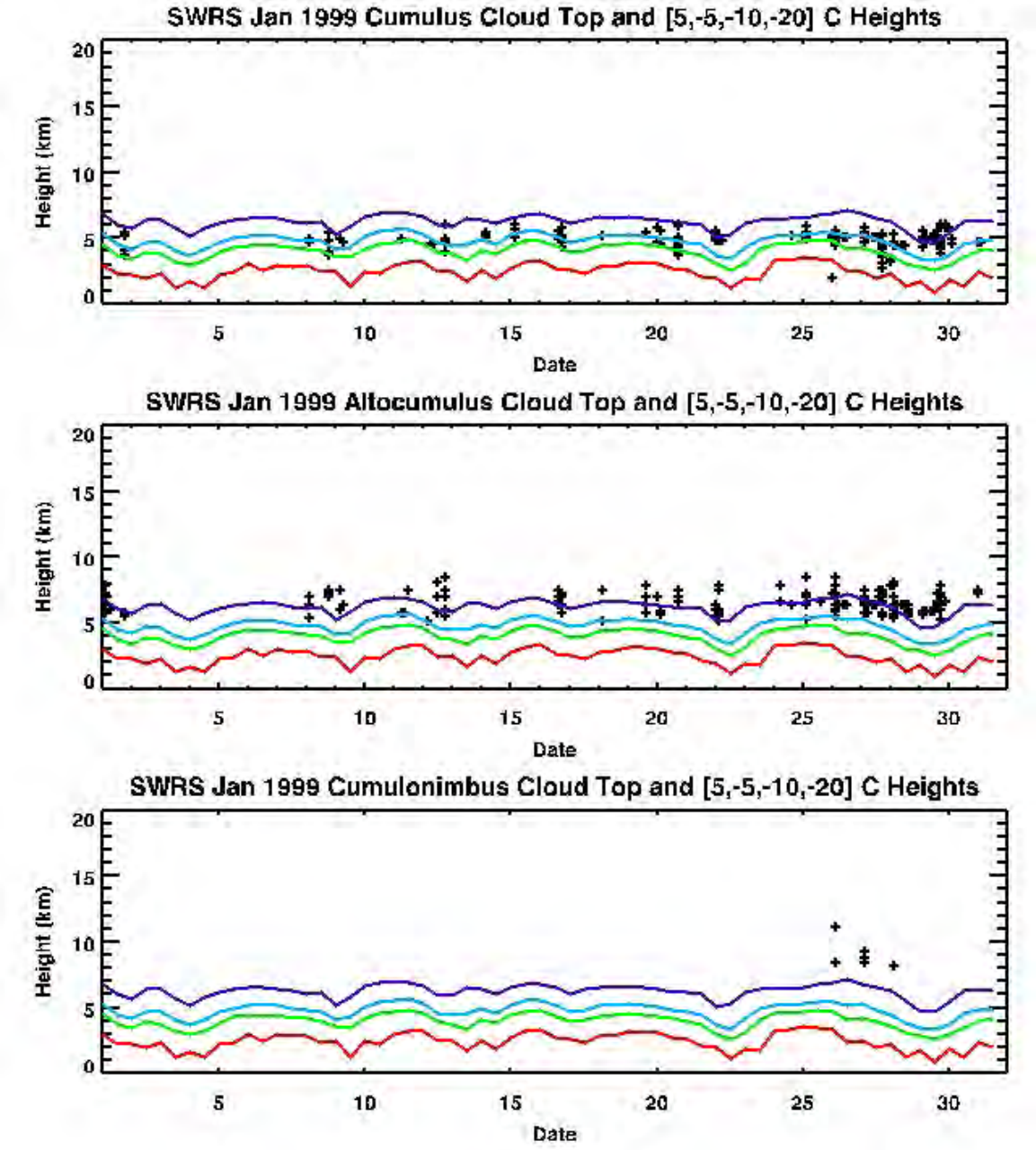

Figure 3-50. Cloud top heights for selected cloud types are shown in black (+). Isotherm heights for 5, –5, –10, and –20°C are shown in red, green, aqua, and blue, respectively.

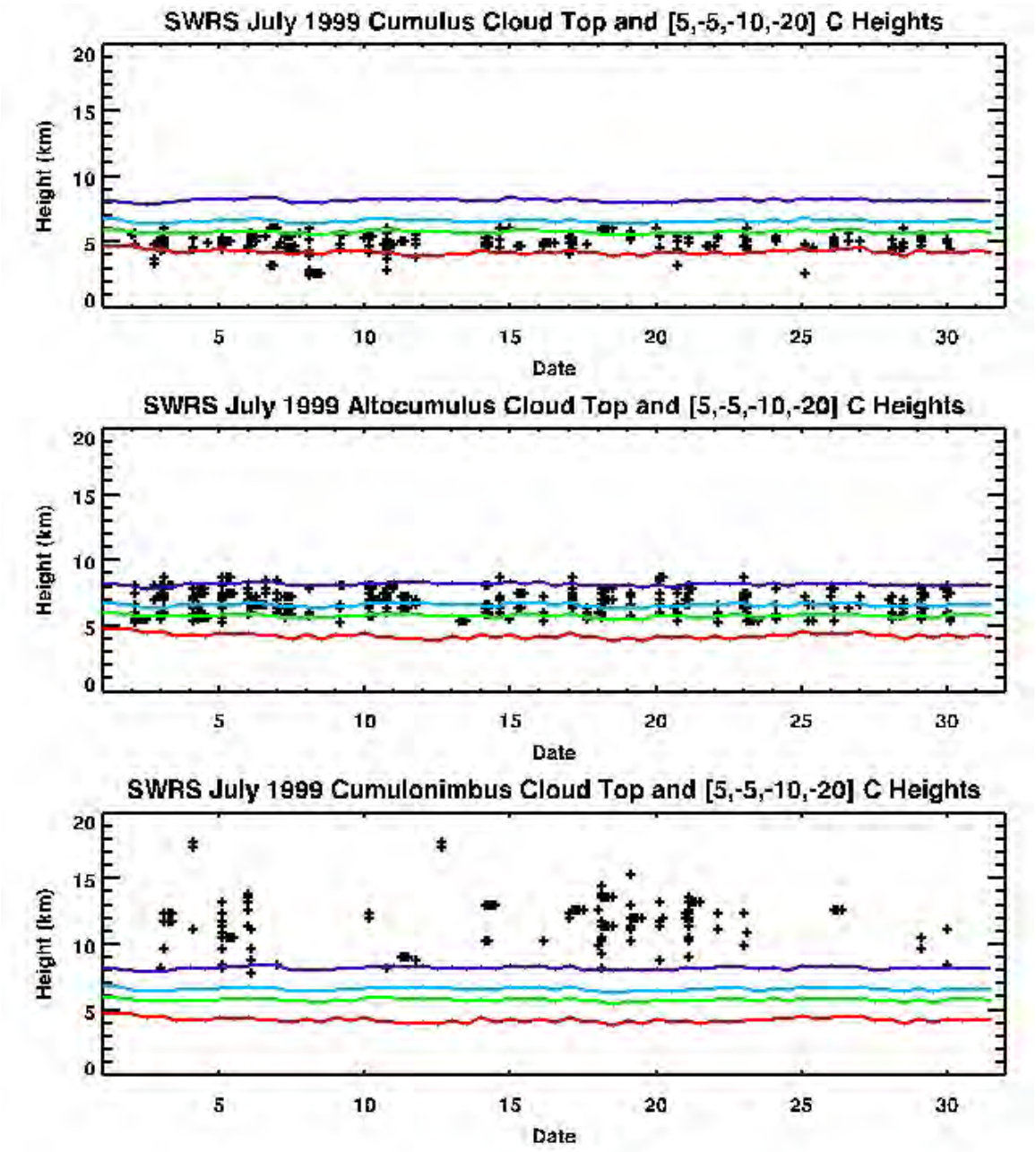

Figure 3-51. Cloud top heights for selected cloud types are shown in black (+). Isotherm heights for 5, –5, –10, and –20°C are shown in red, green, aqua, and blue, respectively.

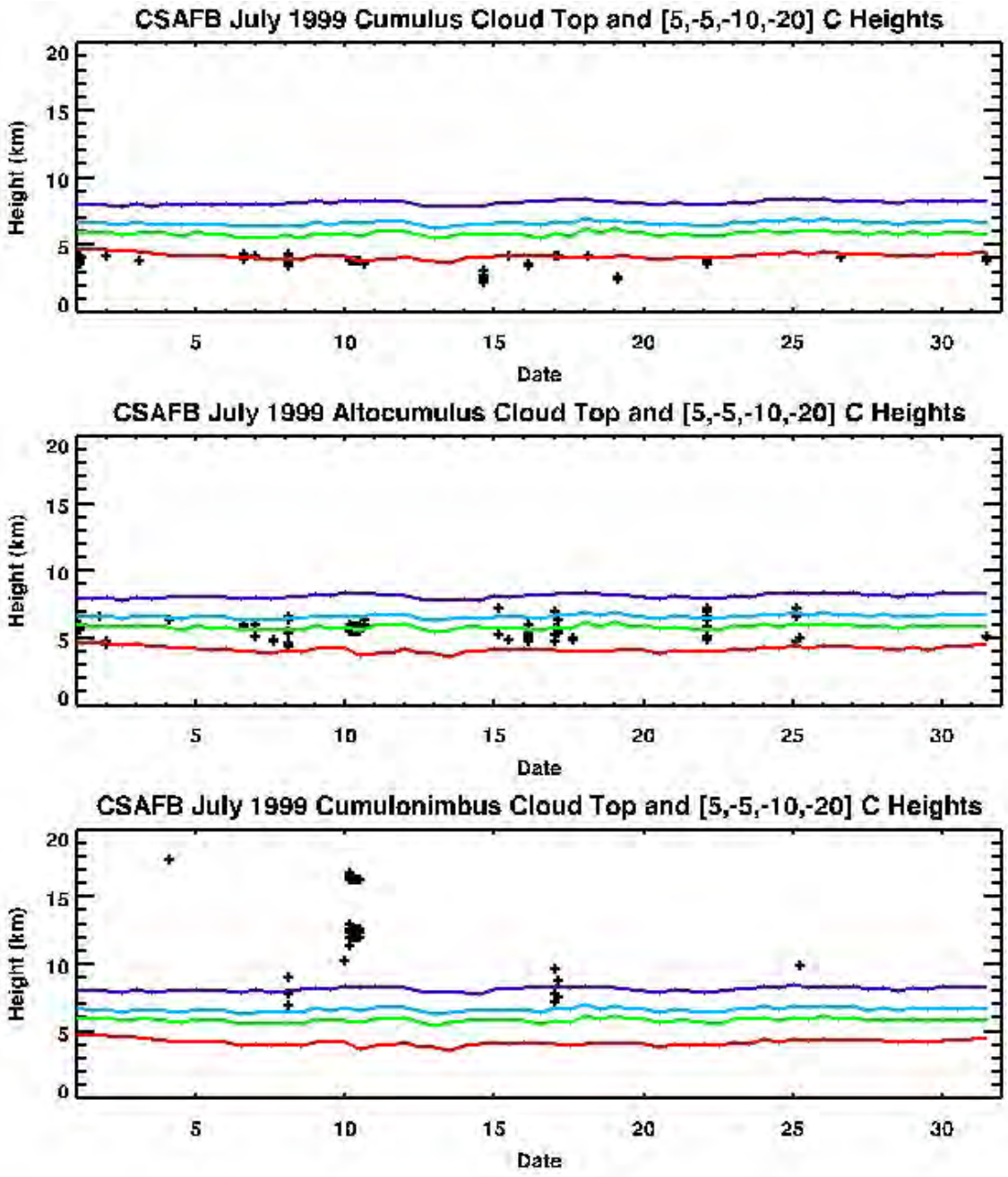

Figure 3-52. Cloud top heights for selected cloud types are shown in black (+). Isotherm heights for 5, –5, –10, and –20°C are shown in red, green, aqua, and blue, respectively. July 1999 was an anomalously thunderstorm-free July at CSAFB.

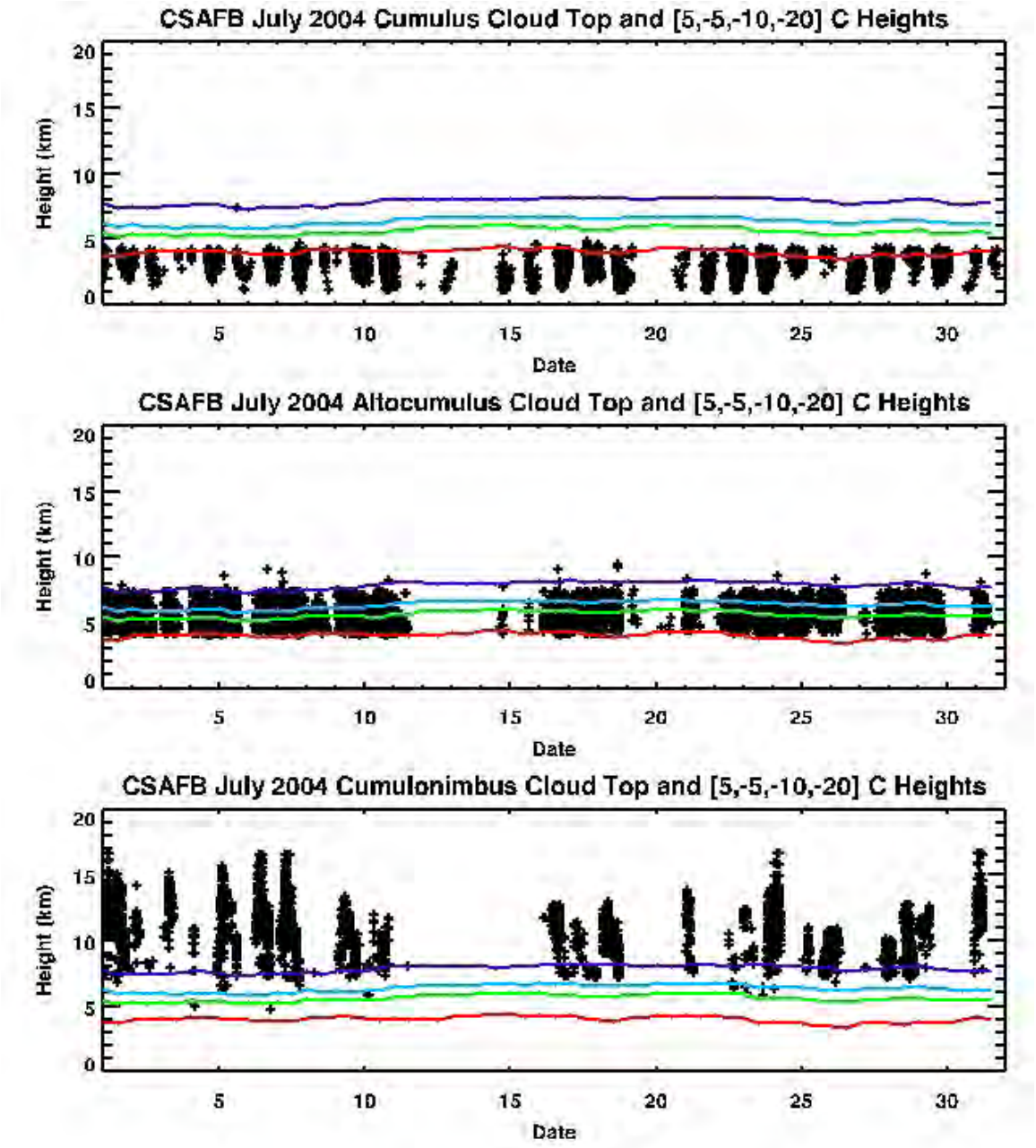

Figure 3-53. Cloud top heights for selected cloud types are shown in black (+). Isotherm heights for 5, –5, –10, and –20°C are shown in red, green, aqua, and blue, respectively.

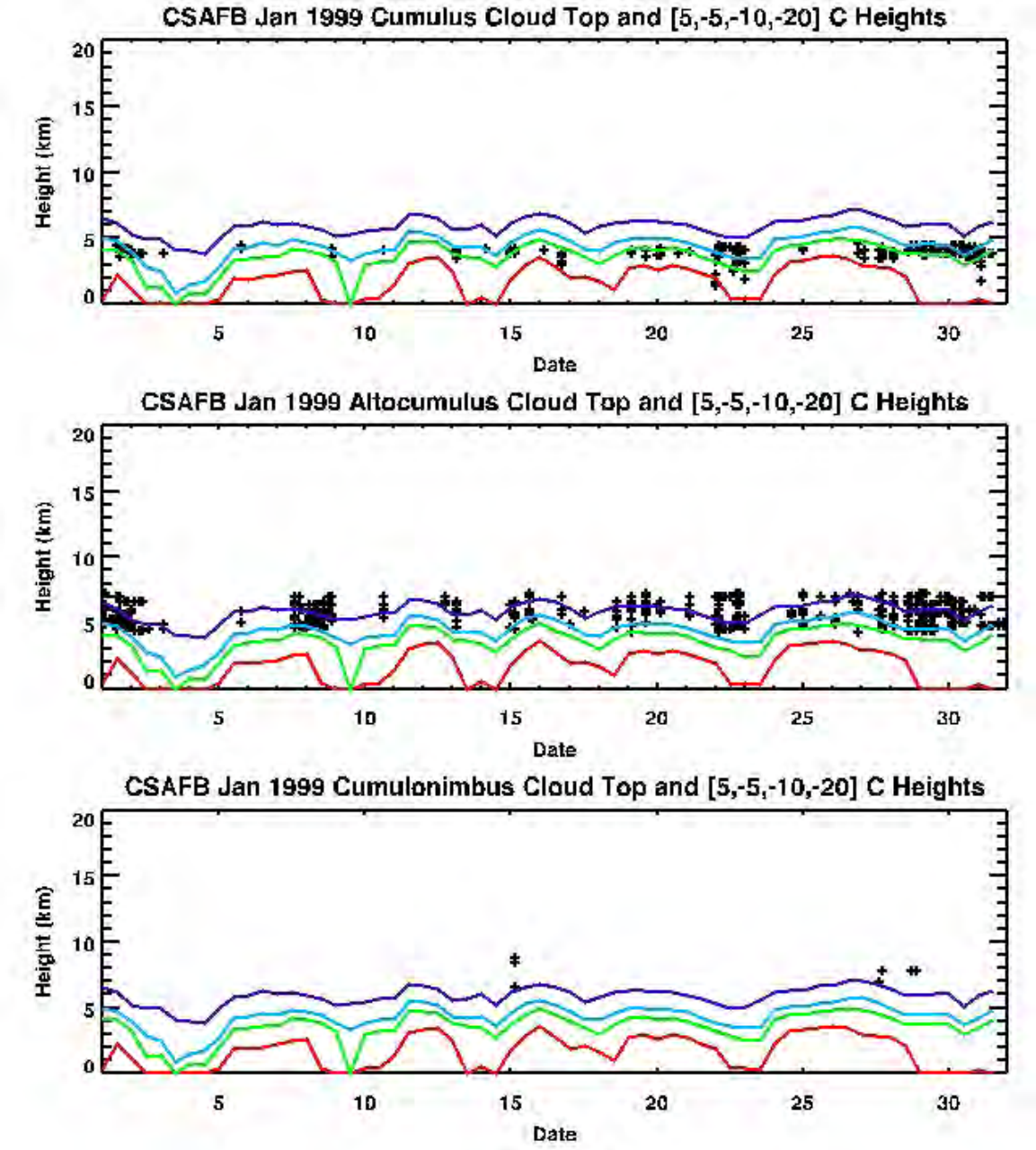

Figure 3-54. Cloud top heights for selected cloud types are shown in black (+). Isotherm heights for 5, –5, –10, and –20ºC are shown in red, green, aqua, and blue, respectively. 5ºC isotherm heights (red) of zero denote places where the surface temperature is colder than 5ºC.

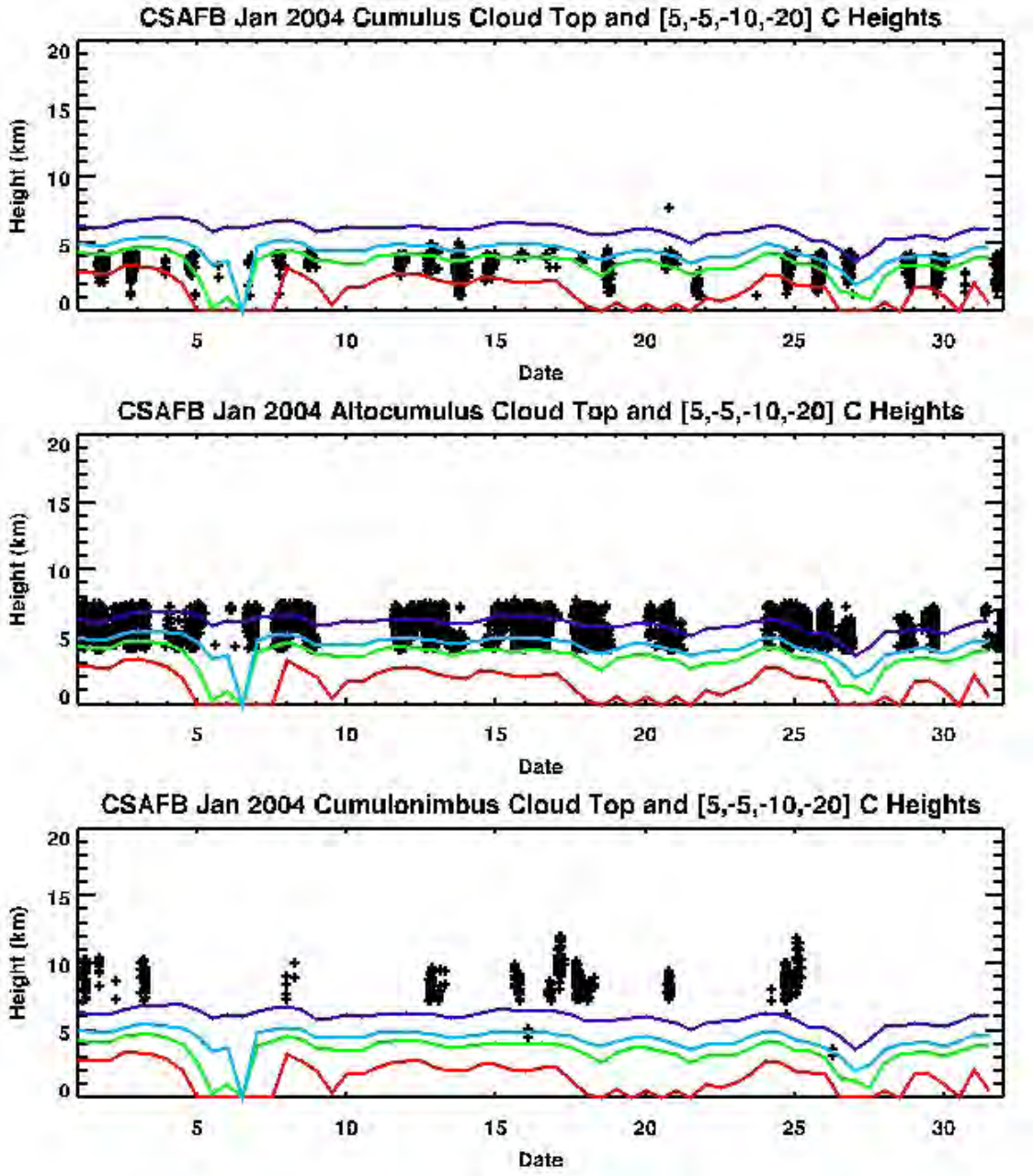

Figure 3-55. Cloud top heights for selected cloud types are shown in black (+). Isotherm heights for 5, –5, –10, and –20°C are shown in red, green, aqua, and blue, respectively. 5°C isotherm heights (red) of zero denote places where the surface temperature is colder than 5°C.

3.3.5 Cloud Coverage Statistics

Heavy cloud cover can delay or scrub launches for reasons other than lightning risk. Figures 3-56 and 3-57 show the monthly percentage cloud coverage for the CDFS2 grid point closest to the locations given in Table 3-6. The red line denotes the monthly mean cloud coverage.

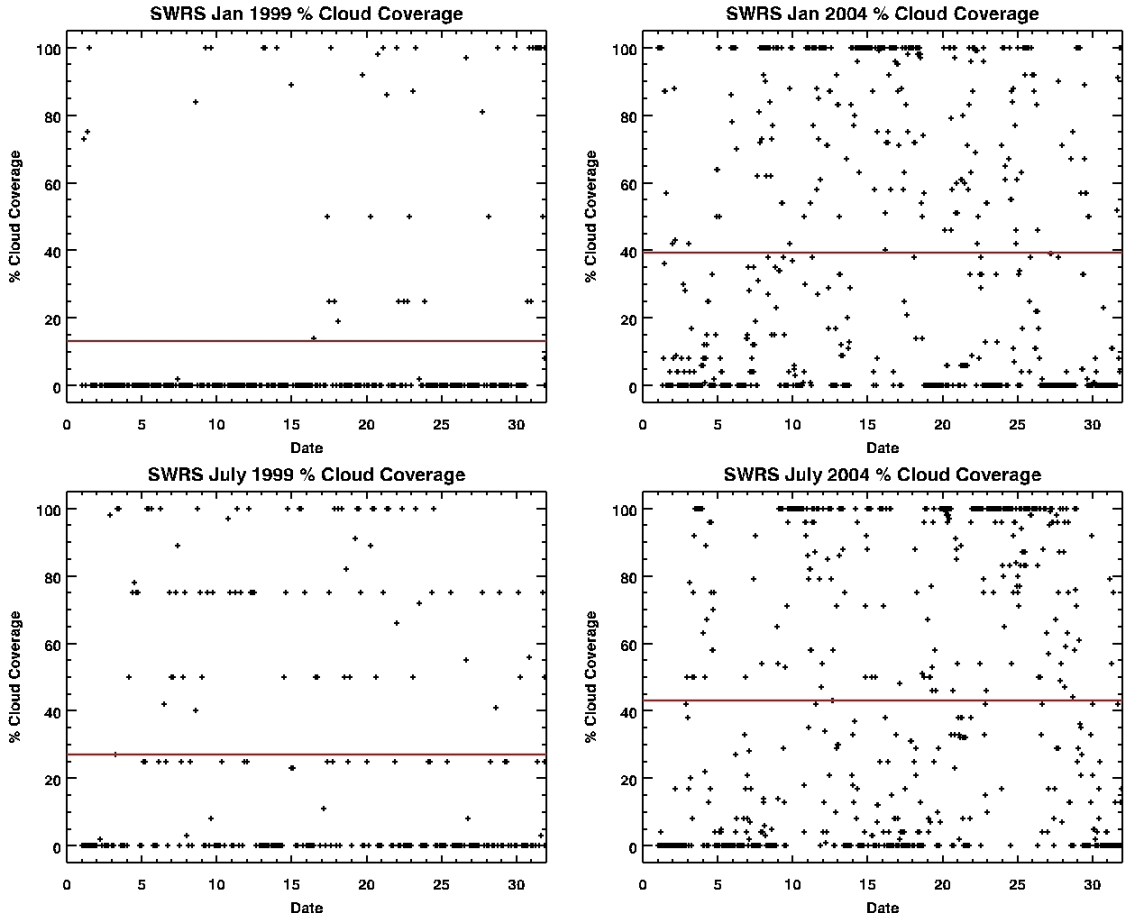

Figure 3-56. Percentage cloud coverage at SWRS. The red line denotes the monthly mean.

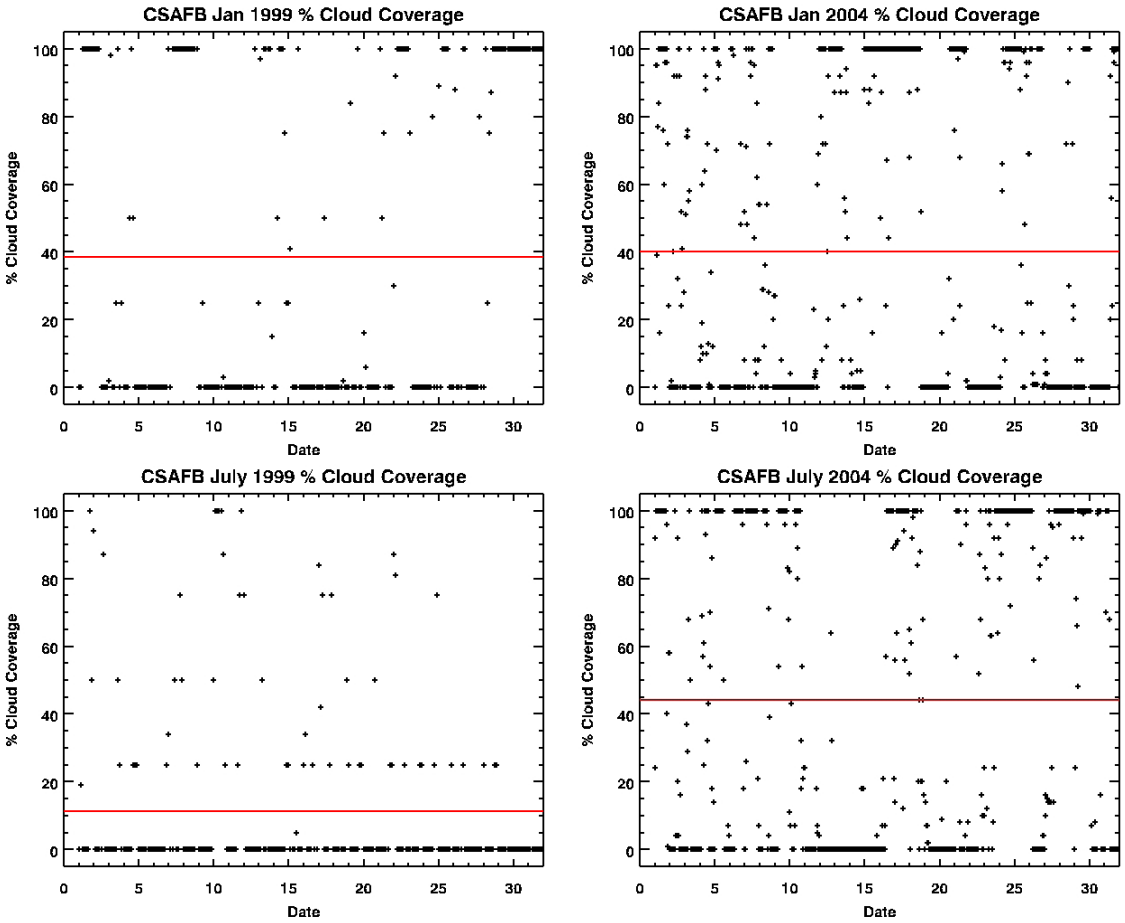

Figure 3-57. Percentage cloud coverage at CSAFB. The red line denotes the monthly mean. The low value of % cloud coverage in July 1999 reflects that it was an anomalously storm-free July at CSAFB.

Figures 3-58 and 3-59 show the mean cloud coverage measured by satellites for April and July. On average, satellite cloud climatology shows that the site of the proposed SWRS is less cloudy than CSAFB except during the monsoonal flow season of July and August. Year-to-year variability is high, as evident in Figure 3-57.

3.3.6 Summary of Lightning and Cloud Climatology

A nearly 15-year climatology study of naturally occurring cloud-to-ground lightning strikes showed that both proposed spaceport sites experienced similar amounts of lightning strikes. Year-to-year variability is high, however. Cloud-to-ground lightning strike data at the proposed OS indicates that it is less than 80% likely to be lightning free for roughly 120 days of the year, from late May through early September. The proposed SWRS is less than 80% likely to be lightning free (or more than 20% likely to experience lightning) for roughly 90 days a year, from late June through early October. Cape Canaveral had the highest number of days that were less than 80% likely to be lightning free at 146 days, while VAFB had the lowest number of days (0).

While this information is useful, it should be kept in mind that launches can safely take place on the same day as a thunderstorm, as long as the launch is sufficiently far away in time and space from the

thunderstorm. In July, the month with the highest amount of lightning occurrence, the proposed OS, has more hours that are likely to be lightning free than the proposed SWRS.

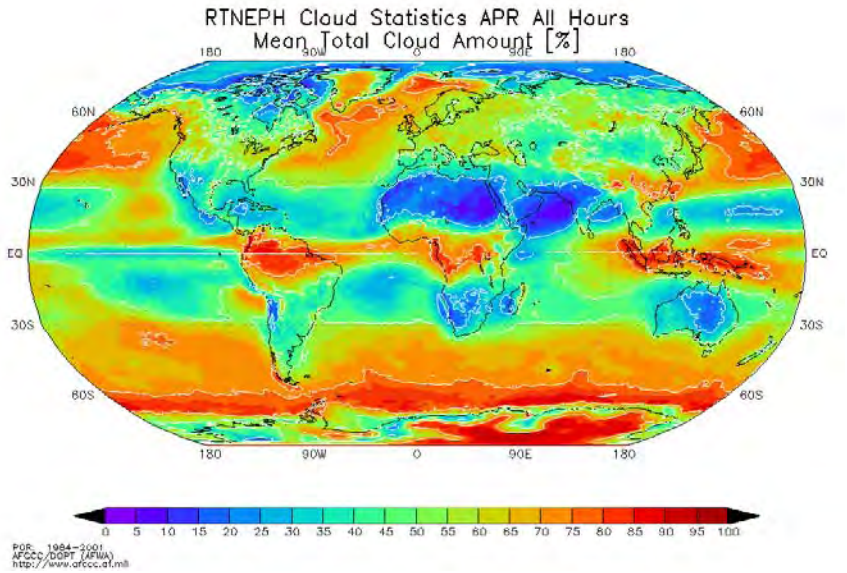

Figure 3-58. Mean total cloud amount from satellite cloud analysis for April. As for most of the year, the Southwest is less cloudy than the Midwest.

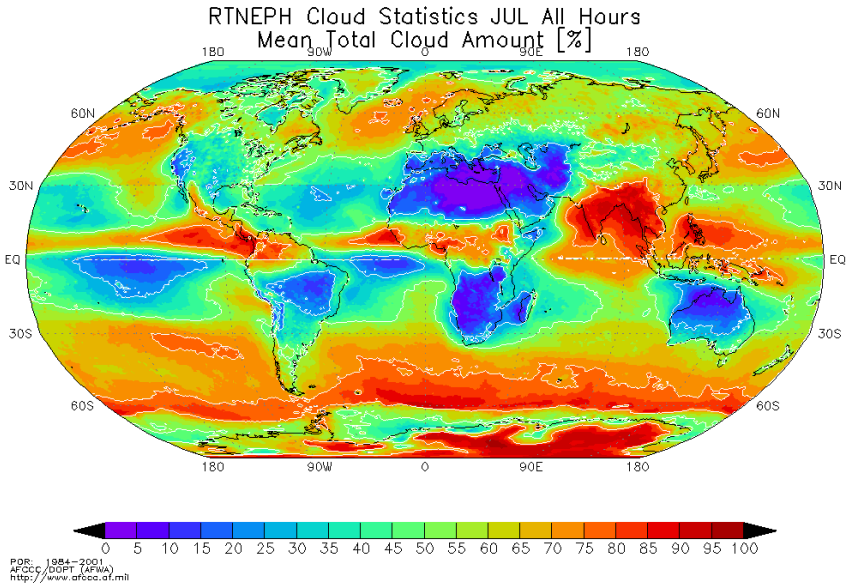

Figure 3-59. Mean total cloud amount from satellite cloud analysis for July. During July and August, New Mexico is cloudier than the Midwest.

3.4 Conclusion: Quantitative Risk Assessment

This section summarizes the extent to which a comprehensive risk assessment for the five concept RLVs at the two proposed spaceports has been achieved and outlines the additional information and analyses that seem necessary to meet this challenge. By "comprehensive risk assessment," we mean a computation of the diurnal and seasonal probability that any particular vehicle will trigger lightning during a particular flight at any particular spaceport, if it is launched without regard to current weather conditions. The following steps have been taken toward such a result:

A. The frequency of natural cloud-to-ground lightning has been determined, both diurnally and seasonally, in the vicinity of each proposed spaceport. Noting that intra-cloud lightning (which is disregarded by the existing national lightning-detection network) constitutes the majority of natural lightning, this frequency gives a *lower bound* on the violation frequency of the LLCC natural-lightning rule, which must certainly be observed during *all* space-launch operations. The resulting statistics are summarized in Section 3.4.1.

B. The frequencies of violations of certain of the cloud-based LLCC have also been estimated, as summarized in Section 3.4.2. Although some portions of the current LLCC may not be applicable for flights of suborbital RLVs, *but only after further analysis* (see Sections 3.2.3, 4.1.1, and 4.1.2), these statistics also constitute an important step toward a comprehensive risk assessment, as outlined below.

C. Estimates of the ambient conditions required to trigger lightning with each of the proposed RLV types are summarized in Section 3.4.3. Knowledge of these conditions enables an operational ABFM to reduce the false alarms that would otherwise result from the application of the LLCC to these vehicles. This knowledge also constitutes another step toward a comprehensive risk assessment.

To make the connection between the LLCC-violation frequencies (B) and the triggering conditions (C), however, more information is required. We also need the probability of occurrence of the relevant electric-field magnitudes in clouds that violate the various LLCC. Some of this information probably already exists in unpublished reports from the ABFM I campaign, and sufficient information certainly exists specific to thunderstorm anvils in Florida from the ABFM II campaign, but it is beyond the scope of this project to collect and re-analyze this data, even assuming that enough such information is available. This approach and its prospects are elaborated on further, however, in Section 3.4.3, and specific recommendations are made in Sections 4.1.1 and 4.1.2.

3.4.1 Probability of Natural Cloud-to-Ground Lightning

The lightning climatologies for the two proposed spaceport sites and three existing launch ranges were examined in detail in Section 3.3. Briefly, both sites experienced similar amounts of natural cloud-to-ground lightning in the fifteen-year period covering 1990–2004. The proposed sites of SWRS and OS have lightning seasons lasting 90 and 120 days, respectively. However, on the days with a high likelihood of lightning, the proposed SWRS is generally likely to be lightning free between 0800 and 1600 UT, 0100 and 0900 local time. In contrast, although CSAFB mainly experiences natural lightning in the early evening, the threat of lightning does not diminish to near zero at any predictable time of day.

3.4.2 Estimated Probability of LLCC Violations

These criteria were analyzed graphically in Sections 3.3.3 and 3.3.4. In general, the lightning database showed that natural cloud-to-ground lightning occurred when the cloud database showed that convective clouds were present. However, the presence of convective clouds does not always correspond to observed natural lightning. Cloud top temperatures over the proposed SWRS are slightly colder for cumulus and altocumulus clouds than over CSAFB. This could elevate the risk of triggered lightning at SWRS during the summer southwest monsoon season. Visual examination of the cloud and lightning data in Figures 3-49 through 3-55 suggests that LLCC will seldom be violated in January but will be violated about 60 to 75% of the time in the late afternoon and evening in July at both sites. Perusal of the July 2004 lightning and cumulus cloud correlation plots in Figures 3-41 and 3-45 shows that those LLCC were violated 30% and 75% of the days, respectively, at CSAFB and the proposed SWRS in the late afternoon and early evening.

3.4.3 Estimated Triggering Conditions

Triggering conditions in terms of ambient electric-field thresholds have been estimated for each of the concept RLVs (except the Concept 5 vehicle, for reasons that are discussed briefly below) in Section 3.1.5.5. Table 3-5 is repeated here for convenience.

Table 3-5 (Repeated). Estimated Triggering Fields

Vehicle	Boost Phase		Glide Phase	
	Surface, kV/m	10 km, kV/m	Surface, kV/m	10 km, kV/m
Concept 1	60	20	125	42
Concept 2	93	31	182	61
Concept 3	83	28	169	56
Concept 4	79	26	—	—
Concept 5	—	—	—	—
Titan IV	16	5	—	—

These field thresholds are quite uncertain in absolute terms, but they should be reasonably comparable between vehicles at the same altitude. Thus, they provide a quantitative basis for the following three conclusions: A) For vehicles that are designed for unpowered horizontal landings (Concept vehicles 1, 2, and 3), there is a significant increase in triggering threshold (qualitatively, a reduction in triggering likelihood) during the glide phase of the flight. B) During the glide phase, these three concept RLVs have higher triggering thresholds than medium-sized aircraft (which have been measured to be on the order of 45 kV/m at 4–5 km altitudes). C) Not surprisingly, all of these concept RLVs have much higher triggering fields than the Titan IV (which is typical of large orbital boosters for which the current LLCC were designed). The following additional conclusion is less certain because conventional aircraft do not have electrically significant exhaust plumes and, consequently, are not strictly comparable to space vehicles during boost phase: D) Although the largest vehicle (Concept 1) has an appreciably lower triggering threshold than the others, during boost phase all of them appear to be roughly comparable to medium-sized aircraft. The last conclusion is not based on quantitative triggering conditions, but rather on the balloon-launched nature of the 5th concept RLV: E) Launch conditions for the Concept 5 vehicle will have to be even more rigorous than provided in the current LLCC because of the huge balloon that is required to lift it to 80,000 ft.

altitude before ignition. Wind shear, turbulence, and icing must all be avoided, in addition to lightning. Therefore, we do not believe that triggered-lightning conditions, nor even the LLCC, are relevant in this case.

3.4.4 Toward a Probability of Triggered Lightning

The triggering fields that are derived in Section 3.1.5 constitute a quantitative metric that may be compared among vehicles. A higher triggering field does correspond to a lower likelihood of triggered lightning, all other circumstances being equal. Note, however, that a given field threshold cannot be translated directly into a probability of triggering. Triggering probability depends primarily on the weather into which a vehicle flies.

One way of estimating the probability of triggering during a single flight of a given vehicle from a given spaceport would be to combine the probabilities of violation of all relevant LLCC rules at that spaceport with the corresponding probabilities of encountering the threshold field for that vehicle during each such violation (remembering, of course, the additional complication that this threshold field is altitude dependent). Suppose, for example, that there were three LLCC, arbitrarily named "Rule D," "Rule E," and "Rule F" that were applicable to the RLV in question. Then the overall triggering probability, *P*, could be written as follows:

$$\begin{aligned} P = {} & P(\mathrm{D}) + P(\mathrm{E}) + P(\mathrm{F}) \\ & - P(\mathrm{D\&E}) - P(\mathrm{D\&F}) - P(\mathrm{E\&F}) \\ & + P(\mathrm{D\&E\&F}) \end{aligned} \tag{8}$$

Equation 8 requires some explanation. *P* on the left-hand side denotes the probability of the INCLUSIVE OR of triggering probabilities due to three separate rules, more than one of which may be violated simultaneously. Each $P(I)$ on the right-hand side denotes the individual triggering probability due to Rule *I*, independent of violations of the other two rules. Therefore, it should be clear that the sum of the $P(I)$, given in the first line of (8), will in general exceed *P*, and may even exceed unity, because of multiple counting of violations of more than one rule for the flight. The $P(I\&J)$ denote the triggering probability due to simultaneous violations of both Rules *I* and *J*, and $P(\mathrm{D\&E\&F})$ represents that of all three rules. These terms are required to correct the sum in the first line of the equation, as can be easily demonstrated with Venn diagrams [e.g., Freund, 1967, Ch. 5].

Each $P(I)$ above can be expressed as the product of the probability with which that rule is violated at the given spaceport, $Q(I)$, from climatological statistics like those in Section 2.4.2, times the probability that such rule violations result in ambient fields in excess of the triggering threshold for the given RLV:

$$P(I) = Q(I)*[1 - B(I)] \tag{9}$$

where $B(I)$ is the probability that *no* hazardous fields occur during Rule *I* violations. Similarly,

$$P(I\&J) = Q(I\&J)*[1 - B(I)*B(J)] \tag{10}$$

and

$$P(\mathrm{D\&E\&F}) = Q(\mathrm{D\&E\&F})*[1 - B(\mathrm{D})*B(\mathrm{E})*B(\mathrm{F})] \tag{11}$$

An example of the estimation of the $B(I)$ in Equations 9 through 11 is provided in Table 3-10 [Willett and Barnes, 2000], based on data collected for large orbital boosters during the ABFM I campaign in the early 1990s. Unfortunately, these results apply to an earlier set of LLCC that were current at the time. Rule D prohibited flight through a cloud layer thicker than 4500 ft that contains temperatures between 0 and –20ºC, Rule E prohibited flight through clouds that extend above 0ºC and are associated with disturbed weather within 5 nmi, and Rule F prohibited flight through thunderstorm debris clouds, nor within 5 nmi of such clouds not monitored by a field mill network or with radar returns greater than 10 dBZ. These results would not be specifically relevant here in any case, since the field thresholds then considered hazardous to large boosters (indicated in the table) were considerably lower than those derived in Section 3.1.5 for the much smaller RLVs presently under consideration.

Table 3-10. ABFM Data on the Occurrence of Hazardous Fields Aloft During LLC Rule Violations (LLC References Superscripted)

			Rule F (Age or Standoff)		
ABFM Statistics	**Rule D**	**Rule E**	**t = 0**	**t > 1 hr**	**Within 5 nmi**
Number of Cases	863	524	150	28	
Number "Hazardous"	121[a]	185[c,e]	95[n]	0[m]	?
Hazardous Field	>3 kV/m	>5 kV/m	>1 kV/m	>3 kV/m	
$B(I)$ — from above	0.860	0.647	0.37	1.0	?

[a] Briefing to LCC "Peer Review Committee" by MSFC at KSC, 2/94
[c] Winter 1991 Deployment Report, MSFC, 2/25/92
[e] Winter 1992 Deployment Report, MSFC, 10/8/92
[m] Mailing to "Peer Review Committee" from NASA/ME, 11/10/93
[n] D. Mach, personal communication, 9/7/94

There might be sufficient data still available from the ABFM I campaign to estimate the probabilities of triggering fields for our RLVs during violations of at least some of the current LLCC, but compiling and analyzing such data would not be feasible within the resources available to this project. There certainly is sufficient data on ambient field vs. radar reflectivity in Florida anvil clouds from the ABFM II campaign in the early 2000s to estimate the probability of triggering fields for these RLVs during violations of the current anvil rules, but even this is beyond the scope of the project and, in any case, is not sufficient for a comprehensive risk assessment.

4. Recommendations for the Future

4.1 Statistical Analysis of Existing Data to Better Determine LLCC and LFCC Applicability to RLVs

In Section 3.2.3 we have attempted to prioritize the application of the existing LLCC and LFCC to the RLVs and launch sites of interest here. Nevertheless, little or no quantitative justification can be offered at present for ignoring even the lower-priority rules in these cases. There is, however, an opportunity to develop such justifications in several cases.

4.1.1 Re-Analysis of ABFM I Data

The ABFM I dataset included measurements of ambient field as a function of distance from the edges of various cloud types, which were originally analyzed to justify the existing standoff distances for large orbital boosters that are embodied in the current rules. Assuming that this data is still available, it could be re-analyzed to determine more appropriate (possibly zero) standoff distances for the higher electric-field triggering thresholds deduced for our small RLVs. It is therefore recommended that NASA/MSFC be requested to perform the appropriate statistical re-analysis of their old dataset.

4.1.2 Re-Analysis of ABFM II Data

Furthermore, as mentioned in Section 3.1.1.2, it would be relatively straightforward to re-analyze existing ABFM II data to determine a radar threshold specifically for anvil clouds that is more appropriate to the higher triggering thresholds of these RLVs. First a small study of the relevant cloud physics should be undertaken to establish that the data on Florida anvils is applicable to midwestern and/or southwestern thunderstorms, as mentioned in Section 3.1.1.1. Assuming that the existing radar-vs.-field relationship for anvil clouds is applicable, a statistical analysis should be undertaken to determine the corresponding radar thresholds.

4.2 Monitor All Lightning Types

Monitor all types of lightning (both cloud-to-ground and intra-cloud) at each launch site. (Note that the detection and location of intra-cloud lightning may require the installation of additional equipment at each site.) This should be done before beginning RLV operations, to the extent possible using the sensors presently installed, both to better quantify the effects of lightning on launch availability vs. time of day, season, etc., and to find any new or unexpected behavior at those locations.

4.2.1 Instrumentation

Instrumentation that is suitable to detect all types of lightning should be installed around each launch site to assure avoidance of natural lightning during all future RLV operations.

4.3 Ground-based Electric Fields and Cloud Types

Monitor ground-based electric fields and cloud types at each launch site. (Note that this may require the installation of additional equipment at each site.) This should be done before beginning RLV operations, to the extent possible using the sensors presently installed, both to better quantify the effects of the modified LLCC on launch availability vs. time of day, season, etc., and to find any new or unexpected behavior at those locations.

4.3.1 Instrumentation

Instrumentation such as field mills suitable to detect significant enhancements or polarity reversals in the normal fair-weather field should be installed near each launch site to aid in the avoidance of unexpected hazards during all future RLV operations.

4.3.2 Observers, Instrumentation, and Radar

Observers and instrumentation, including a dedicated weather radar, that are suitable to identify cloud types, measure cloud heights and thicknesses, and monitor radar reflectivities should be installed near each launch site to verify the modified LLCC during all future RLV operations.

4.4 Quantification of Electric-field Triggering Conditions and Effects of Vehicle Plumes

Continue both theoretical and experimental efforts to quantify the electric-field triggering conditions and the effects of the vehicle exhaust plumes in order to obtain more accurate triggering thresholds for the various RLVs. Specific topics in need of further research include experimental and/or theoretical determinations of (A) which of the two positive-leader models described in Section 3.1.2 (or some other model entirely) is more nearly correct, (B) what is the true altitude dependence of the positive-leader-viability condition (see Section 3.1.3), (C) how the exhaust plume actually affects the triggering process (not only in terms of its conductivity distribution, as discussed in Section 3.1.5.3, but also in terms of its total action, as outlined in Section 3.1.5.4), and finally (D) whether the focus on positive-leader viability (as advocated in Section 2.2.2) is fully justified.

4.4.1 Specific Experiment on Plume Conductivity Distributions

As recommended at the end of Section 3.1.5.3, a small experiment should be conducted on a static test stand to measure the actual conductivity distributions in exhaust plumes from the engine types under consideration here. Such data would serve as a better “paradigm” from which to scale the electrical length to the various RLVs. The Aerospace Testing Alliance and/or the NASA Glenn Laboratory would be capable of conducting such experiments.

4.4.2 Specific Modeling of Plume Conductivity Distributions and Scaling

First determine (presumably from data in the literature) both the variation with temperature of the ionization rates of sodium and potassium and the typical amounts of these trace constituents in the various rocket fuels of interest to RLVs. Then use a theoretical model to predict temperature distributions in plumes of various thrust levels as functions of altitude. This would result in a better basis for scaling electrical length than what was done in Sections 3.1.5.3 and 3.1.5.4. The Aerospace Corporation has experts with access to the appropriate plume codes.

4.5 ABFM System to Provide Measurements of Electric Field Aloft in Support of RLV Operations

Consider further the feasibility of an ABFM system to provide measurements of the electric field aloft in support of RLV operations.

4.6 Consider Further Enhancements of Radar-based LLCC to Include Other Cloud Types

Consider further enhancements of the radar-based LLCC to include other cloud types in addition to anvils.

5. Acronyms and Abbreviations

ABFM	Airborne Field Mill
Ac	altocumulus
AFB	Air Force Base
AFCCC	Air Force Combat Climatology Center
AEDC	Arnold Engineering Development Center (Tullahoma)
AIAA	American Institute of Aeronautics and Astronautics
As	altostratus
AST	Office of Commercial Space Transportation
CAPE	Cape Canaveral Air Force Station, Florida
Cb	cumulonimbus
Cc	cirrocumulus
CDFS2	Cloud Depiction and Forecast System V2
CFR	Code of Federal Regulations
CG	cloud-to-ground
Ci	cirrus
cm	centimeter
CONUS	Continental United States
COTR	Contracting Officer's Technical Representative
Cs	cirrostratus
CSAFB	Clinton-Sherman Air Force Base
Cu	cumulus
CVC	current-voltage characteristic
dBZ	Radar reflectivity units
DC	direct current
ºC	degrees Centigrade
DMSP	Defense Meteorological Satellite Program
DOT	Department of Transportation
DOY	day of year
ΔE	change in electric field
E	electric field
ECMWF	European Center for Medium Range Forecasting
FAA	Federal Aviation Administration
ft	foot
GBFM	Ground-Based Field Mill
ILS	instrument landing system
IR	infrared
ISCCP	International Satellite Cloud Climatology Project
JP-1	Fuel Oil Number 1, Kerosene
K	degrees Kelvin
km	kilometer
KSC	Kennedy Space Center (NASA)
kV	kilovolt
lb	pound
lbf	pound force
LDAR	Lightning Detection and Ranging
LFCC	Proposed FAA Natural and Triggered Lightning Flight Commit Criteria

LLC	limited liability company
LLCC	Lightning Launch Commit Criteria
LLJ	low-level jet
LLL	liquid-like layer
LMA	lightning mapping array
LT	local time
LWC	liquid water content
MHz	megahertz
NASA	National Aeronautics and Space Administration
nmi	nautical mile
m	meter
MCS	mesoscale convective system
µA	microampere
MDA	Missile Defense Agency
MSFC	Marshall Space Flight Center (NASA)
MV	megavolt
NCAR	National Center for Atmospheric Research
NLDN	National Lightning Detection Network
Ns	nimbostratus
O_2	oxygen
ONERA	*Office National d'Études et de Recherches Aérospatiales* (French Aeronautics and Space Research Center)
OS	Oklahoma Spaceport
PPCG	predominantly positive cloud-to-ground
RF	radio frequency
RLV	Reusable Launch Vehicle
RMS	root mean square
RP-1	Rocket Propellant 1 (standard kerosene rocket fuel, MIL-P-25576)
RPV	remotely piloted vehicle
s	second
Sc	stratocumulus
sec	second
SRB	solid rocket booster
St	stratus
STP	standard temperature and pressure
SWRS	Southwest Regional Spaceport
UHF	Ultra High Frequency (300–3000 MHz; 1 m – 10 cm)
USAF	United States Air Force
UT	Universal Time
VAFB	Vandenberg Air Force Base
VAHIRR	volume-averaged, height-integrated radar reflectivity
VHF	very high frequency
WSMR	White Sands Missile Range

6. References

Aleksandrov, N. L., E. M. Bazelyan, and Yu P. Raizer. Forthcoming. Initiation and development of first lightning leader: The effects of coronae and position of lightning origin. ICAE special issue, *Atmospheric Research*, in press, 2005.

Avila, E. E., C. P. R. Saunders, H. Bax-Norman, and N. E. Castellano. 2005. Charge sign reversal in ice particle-graupel collisions. *Geophys. Res. Lett*. 32, L01801, doi:10.1029/2004GL020761.

Bailey, J. C., and R. V. Anderson. March 13, 1987. *Experimental calibration of a vector electric field meter measurement system on an aircraft.* Memorandum Report 5900, Naval Research Laboratory, Washington, DC.

Baker, M. B., E. R. Jayarantne, J. Latham, and C. P. Saunders. 1987. The influence of diffusional growth rates on the charge transfer accompanying rebounding collisions between ice crystals and soft hailstones. *Quart. J. Roy. Meteorol. Soc.* 113, 1193–1215.

Baker, M. B., and J. G. Dash. 1989. Charge transfer in thunderstorms and the surface melting of ice. *J. Crystal Growth* 97, 770–776.

Baker, M. B., H. J. Christian, and J. Latham. 1995. A computational study of the relationships linking lightning frequency and other thundercloud parameters. *Quart. J. Roy. Meteorol. Soc.* 121, 1525–1548.

Baker, M. B., A. M. Blyth, H. J. Christian, J. Latham, K. L. Miller, and A. M. Gadian. 1999. *Atmos. Res*. 51, 221–236.

Barnes, A. A. Jr., and J. I. Metcalf. Summary of the triggered lightning workshop held at Cape Canaveral AFS, Florida. AFGL Technical Memorandum No. 151, 17–19 February 1988.

Bateman, M. G., D. M. Mach, S. Lewis, J. E. Dye, E. Defer, C. A. Grainger, P. T. Willis, H. J. Christian, and F. J. Merceret. 9–13 June 2003. Comparison of in situ electric field and radar derived parameters for stratiform clouds in central Florida. In *Proceedings of the 12th International Conference on Atmospheric Electricity*, Versailles, France, International Commission on Atmospheric Electricity.

Bazelyan, E. M., and Yu P. Raizer. 1998. *Spark Discharge*. Boca Raton: CRC Press, 294 pp.

Bazelyan, E. M., and Yu P. Raizer. 2000. *Lightning Physics and Lightning Protection*. Bristol: Institute of Physics Publishing, 325 pp.

Black, R., and J. Hallett. The Mystery of Cloud Electrification. *American Scientist* 86 (6), Nov–Dec 1998.

Boccippio, D. J., D. J. Heckman, and S. J. Goodman. 2001a. A diagnostic analysis of the Kennedy Space Center LDAR network 1. Data characteristics. *J. Geophys. Res*. 106 (D5), 4769–4786.

Boccippio, D. J., D. J. Heckman, and S. J. Goodman. 2001b. A diagnostic analysis of the Kennedy Space Center LDAR network 2. Cross-sensor studies. *J. Geophys. Res*. 106 (D5), 4787–4796.

Bondiou, A., and I. Gallimberti. 1994. Theoretical modeling of the development of positive sparks in long gaps. *J. Phys. D* 27, 1252–1266.

Boulay, J. L., J. P. Moreau, A. Asselineau, and P. L. Rustan. April 19–22, 1988. Analysis of recent in-flight lightning measurements on different aircraft. Paper presented at the Aerospace and Ground Conference on Lightning and Static Electricity, Oklahoma City.

Brook, M., G. Armstrong, R. P. H. Winder, B. Vonnegut, and C. B. Moore. 1961. Artificial initiation of lightning discharges. *J. Geophys. Res*. 66, 3967–3969.

Brook, M., C. R. Holmes, and C. B. Moore. 1970. Lightning and rockets: Some implications of the Apollo 12 lightning event. *Naval Research Reviews* 23(4), 1–17.

Brooks, I. M., and C. P. R. Saunders. 1995. Thunderstorm charging: Laboratory experiments clarified. *Atmos. Res*. 39, 263–273.

Brown, K. A., P. R. Krehbiel, C. B. Moore, and G. N. Sargent. 1971. Electrical screening layers around charged clouds. *J. Geophys. Res.* 76, 2825–2835.

Byrne, G. J., A. A. Few, and M. E. Weber. 1983. Altitude thickness and charge concentration of charge regions of four thunderstorms during TRIP 81, based on in situ balloon electric field measurements. *Geophys. Res. Lett*. 10, 39–42.

Byrne, G. J., A. A. Few, and M. F. Stewart. 1989. Electric field measurements within a severe thunderstorm anvil. *J. Geophys. Res.* 94, 6297–6307.

Christian, H. J., V. Mazur, B. D. Fisher, L. H. Ruhnke, K. Crouch, and R. P. Perala. 1989. The Atlas/Centaur lightning strike incident. *J. Geophys. Res*. 94 (D11), 13,169–13,177.

Clothiaux, E. E., T. P. Ackerman, G. G. Mace, K. P. Moran, R. T. Marchand, M. A. Miller, and B. E. Martner. May 2000. Objective determination of cloud heights and radar reflectivities using a combination of active remote sensors at the ARM CART sites. *J. Applied Meteorology* 39, 645–665.

Cohen, I. Bernard. 1990. The kite, the sentry box, and the lightning rod. Chap. 6 in *Benjamin Franklin's Science.* Cambridge: Harvard Univ. Press.

Dash, J. G., B. L. Mason, and J. S. Wettlaufer. 2001. Theory of charge and mass transfer in ice-ice Collisions. *J. Geophys. Res*. 106, (D17), 20,395–20,402.

Davydenko, S. S., E. A. Mareev, T. C. Marshall, and M. Stolzenburg. 2004. On the calculation of electric fields and currents of mesoscale convective systems. *J. Geophys. Res.* 109, D11103, doi:10.1029/2003JD003832.

Dawson, G. A., and W. P. Winn. 1965. A model for streamer propagation. *Z. Phys.* 183, 159–171.

Drake, J. C. 1968. Electrification accompanying the melting of ice particles. *Quart. J. Roy. Meteorol. Soc*. 94, 176–191.

Dye, J. E., J. J. Jones, A. J. Weinheimer, and W. P. Winn. 1988. Observations within two regions of charge during initial thunderstorm electrification. *Quart. J. Roy. Meteorol. Soc*. 114, 1271–1290.

Dye, J. E., J. J. Jones, A. J. Weinheimer, and W. P. Winn. 1992. Reply to comments by C. B. Moore and B. Vonnegut: Further analysis of two regions of charge during initial thunderstorm electrification. *Quart. J. Roy. Meteorol. Soc.* 118, 401–412.

Dye, J. E., and S. Lewis. June 4, 2004a. Summary of the Final Report to NASA KSC on the Airborne Field Mill Project. (ABFM) Under NASA Grant NAG10-284.

Dye, J. E., and S. Lewis. June 4, 2004b. Final Report to NASA KSC on the Airborne Field Mill Project. (ABFM) Under NASA Grant NAG10-284.
http://box.mmm.ucar.edu/abfm/webpage/Reports/FinalReport_0604.pdf

Dye, J. E., M. Bateman, D. Mach, H. J. Christian, C. A. Grainger, H. C. Koons, E. P. Krider, F. J. Merceret, and J. C. Willett. January 29–February 2, 2006. The scientific basis for a radar-based, Lightning Launch Commit Criteria for anvil clouds. Paper No. 8.7, presented at the 12th Conference on Aviation, Range, and Aerospace Meteorology (ARAM), Atlanta, Georgia.

Edels, H., and E. Graffmann. 1969. Time constant measurements of high pressure arc columns. *Z. Phys.* 228, 396–415.

Ely, B. L., and R. E. Orville. 2005. High percentage of positive lightning along the USA west coast. *Geophys. Res. Lett*. 32.

Farrell, W. M., R. A. Goldberg, R. J. Blakeslee, M. D. Desch, J. G. Houser, J. D. Mitchell, C. L. Crosky, D. M. Mach, and J. C. Bailey. 9–13 June 2003. ACES: a unique platform for electrodynamic studies of upward currents into the middle atmosphere. In *Proceedings of the 12th International Conference on Atmospheric Electricity*, Versailles, France, International Commission on Atmospheric Electricity.

Fisher, F. A., J. A. Plumer, and R. A. Perala. 1999. *Lightning protection of aircraft.* Report, Lightning Technologies, Inc., 10 Downing Parkway, Pittsfield, MA 01201, Second printing.

Fisher, B. D., M. R. Phillips, and L. M. Maier. August 24–26, 1992. Joint NASA/USAF airborne field mill program — operation and safety considerations during flights of a Lear 28 airplane in adverse weather. AIAA-92-4093, paper presented at the 6th Biennial Flight Test Conference, Hilton Head I., SC, American Institute of Aeronautics and Astronautics.

Freund, J. E. 1967. *Modern elementary statistics.* 3rd ed. Englewood Cliffs, NJ: Prentice-Hall, Inc., pp. 432.

Gallimberti, I., G. Bacchiega, A. Bondiou-Clergerie, and P. Lalande. 2002. Fundamental processes in long air gap discharges. *C. R. Physique* 3, 1335–1359.

Harrison, H. T. United Air Line Turbojet experience with electrical discharges. UAL Meteorological Circular, no. 57, 1965.

Hays, R. B., and R. G. Roble. 1979. A quasi-static model of atmospheric electricity: 1. The lower atmosphere. *J. Geophys. Res*. 84, 3291–3305.

Helsdon, J. H., W. A. Wojcik, and R. D. Farley. 2001. An examination of thunderstorm-charging mechanisms using a two-dimensional storm electrification model. *J. Geophys. Res.* 106, (D1) 1165–1192.

Helsdon, J. H., S. Gattaleeradapan, R. D. Farley, and C. C. Waits. 2002. An examination of the convective charging hypothesis: Charge structure, electric fields, and Maxwell currents. *J. Geophys. Res.* 107, (D22), ACL 9-1 to ACL 9-26, doi:10.1029/2001JD001495.

Holle, R. L., R. E. López and C. Zimmermann. 1999. Updated recommendations for lightning safety-1998. *Bull. Am. Meteorol. Soc.* 80, 2035–2041.

Holle, R. L., M. Murphy, and R. E. Lopez. September 2003. Distances and times between cloud-to-ground flashes in a storm, Paper 103-79KMI, presented at the International Conference on Lightning and Static Electricity, Blackpool, U.K.

Holzer, R. E., and D. S. Saxon. 1952. Distribution of electrical conduction currents in the vicinity of thunderstorms. *J. Geophys. Res*. 57, 207–216.

Idone, V. P. 1992. The luminous development of Florida triggered lightning. *Res. Lett. Atmos. Electr*. 12, 23–28.

Idone, V. P., and R. E. Orville. 1988. Channel tortuosity variations in Florida triggered lightning. *Geophys. Res. Lett*. 15, 645–648.

Imyanitov, I. M., Ye V. Chubarina, and Ya M. Shvarts. February 1972. *Electricity of clouds.* NASA Technical Translation. NASA TT F-718, 122 pp.

Jacobson, E. A., and E. P. Krider. 1976. Electrostatic field changes produced by Florida lightning. *J. Atmos. Sci*. 33, 103–117.

Jayaratne, E. R., C. P. R. Saunders, and J. Hallett. 1983. Laboratory studies of the charging of soft hail during ice crystal interactions. *Quart. J. Roy. Meteorol. Soc*. 109, 609–630.

Jones, J. J., W. P. Winn, and F. Han. 1993. Electric field measurements with an airplane: problems caused by emitted charge. *J. Geophys. Res*. 98, 5235–5244.

Kasemir, H. W. 1959. The thunderstorm as a generator in a global electric circuit (in German). *Z. Geophys*. 25, 33–64.

King, L. A. 1961. *The voltage gradient in the free-burning arc in air or nitrogen,* British Electrical and Allied Industries Research Association Report G/XT172. Surrey, England: Leatherhead.

Koshak, W. J., J. C. Bailey, H. J. Christian, and D. M. Mach. 1994. Aircraft electric field measurements: calibration and ambient field retrieval. *J. Geophys. Res*. 99, 22,781–22,792.

Koshak, W. J., and E. P. Krider. 1989. Analysis of lightning field changes during active Florida thunderstorms. *J. Geophys. Res*. 94, 1165–1186.

Koshak, W. J., D. M. Mach, H. J. Christian, and M. F. Stewart. 2005. Forthcoming. A mathematical method for retrieving storm electric fields from aircraft field mill data. *J. Oceanic and Atmosph. Tech*., in preparation.

Kositsky, J., K. L. Giori, R. A. Maffione, D. H. Cronin, J. E. Nanevicz, and R. Harris-Hobbs. January 1991. *Airborne field mill (ABFM) system calibration report.* PIIN No. F04701-90-C-0023, The Aerospace Corporation, El Segundo, CA.

Krehbiel, P. R., M. Brook, and R. A. McCrory. 1979. An analysis of the charge structure of lightning discharges to ground. *J. Geophys. Res*. 84, 2432–2456.

Krehbiel, P. R. 1986. The electrical structure of thunderstorms. Chap. 8 in *The Earth's electrical environment.* Washington, DC: National Academy Press.

Krehbiel, P. R., R. J. Thomas, W. Rison, T. Hamlin, J. Harlin, and M. Davis. January 2000. Lightning mapping observations in central Oklahoma. *Eos*, 21–25.

Krider, E. P., R. C. Noggle, M. A. Uman, and R. E. Orville. 1974. Lightning and Apollo 17/Saturn V exhaust plume. *J. Spacecraft* 11(2), 72–75.

Krider, E. P. Electric field changes and the cloud electrical structure. *J. Geophys. Res.* 94, 13145–13149, 1989.

Krider, E. P., H. C. Koons, R. L. Waltersheid, W. D. Rust, and J. C. Willett. 15 January 1999. *Natural and triggered Lightning Launch Commit Criteria (LCC)*, SMC-TR-99-20, Aerospace Report TR-99(1413)-1, Air Force Materiel Command, Space and Missile Systems Center, Los Angeles, CA.

Krider, E. P., H. J. Christian, J. E. Dye, H. C. Koons, J. Madura, F. Merceret, W. D. Rust, R. L. Walterscheid, and J. C. Willett. January 29–February 2, 2006. Natural and triggered lightning launch commit criteria, Paper No. 8.3, presented at the 12th Conference on Aviation, Range, and Aerospace Meteorology (ARAM), Atlanta, Georgia.

Labaree, L. W., et al., eds. 1962. *The Papers of Benjamin Franklin.* Yale University Press, Vol. 5, p. 69.

Lalande, P., and A. Bondiou-Clergerie. 24 February 1997. Collection and analysis of available in-flight measurement of lightning strikes to aircraft. Report AI-95-SC.204-RE/210-D2.1, ONERA (France) Transport Research and Technological Development Program DG VII.

Lalande, P., A. Bondiou-Clergerie, P. Laroche, A. Eybert-Bérard, J. P. Berlandis, B. Bador, A. Bonamy, M. A. Uman, and V. A. Rakov. 1998. Leader properties determined with triggered lightning techniques. *J. Geophys. Res.* 103, 14,109–14,115.

Lalande, P., A. Bondiou-Clergerie, G. Bacchiega, and I. Gallimberti. 2002. Observations and modeling of lightning leaders. *C. R. Physique* 3, 1375–1392.

Laroche, P., A. Eybert-Bérard, L. Barret, and J. P. Berlandis. 13–16 June 1988. Observations of preliminary discharges initiating flashes triggered by the rocket and wire technique. Paper presented at the 8th International Conference on Atmospheric Electricity, Uppsala, Sweden.

Laroche, P., A. Delannoy, and H. Le Court de Béru. September 26–28, 1989a. Electrostatic field conditions on an aircraft stricken by lightning. Paper presented at the International Conference on Lightning and Static Electricity, University of Bath, UK.

Laroche, P., A. Bondiou, A. Eybert-Bérard, L. Barret, J. P. Berlandis, G. Terrier, and W. Jafferis. September 26–28, 1989b. Lightning flashes triggered in altitude by the rocket and wire technique. Paper presented at the International Conference on Lightning and Static Electricity, University of Bath, UK.

Latham, J. 1981. The electrification of thunderstorms. *Quart. J. Roy. Meteorol. Soc.* 107, 277–298.

Latham, D. J. 1986. Anode column behavior of long vertical air arcs at atmospheric pressure. *IEEE Trans. Plasma Sci*. PS-14, 220–227.

Latham, D. 1991. Lightning flashes from a prescribed fire-induced cloud. *J. Geophys. Res.* 96 (D9), 17,151–17,157.

Launch vehicle lightning/atmospheric electrical constraints post-Atlas/Centaur 67 incident. 31 August 1988. TOR-0088(3441-45)-2, The Aerospace Corporation, El Segundo, CA.

Lightning Review Committee. 31 August 1988. *Launch vehicle lightning/atmospheric electrical constraints post-Atlas/Centaur 67 incident.* TOR-0088(3441-45)-2, The Aerospace Corporation, El Segundo, CA.

MacGorman, D. R., and W. D. Rust. 1998. *The electrical nature of storms.* Oxford University Press, 422 pp.

Mach, D. M., and W. J. Koshak. 9–13 June 2003. General matrix inversion technique for the calibration of electric field sensor arrays on aircraft platforms. In *Proceedings of the 12th International Conference on Atmospheric Electricity,* Versailles, France, International Commission on Atmospheric Electricity.

Maier, L. M., and E. P. Krider. 1986. The charges that are deposited by cloud-to-ground lightning in Florida. *J. Geophys. Res*. 91, 13,275–13,289.

Marshall, T. C., W. D. Rust, W. P. Winn, and K. E. Gilbert. 1989. Electrical structure in two thunderstorm anvil clouds. *J. Geophys. Res*. 94 (D2), 2171–2181.

Marshall, T. C., and B. Lin. 1992. Electricity in dying thunderstorms. *J. Geophys. Res*. 97 (D9), 9913–9918.

Marshall, T. C., and W. D. Rust. 1993. Two types of vertical electrical structures in stratiform precipitation regions of mesoscale convective regions. *Bull. Am. Meteorol. Soc*. 78(11), 2159–2170.

Marshall, T. 2000. Comment on "'Spider' lightning in intracloud and positive cloud-to-ground flashes" by Vladislav Mazur, Xuan-Min Shao, and Paul R. Krehbiel. *J. Geophys. Res.* 105 (D6), 7397–7399.

Marshall, T. C., M. Stolzenburg, W. D. Rust, E. R. Williams, and R. Boldi. 2001. Positive charge in the stratiform cloud of a mesoscale convective system. *J. Geophys. Res*. 106 (D1), 1157–1163.

Mason, B. J. 1971. The electrification of clouds. Chap. 9 in *The physics of clouds.* 2nd ed. Oxford: Clarendon.

Mason, J. 1988. The generation of electric charges and fields in thunderstorms. *Proc. Roy. Soc. London* A415, 303–315.

Mason, B. L., and J. G. Dash. 2000. Charge and mass transfer in ice-ice collisions: Experimental observations of a mechanism in thunderstorm electrification. *J. Geophys. Res*. 105, (D8), 10,185–10,192.

Mazur, V., B. D. Fisher, and J. C. Gerlach. 1984. Lightning strikes to an airplane in a thunderstorm. *J. Aircraft* 21, 607–611.

Mazur, V., X-M. Shao, and P. R. Krehbiel. 1988. "Spider" lightning in intracloud and positive cloud-to-ground flashes. *J. Geophys. Res*. 103, 19,811–19,822.

Mazur, V. 1989b. A physical model of lightning initiation on aircraft in thunderstorms. *J. Geophys. Res*. 94, 3326–3340.

McNamara, T. M. 2002. The horizontal extent of cloud-to-ground lightning over the Kennedy Space Center. M.S. thesis, Air Force Institute of Technology, Wright-Patterson AFB, Ohio, AFIT/GM/ENP/02M-06.

Mo, Q., A. E. Ebneter, P. Fleischhacker, and W. P. Winn. 1998. Electric field measurements with an airplane: A solution to problems caused by emitted charge. *J. Geophys. Res*. 103, 17,163–17,173.

Moore, C. B., and B. Vonnegut. 1992. Comments on 'Observations of two regions of charge during initial thunderstorm electrification' by J. E. Dye, J. J. Jones, A. J. Weinheimer, and W. P. Winn (July 1988, 114, 1271–1290). *Quart. J. Roy. Meteorol. Soc*. 118, 395–400.

Moore, C. B., G. D. Aulich, and W. Rison. 2000. Measurements of lightning rod responses to nearby strikes. *Geophys. Res. Lett*. 27, 1487–1490.

Morse, P. M., and H. Feshbach. 1953. *Methods of theoretical physics*, Vol. 2, p. 1284. New York, NY: McGraw-Hill.

Murphy, M. J., E. P. Krider, and M. W. Maier. 1996. Lightning charge analyses in small Convection and Precipitation Experiment (CaPE) storms. *J. Geophys. Res.* 101 (D23), 29,615–29,626.

Murphy, M. J., and R. L. Holle. 2005. A warning method for cloud-to-ground lightning based on total lightning and radar information, preprints, International Conference on Lightning and Static Electricity, 19–23 September 2005, Seattle, Washington, paper LDM-36, 2005.

Nanevicz, J. E., and G. R. Hilbers. 1973. *Environment Titan vehicle electrostatic*. Air Force Avionics Laboratory, AFAL-TR-73-170, Wright-Patterson AFB, Ohio.

NAS, 1986. *The Earth's electrical environment.* Washington, DC: National Academy Press.

Naud, C. M, J-P Muller, and E. E. Clothiaux. 2003. Comparison between active sensor and radiosonde cloud boundaries over the ARM southern Great Plains site. *J. Geophys. Res*. 108(D4), 4140.

Naud, C. M, J-P Muller, M. Haeffelin, Y. Morille, and A. Delaval. 2004. Assessment of MISR and MODIS cloud top heights through inter-comparison with a back-scattering lidar at SIRTA, *Geophys. Res. Lett.* 31, L04114.

Nelson, L. A. 2002. Synthesis of 3-dimensional lightning data and weather radar data to determine the distance that naturally occurring lightning travels from thunderstorms. M.S. thesis, Air Force Institute of Technology, Wright-Patterson AFB, Ohio, AFIT/GM/ENP/02M-07.

Newman, M. M. 1958. Lightning discharge channel characteristics and related atmospherics. In *Recent advances in atmospheric electricity.* Ed. L. G. Smith. New York: Pergamon Press, pp. 475–484.

Newman, M. M., J. R. Stahmann, J. D. Robb, E. A. Lewis, S. G. Martin, and S. V. Zinn. 1967. Triggered lightning strokes at very close range. *J. Geophys. Res*. 72, 4761–4764.

Panel on Meteorological Support for Space Operations. 1988. *Meteorological Support for Space Operations, Review and Recommendations.* National Academy Press, 77 pp. Washington, DC.

Peng, G. S. February 1, 2006. An analysis of lightning risk and convective cloud cover for two proposed commercial spaceport sites. Paper 8.10, presented at the 12th Conference on Aviation, Range, and Aerospace Meteorology (ARAM), Atlanta, GA.

Perala, R. A., T. H. Rudolph, D. A. Steffen, G. J. Rigden, and H. S. Weigel IV. 1994. *A model for predicting the triggering of lightning by launch vehicles*, Electromagnetic Applications, Inc., EMA-93-R-035, Denver, CO.

Phelps, C. T., and R. F. Griffiths. 1976. Dependence of positive corona streamer propagation on air pressure and water vapor content. *J. Appl. Phys.* 47, 2929–2934.

Proctor, D. E. 1971. A hyperbolic system for obtaining VHF radio pictures of lightning. *J. Geophys. Res*. 76, 1478–1489.

Raizer, Yu P. 1991. *Gas discharge physics.* Berlin: Springer-Verlag, 449 pp.

Rakov, V. A., and M. A. Uman. 2003. *Lightning physics and effects*. Cambridge University Press, 687 pp.

Reynolds, S. E., M. Brook, and M. F. Gourley. 1957. Thunderstorm charge separation. *J. Meteorol*. 14, 426–436.

Rison, W., R. J. Thomas, P. R. Krehbiel, T. Hamlin, and J. Harlin. 1999. A GPS-based three-dimensional lightning mapping system: Initial observations in central New Mexico. *Geophys. Res. Lett*. 26, 3573–3576.

Roeder, W. P., J. E. Sardonia, S. C. Jacobs, M. S. Hinson, A. A. Guiffrida, and J. T. Madura. January 11–14, 1999. Lightning Launch Commit Criteria at the Eastern Range/Kennedy Space Center. Paper presented at the 37th AIAA Aerospace Sciences Meeting and Exhibit. AIAA-99-0890.

Rust, W. D., and D. R. MacGorman. 2002. Possibly inverted-polarity electrical structures in thunderstorms. *Geophys. Res. Lett*. 29 (12), 12-1 to 12-4.

Rust, W. D., and R. J. Trapp. 2002. Initial balloon soundings of the electric field in winter nimbostratus clouds in the USA. *Geophys. Res. Lett*. 29 (20), 20-1 to 20-4.

Saunders, C. P. R. 1988. Thunderstorm electrification. *Weather* 43, 318–324.

Saunders, C. P. R., W. D. Keith, and R. P. Mitzeva. 1991. The effect of liquid water on thunderstorm charging. *J. Geophys. Res*. 96, 11007–11017.

Schaub, W. R. Jr. Feb. 1996. *Nationwide lightning climatology, Air Force Combat Climatology Center Report*. AFCCC/TN-96/002.

Schaub, W. R. Jr. March 1996. *Lightning climatology for Holloman AFB, New Mexico*. Air Force Combat Climatology Center Report AFCCC/TN-96/005.

Schonland, B. F. J. 1950. *The flight of thunderbolts.* Oxford: Clarendon, p. 22.

Schuur, T. J., B. F. Smull, W. D. Rust, and T. C. Marshall. 1991. Electrical and kinematic structure of the stratiform precipitation region trailing an Oklahoma squall line. *J. Atmos. Sci*. 48 (6), 825–842.

Scott, R. D., P. R. Krehbiel, and W. Rison. 2001. The use of simultaneous horizontal and vertical transmissions for dual-polarization radar meteorological observations. *J. Atmos. Ocean. Tech*. 18, 629–648.

Shepherd, T. R., W. D. Rust, and T. C. Marshall. 1996. Electric fields and charges near 0ºC in stratiform clouds. *Mon. Wea. Rev*. 124, 919–938.

Simmons, F. S. 2000. *Rocket exhaust plume phenomenology.* The Aerospace Press and American Institute of Aeronautics and Astronautics, ISBN 1-884989-08-X.

Simpson, G. 1949. Atmospheric electricity during disturbed weather. *Geophysical Memoirs* No. 84, Vol. 4, Meterological Office, London, 51 pp.

Smythe, W. R. 1968. *Static and dynamic electricity*. 3rd ed. New York: McGraw-Hill Book Company, 623 pp.

Standler, R. B., and W. P. Winn. 1079. Effects of coronae on electric fields beneath thunderstorms, *Quart J. Roy. Meteorol. Soc*. 105, 285–302.

Stolzenburg, M., T. C. Marshall, W. D. Rust, and B. F. Smull. 1994. Horizontal distribution of electrical and meteorological conditions across the stratiform region of a mesoscale convective system. *Mon. Wea. Rev*. 122, 1777–1797.

Stolzenburg, M., W. D. Rust, B. F. Smull, and T. C. Marshall. 1998a. Electrical structure in thunderstorm convective regions: 1. Mesoscale convective systems. *J. Geophys. Res.* 103, 14,059–14,078.

Stolzenburg, M., W. D. Rust, B. F. Smull, and T. C. Marshall. 1998b. Electrical structure in thunderstorm convective regions: 2. Isolated storms. *J. Geophys. Res.* 103, 14,079–14,096.

Stolzenburg, M., W. D. Rust, B. F. Smull, and T. C. Marshall. 1998c. Electrical structure in thunderstorm convective regions: 3. Synthesis. *J. Geophys. Res*. 103 14,097–14,108.

Stolzenburg, M., T. C. Marshall, and W. D. Rust. 2001. Serial soundings of electric field through a mesoscale convective system. *J. Geophys. Res*. 106 (D12), 12371–12380.

Stolzenburg, M., and T. C. Marshall. 2002. Two simultaneous charge structures in thunderstorm convection. *J. Geophys. Res*. 107, D18, ACL 5-1 – ACL 5-12.

St. Privat D'Allier Group. 5–7 March 1985. Artificially triggered lightning in France. Applications: possibilities, limitations paper presented at the 6th Symposium on Electromagnetic Compatibility, Zurich.

Szymanski, E. W., S. J. Szymanski, C. R. Holmes, and C. B. Moore. 1980. An observation of a precipitation echo intensification associated with lightning. *J. Geophys. Res*. 85 (C4), 1951–1953.

Takahashi, T. 1978. Riming electrification as a charge generation mechanism in thunderstorms. *J. Atmos. Sci*. 35, 1536–1548.

Takahashi, T., and K. Miyawaki. 2002. Reexamination of riming electrification in a wind tunnel. *J. Atmos. Sci*. 59, 1018–1025.

Thomas, R. J., P. R. Krehbiel, W. Rison, T. Hamlin, J. Harlin, and D. Shown. 2001. Observations of VHF source powers radiated by lightning. *Geophys. Res. Lett*. 28, 143–146.

Thomas, R. J., P. R. Krehbiel, W. Rison, S. J. Hunyady, W. P. Winn, T. Hamlin, and J. Harlin. 2004. Accuracy of the lightning mapping array. *J. Geophys. Res*. 109, (D14207, doi:10.1029/2004JD004549).

Titan Programs. 1988. *Launch vehicle lightning/atmospheric electrical constraints post-Atlas/Centaur 67 incident*, TOR-0088(3441-45)-2, The Aerospace Corporation.

Uman, M. A. 1987. *The lightning discharge.* Orlando: Academic Press, 377 pp.

Uman, M. A., and V. A. Rakov. 2003. The interaction of lightning with airborne vehicles. *Prog. in Aerospace Sciences* 39, 61–81.

Vonnegut, B. 1991. How the external currents flowing to a thundercloud influence its electrification. *Ann. Geophysicae* 9, 34–36.

Vonnegut, B., D. J. Latham, C. B. Moore, and S. J. Hunyady. 1995. *J. Geophys. Res.* 100 (D3), 5037–5050.

Willett, J. C., D. A. Davis, and P. Laroche. 1999. An experimental study of positive leaders initiating rocket-triggered lightning. *Atmospheric Research* 51, 189–219.

Willett, J. C., and A. A. Jr. Barnes. 2 June 2000. *Feasibility analysis for measuring electric field aloft*, unpublished report prepared for the Weather Integrated Product Team, Range Standardization and Automation Program.

Willett, J. C., E. P. Krider, G. S. Peng, F. S. Simmons, G. W. Law, R. W. Seibold, and K. Shelton-Mur. January 29 – February 2, 2006. Triggered lightning risk assessment for reusable launch vehicles at the Southwest Regional and Oklahoma Spaceports. Paper 8.9, presented at the 12th Conference on Aviation, Range, and Aerospace Meteorology (ARAM), Atlanta, Georgia.

Williams, E. R. 1988. The electrification of thunderstorms. *Scientific American*, 259, 88–99.

Williams, E. R. 1989. The tripole structure of thunderstorms. *J. Geophys. Res.* 94, 13,151–13,167.

Williams, E. R., R. Zhang, and J. P. Rydock. 1991. Mixed-phase microphysics and cloud electrification. *J. Atmos. Sci.* 48, 2195–2203.

Wilson, C. T. R. 1920. Investigations on lightning discharges and on the electric field of thunderstorms. *Phil. Trans. Roy. Soc. London* A221, 73–115.

Winn, W. P. 1993. Aircraft measurement of electric field: self calibration. *J. Geophys. Res*. 98, 7351–7365.

Workman, E. J., and R. E. Holzer. 1939. Quantities of charge transfers in lightning discharges. *Phys. Rev*. 55, 2nd ser., 598.

Workman, E. J., and R. E. Holzer. 1942. A preliminary investigation of the electrical structure of thunderstorms NACA Tech. Note 850, National Advisory Committee for Aeronautics, Washington, DC.

Zamiska, A., and P. Giese. RTNEPH AFCCC Climatic Database Users Handbook No. 1, Air Force Combat Climatology Center Report USAFETAC/UH-86/001. Sept. 1986 (Revised Nov. 1996).

Ziegler, C. L., D. R. MacGorman, J. E. Dye, and P. S. Ray. 1991. A model evaluation of noninductive graupel-ice charging in the early electrification of a mountain thunderstorm. *J. Geophys. Res*. 96, 12,833–12,855.

Ziegler, C. L., and D. R. MacGorman. 1994. Observed lightning morphology relative to modeled space charge and electric field distributions in a tornadic storm. *J. Atmos. Sci*. 51, 833–851.

Appendix A
Airborne Field Mill Project (ABFM) Summary

Final Report to NASA KSC on the Airborne Field Mill Project (ABFM) under NASA Grant NAG10-284

James E. Dye and Sharon Lewis
National Center for Atmospheric Research
Boulder, Colorado

June 4, 2004

The following is the Summary of Results Section from the NCAR Final Report on the ABFM project. For information on the project and the basis for these conclusions see the full NCAR FINAL REPORT: Dye, J. E., and S. Lewis, Final Report to NASA KSC on the Airborne Field Mill Project (ABFM) Under NASA Grant NAG10-284, June 4, 2004.

8. Summary of Results

Three field campaigns were conducted during the Airborne Field Mill Project II (ABFM) to investigate the relationships between electric field intensity, reflectivity, and particle microphysics. The June 2000 and May/June 2001 campaigns were very successful in providing many measurements in anvils, convective debris, weak to moderate intensity deep convection, and stratiform situations. The February 2001 campaign, conducted during conditions of severe drought in central Florida, provided limited measurements in thick clouds. As a result most of the analysis of ABFM observations have focused on anvils. We have gathered over or near KSC an excellent, unique data set, hitherto unavailable in the scientific community, with 3-dimensional electric field and detailed microphysical measurements in coordination with radar measurements. This data set is valuable for use in developing new Lightning Launch Commit Criteria rules but also for scientific investigations.

The primary results from ABFM II for anvils are as follows:

8.1 Electric Fields and Microphysics

- In regions of anvils with strong electric fields (in large degree also for debris cases), there was a surprising degree of consistency of observed particle concentrations in different size ranges from flight to flight.
- When strong electric fields (>10 kV/m) occurred, the particle concentrations in all size ranges from tens of microns to several millimeters were high, but higher particle concentrations did not necessarily indicate regions of strong electric field.
- The smaller ice particles in the anvils (<50 μm) are primarily spherical, thereby suggesting frozen cloud droplets. Almost all particles >100 μm are irregular with little evidence of riming except near storm cores. Pristine ice crystals were observed infrequently. Most particles > 500 μm have the appearance of aggregates. Long chains of aggregates were frequently seen, suggesting

enhancement of aggregation by the strong electric fields. Additional research could be done on this topic using this unique data set.

- Scatter plots of the anvil data set showed an unexpected, complex relationship between electric field and particle concentrations for all size ranges. For electric fields >3 kV/m up to the maximum of ~45 kV/m there is not much change of concentration with increasing field, but for Emag < 3 kV/m there are wide ranges of concentration for relatively small changes of field and a knee or inflection point in the plots.
- At this time, we have no explanation for the change in character of the electric field and particle concentration relationship near 3 kV/m.
- There was no evidence of supercooled liquid water being present in the anvils. This suggests that active electrification via the non-inductive charging mechanism is probably not occurring to any significant degree in these anvils.
- However, in several cases we observed the transition of anvils into a secondary development, a stratiform-like layer. During this secondary development electric fields persisted for extended periods of time and perhaps even intensified. Reflectivity persisted for long periods and sometimes increased, especially near the 0°C level but also aloft. (See Dye et al., (ICCP2004 preprint) for the example of the June 4, 2001, case and J. Willett's Final Report on the ABFM Web Report page). This topic warrants further investigation.
- Even though this stratiform-like development occurred in some anvils, column averaged or volume integral reflectivity continued to provide good guidance on the presence of strong electric fields. The behavior of the Emag vs. reflectivity scatter plots was the same when these secondary development regions were included as well as when they were not.

8.2 Reflectivity and Microphysics

- The relationship between reflectivity (of a 3 km cube near the aircraft) and particle concentration was found to be consistent with a power law in all size ranges from the smallest to the largest, but with more variation for the small and intermediate-sized particles than for the particles > 1 mm.
- The particles > 3 mm, our largest size category, exhibited the best correlation with reflectivity, as expected.
- The scatter plots of reflectivity versus particle concentration did not exhibit a complex behavior, unlike the scatter plots of electric field versus particle concentration.
- Measurements near anvil edge clearly showed that particles extend out to or beyond the 0 dBZ radar contour and well beyond the 10 dBZ radar contour. As a result of ABFM observations the LAP changed the definition of "anvil edge" in the LLCC rules from +10 dBZ to 0 dBZ.

8.3 Electric Field Reflectivity

- Strong electric fields were found to be associated with regions of higher reflectivity (>~5 to 10 dBZ) above the freezing level (assumed to be >= 5 km MSL), but higher reflectivity did not necessarily indicate regions of strong electric field.
- The change in behavior of the character of the electric field and particle relationship near 3 kV/m carries over to and impacts the relationship of electric field with reflectivity and with electrical decay times.

- Reflectivity at the aircraft location or in the 1 × 1 km column above the aircraft measured by the 74C and NEXRAD radars at anvil altitudes over KSC is not a suitable parameter for comparing to electric field strength because of scan gaps between antenna sweeps of both radars. Additionally, strong temperature gradients can at times cause significant refraction of the radar beam.
- A reflectivity parameter, the 11 × 11 or 21 × 21 column average, was developed to minimize the effects of scan gaps and also to detect possible sources of strong electric fields in the large volume near but not at the aircraft location.

8.4 Electrical Decay Time Scale, Microphysics, Reflectivity and Electric Field

- A simple model was developed to estimate the decay of electric field in the ABFM anvils based upon the observed particle size distributions (Willett, Final Report, 2003). Because the model assumes constant microphysics during the field decay, the model times are considered upper limits.
- An electrical decay time scale, ETmScl (or τ_E in Willett's reports) is calculated for each 30 s average of aircraft data in anvil to estimate from the model the time for the electric field to decay from 50 to 0 kV/m. In the high field limit, i.e., for fields approximately > 2 kV/m, the decay is linear.
- The particle cross sectional area, particularly in the size range 0.2 to 2 mm, largely controls the calculated electric field decay time scales for anvils in the model.
- The optical extinction coefficient (as well as electrical decay time) is also weighted toward mid-sized particles 200 to 2000 μm. (See Willett (2003b) on Optical Extinction Coefficient.)
- The observed particle size distributions yield calculated electric field decay time scales ranged from 3 hours near the core of active storms to only a few minutes near the edge of anvils.
- Plots of the electrical decay time scale versus electric field show a large change in the plots near 3 kV/m similar to those of electric field versus particle concentration. This is a result of the change in character of the electric field and particle concentration relationship.
- Comparisons for case study days of electric field decay time scale from the model with observed decay times were generally consistent, but only one ABFM anvil case permitted a meaningful comparison.
- Neither reflectivity nor electrical time scale are a suitable proxy for electric field.

8.5 Consideration of Possible Radar Variables for an LLCC Rule

- Scatter plots of the 11 × 11 or 21 × 21 column average versus the magnitude of the electric field, Emag have been useful for considering a possible radar-based LLCC rule. Such plots have the behavior that for reflectivity less than some threshold value, no points with moderate or strong electric fields (> 3 kV/m) were observed.
- The 11 × 11 column is preferable to the 21 × 21 column for the purpose of calculating either average or another radar variable for use in an LLCC.
- The arithmetic average of dBZ values is preferable to a geometric average (in which dBZ is converted to Ze, averaged, and then converted back to dBZ), because the geometric average gives most weight to the very largest reflectivity. Similarly this is true for the maximum reflectivity.
- The 11 × 11 volume integral (the product of the 11 × 11 column average and the average 11 × 11 thickness) was found to have a smaller false alarm rate than the 11 × 11 column average. The

volume integral was also less sensitive to the reflectivity cutoff being used, –10 or 0 dBZ, and therefore more robust.

- At this time, the 11 × 11 volume integral appears to be the most promising radar variable for use in an LLCC rule.
- If the primary consideration is to prevent statistical bias, a cutoff threshold for the radar measurements of –10 dBZ is preferable to a 0 dBZ cutoff for use in calculating column average or anvil thickness.
- There was considerable debate about whether a cutoff of –10 dBZ or a cutoff of 0 dBZ was preferable for use in an LLCC. This is a topic for further investigation and discussion.
- An examination of the entire ABFM data set (not just anvils) showed that the electric field falls off rapidly from the cloud edge. By a 9 km distance from the cloud edge electric fields are <1.5 kV/m.
- For debris clouds, the scatter plots of reflectivity parameters versus electric field were very similar in nature to the scatter plots for anvils. A radar-based LLCC for debris clouds might be very similar to the one presently being developed for anvils.

Appendix B
Proposed Natural and Triggered Lightning Flight Commit Criteria

A. G417.1 General

Each of the Lightning Flight Commit Criteria (LFCC) requires ***clear and convincing*** evidence to trained weather personnel that its constraints are not violated. Under some conditions trained weather personnel can make a clear and convincing determination that the LFCC are not violated based on visual observations alone. However, if the weather personnel have access to additional information such as measurements from weather radar, lightning sensors, electric field mills, and/or aircraft, this information can be used to increase both safety and launch availability. If the additional information is within the criteria outlined in the LFCC, it would allow a launch to take place where a visual observation alone would not.

(a) This appendix provides flight commit criteria to protect against natural lightning and lightning triggered by the flight of a launch vehicle. A launch operator must apply these criteria under § 417.113 (c) for any launch vehicle that utilizes a flight safety system.

(b) The launch operator must employ:

(1) Any weather monitoring and measuring equipment needed to satisfy the lightning flight commit criteria.

(2) Any procedures needed to satisfy the lightning flight commit criteria.

(c) If a launch operator proposes any alternative lightning flight commit criteria, the launch operator must clearly and convincingly demonstrate that the alternative provides an equivalent level of safety.

B. G417.3 Definitions, Explanations and Examples

For the purpose of this appendix:

Anvil cloud means a stratiform or fibrous cloud produced by the upper-level outflow or blow-off from thunderstorms or convective clouds.

Associated means that two or more clouds are causally related to the same weather disturbance or are physically connected. Associated does not have to mean occurring at the same time. A cumulus cloud formed locally and a cirrus layer that is physically separated from that cumulus cloud and that is generated by a distant source are not associated, even if they occur over or near the launch point at the same time.

Average Cloud Thickness is the altitude difference (in kilometers) between the average top and the average base of all clouds within the Specified Volume. The cloud base to be averaged is the higher of (1) the 0 degree Celsius level and (2) the lowest extent (in altitude) of all cloud radar reflectivities 0 dBZ or greater. Similarly, the cloud top to be averaged is the highest extent (in altitude) of all cloud radar reflectivities 0 dBZ or greater. Given the grid-point representation of a typical radar processor, allowance must be made for the vertical separation of grid points in

computing cloud thickness: The cloud base at any horizontal position shall be taken as the altitude of the corresponding base grid point *minus* half of the grid-point vertical separation. Similarly, the cloud top at that horizontal position shall be taken as the altitude of the corresponding top grid point *plus* half of this vertical separation. Thus, a cloud represented by only a single grid point having a radar reflectivity equal to or greater than 0 dBZ within the Specified Volume would have an Average Cloud Thickness equal to the vertical grid-point separation in its vicinity.

Bright band means an enhancement of radar reflectivity caused by frozen hydrometeors falling and beginning to melt at any altitude where the temperature is 0 degrees Celsius or warmer.

Cloud means a visible mass of water droplets or ice crystals produced by condensation of water vapor in the atmosphere.

Cloud edge means the visible boundary, including the sides, base, and top, of a cloud as seen by an observer. In the absence of a visible boundary as seen by an observer, the 0 dBZ radar reflectivity boundary defines a cloud edge.

Cloud layer means a vertically continuous array of clouds not necessarily of the same type whose bases are approximately at the same level.

Cumulonimbus cloud means any convective cloud with any part at an altitude where the temperature is colder than –20 degrees Celsius.

Debris cloud means any cloud, except an anvil cloud, that has become detached from a parent cumulonimbus cloud or thunderstorm, or that results from the decay of a parent cumulonimbus cloud or thunderstorm.

Disturbed weather means a weather system where dynamical processes destabilize the air on a scale larger than the individual clouds or cells. Examples of disturbed weather include fronts and troughs.

Electric field measurement at the surface of Earth means the 1-minute arithmetic average of the vertical electric field (E_z) at the ground measured by a ground-based field mill. The polarity of the electric field is the same as that of the potential gradient; that is, the polarity of the field at Earth's surface is the same as the dominant charge overhead. An interpolation based on electric field contours is not a measurement for purposes of this appendix.

Field mill is a specific class of electric-field sensor that uses a moving, grounded conductor to induce a time-varying electric charge on one or more sensing elements in proportion to the ambient electrostatic field.

Flight path means the planned normal flight trajectory, including its vertical and horizontal uncertainties to include the sum of the wind effects and the three-sigma guidance and performance deviations.

Moderate precipitation means a precipitation rate of 0.1 inches/hr or a radar reflectivity factor of 30 dBZ.

Nontransparent Cloud cover is nontransparent if (1) forms seen through it are blurred, indistinct, or obscured; or (2) forms are seen distinctly only through breaks in the cloud cover. Clouds with a radar reflectivity factor of 0 dBZ or greater are also nontransparent.

Ohms/Square means the surface resistance in ohms when a measurement is made from an electrode on one surface extending the length of one side of a square of any size to an electrode on the same surface extending the length of the opposite side of the square. The resistance measured in this way is independent of the area of a square.

Precipitation means detectable rain, snow, hail, graupel, or sleet at the ground; virga, or a radar reflectivity factor greater than 18 dBZ at altitude.

Specified Volume – The volume bounded in the horizontal by vertical, plane, perpendicular sides located 5.5 km (3 NM) north, east, south, and west of the point on the flight track. The volume is bounded on the bottom at the altitude where the temperature is 0 degrees Celsius, and on the top by the upper extent of all clouds.

Thick cloud layer means one or more cloud layers whose combined vertical extent from the base of the bottom layer to the top of the uppermost layer exceeds a thickness of 4,500 feet. Cloud layers are combined with neighboring layers for determining total thickness only when they are physically connected by vertically continuous clouds, as, for example, when towering clouds in one layer contact or merge with clouds in a layer (or layers) above.

Thunderstorm means any convective cloud that produces lightning.

Transparent Cloud cover is transparent if objects above, including higher clouds, blue sky, and stars can be distinctly seen from below; or objects, including terrain, buildings, and lights on the ground, can be distinctly seen from above. Transparency is defined only for the visible wavelengths.

Triboelectrification means the transfer of electrical charge from ice particles to the launch vehicle when the ice particles rub against the vehicle during impact.

Volume-Averaged, Height-Integrated Radar Reflectivity (VAHIRR) is the product of the Volume-Averaged Radar Reflectivity and the Average Cloud Thickness within a Specified Volume relative to a point along the flight track (units of dBZ-kilometers). The Volume-Averaged, Height-Integrated Radar Reflectivity measurement must be made in the absence of significant attenuation by intervening storms or by water or ice on the radome itself. The Volume-Averaged, Height-Integrated Radar Reflectivity measurement is invalid at any point on the flight track that is within 20 km of any radar reflectivity of 35 dBZ or greater at altitudes of 4 kilometers above mean sea level or greater, and at any point that is within 20 km of any type of lightning that has occurred in the previous 5 minutes. The Specified Volume must not contain any portion of the cone of silence above the radar, nor any portion of any sectors that may have been blocked out for payload-safety reasons. The individual grid-point reflectivities used to determine either the Volume-Averaged Radar Reflectivity or the Average Cloud Thickness must be meteorological reflectivities.

Volume-Averaged Radar Reflectivity is the arithmetic average (in dBZ) of the cloud radar reflectivity within the Specified Volume. Normally, a radar processor will report reflectivity values interpolated onto a regular, three-dimensional array of grid points. Any such grid point within the Specified Volume is included in the average if and only if it has a radar reflectivity equal to or greater than 0 dBZ.

Within is a function word used to specify a distance in all directions (horizontal, vertical, and slant separation) between a cloud edge and a flight path. For example, "within 10 nautical miles of a thunderstorm cloud" means that there must be a 10-nautical-mile margin between every part of a thunderstorm cloud and the flight path.

C. G417.5 Lightning

(a) A launch operator must not initiate flight for 30 minutes after any type of lightning occurs in a thunderstorm if the flight path will carry the launch vehicle within 10-nautical-miles of that thunderstorm.

(b) A launch operator must not initiate flight for 30 minutes after any type of lightning occurs within 10 nautical miles of the flight path ***unless all of the following conditions are satisfied:***

(1) The cloud that produced the lightning is not within 10 nautical miles of the flight path;

(2) There is at least one working field mill within 5 nautical miles of each such lightning flash; and

(3) The absolute values of all electric field measurements made at the Earth's surface within 5 nautical miles of the flight path and at each field mill specified in paragraph (b)(2) of this section have been less than 1000 volts/meter for 15 minutes or longer.

(c) If a cumulus cloud remains 30 minutes after the last lightning occurs in a thunderstorm, Section D applies. Sections E and F apply to any anvil or detached anvil clouds. Section G applies to debris clouds.

D. G417.7 Cumulus Clouds

For the purposes of this section, "cumulus clouds" do not include altocumulus, cirrocumulus, or stratocumulus clouds.

(a) A launch operator must not initiate flight if the flight path will carry the launch vehicle within 10 nautical miles of any cumulus cloud that has a cloud top at an altitude where the temperature is colder than –20 degrees Celsius.

(b) A launch operator must not initiate flight if the flight path will carry the launch vehicle within 5 nautical miles of any cumulus cloud that has a cloud top at an altitude where the temperature is colder than –10 degrees Celsius.

(c) A launch operator must not initiate flight if the flight path will carry the launch vehicle through any cumulus cloud with its cloud top at an altitude where the temperature is colder than –5 degrees Celsius.

(d) A launch operator must not initiate flight if the flight path will carry the launch vehicle through any cumulus cloud that has a cloud top at an altitude where the temperature is between +5 degrees Celsius and –5 degrees Celsius ***unless all of the following conditions are satisfied:***

(1) The cloud is not producing precipitation;

(2) The horizontal distance from the center of the cloud top to at least one working field mill is less than 2 nautical miles; and

(3) All electric field measurements made at the Earth's surface within 5 nautical miles of the flight path and at each field mill specified in paragraph (d)(2) of this section have been between −100 volts/meter and +500 volts/meter for 15 minutes or longer.

E. G17.9 Attached Anvil Clouds

(a) A launch operator must not initiate flight if the flight path will carry the launch vehicle through or within 10 nautical miles of a nontransparent part of any attached anvil cloud for the first 30 minutes after the last lightning discharge in or from the parent cloud or anvil cloud.

(b) A launch operator must not initiate flight if the flight path will carry the launch vehicle through or within 5 nautical miles of a nontransparent part of any attached anvil cloud between 30 minutes and three hours after the last lightning discharge in or from the parent cloud or anvil cloud unless both of the following conditions are satisfied:

(1) The portion of the attached anvil cloud within 5 nautical miles of the flight path is located entirely at altitudes where the temperature is colder than 0 degrees Celsius; and

(2) The volume-averaged, height-integrated radar reflectivity is less than +33 dBZ-kft (+10 dBZ-km) everywhere along the portion of the flight path where any part of the attached anvil cloud is within the specified volume.

(c) A launch operator must not initiate flight if the flight path will carry the launch vehicle through a nontransparent part of any attached anvil cloud more than 3 hours after the last lightning discharge in or from the parent cloud or anvil cloud unless all of the following conditions are satisfied:

(1) The portion of the attached anvil cloud within 5 nautical miles of the flight path is located entirely at altitudes where the temperature is colder than 0 degrees Celsius; and

(2) The volume-averaged, height-integrated radar reflectivity is less than +33 dBZ-kft (+10 dBZ-km) everywhere along the portion of the flight path where any part of the attached anvil cloud is within the specified volume.

F. G17.11 Detached Anvil Clouds

For the purposes of this section, detached anvil clouds are never considered debris clouds.

(a) A launch operator must not initiate flight if the flight path will carry the launch vehicle through or within 10 nautical miles of a nontransparent part of a detached anvil cloud for the first 30 minutes after the last lightning discharge in or from the parent cloud or anvil cloud before detachment or after the last lightning discharge in or from the detached anvil cloud after detachment.

(b) A launch operator must not initiate flight if the flight path will carry the launch vehicle between 0 (zero) and 5 nautical miles from a nontransparent part of a detached anvil cloud between 30 minutes and 3 hours after the time of the last lightning discharge in or from the parent cloud or anvil cloud before detachment or after the last lightning discharge in or from the detached anvil cloud

after detachment unless Section (1) or Section (2) is satisfied:

(1) This section is satisfied if all three of the following conditions are met:

(i) There is at least one working field mill within 5 nautical miles of the detached anvil cloud; and

(ii) The absolute values of all electric field measurements at the surface within 5 nautical miles of the flight path and at each field mill specified in (i) above have been less than 1000 V/m for 15 minutes; and

(iii) The maximum radar return from any part of the detached anvil cloud within 5 nautical miles of the flight path has been less than 10 dBZ for 15 minutes.

(2) This section is satisfied if both of the following conditions are met:

(i) The portion of the detached anvil cloud within 5 nautical miles of the flight path is located entirely at altitudes where the temperature is colder than 0 degrees Celsius; and

(ii) The volume-averaged, height-integrated radar reflectivity is less than +33 dBZ-kft (+10 dBZ-km) everywhere along the portion of the flight path where any part of the detached anvil cloud is within the specified volume.

(c) **A launch operator must not initiate flight** if the flight path will carry the launch vehicle through a nontransparent part of a detached anvil cloud unless Section (1) or Section (2) is satisfied

(1) This section is satisfied if both of the following conditions are met.

(i) At least 4 hours have passed since the last lightning discharge in or from the detached anvil cloud; and

(ii) At least 3 hours have passed since the time that the anvil cloud is observed to be detached from the parent cloud.

(2) This section is satisfied if both of the following conditions are met.

(i) The portion of the detached anvil cloud within 5 nautical miles of the flight path is located entirely at altitudes where the temperature is colder than 0 degrees Celsius; and

(ii) The volume-averaged, height-integrated radar reflectivity is less than +33 dBZ-kft (+10 dBZ-km) everywhere along the portion of the flight path where any part of the detached anvil cloud is within the specified volume.

G. G417.13 Debris Clouds

(a) A launch operator must not initiate flight if the flight path will carry the launch vehicle through any nontransparent part of a debris cloud for 3 hours after the debris cloud is observed to be detached from the parent cloud, or after the debris cloud is observed to have formed from the decay of the parent cloud top to an altitude where the temperature is warmer than −10 degrees Celsius. The 3-hour period must begin again at the time of any lightning discharge in or from the debris cloud.

(b) A launch operator must not initiate flight if the flight path will carry the launch vehicle within 5 nautical miles of a nontransparent part of a debris cloud during the 3-hour period defined in paragraph (a) of this section, ***unless all of the following conditions are satisfied:***

(1) There is at least one working field mill within 5 nautical miles of the debris cloud;

(2) The absolute values of all electric field measurements ***made*** at the Earth's surface within 5 nautical miles of the flight path ***and at*** each field mill ***employed*** by paragraph (b)(1) of this section has been less than 1000 volts/meter for 15 minutes or longer; and

(3) The maximum radar return from any part of the debris cloud within 5 nautical miles of the flight path has been less than 10 dBZ for 15 minutes or longer.

H. G417.15 Disturbed Weather

(a) A launch operator must not initiate flight if the flight path will carry the launch vehicle through a nontransparent cloud associated with disturbed weather that has clouds with cloud tops at altitudes where the temperature is colder than 0 degrees Celsius and that contains, within 5 nautical miles of the flight path:

(1) Moderate or greater precipitation; or

(2) Evidence of melting precipitation such as a radar bright band.

I. G417.17 Thick Cloud Layers

(a) A launch operator must not initiate flight if the flight path will carry the launch vehicle through a nontransparent part of a cloud layer that is:

(1) Greater than 4,500 feet thick and any part of the cloud layer along the flight path is located at an altitude where the temperature is between 0 degrees Celsius and –20 degrees Celsius; or

(2) Connected to a thick cloud layer that, within 5 nautical miles of the flight path, is greater than 4,500 feet thick and has any part located at any altitude where the temperature is between 0 degrees Celsius and –20 degrees Celsius.

(b) A launch operator need not apply the lightning commit criteria in paragraphs (a)(1) and (a)(2) of this section if the thick cloud layer is a cirriform cloud layer that has never been associated with convective clouds, is located only at temperatures of –15 degrees Celsius or colder, and shows no evidence of containing liquid water.

J. G417.19 Smoke Plumes

(a) A launch operator must not initiate flight if the flight path will carry the launch vehicle through any cumulus cloud that has developed from a smoke plume while the cloud is attached to the smoke plume, or for the first 60 minutes after the cumulus cloud is observed to be detached from the smoke plume.

(b) Section D applies to cumulus clouds that have formed above a fire but have been detached from the smoke plume for more than 60 minutes.

K. G417.21 Surface Electric Fields

(a) A launch operator must not initiate flight for 15 minutes after the absolute value of any electric field measurement at the Earth's surface within 5 nautical miles of the flight path has been greater than 1500 volts/meter.

(b) A launch operator must not initiate flight for 15 minutes after the absolute value of any electric field measurement at the Earth's surface within 5 nautical miles of the flight path has been greater than 1000 volts/meter unless:

(1) All clouds within 10 nautical miles of the flight path are transparent; or

(2) All nontransparent clouds within 10 nautical miles of the flight path have cloud tops at altitudes where the temperature is warmer than +5 degrees Celsius and have not been part of convective clouds that have cloud tops at altitudes where the temperature is colder than −10 degrees Celsius within the last 3 hours.

L. G417.25 Triboelectrification

(a) A launch operator must not initiate flight if the flight path will go through any part of a cloud at an altitude where the temperature is colder than −10 degrees Celsius up to the altitude at which the launch vehicle's velocity exceeds 3000 feet/second; unless

(1) The launch vehicle is "treated" for surface electrification; or

(2) A launch operator demonstrates by test or analysis that electrostatic discharges on the surface of the launch vehicle caused by triboelectrification will not be hazardous to the launch vehicle or the spacecraft.

(b) A launch vehicle is treated for surface electrification if

(1) All surfaces of the launch vehicle susceptible to ice particle impact are such that the surface resistivity is less than 10^9 ohms/square; and

(2) All conductors on surfaces (including dielectric surfaces that have been treated with conductive coatings) are bonded to the launch vehicle by a resistance that is less than 10^5 ohms.